Development of Mathematical Models and Mathematical, Computational Framework for Multi-media Interaction Processes

by

Yongting Ma

B.S. (Physics), Shandong Normal University, China, 2001

M.S. (Physics), Huazhong University of Science and Technology, China, 2003

M.S. (Mechanical and Aerospace Engineering), George Washington University, 2005

Submitted to the graduate degree program in Department of Mechanical Engineering and the Graduate Faculty of the University of Kansas in partial fulfillment of the requirements for the degree of Doctor of Philosophy.

_____

Dr. Albert Romkes (Advisor), Chairperson

_____

Dr. Karan S. Surana (Co-advisor)

_____

Dr. Peter W. TenPas

_____

Dr. Ray Taghavi

_____

Dr. Bedru Yimer

_____

Date Defended:

The dissertation committee for Yongting Ma certifies that this is the approved version of the following dissertation:

Development of Mathematical Models and Mathematical, Computational Framework for Multi-media Interaction Processes

Dr. Albert Romkes (Advisor), Chairperson

Date Approved:

Abstract

This thesis presents development of mathematical models for multi-media interaction process using Eulerian description and associated computational infrastructure to obtain numerical solution of the initial value problems described by these mathematical models using finite element method. In the development of mathematical models for multi-media interaction processes the physics of solids, liquids and gases are described using conservation laws, appropriate constitutive equations and equations of state in Eulerian description. The use of conservation laws in Eulerian description for all media of an interaction process and the use of the same dependent variables in the resulting governing differential equations (GDEs) for solids, liquids and gases ensure that their interactions are intrinsic in the mathematical model. In the development of the constitutive equations and the equations of state, the same dependent variables are utilized as those in the conservation laws. The dependent variables of choice due to the Eulerian description (which is necessitated due to liquids and gases) are density, pressure, velocities, temperature, heat fluxes and stress deviations. When the mathematical models of the deforming matter for progressively increasing deformation are derived using conservation laws in Eulerian description, the constitutive equations must be derived using rate constitutive theories [1–3] regardless of whether the deforming matter is solid or fluid. Thus complete mathematical description of the deforming matter is highly dependent on the appropriate choice of the specific constitutive equations. Assessment of the validity of various rate constitutive equations is an integral part of the present research. In this proposed approach, the physics of all interacting media of an interaction process are described by a single mathematical model (conservation laws) in the same dependent variables and hence their interactions are inherent in the mathematical model and require no further considerations.

The resulting GDEs from these mathematical models are generally a system of non-linear partial differential equations in space coordinates and time. The hpk mathematical and computational finite element framework with space-time variationally consistent (STVC) integral forms is utilized to obtain the numerical solutions of the initial value problems described by the mathematical models. The proposed computational methodology permits higher order global differentiability approximations, ensures time accuracy of evolutions as well as unconditional stability of computations during the entire evolution. The methodology presented here for multi-media interaction processes is rather natural and lends itself naturally to accurate finite element computations in hpk framework when the integral forms are space-time variationally consistent (STVC).

In most of the currently used methodologies, the interaction between the different media is established using constraint equations at the interfaces between the media. Thus, these approaches are error prone and the validity and accuracy of the computed solutions is highly dependent on the physics described by the constraint equations. In the proposed methodology, the constraint equations are completely eliminated.

This work is dedicated to my beloved parents, to my family and to my sister Liyan Ma.

Acknowledgments

I would like to thank and express my sincere gratitude to my advisor, Dr. Albert Romkes and my co-advisor, Dr. Karan S. Surana (Deane E. Ackers Distinguished Professor of Mechanical Engineering) for providing able guidance and encouragement for fruitful completion of the work presented here. I would also like to thank Dr. Peter W. Tenpas, Dr. Ray Taghavi and Dr. Bedru Yimer for serving as members of my thesis committee.

I would also like to extend my thanks to Dr. Albert Romkes, Dr. Karan S. Surana and the Department of Mechanical Engineering for providing me financial assistance during my graduate studies. The infrastructure provided by the Computational Mechanics Laboratory (CML) is worth mentioning, as it helped immensely to complete this thesis work within time schedule.

Special thanks goes to my parents for encouraging and their support throughout my academic life and thanks to my wife, Ningning Wang for her love, care and encouragement which allowed me to remain focused on my research.

I appreciate and thank all of my friends and colleagues for providing good suggestions and fruitful discussions for completion of this work.

Yongting Ma

Contents

List of Tables

List of Figures

Nomenclature

$\hat{\mathbf{U}}$	:	Velocity Vector
$\mathbf{U}$	:	Dimensionless Velocity Vector
$\hat{\rho}$	:	Density
ρ	:	Dimensionless Density
$\hat{\eta}$	:	Zero Shear Rate Viscosity
η	:	Dimensionless Zero Shear Rate Viscosity
$\hat{\boldsymbol{\tau}}$	:	Stress Derivation Tensor
$\boldsymbol{\tau}$	:	Dimensionless Stress Tensor
$\hat{\mathrm{p}}$	:	Pressure
p	:	Dimensionless Pressure
$\hat{u}$	:	Velocity in x direction
u	:	Dimensionless Velocity in x direction
$\hat{v}$	:	Velocity in y direction
v	:	Dimensionless Velocity in y direction
$\hat{\tau}_{xx}$	:	Normal Stress in x direction
τ_{xx}	:	Dimensionless Normal Stress in x direction
$\hat{\tau}_{yy}$	:	Normal Stress in y direction
τ_{yy}	:	Dimensionless Normal Stress in y direction
$\hat{\tau}_{xy}$	:	Shear Stress in xy plane
τ_{xy}	:	Dimensionless Shear Stress in xy plane
ω	:	Dimensionless vorticity
Re	:	Reynolds number
Ec	:	Eckert number
Br	:	Brinkman number
Pr	:	Prandtl number
De	:	Deborah number

λ_1 : Relaxation time

λ_2 : Retardation time

α : dimensionless mobility factor

$\hat{x}$: x coordinate

x : Dimensionless x coordinate

$\hat{y}$: y coordinate

y : Dimensionless y coordinate

τ_0 : Reference Stress

p_0 : Reference Pressure

ρ_0 : Reference Density

U_0 : Reference Velocity

L_0 : Reference Length

η_0 : Reference Viscosity

φ : Vector of Field Variables

φ_h : Interpolation of φ over an element 'e'

u_h : Interpolation of velocity u over an element 'e'

v_h : Interpolation of velocity v over an element 'e'

p_h : Interpolation of pressure p over an element 'e'

Chapter 1

Literature Review, Scope and Outline of the Work

1.1 Literature Review

The interactions of diversely different media such as solids, liquids and gases with varied physics occur routinely in many areas of engineering, physics and sciences. The development of mathematical models and the numerical simulation of associated boundary value problems (BVPs) and initial value problems (IVPs) for multi-media processes containing diversely different media have been a subject of study and many research writings for over four decades. While many application specific developments may be found in the published literature, there is lack of general mathematical modeling infrastructure and associated computational methodology that is application and problem independent and addresses all interaction processes with the same generality, rigour and accuracy. The basic philosophy adopted in the currently published literature for multi-media interaction processes consists of the following :

(1) The mathematical model for each medium of an interaction process is devel-

oped based on what is ideally suited for the media. This often leads to different choices of the descriptions (Lagrangian description or Eulerian description) as well as different choices of dependent variables in the development of the mathematical models for each media of an interaction process. For example, the use of Lagrangian description with displacements as dependent variable of choice for solids and Eulerian description for liquids and gases in which velocities are dependent variables of choice.

(2) In the development of the mathematical and computational infrastructure to obtain numerical solution of the boundary value problems (BVPs) or the initial value problems (IVPs) associated with these mathematical models, most suitable strategies of discretization for each media are employed as well.

(3) As a consequence of the first two steps, in the development of the mathematical models as well as the methods of approximations utilized for obtaining numerical solutions of the associated BVPs and IVPs, there is no inherent interaction between a medium and its neighbors.

(4) The interactions between a medium and its neighbors are generally established through constraint equations (generally a set of algebraic relations enforcing the desired physics) at the interfaces between the interacting media. This philosophy and its variation have led to many different strategies out of which, perhaps the 'Arbitrary Lagrangian Eulerian (ALE)' methodology is most commonly accepted as a viable approach and is currently used for multi-media interaction processes.

There is a vast amount of literature on this subject, a detailed discussion of all relevent works is beyond the scope of the thesis. Instead we classify various approaches and published works in groups and then simply present their salient features primarily in

context with finite element method. We consider fluid-solid interaction as a model problem of multi-media interaction process to present the literature review. In the literature review presented in the following, the published work is grouped in two specific areas: development of mathematical models, and development and use of the methods of approximations to obtain the numerical solutions of the associated BVPs and the IVPs described by the mathematical models.

1.1.1 Mathematical models

Broadly speaking, the published works in the area of the development of the mathematical models for various media of an interaction process can be divided into four categories

(i) The first category consists of mathematical models that utilize purely Lagrangian descriptions [10–13]. The formulation in reference [10] is based on conservation of mass and balance of momenta and claims to eliminate non-zero frequency modes. A partitioned formulation presented in reference [11] using an interface compliance normalization and a transformation of the displacement that correctly describes the presence of zero-energy modes in the fluid without which incorrect vibration characterization would result. In reference [12] partitioned and monolithic approach are compared in terms of stability, accuracy and computational cost for the numerical simulation of fluid-structure interactions. In contrast to partitioned schemes, monolithic schemes are claimed to be unconditionally stable and considerably more accurate. Least squares finite element formulations using first order system of equations in displacements for solid and Navier-Stokes equations in velocity for fluid are presented in reference [13]. The solution strategy alternates between fluid and solid with load transfer at the interface. Flow

in an elastic pipe, L-shaped domain and cross flow problems are used as model problems. The Lagrangian descriptions are ideally suited for solids in which the motions of the material particles can be easily described using reference configuration and time. Use of such mathematical models using Lagrangian description for liquids and gases obviously limits the range of application due to the fact that complex motion of the fluid particles becomes difficult to describe using reference configuration and time.

(ii) The second category of approaches are those in which purely Eulerian descriptions are utilized [14–21] for all media of an interaction process. A multi-material Eulerian approach for impact and penetration problems is presented by Benson [14]. This approach is a combination of finite different, finite element, operator splitting, sequential solution strategies with the objective of improving efficiency of transport calculations. Fedkiw *e*t al. [15] employ non-oscillatory Eulerian approach to two-phase compressible flow along with Ghost Fluid Method. A level set function is used to track the motion of the multimaterial interfaces. The authors claim success in preserving continuous pressure and velocity profiles at contact discontinuity. Various numerical results are presented using third order ENO-local Lax-Friedrich and third order TVD-RK schemes. Implicit multi-material Eulerian formulations [16] are developed to extend the range of applicability to quasi-static problems. The mixture theory for the multi-material elements and the transport step is included. Benson et. al. [17] consider Eulerian cell formulation due to its ability to permit large motions for fluid-solid interaction. In this work, Eulerian formulations are extended to handle large structural deformations and rotations. An Eulerian, sharp interface, Cartesian grid method is developed in references [18, 19]. The mass, momentum and energy equations

are used in conjunction with evolution equations for deviatoric stress and equivalent plastic strain. The Mie-Gruneisen equation of state is used and the material is modeled as a Johnson-Cook solid. An Eulerian-approach for fluid-structure coupling is presented in reference [20] for an elastic body and an incompressible fluid. Level set is used to determine the fluid-solid interfaces. Biophysical applications are presented using this approach. Dunne [21] presented a fully variational Eulerian approach for fluid-structure interaction. In this approach, the displacement appears as a primary variable and the set of initial positions (IP) is used to monitor the structure displacements. The author showed the main advantage of the set of initial positions (IP) approach with respect to the level set approach is the improved handing of geometries containing corners. In this approach, the mesh points or monitoring locations remain fixed and the material particles pass through these locations. In this approach, the mathematical models always result into a system of non-linear partial differential equations even for linear problems. This approach is not very popular for solid mechanics because of its inability to follow material particles. Due to the use of velocity as dependent variable in the conservation laws, the constitutive equations for solids need to be rate constitutive equations such as upper convected, Jaumann, lower convected etc. These are known to produce different response for the same material constants. This has been a subject of research for some time without any consensus [22] and is a subject of investigation in the present work also. Another issue of concern and of further investigation is the choice of total stresses or stress deviations and pressure as dependent variables. The use of Galerkin method with weak form requiring stabilization methods (upwinding) has hampered the success of finite element method for obtaining numerical solutions of IVPs described by mathematical models containing non-linear space-time differential operators.

(iii) Third category of approaches are those that utilize Eulerian as well as Lagrangian descriptions in the development of the mathematical models as deemed appropriate for the media [23–28]. Sussman *e*t al. [23] utilize the level set approach for computing solutions of incompressible two phase flow. A second-order projection method implementing a second-order upwinded procedure for differencing the convection terms is used. The level set is used as a signed distance function. The air bubble problem is analyzed in which the effects of surface tension, viscous terms and density ratios are studied.

Arienti *e*t al. [24] use level set to track the moving interface. The Eulerian and Lagrangian subdomains are modeled and discretized individually. The boundary conditions at the interface are established enforcing conservation of mass and continuity of the stress tensor in direction normal to the boundary.

Caiden *e*t al. [25] propose a numerical method for modeling two phase flow consisting of separate compressible and incompressible regions. A level set method to track the interface between the compressible and incompressible regions, as well as the Ghost Fluid Method(GFM) to create accurate discretization across the interface.The ability of the method to compute compressible/incompressible flow interaction when the compressible flow contains shocks is also investigated.

Koren *e*t al. [26] present solutions of two fluid flows with finite volume technique. Level set method is used to track the interface. The authors propose numerous remedies to control solution errors. These remedies are problem specific in nature. For large density ratios, a simple variant of ghost fluid method is employed.

Gr*öb e*t al. [27] present a finite element method based on level set method for two phase incompressible flows. Level set technique is applied for determining the interface between flows. Surface tension effects are taken into consideration. For

time discretization a variant of the fractional step θ-scheme is applied. Numerical studies demonstrate reparameterization and smoothing of level sets, effect of surface tension and levitated drop in a measuring cell.

Chessa and Belytschko [28] employ enriched finite element formulation for computing solutions for axisymmetric two phase flow. The enrichment of the elements implemented by the extended finite element method (X-FEM) allows the discontinuity in the velocity gradient at the interface to be modeled by a local partition of unity. Level -set technique is used to monitor the movement of the interface. Surface tension effects are also taken into consideration. The numerical examples include fully developed Couette flow, velocity of rising bubble, drop falling onto a thin film and bubbles rising to a surface.

For different media of an interaction process, the mathematical models are generally developed using Lagrangian description for solids while Eulerian description is used for liquids and gases. This generally necessitates the use of different variables in the two descriptions. For example, displacements in Lagrangian description but velocities in Eulerian description. There are some difficulties associated with this approach: (a) Due to different choices descriptions as well as dependent variables for solids and liquids, the mathematical models do not contain their interactions (b) The interaction between the mating media must be described through constraint equations related to the interface physics. Thus the validity of the constraint equations largely controls accuracy of the interaction at and in the neighborhood of the interfaces. This approach is highly prone to judgemental errors. (c) When solving the BVPs and IVPs associated with these mathematical models numerically, the interface boundaries may move into or away from the Eulerian mesh. This is due to the fact that in Lagrangian description the particles

i.e. mesh points or grid points move and their displacements are monitored while in Eulerian description, computations are performed on a fixed mesh. To avoid this problem, generally moving mesh strategies or ghost inferface element methods are employed which may contain approximations and are generally problem dependent.

(iv) The fourth category of methods consists of ALE methods [29–38].

In a technical report [29], Amsden and Hirt combine implicit continuous fluid Eulerian and the ALE methods to present a numerical scheme for fluid flow at various speeds. The numerical scheme is described in connection with the framework of a computer program, YAQUI. This approach was further developed in [30]. It is one of the earliest works introducing ALE methods. In this work a numerical technique for finite difference approach is presented consisting of ALE and an implicit formulation similar to implicit continuous fluid Eulerian technique. The basic methodology and the corresponding finite difference approximations are discussed in details. Computational stability, accuracy and other relevant topics are discussed as well.

Hughes *e*t al. [31] present theoretical development of finite element method using ALE approach for incompressible viscous flows, which is appropriate for modeling the fluid subdomain of many fluid-structure interactions. The scheme is implemented using two dimensional iso-parametric finite elements and is applied to a free-surface wave propagation problem to demonstrate its effectiveness.

Lepage and Habashi [32] presented a three dimensional finite element Euler/Navier-Stokes solver based on the ALE formulation. A two zone node movement scheme based on Laplacian smoothing is used. Equilibrium between fluid and solid media is achieved iteratively. ALE formulation is used to account for moving bound-

aries. Even though the framework presented is for 3D problems, the numerical studies are only given for two dimensional cases, these include the past oscillating airfoil, oscillating cylinder and modeling of ice-accretion.

In reference [33], large rotations and large displacements in geometrically nonlinear structural behavior is considered. The ALE finite element formulation using triangular elements is presented for compressible inviscid fluid flow. The beam arch elements are developed to account for large displacements and large rotations of the structure. Newmark time integration is employed for obtaining structural response while Lax-Wendroff scheme with shock capturing technique is used for the fluid.

Mendes and Branco [34] analyze the fluid-rigid body interaction using ALE approach with finite element method and a two step projection scheme. The flow is assumed to be two dimensional, incompressible, laminar and viscous in Lagrangian-Eulerian framework. In the two step projection scheme, the pressure is calculated by solving a consistent discrete analogue of the Poisson equation for the pressure field.

In reference [35], ALE formulation for fluid-structure interaction problem is applied to an underwater explosion. For the fluid close to the interface, an ALE formulation is used, whereas in areas away from the structure, an Eulerian formulation is employed. The structure is described using Lagrangian approach. This formulation allows two different materials within a single element. The purpose of the ALE formulation is to demonstrate the ability of the ALE smoothing method to continue the calculation beyond the point where the pure Lagrangian calculations fail.

ALE finite element method with automatic mesh updating [36] is formulated for

analyzing fluid-structural buckling and problems involving large domain changes. ALE finite element formulation is employed for the fluid, and the total Lagrangian for the structure. From numerical analysis of 2D artificial heart, it is concluded that the Laplace equation based on ALE mesh updating algorithm works well for large deformation of fluid domain. The 3D model is analyzed by using strong coupling, numerical stabilization methods and extended predictor-multicorrector algorithm time integration method with automatic time step control.

In reference [37], an ALE formulation is used for large structural displacements. The ALE formulation is employed for the fluid part while the elastic structure has total Lagrangian description. The interface boundary conditions are purely kinematic. The coupled algebraic system is solved by relaxation algorithm, in which the fluid and structural parts of the problem are tracked with Dirichlet and Neumann boundary conditions respectively.

Pishevar [38] proposed an ALE scheme for compressible multiphase fluids. The gas-phase is separated from the liquid-phase by an immiscible interface. The interface remains Lagrangian at all times and the ALE behavior is allowed only within materials. The grid of the interface is moved with a velocity obtained from the exact solution of Riemann problem at the interface. The mesh velocity is obtained by solving Laplace equation using interface velocity as boundary condition.

The ALE methods have no basic dependence on particles and treat the computational mesh as a reference frame which may be moving at an arbitrary velocity other than the velocities of the particles. Since the reference frame moves in space with an arbitrary velocity, the ALE description does not refer directly to particles in motion, it is only useful for describing a flow only if it is linked to

either classical Lagrangian or Eulerian description. This is exactly what is done in the approach.

1.1.2 Methods of approximation

The mathematical models resulting from the use of conservation laws, constitutive equations and the equations of state (for compressible matter) are generally a system of nonlinear partial differential equations in space coordinate and time. Thus, an unconditionally stable computational methodology to obtain their accurate numerical solutions is of critical importance. In the following we describe currently used approaches. The methodologies to obtain approximate numerical solutions (methods of approximation) of the BVPs and IVPs described by these mathematical models fall into three distinct and popular categories (among others): finite difference methods, finite volume methods and finite element methods. Since the research described in this thesis only considers finite element method, we present pertinent and commonly used methodologies in this area. A closer examination of the mathematical models reveals that these naturally lead to IVPs for multi-media interaction process, i.e. we need to examine finite element methodologies related to IVPs in which the space-time differential operators are nonlinear. Generally speaking the methods of approximation for IVPs can be classified in two groups: space-time decoupled methods and space-time coupled methods.

In space-time decoupled approaches non-concurrent treatments i.e. integral forms, discretizations etc. are used in space and time. In such approaches a spatial finite element discretization may be performed independently from finite element or finite difference discretization in time. In contrast, space-time coupled methods construct space-time integral forms based on fundamental lemma or the residual functional [39–41] using

the mathematical model. This is followed by a space-time local approximation over a space-time finite element. The space-time coupled approaches can be applied to the whole space-time domain by discretizating it, or one could use a space-time discrezation for an increment of time resulting in a space-time strip or slab for an incremental of time and then time march the solution [7]. The space-time strip approach with time marching is more efficient as in this case a small problem is solved for each incremental of time. The time-dependent processes are evolutions where the solutions naturally exhibit simultaneous dependence on space coordinates and time. For such processes the incentive to use decoupled methods may be to reduce computational effort. However, space-time decoupling may lead to serious loss of accuracy and unusually small time steps may be required to ensure stability. We also remark that in the space-time coupled methods the space-time differential operators can be classified mathematically for all IVPs either using the whole space-time domain or a space-time strip or a slab. This permits unified treatment for all IVPs using methods of approximations. Surana et. al. [7] have shown that the space-time differential operators are either non-self adjoint or non-linear and as a consequence all space-time methods of approximation except space-time least squares processes are space-time variationally inconsistent (STVIC) i.e. will yield integral forms that may not lead to unconditionally stable computations. In space-time decoupled methods there is no such concept of operator classification thus, each IVP must be treated individually to ensure stability of computations.

In the currently used finite element approaches for multi-media interaction processes, the space-time decoupled methods are generally used. An integral form is constructed using Galerkin method with weak form (GM/WF) in the spatial domain assuming all time derivatives to be constant. This is followed by local approximation over the spatial domain in which the local approximation functions are functions of spatial coordinates

but the nodal degrees of freedoms are functions of time. Upon substituting the local approximation into the integral form one obtains a system of ordinary differential equations in time that are integrated numerically using implicit or explicit time integration methods or discretized and solved numerically using finite element method in time. In this approach, when the differential operator contains odd derivatives of the dependent variables with respect to spatial coordinates or is non-linear, the coefficient matrices are not symmetric and many of the problems associated with GM/WF for non-linear or non-self adjoint operators for BVPs may be encountered in this case also. This approach may require use of stabilization methods which eventually results in addition of artificial diffusion. The use of space-time coupled methods in the published work is not common and is primarily dominated by GM/WF, which in case of the IVPs under consideration, will lead to space-time variationally inconsistence (STVIC) integral forms that would undoubtedly require stabilization of the computation using upwinding methods. In summary, dominance and use of GM/WF in the published work for interaction processes raises very serious questions regarding stability of the computational processes, their accuracy as well as time accuracy of evolutions. The stabilization methods very rarely have rigorous mathematical basis [42].

1.2 Rationale, Scope and Outline of Present Work

The work of Benson et al. [14, 16, 17] using Eulerian description for all media of an interaction process with finite difference, finite volume and finite element method (GM/WF) is noteworthy in context with the research presented here. In the development of the mathematical models in these works, choice of variables, rate constitutive equations and rationale for specific choices are not clear. Furthermore, the clear demarcation between the development mathematical models and the methods of approxima-

tions for obtaining their solution is not clear either. In many instances a mix of finite difference, finite volume and finite element methods has been used that lacks rationale from the point of view of computational mathematics. The other significant series of works is due to Udaykumar et al. [18, 19, 43–47] using purely Eulerian description for elastic-plastic solid behavior, Newtonian fluid and compressible gases with finite difference and finite volume methods including level set for tracking moving boundaries and interface. These works concentrated primarily on level set and finite difference tricks with the objective of sharp interface resolutions. Rotionale for the models, choice of variable and the choice of constitutive theory for the most part is not discussed but simply stated, presented and used by the authors. Many of the problems associated with these works are some what due to mathematical models but are also due to use of space-time decoupled finite difference and finite volume methods for obtaining numerical solution of the associated IVPs of the interaction problems. The work presented in this thesis attempts to address all of the issues related to mathematical models as well as computational methods for obtaining their numerical solutions that arise in the interaction processes. The following is an outline of the work presented in this thesis. The necessity of the approach presented here and the rationale behind it are clearly stated and discussed.

1.2.1 Mathematical models

(1) The most accurate, problem independent and the straight forward means of accounting for the interactions of diversely different media in an interaction process is to ensure that a single mathematical model describes the physics of all media of an interaction process. In doing so we ensure that their interactions are inherent in the mathematical model.

(2) The development of the mathematical model must utilize Eulerian descriptions for solids as well as fluids. This is necessitated due to the fact that complex motion of particles can not be described using Lagrangian description.

(3) The choice of dependent variables must be the same for all media (i.e. solids and fluids) of an interaction process and must be such that the same governing differential equations (GDEs) from the conservation laws can be used for all media of an interaction process. Furthermore, the constitutive theory and the equations of state must also be derivable for all interacting media using the same dependent variables that are used in the conservation laws.

(4) The GDEs resulting from the conservation laws (conservation of mass, balance of momenta and conservation of energy) can be easily derived using density, velocities, total stress tensors, specific internal energy and heat fluxes as dependent variables in Eulerian description, which remain valid for all media of an interaction process. These equations obviously do not have closure without the constitutive equations describing the constitution of the specific media of interest and the equations of state.

(5) If the deforming matter is to be in thermodynamic equilibrium, then in addition to conservation of mass, balance of momenta and conservation of energy, the second law of thermodynamics (entropy inequality) must also be satisfied for the deformation to be admissible. As well known conservation of mass, balance of momenta and conservation of energy yield continuity, momentum and energy equations in which we assume existence of stress field and heat flux in the deforming matter. Thus the second law of thermodynamics must provide the basis for the development of the constitutive theory for the stress tensor and heat vector [1–4] for all media of an interaction process.

It has been shown by Surana [4] and Surana et. al. [1–3] that in Eulerian descriptions the constitutive equations for the stress tensor must be derived using ordered rate constitutive theories based entropy inequality and the theory of generators and invariants. In this approach many possibilities exists for deriving various theories, however the main limitation in the use of these theories arise from the design of valid experiments to determine the values of the coefficients in the constitutive relations. In the work presented in this thesis we borrow the constitutive relations from references [1–4] but present discussions and investigations of their validity and usefulness in multi-media interaction processes. We discuss the inherent limitations of the presently used theories due to the assumption employed in their derivations and present some theoretical and computational evidence to support usefulness of some constitutive relations over the others from the point of view of their use in the interaction processes.

1.2.2 Methods of approximation

The mathematical models for multi-media interaction processes generally result in a system of nonlinear partial differential equations in space coordinates and time containing density, velocities, pressure, stress tensors, heat vectors and temperature as dependent variables. This work utilizes space-time finite element method based on space-time least squares processes for a space-time strip or slab that corresponds to an increment of time and then time maches the solution to compute the desired evolution. In the computations of the numerical solutions of the associated IVPs describing interaction processes we view: (i) higher order global differentiability of approximation in space and time and (ii) unconditional stability of the computational process during the entire evolution as two most significant aspects. We must keep in mind that sta-

bilizing computations using upwinding method is not a viable option due to the fact that upwinding methods neither have physical nor mathematical basis [42]. Surana et al. [7, 48–50] have shown that the order k of the approximation space defining global differentiability of order $(k-1)$ of the approximations is an independent parameter in all finite element computations in addition to h, the characteristic length of the discretization and p, the degree of local approximation. h, p -refinements can not alter k. For example, local approximation of class C^0 ($k = 1$) remain of class C^0 regardless of the choices of h and p. Thus, in the finite element processes and computations, h, p and k are independent parameters as opposed to h and p used currently with local approximation generally of class C^0. Thus, "h, p, k as independent parameters" and calculus of variations form the basis for mathematical and computational framework for the finite element processes used in the present work, hence forth referred to as "hpk mathematical and computational framework". The hpk framework allows higher degree local approximations of higher order global differentiabilities in space and time and variational consistency of the space-time integral forms result in unconditionally stable computations.

Thus the space-time local approximations are in $H^{k,p}(\bar{\Omega}^e_{xt})$ spaces in which $k = (k_1, k_2)$ are the orders of the spaces in space and time, $p = (p_1, p_2)$ are the p-level in space and time and $\bar{\Omega}^e_{xt}$ is the space-time domain of a typical space-time element 'e'. Since the differential operators in the IVPs in the interaction processes are non-linear, only space-time least squares processes yield STVC integral forms ensuring that the coefficient matrices in the algebraic systems are symmetric with real basis and eigenvalues greater than zero and hence yield unconditionally stable computations during the entire evolution for all choices of h, p and k and the dimensionless parameters appearing in the mathematical models.

The main emphasis of the work presented here is first, to establish and demonstrate that it is possible to derive a single mathematical model that describes all media of an interaction process and thus their interactions are intrinsic in the mathematical model and hence, do not require the use of constraint equations at the interfaces between the media to establish their interactions. Secondly, to demonstrate that hpk framework with STVC integral forms is ideally suited for obtaining numerical solutions of the IVPs described by these mathematical models. For simplicity we have chosen to restrict this work to applications in which the movement of the interfaces, free surfaces and boundaries is very small and hence Eulerian descriptions with computations on a fixed grid suffice. Large movements of the interfaces, free surfaces and boundaries will be considered in the future work.

1.2.3 An outline of the work in various chapters

An outline of the work presented in various chapters of this thesis is described in the following. The mathematical models including constitutive equations for stress tensor and heat vector for solids and fluids (both incompressible and compressible) are presented in chapter 2. The details of the mathematical and computational finite element framework used for obtaining numerical solutions of the IVPs described by the mathematical models are given in chapter 3. Chapter 4 presents some derivations and investigations of the validity and limitations of the rate constitutive theories by Surana [4] and Surana et. al. [1–3] and their usefulness in the mathematical models. The speed of propagation of a disturbance in an inelastic and/or incompressible media is infinity, however such assumptions are often used in constructing mathematical models, it is essential to investigate if the IVPs associated with these assumptions can be solved numerically without problem dependent treatments while still maintaining bounded computed evolutions.

The investigations related to this aspect of the work are presented in chapter 5. Various multi-media interaction processes and 1D numerical studies are considered in chapter 6 to illustrate how such processes are to be viewed and simulated using the approach presented in this thesis. Chapter 7 contains 2D numerical studies for various multi-media interaction model problems to demonstrate the usefulness, rigour and accuracy of the proposed methodology. Summary and conclusions are presented in chapter 8.

Chapter 2

Development of Mathematical Models for Multi-media Processes Using Eulerian Description

The mathematical description of the physics of deforming matter can be established using conservation laws: conservation of mass, balance of momenta and conservation of energy. These yield continuity equation, momentum equations and energy equation. In this derivation we have two choices: (i) The mathematical model can utilize material point coordinates (x_i) in the reference or the initial configuration and time (t) in which case the deformed position coordinates $\bar{x}_i$ are given by

$$\bar{x}_i = \bar{x}_i(x_i, t) \tag{2.1}$$

In such description all dependent variables or quantities of interest become function of x_i and t. The mathematical models derived using this approach are called Lagrangian descriptions. The PDEs resulting in such descriptions contain dependent variables,

position coordinates x_i and time t. Thus if Q is a dependent variable, we write

$$Q = Q(x_i, t) \tag{2.2}$$

Thus in this approach we follow the material particles in time during evolution. (ii) On the other hand, we can use inverse of (2.1) i.e.

$$x_i = x_i(\bar{x}_i, t) \tag{2.3}$$

In this approach we consider fixed location $\bar{x}_i$ that are occupied by different material particles at different values of time allowing us to monitor the state of the evolution of the matter at $\bar{x}_i$. The mathematical models derived using this approach are called Eulerian descriptions. The PDEs resulting in such descriptions contain dependent variables, position coordinates $\bar{x}_i$ in the current configuration and time t as independent variables. Thus if $\bar{Q}$ is a dependent variable, we write

$$\bar{Q} = \bar{Q}(\bar{x}_i, t) \tag{2.4}$$

Over bar on Q emphasizes Eulerian description. Thus we note that in Eulerian description, we monitor the state of evolution of the deforming matter at a fixed spatial location in the current configuration occupied by different material particles during the evolution rather than following the material particles as in Lagrangian description. This approach is obviously ideal for fluids which may have complex motion during the evolution.

Based on these two approaches of describing the state of the deforming matter, it is straight forward to conclude that in multi-media interaction processes which may involve interactions between solids and fluids, the Eulerian descriptions are meritorious

to describe behaviors of deforming fluids. And if we insist that a single mathematical model describe the deformation of all media of an interaction process then we must employ conservation laws (conservation of mass, balance of momenta and conservation of energy) in Eulerian description without regard to the constitution of the matter but with the assumption of the existence of a stress tensor and a heat vector. The mathematical description so derived will naturally be applicable to all media of an interaction process as does not contain media specific physics i.e. constitutive equations and equations of state.

A single mathematical model derived using conservation laws, though describes all media of an interaction process, does not have closure due to the lack of media specific physics that is essential in complete mathematical descriptions i.e. constitutive equations and the equations of state. These obviously will be media specific but must utilize the same description (i.e. Eulerian description) as well as the same dependent variables as used in the conservation laws. For the deforming matter to be in thermodynamic equilibrium, in addition to conservation laws, the second law of thermodynamics (entropy inequality) must be satisfied. Since the conservation laws assume existence of stress tensor and heat vector without regard to the deformation and properties of the matter, these are applicable to all deforming matter but contain no mechanism for developing the constitutive theory. Thus we must consider the second law of thermodynamics to derive constitutive theory for the stress tensor and heat vector for all deforming matters [5,6]. This would ensure thermodynamic equilibrium of the deforming matter. In deriving constitutive theory for the stress tensor from the conditions resulting from the entropy inequality it is necessary to decompose the total stress tensor into the equilibrium stress and the deviatoric stress and then establish constitutive relations for each one individually. The equilibrium stress results in mechanical pressure for incom-

pressible matter and thermodynamic pressure for compressible matter. The constitutive relations for the heat vector in the simplest form result in Fourier heat conduction law. Thus in Eulerian descriptions, the constitutive theory for the stress tensor is essentially the development of the constitutive relations for the deviatoric stress tensor.

In addition to constitutive relations, equations of state is needed if the matter is compressible. The equation of state defines dependence of thermodynamic pressure on temperature and density. These are well established for commonly used materials. In the development of the mathematical models using principles of continuum mechanics it is sufficient to assume dependence of the thermodynamic pressure on density and temperature rather than a specific form.

The conservation laws, constitutive theory (second law of thermodynamics) and equations of state provide complete mathematical description of all deforming media of an interaction process. A single mathematical model resulting from the conservation laws holds for each media while the media specific physics is described by the constitutive equations and the equations of state. In this process, choice of a single description (i.e. Eulerian) and a consistent single set of dependent variables ensure that the interactions of the various media of a process remain inherent in the mathematical model and thus eliminating the need for constraint equations at the interfaces between the media as used presently. Details of the various aspects of the mathematical models are presented in the following.

Notations

Based on [4–6], the distinction between Lagrangian and Eulerian descriptions can be

made by using x_i (coordinates in the reference configuration) and $\bar{x}_i$ (fixed coordinates location in the current configuration) and likewise $Q = Q(x_i, t)$ and $\bar{Q} = \bar{Q}(\bar{x}_i, t)$ implying Lagrangian and Eulerian descriptions of a dependent variable Q. This distinction helps and results in more clarity in the development and representation of the constitutive theories as well as conservation laws. For the dependent variables we employ standard notation i.e. ρ, $\boldsymbol{v}$, $\boldsymbol{\sigma}$ or $\boldsymbol{\tau}$, T and $\boldsymbol{q}$ meaning density, velocity vector, stress tensor, temperature and heat vector. When used in Eulerian description, these will obviously contain over bar. Other notations used in this thesis are either defined where they are used or are given in the list of nomenclatures.

The material presented in this chapter is divided in the following sections.

(a) Preliminary considerations;

(b) Conservation laws;

(c) Rate constitutive equations;

(d) Equations of state and specific internal energy;

(e) Complete mathematical models and their dimensionless forms;

(f) Summary.

2.1 Preliminary Considerations [1, 4–6]

Consider a fixed Cartesian coordinate system o-$x_1x_2x_3$ or x-frame. Let x_i be the position coordinates of each material point in the reference configuration (assumed same as initial configuration at time t_0, time at the commencement of the evolution). Let $\bar{x}_i$ be the coordinates of the material points in the current configuration, also defined in the

fixed x-frame. Consider the matter to be homogeneous and isotropic, hence the mathematical descriptions of the deforming matter developed at a material point are valid for the entire volume of the deforming matter.

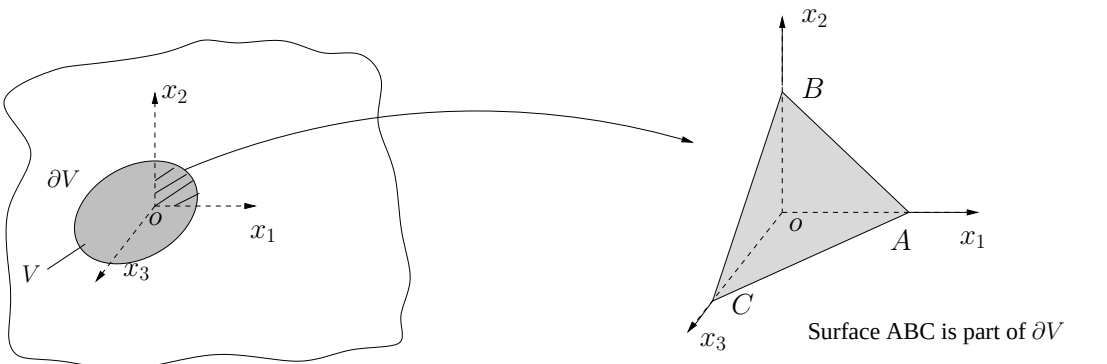

(a) Reference configuration

(b) Elementary tetrahedron in reference configuration

Figure 2.1: Elementary tetrahedron in the reference configuration

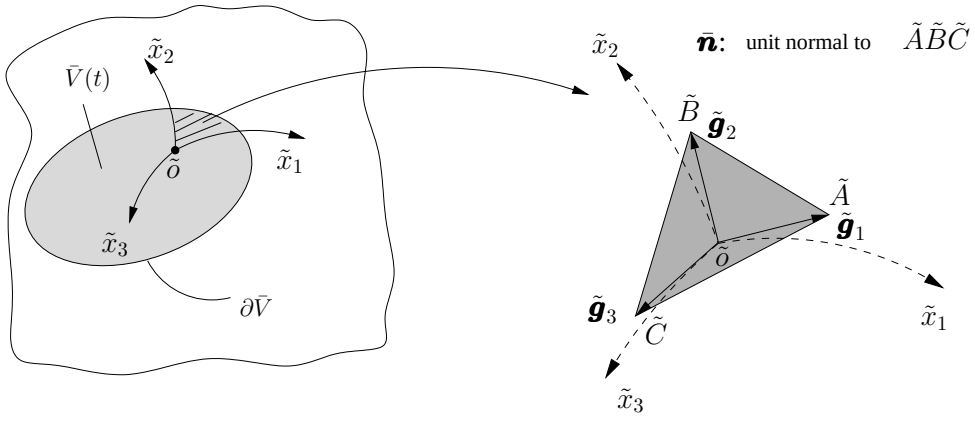

(a) Current configuration

(b) Deformed tetrahedron with covariant base vectors

Figure 2.2: Elementary tetrahedron in the current configuration

Consider an elementary tetrahedron $oABC$ in the reference configuration with oblique plane ABC and its faces oBC, oCA and oAB parallel to the x_1, x_2, x_3 planes (figure

2.1). In the current configuration the tetrahedron deforms into $\bar{o}\bar{A}\bar{B}\bar{C}$ (figure 2.2). The faces of the deformed tetrahedron are flat but not mutually perpendicular (due to finite deformation). The oblique face $\bar{A}\bar{B}\bar{C}$ is also flat and has external traction acting on it. The edges of deformed tetrahedron ($\bar{o}\bar{A}$, $\bar{o}\bar{B}$ and $\bar{o}\bar{C}$) are covariant base vectors $\tilde{\boldsymbol{g}}_i$. These form a nonorthogonal basis. The vectors normal to the faces of the deformed tetrahedron form contravariant base vectors $\tilde{\boldsymbol{g}}^i$ defining the reciprocal nonorthogonal basis. If we consider oA, oB and oC as material lines in the reference configuration then the covariant base vectors are the tangent vectors to the deformed material lines at material point $\bar{o}$ in the current configuration. Let $\{\bar{P}\}$ be the average stress vector on the oblique plane $\bar{A}\bar{B}\bar{C}$ with normal $\{\bar{n}\}$. Using $\tilde{\boldsymbol{g}}^i$ basis and the dyads $\tilde{\boldsymbol{g}}^i \otimes \tilde{\boldsymbol{g}}^j$ we can define a stress tensor $\bar{\boldsymbol{\varrho}}^{(0)}$ with components $(\bar{\varrho}^{(0)})_{ij}$. Lisewise, using $\tilde{\boldsymbol{g}}_i$ basis and the dyads $\tilde{\boldsymbol{g}}_i \otimes \tilde{\boldsymbol{g}}_j$ we can also define a stress tensor $\bar{\boldsymbol{\varrho}}_{(0)}$ with components $(\bar{\varrho}_{(0)})_{ij}$. The Cartesian components of $\bar{\boldsymbol{\varrho}}^{(0)}$ denoted by $\bar{\sigma}^{(0)}_{ij}$ and hence the tensor $\bar{\boldsymbol{\sigma}}^{(0)}$ is called contravariant Cauchy stress tensor derived used contravariant basis. Similary, the Cartesian components of $\bar{\boldsymbol{\varrho}}_{(0)}$ denoted by $(\bar{\sigma}_{(0)})_{ij}$ and hence the tensor $\bar{\boldsymbol{\sigma}}_{(0)}$ is called the covariant Cauchy stress tensor derived using covariant description. The Cauchy stress tensors $\bar{\boldsymbol{\sigma}}^{(0)}$ and $\bar{\boldsymbol{\sigma}}_{(0)}$ are in the deformed configuration for a tetrahedron located at a material point $\bar{o}$ with position coordinates $\bar{x}_i$ in the fixed x-frame, hence these are Eulerian measures of stress with their components in the x-frame (see references [1, 4–6]). Thus, these stress measures can be used in the conservation laws in Eulerian description. Equilibrium of the tetrahedron with these stress tensors and $\{\bar{P}\}$ requires stress tensors $\bar{\boldsymbol{\sigma}}^{(0)}$ and $\bar{\boldsymbol{\sigma}}_{(0)}$ to be symmetric. Development of the constitutive theory for the stress tensors $\bar{\boldsymbol{\sigma}}^{(0)}$ and $\bar{\boldsymbol{\sigma}}_{(0)}$ using second law of thermodynamics [1, 4–6] requires decomposition of the stress tensors $\bar{\boldsymbol{\sigma}}^{(0)}$ and $\bar{\boldsymbol{\sigma}}_{(0)}$ into equilibrium stress and deviatoric

stress

$$\bar{\boldsymbol{\sigma}}^{(0)} = {}_e\bar{\boldsymbol{\sigma}}^{(0)} + {}_d\bar{\boldsymbol{\sigma}}^{(0)} \tag{2.5}$$

$$\bar{\boldsymbol{\sigma}}_{(0)} = {}_e\bar{\boldsymbol{\sigma}}_{(0)} + {}_d\bar{\boldsymbol{\sigma}}_{(0)} \tag{2.6}$$

The equilibrium stress tensors ${}_e\bar{\boldsymbol{\sigma}}^{(0)}$ or ${}_e\bar{\boldsymbol{\sigma}}_{(0)}$ can be established using entropy inequality. For compressible matter, we obtain

$$\bar{\boldsymbol{\sigma}}^{(0)} = -p(\bar{\rho}, T)[I] + {}_d\bar{\boldsymbol{\sigma}}^{(0)} = -p(\bar{\rho}, T)[I] + \bar{\boldsymbol{\tau}}^{(0)} \tag{2.7}$$

$$\bar{\boldsymbol{\sigma}}_{(0)} = -p(\bar{\rho}, T)[I] + {}_d\bar{\boldsymbol{\sigma}}_{(0)} = -p(\bar{\rho}, T)[I] + \bar{\boldsymbol{\tau}}_{(0)} \tag{2.8}$$

in which, $p(\bar{\rho}, T)$ is thermodynamic pressure dependent on the density $\bar{\rho}$ and temperature T in the current configuration. $p(\bar{\rho}, T)$ is assumed positive when compressive. $p(\bar{\rho}, T)$ defines equation of state and is completely deterministic from the deformation field. $\bar{\boldsymbol{\tau}}^{(0)}$ and $\bar{\boldsymbol{\tau}}_{(0)}$ are deviatoric Cauchy stress tensors based on contra- and co- variant bases. In case of incompressible matter, the incompressibility constraint in conjunction with entropy inequality yields

$$\bar{\boldsymbol{\sigma}}^{(0)} = -p(T)[I] + {}_d\bar{\boldsymbol{\sigma}}^{(0)} = -p(T)[I] + \bar{\boldsymbol{\tau}}^{(0)} \tag{2.9}$$

$$\bar{\boldsymbol{\sigma}}_{(0)} = -p(T)[I] + {}_d\bar{\boldsymbol{\sigma}}_{(0)} = -p(T)[I] + \bar{\boldsymbol{\tau}}_{(0)} \tag{2.10}$$

in which $p(T)$ is mechanical pressure, assumed positive when compressible. Clearly $p(T)$ is not deterministic from the deformation field. We remark that in the conservation laws we could use $\bar{\boldsymbol{\sigma}}^{(0)}$ and $\bar{\boldsymbol{\sigma}}_{(0)}$ or their decompositions as shown by (2.7) - (2.10). In the conservation laws we consider $\bar{\boldsymbol{\tau}}$ to be deviatoric Cauchy stress tensor which could be $\bar{\boldsymbol{\tau}}^{(0)}$ or $\bar{\boldsymbol{\tau}}_{(0)}$ depending upon the choice of basis i.e. contra- or co- variant basis.

2.2 Conservation Laws

If we assume the matter to be compressible then to apply conservation laws to the deformed volume $\bar{V}$ we choose density $\bar{\rho}$, velocities $\boldsymbol{v}$, Cauchy stress tensor $\bar{\boldsymbol{\sigma}}$ (or its decomposition into p and $\bar{\boldsymbol{\tau}}$), specific internal energy (energy/unit mass) $\bar{e}$ and heat vector $\bar{\boldsymbol{q}}$ as dependent variables. Conservation of mass, balance of momenta and conservation of energy for volume $\bar{V}$ yield continuity equation (2.11), momentum equations (2.12) and energy equation (2.13) (see reference [4–6] for derivation). Using Einstein's notation we can write

Compressible matter

$$\frac{\partial \bar{\rho}}{\partial t} + \frac{\partial (\bar{\rho} v_i)}{\partial \bar{x}_i} = 0 \tag{2.11}$$

$$\bar{\rho}\frac{\partial v_i}{\partial t} + \bar{\rho}\frac{\partial v_i}{\partial \bar{x}_j} v_j + \frac{\partial p}{\partial \bar{x}_j} - \frac{\partial \bar{\tau}_{ij}}{\partial \bar{x}_j} - \bar{\rho}\bar{F}_i^b = 0 \tag{2.12}$$

$$\bar{\rho}\frac{D\bar{e}}{Dt} + \frac{\partial \bar{q}_i}{\partial \bar{x}_i} - \bar{\sigma}_{ij}\frac{\partial v_i}{\partial \bar{x}_j} = 0 \tag{2.13}$$

in which $\bar{F}_i^b$ are body forces per unit mass in the x-frame and $\frac{D}{Dt}$ is the material derivative.

Incompressible matter

For incompressible matter $\bar{\rho} = \rho$ i.e. density in the current configuration is same as the density in the reference configuration, thus density remains constant during evolution. This obviously implies that $\bar{V} = V$. Thus for incompressible matter (2.11) - (2.13)

reduce to

$$\rho\left(\frac{\partial v_i}{\partial \bar{x}_i}\right) = 0 \tag{2.14}$$

$$\rho\frac{\partial v_i}{\partial t} + \rho\frac{\partial v_i}{\partial \bar{x}_j}v_j + \frac{\partial p}{\partial \bar{x}_j} - \frac{\partial \bar{\tau}_{ij}}{\partial \bar{x}_j} - \rho\bar{F}_i^b = 0 \tag{2.15}$$

$$\rho\frac{D\bar{e}}{Dt} + \frac{\partial \bar{q}_i}{\partial \bar{x}_i} - \bar{\sigma}_{ij}\frac{\partial v_i}{\partial \bar{x}_j} = 0 \tag{2.16}$$

We note that (2.11) - (2.13) and (2.14) - (2.16) do not have closure. In case of compressible matter, we have five partial differential equations in fourteens variables: $\bar{\rho}$, v_i, $\bar{\sigma}_{ij}$, $\bar{e}$, $\bar{q}_i$, whereas in incompressible case we have five partial differential equations in thirteen variables v_i, $\bar{\sigma}_{ij}$, $\bar{e}$, $\bar{q}_i$. The additional equations needed to provide closure of these two mathematical models are provided by the constitutive theory.

2.3 Rate Constitutive Equations for Stress Tensors [1–6]: General and Theoretical Considerations

As mentioned earlier, the second law of thermodynamics (entropy inequality) forms the basis for deriving constitutive relations for stress tensor $\bar{\boldsymbol{\sigma}}$ and heat vector $\bar{\boldsymbol{q}}$. First we note that in Eulerian description, the strain tensors are not obtainable, instead we must consider the convected time derivatives of the strain tensors in contra- and co- variant bases. Surana [4] and Surana et. al. [1–3] have presented the ordered rate constitutive theories for compressible and incompressible solids and fluids. Authors have shown that almost all commonly used constitutive relations for solids and fluids in Eulerian description can be derived as special cases of general ordered rate constitutive theories presented in reference [1–4]. A summary of the derivations of the constitutive theory for simple materials considered in this thesis is presented in the following.

In the development of the mathematical models for deforming matter based on conservation laws, the constitutive equations describing the constitution of the matter are essential to provide closure to the mathematical models and to incorporate material specific physics in the mathematical models derived using conservation laws. The constitutive equations must satisfy certain physical and mathematical requirements. Based on [6, 51, 52], the principles of casualty, determinism, equipresence, objectivity, material invariance, neighborhood, memory and admissibility are fundamental in the development of the constitutive relations for the matter. In general, for a thermo-mechanical process the constitutive equation: (1) must describe how heat flux is related to temperature gradients and conductivity. This is adequately described by Fourier heat conduction law. (2) must describe a relationship between stresses and deformation. This aspect is considered in this chapter. A detailed discussion of all of the principles is beyond the scope of this chapter. Instead we only elaborate on two principles that are most relevant in view of the work considered in this chapter: (1) The principle of material objectivity or frame invariance. The constitutive equation must be form-invariant with respect to rigid motions of the spatial frame of reference i.e. the form of the constitutive equations should not change due to rigid rotation of the spatial frame of reference. (2) The principle of admissibility. According to the principle of admissibility all constitutive equations must be consistent with the basic principles of continuum mechanics, that is, they are subjected to the principles of conservation of mass, balance of momenta, conservation of energy (first law of thermodynamics), and the Clausius-Duhem inequality (second law of thermodynamics). The first three conservation laws yield well known continuity, momentum and energy equations. The second law of thermodynamics yields a set of conditions that must be satisfied to ensure thermodynamics equilibrium of deforming matter. These conditions establish dependence of Helmholtz

free energy density on tensors describing the deformation and provide information regarding heat flux and temperature gradient among others. The specific form of these conditions vary depending upon the assumed physics of the deforming matter.

Following references [1–4], we find that the condition resulting from the Clausius-Duhem inequality do not directly provide a mechanism to establish the constitutive theory for the total Cauchy stress tensor $\bar{\boldsymbol{\sigma}}$. As shown earlier the total Cauchy stress tensor is decomposed into equilibrium stress tensor and deviatoric Cauchy stress tensor. The condition resulting from the entropy inequality can be used to establish constitutive relations for equilibrium stress for both compressible and incompressible matter regardless of whether it is a solid or a fluid. In case of compressible matter the equilibrium stress becomes thermodynamic pressure $p = p(\bar{\rho}, T)$ and for incompressible matter, the mechanical pressure $p = p(T)$. Thus, the constitutive theory for stress tensor reduces to determination of deviatoric Cauchy stress tensor $\bar{\boldsymbol{\tau}}$ (in contra- or co- variant basis) as a function of deformation and properties of the matter. Since entropy inequality does not provide a mechanism for determing the constitutive theory for deviatoric Cauchy stress tensor, we utilize the theory of generators and invariants [1–4] to establish constitutive relation for it. Due to Eulerian description, it becomes necessary to use the convected time derivatives of the chosen stress and strain tensors in the development of the constitutive theory.

2.4 Convected Time Derivatives of Stress and Strain Tensors [1–4]

If the edges oA, oB and oC of the tetrahedron $oABC$ in the reference configuration represent material lines, then upon deformation the material lines associated with oA, oB and oC become curvilinear in the current configuration defining the convected or convective coordinate system. The tangent vectors of these material lines forming edges of the deformed tetrahedron in the current configuration are covariant vectors. The vectors normal to the faces of the deformed tetrahedron are called contravariant vectors. The covariant vectors form a nonorthogonal basis. The contravariant vectors also form a nonorthogonal basis reciprocal to the covariant basis. The convective or convected coordinate system is the most natural way for the development of the constitutive theory due to the fact that in this coordinate system deformed material lines are identified.

In Lagrangian descriptions the strain measures are available and hence can be used in the development of the constitutive theories. In Eulerian description the strain measures requiring material particle displacements are naturally not available, thus for deriving constitutive theories in Eulerian description, we must consider time derivatives of the strain measures in the convected coordinate system. This is a fundamental difference between the constitutive theories in Lagrangian and Eulerian descriptions. The constitutive theories in the Eulerian description are called rate constitutive theories due to the fact that these require convected time derivatives of the chosen conjugate stress and strain tensors. The covariant and contravariant bases provide two obvious alternatives for the development of the rate constitutive theories. We consider contravariant Cauchy stress tensor $\bar{\boldsymbol{\tau}}^{(0)}$ and Almansi strain tensor $\bar{\boldsymbol{\varepsilon}}$ in contravariant basis and $\bar{\boldsymbol{\tau}}_{(0)}$, the covariant Cauchy stress tensor and $\boldsymbol{\varepsilon}$, Green's strain tensor in covariant bases as

conjugate measures of deviatoric Cauchy stress tensor and strain tensor. The convected time derivatives of these measures in contra- and co- basis are needed for rate constitutive theories.

2.4.1 Convected time derivatives of deviatoric Cauchy stress tensor [1, 4]

These must be derived for compressible as well as incompressible matter in contra- and co- variant bases.

Incompressible matter : contravariant basis

Let $\bar{\boldsymbol{\tau}}^{(0)}$ be contravariant deviatoric Cauchy stress tensor and $\boldsymbol{\tau}^{[0]}$ be the second Piola-Kirchhoff stress tensor derived from it, then

$$[\tau^{[0]}] = [\bar{J}][\bar{\tau}^{(0)}][\bar{J}]^T \tag{2.17}$$

If $[\bar{\tau}^{(k)}]$ is the k^{th} convected time derivative of $[\bar{\tau}^{(0)}]$ in the contravariant basis, then following Surana et.al. [1, 4] we can write the following:

$$\left.\begin{aligned} &\frac{D}{Dt}[\tau^{[k-1]}] = [\tau^{[k]}] \\ &[\tau^{[k]}] = [\bar{J}][\bar{\tau}^{(k)}][\bar{J}]^T \\ &[\bar{\tau}^{(k)}] = \frac{D}{Dt}[\bar{\tau}^{(k-1)}] - [L][\bar{\tau}^{(k-1)}] - [\bar{\tau}^{(k-1)}][L]^T \end{aligned}\right\} \quad k = 1, 2, \ldots \tag{2.18}$$

where

$$\bar{J}_{ij} = \frac{\partial x_i}{\partial \bar{x}_j}, \quad L_{ij} = \frac{\partial v_i}{\partial \bar{x}_j} \tag{2.19}$$

$[\bar{\tau}^{(1)}]$ is the first convected time derivative of the contravariant Cauchy stress deviation tensor $[\bar{\tau}^{(0)}]$ generally referred to as upper convected time derivative of tensor $[\bar{\tau}^{(0)}]$. The first upper convected time derivative of $[\bar{\tau}^{(0)}]$ in contravariant basis is denoted by

$$[\overset{\nabla}{\tau}] = [\bar{\tau}^{(1)}] \tag{2.20}$$

Incompressible matter : covariant basis

Let $\bar{\boldsymbol{\tau}}_{(0)}$ be covariant deviatoric Cauchy stress tensor and $\boldsymbol{\tau}_{[0]}$ be the second Piola-Kirchhoff stress tensor derived using $\bar{\tau}_{(0)}$, then

$$[\tau_{[0]}] = [J]^T[\bar{\tau}_{(0)}][J] \tag{2.21}$$

If $[\bar{\tau}_{(k)}]$ is the k^{th} convected time derivative of $[\bar{\tau}_{(0)}]$ in the covariant basis, then following Surana et.al. [1, 4] we can write the following:

$$\left.\begin{aligned} &\frac{D}{Dt}[\tau_{[k-1]}] = [\tau_{[k]}] \\ &[\tau_{[k]}] = [J]^T[\bar{\tau}_{(k)}][J] \\ &[\bar{\tau}_{(k)}] = \frac{D}{Dt}[\bar{\tau}_{(k-1)}] + [L]^T[\bar{\tau}_{(k-1)}] + [\bar{\tau}_{(k-1)}][L] \end{aligned}\right\} \quad k = 1, 2, \ldots \tag{2.22}$$

where

$$J_{ij} = \frac{\partial \bar{x}_i}{\partial x_j} \tag{2.23}$$

$[\bar{\tau}_{(1)}]$ is the first convected time derivative of the covariant Cauchy stress deviation tensor $[\bar{\tau}_{(0)}]$ generally referred to as lower convected time derivative of tensor $[\bar{\tau}_{(0)}]$. It is

denoted by $[\overset{\Delta}{\tau}]$

$$[\overset{\Delta}{\tau}] = [\bar{\tau}_{(1)}] \tag{2.24}$$

Incompressible matter : Jaumann rate

Jaumann rate is the average of the upper convected and lower convected stress rates when the velocity fields in the upper convected and lower convected cases are the same which is only possible if the deformation is not finite. If we define $[\bar{\tau}^{(0)}] = [\bar{\tau}_{(0)}] = [\bar{\tau}^{J}]$ as the Jaumann stress in contra- and co- variant bases and take their average (i.e. add and divide by two) and use the definition of the spin tensor $[W]$

$$[W] = \frac{1}{2}([L] - [L]^T) \tag{2.25}$$

then we can write the following

$$\left.\begin{aligned} &\frac{D}{Dt}[{}^{[k-1]}\tau^{J}] = [{}^{[k]}\tau^{J}] \\ &[{}^{(k)}\bar{\tau}^{J}] = \frac{D}{Dt}[{}^{(k-1)}\bar{\tau}^{J}] - [W][{}^{(k-1)}\bar{\tau}^{J}] + [{}^{(k-1)}\bar{\tau}^{J}][W] \end{aligned}\right\} \quad k = 1, 2, \ldots \tag{2.26}$$

The back subscript implies that this description is neither contravariant nor covariant. Furthermore, in this derivation we have used

$$[{}^{(k)}\bar{\tau}^{J}] = [\bar{\tau}^{(k)}] = [\bar{\tau}_{(k)}] \tag{2.27}$$

Remarks

We note that the expression for $[\bar{\tau}^{(1)}]$ and $[\bar{\tau}_{(1)}]$ contain material derivatives plus some more terms, so we can introduce a new notation similar to the material derivative if we drop the over bar and super and subscript in their definitions. We can write the following

for the contra- and co- variant first convected time derivatives of the corresponding stress tensors

$$\overset{\nabla}{\frac{D}{Dt}}[\tau] = \frac{D}{Dt}[\tau] - [L][\tau] - [\tau][L]^T \tag{2.28}$$

$$\overset{\triangle}{\frac{D}{Dt}}[\tau] = \frac{D}{Dt}[\tau] + [L]^T[\tau] + [\tau][L] \tag{2.29}$$

In (2.28) and (2.29) it is understood that $[\tau]$ on the right sides of the equations are contra- and co-variant Cauchy stress tensors and the left sides of (2.28) and (2.29) are their first convected time derivatives. Likewise the first Jaumann rate can be written as

$$\frac{^J D}{Dt}[\tau] = \frac{D}{Dt}[\tau] - [W][\tau] + [\tau][W] \tag{2.30}$$

Compressible matter : contravariant basis

Following the notations used for incompressible case, the convected time derivative of order 'k' of $[\bar{\tau}^{(0)}]$ can be defined as

$$\left.\begin{aligned} &\frac{D}{Dt}[\tau^{[k-1]}] = [\tau^{[k]}] \\ &[\tau^{[k]}] = |J|[\bar{J}][\bar{\tau}^{(k)}][\bar{J}]^T \\ &[\bar{\tau}^{(k)}] = \frac{D}{Dt}[\bar{\tau}^{(k-1)}] - [L][\bar{\tau}^{(k-1)}] - [\bar{\tau}^{(k-1)}][L]^T + [\bar{\tau}^{(k-1)}]\text{tr}([L]) \end{aligned}\right\} \quad k = 1, 2, \ldots \tag{2.31}$$

Compressible matter : covariant basis

The convected time derivative of order 'k' of the covariant deviatoric Cauchy stress

$[\bar{\tau}_{(0)}]$ can be defined as

$$\left.\begin{aligned} &\frac{D}{Dt}[\tau_{[k-1]}] = [\tau_{[k]}] \\ &[\tau_{[k]}] = |J|[J]^T[\bar{\tau}_{(k)}][J] \\ &[\bar{\tau}_{(k)}] = \frac{D}{Dt}[\bar{\tau}_{(k-1)}] + [L]^T[\bar{\tau}_{(k-1)}] + [\bar{\tau}_{(k-1)}][L] + [\bar{\tau}_{(k-1)}]\text{tr}([L]) \end{aligned}\right\} \quad k = 1, 2, \ldots \tag{2.32}$$

Compressible matter : Jaumann rates

Following the incompressible case, 'k' order convected time derivative of Jaumann stress can be written as

$$\left.\begin{aligned} &\frac{D}{Dt}[{}^{[k-1]}\tau^J] = [{}^{[k]}\tau^J] \\ &[{}^{(k)}\bar{\tau}^J] = \frac{D}{Dt}[{}^{(k-1)}\bar{\tau}^J] - [W][{}^{(k-1)}\bar{\tau}^J] + [{}^{(k-1)}\bar{\tau}^J][W] + [{}^{(k-1)}\bar{\tau}^J]\text{tr}([L]) \end{aligned}\right\} \quad k = 1, 2, \ldots \tag{2.33}$$

Equation (2.33) is valid only if the velocity fields in contra- and co-variants bases are the same and when

$$[{}^{(k)}\bar{\tau}^J] = [\bar{\tau}^{(k)}] = [\bar{\tau}_{(k)}] \tag{2.34}$$

Remarks

Following the remarks presented for incompressible case, here also we introduce upper convected, lower convected and Jaumann derivatives to define the first convected time derivatives of the deviatoric Cauchy stress tensor for compressible matter

$$\overset{\nabla}{\frac{D}{Dt}}[\tau] = \frac{D}{Dt}[\tau] - [L][\tau] - [\tau][L]^T + [\tau]\text{tr}([L]) \tag{2.35}$$

$$\overset{\Delta}{\frac{D}{Dt}}[\tau] = \frac{D}{Dt}[\tau] + [L]^T[\tau] + [\tau][L] + [\tau]\text{tr}([L]) \tag{2.36}$$

$$\overset{J}{\frac{D}{Dt}}[\tau] = \frac{D}{Dt}[\tau] - [W][\tau] + [\tau][W] + [\tau]\text{tr}([L]) \tag{2.37}$$

It is understood that $[\tau]$ in (2.35)- (2.37) refer to contravariant, covariant and Jaumann deviatoric Cauchy stress tensors.

2.4.2 Convected time derivatives of the strain tensors

We consider Almansi and Green's strain measures in contra- and co- variant bases to derive their convected time derivatives of an arbitrary order k. Unlike convected time derivatives of the stress tensors, here the distinction between compressible and incompressible matter does not exist.

Covariant basis

If consider Green's strain $[\varepsilon]$ and take its material derivative then we can extract the convected time derivative of order one from it. Following the same procedure we can obtain convected time derivative of any desired order 'k' of the Green's strain tensor $[\varepsilon]$ [1, 4].

$$\left.\begin{aligned} &\frac{D}{Dt}[\gamma_{[k-1]}] = [\gamma_{[k]}] \\ &[\gamma_{[k]}] = [J]^T[\gamma_{(k)}][J] \\ &[\gamma_{(k)}] = \frac{D}{Dt}[\gamma_{(k-1)}] + [L]^T[\gamma_{(k-1)}] + [\gamma_{(k-1)}][L] \end{aligned}\right\} \quad k = 2, 3, \ldots \tag{2.38}$$

where

$$[\gamma_{[1]}] = \frac{D}{Dt}[\varepsilon] = [J]^T[\gamma_{(1)}][J] \tag{2.39}$$

$$[\gamma_{(1)}] = \frac{1}{2}\big([L] + [L]^T\big) = [D] \tag{2.40}$$

Contravariant basis

In this case we consider Almansi strain tensor $[\bar{\varepsilon}]$ and takes its material derivative to extract its first convected time derivative. In general, the convected time derivative of order 'k' of the Almansi strain $[\bar{\varepsilon}]$ can be defined by the following:

$$\left.\begin{aligned} &\frac{D}{Dt}[\gamma^{[k-1]}] = [\gamma^{[k]}] \\ &[\gamma^{[k]}] = [\bar{J}][\gamma^{(k)}][\bar{J}]^T \\ &[\gamma^{(k)}] = \frac{D}{Dt}[\gamma^{(k-1)}] - [L][\gamma^{(k-1)}] - [\gamma^{(k-1)}][L]^T \end{aligned}\right\} \quad k = 2, 3, \ldots \tag{2.41}$$

where

$$[\gamma^{[1]}] = \frac{D}{Dt}[\bar{\varepsilon}] = [\bar{J}][\gamma^{(1)}][\bar{J}]^T \tag{2.42}$$

$$[\gamma^{(1)}] = \frac{1}{2}\big([L] + [L]^T\big) = [D] \tag{2.43}$$

Remarks

(1) We note that $[\gamma^{(1)}] = [\gamma^{(1)}] = \frac{1}{2}\big([L] + [L]^T\big) = [D]$

(2) $[\gamma_{(i)}]$ and $[\gamma^{(i)}]$; $i = 1, 2, \ldots$ are fundamental kinematic tensors in co- and contra-variant bases. These are convected time derivatives of orders $i = 1, 2, \ldots$ of Green's and Almansi strain tensors.

2.5 Constitutive Equations for Deviatoric Cauchy Stress for Viscous Fluids, Polymeric Fluids and Elastic Solids

In this section we present constitutive equations for thermoviscous fluids, polymeric liquids and elastic solids in Eulerian description. References containing their detailed derivations are cited. Surana et.al. [1–3] have presented derivations of the rate constitutive theories for all three cases using the theory of generators and invariants.

2.5.1 Thermoviscous fluids

The simplest form of the constitutive equations for such fluids are well known Newton's law of viscosity. Surana et. al. [1] have shown that these can be derived by considering rate constitutive theory of order one (special case of general ordered rate constitutive theory for thermoviscous fluids) in which second and higher degree terms in the components of the first convected time derivative of the strain tensor are neglected. Using contra- and co- variant bases, the constitutive equation for the deviatoric Cauchy stress tensors $\bar{\boldsymbol{\tau}}^{(0)}$ and $\bar{\boldsymbol{\tau}}_{(0)}$ can be derived.

$$[\bar{\tau}^{(0)}] = [\bar{\tau}^{(0)}]_0 + 2\eta(\bar{\rho},T)\,[\gamma^{(1)}] + \kappa(\bar{\rho},T)\,\text{tr}([\gamma^{(1)}])[I] - \alpha_{tm}(T-T_0)[I] \quad (2.44)$$

$$[\bar{\tau}_{(0)}] = [\bar{\tau}_{(0)}]_0 + 2\eta(\bar{\rho},T)\,[\gamma_{(1)}] + \kappa(\bar{\rho},T)\,\text{tr}([\gamma_{(1)}])[I] - \alpha_{tm}(T-T_0)[I] \quad (2.45)$$

in which $\eta(\cdot)$ and $\kappa(\cdot)$ are first and second viscosities that may be dependent on density and temperature in the current configuration. Other quantities have their usual meaning.

Since $[\gamma^{(1)}] = [\gamma^{(1)}] = [D]$ and if we drop over bar on $[\tau^{(0)}]$ and $[\tau_{(0)}]$ and also drop

super- and sub- script '(0)' then we can write (2.44) and (2.45) as

$$[\tau] = [\tau]_0 + 2\eta(\bar{\rho}, T)\,[D] + \kappa(\bar{\rho}, T)\,\text{tr}([D])[I] - \alpha_{tm}(T - T_0)[I]\ , \quad \text{compressible matter} \tag{2.46}$$

In case of incompressible thermoviscous fluids (2.46) reduces to

$$[\bar{\tau}] = [\tau]_0 + 2\eta(T)\,[D] - \alpha_{tm}(T - T_0)[I]\ , \quad \text{incompressible matter} \tag{2.47}$$

due to the fact that for incompressible thermoviscous fluids the density is constant, hence $\eta = \eta(T)$ and $\text{tr}([D]) = 0$.

2.5.2 Thermoviscoelastic fluid - polymeric fluids

Polymeric fluids are viscous as well as elastic. These fluids have memory characterized by a characteristic time constant for the fluids called relaxation time. Following the derivation of the ordered rate constitutive theory for polymeric fluids presented by Surana et.al. [3, 4] and their simplifications giving Maxwell model, Oldroyd-B model and Giesekus constitutive model, we can summarize the final form of the constitutive equations for these three models in the following. Since the constitutive theory utilize convected time derivatives of order one of the deviatoric Cauchy stress tensor, it becomes necessary to present these in contra- and co- variant descriptions. Without loss of generality we neglect the initial stress field in the reference configuration as well as stress field due to thermal effects.

Maxwell model

The constitutive model is generally used for dilute polymeric fluids in which viscous

effects dominate. That is such fluids are essentially viscous with some elasticity. We have the following constitutive equation in contra- and co- variant descriptions (upper convected and lower convected) based on references [3, 4, 53]:

Compressible matter

$$[\bar{\tau}^{(0)}]+ \lambda_1 \, [\bar{\tau}^{(1)}]= 2\eta_0(\bar{\rho}, T) \, [\gamma^{(1)}] + \kappa_0(\bar{\rho}, T) \, \text{tr}([\gamma^{(1)}])[I] \tag{2.48}$$

$$[\bar{\tau}_{(0)}]+ \lambda_1 \, [\bar{\tau}_{(1)}]= 2\eta_0(\bar{\rho}, T) \, [\gamma_{(1)}] + \kappa_0(\bar{\rho}, T) \, \text{tr}([\gamma_{(1)}])[I] \tag{2.49}$$

Incompressible matter

In case of incompressible polymeric fluid $\text{tr}([\gamma^{(1)}]) = \text{tr}([\gamma_{(1)}]) = \text{div}(\boldsymbol{v}) = 0$; $\eta_0 = \eta_0(T)$ hence (2.48) and (2.49) reduce to

$$[\bar{\tau}^{(0)}]+ \lambda_1 \, [\bar{\tau}^{(1)}]= 2\eta_0(T) \, [\gamma^{(1)}] \tag{2.50}$$

$$[\bar{\tau}_{(0)}]+ \lambda_1 \, [\bar{\tau}_{(1)}]= 2\eta_0(T) \, [\gamma_{(1)}] \tag{2.51}$$

In which λ_1 is called relaxation time, $\eta_0(\cdot)$ and $\kappa_0(\cdot)$ are first and second zero shear rate viscosities. We keep in mind that definitions of $[\bar{\tau}^{(1)}]$ as well as $[\bar{\tau}_{(1)}]$ for compressible and incompressible matter are not the same.

Oldroyd-B model

This constitutive model is also used for dilute polymeric fluids. Following references [3, 4, 53], we have the following in contra- and co- variant bases (upper and lower convected rate constitutive equations). For simplicity we consider incompressible matter

only.

$$[\bar{\tau}^{(0)}] + \lambda_1 [\bar{\tau}^{(1)}] = 2\eta_0(T) ([\gamma^{(1)}] + \lambda_2 [\gamma^{(2)}]) \tag{2.52}$$

$$[\bar{\tau}_{(0)}] + \lambda_1 [\bar{\tau}_{(1)}] = 2\eta_0(T) ([\gamma_{(1)}] + \lambda_2 [\gamma_{(2)}]) \tag{2.53}$$

λ_2 is called relaxation time, a time constant of the fluid.

Giesekus model

This model is generally used for dense polymeric liquids (polymer melts) whose behavior is elastically dominated. Based on the ordered rate constitutive theory presented by Surana [4] and Surana et.al. [3] for thermoviscoelastic fluids, the simplified form can be shown to yield the following in contra- and co- variant descriptions (upper convected and lower convected rate stress rates) for the incompressible case.

$$[\bar{\tau}^{(0)}] + \lambda_1 [\bar{\tau}^{(1)}] - \alpha \frac{\lambda_1}{\eta_0(T)} ([\bar{\tau}^{(0)}] \cdot [\bar{\tau}^{(0)}]) = 2\eta_0(T) [\gamma^{(1)}] \tag{2.54}$$

$$[\bar{\tau}_{(0)}] + \lambda_1 [\bar{\tau}_{(1)}] - \alpha \frac{\lambda_1}{\eta_0(T)} ([\bar{\tau}_{(0)}] \cdot [\bar{\tau}_{(0)}]) = 2\eta_0(T) [\gamma_{(1)}] \tag{2.55}$$

α is known mobility factor and η_0 is total viscosity of the fluid.

We remark that the Giesekus constitutive equations in polymer science works are presented and used in terms of polymer stress based on the following decomposition for the deviatoric Cauchy stress.

$$[\bar{\tau}] = [\bar{\tau}^{p}] + [\bar{\tau}^{sv}] \tag{2.56}$$

That is, the deviatoric Cauchy stress is assumed to consist of deviatoric polymer Cauchy stress $[\bar{\tau}^{p}]$ and solvent viscous stress $[\bar{\tau}^{sv}]$ with the assumption that solvent viscous stress $[\bar{\tau}^{sv}]$ can be described by Newton's law of viscosity. The constitutive equations for $[\bar{\tau}^{p}]$ (as used currently) are obtained by replacing $[\bar{\tau}]$ by $[\bar{\tau}^{p}]$ and η_0 by η_p in (2.54) and (2.55).

$$[\bar{\tau}^{p(0)}]+ \lambda_1 \, [\bar{\tau}^{p(1)}]- \alpha\frac{\lambda_1}{\eta_p}([\bar{\tau}^{p(0)}] \cdot [\bar{\tau}^{p(0)}]) = 2\eta_p \, [\gamma^{(1)}] \tag{2.57}$$

$$[\bar{\tau}^{p}_{(0)}]+ \lambda_1 \, [\bar{\tau}^{p}_{(1)}]- \alpha\frac{\lambda_1}{\eta_p}([\bar{\tau}^{p}_{(0)}] \cdot [\bar{\tau}^{p}_{(0)}]) = 2\eta_p \, [\gamma_{(1)}] \tag{2.58}$$

The origin of (2.57) and (2.58) is from the kinetic theory and anisotropic drag due to Brownian motion of polymer molecules [53] (also see Surana [4] and Surana et.al. [3]).

2.5.3 Thermoelastic solid matter

The development of the ordered rate constitutive theory for thermoelastic solid matter in Eulerian description has been presented by Surana [4] and Surana et.al. [2]. The most simplified form of the theory yields rate constitutive theory for hypo-elastic materials in contra- and co- variant descriptions (or upper convected and lower convected rate constitutive equations). For compressible hypo-elastic material we can write

$$[\bar{\tau}^{(1)}]= [\bar{\tau}^{(0)}]_0 + 2\mu(\bar{\rho},T) \, [\gamma^{(1)}] + \kappa(\bar{\rho},T) \, \text{tr}([\gamma^{(1)}])[I] - \alpha_{tm}(T-T_0)[I] \tag{2.59}$$

$$[\bar{\tau}_{(1)}]= [\bar{\tau}_{(0)}]_0 + 2\mu(\bar{\rho},T) \, [\gamma_{(1)}] + \kappa(\bar{\rho},T) \, \text{tr}([\gamma_{(1)}])[I] - \alpha_{tm}(T-T_0)[I] \tag{2.60}$$

In which $\mu(\cdot)$ and $\kappa(\cdot)$ are shear modulus and bulk modulus that may be dependent on density and temperature in the current configuration. For incompressible hypo-elastic solids $\kappa(\cdot) = 0$, $\mu = \mu(T)$ and $\text{tr}([\gamma^{(1)}]) = \text{tr}([\gamma_{(1)}]) = 0$ in (2.59) and (2.60). We must

note that the definition of the first convected time derivative of the deviatoric Cauchy stress tensor $[\bar{\tau}^{(1)}]$ as well as $[\bar{\tau}_{(1)}]$ are different for compressible and incompressible cases. $[\bar{\tau}^{(0)}]_0$ and $[\bar{\tau}_{(0)}]_0$ are initial stress tensors in the reference configuration and α_{tm} is thermal modulus of the solid matter related to coefficient of thermal expansion. These materials do not have memory.

Remarks

(1) Almost all of the constitutive equations presented here are commonly used for finite as well as infinitesimal deformation.

(2) The distinction between contra- and co- variant bases is critical in case of rate theories that utilize first and higher convected time derivatives of stress tensors as these are not same in the two bases. This is also true if the rate theories utilize second and higher ordered convected time derivatives of the strain tensors.

2.6 Constitutive Equations for Heat Vector $\bar{\boldsymbol{q}}$

In references [1–4], Surana and Surana et. al. have also presented ordered rate constitutive theories for heat vectors for thermoviscous fluids, thermoelastic solids and polymeric fluids. The most simplified form of the constitutive equation for heat vector results in Fourier heat conduction law.

$$\bar{\boldsymbol{q}} = -k(T)\text{div}(T) \tag{2.61}$$

in which $k(T)$ is temperature dependent thermal conductivity.

2.7 Equations of State

For a compressible matter, the thermodynamic pressure p is a function of density $\bar{\rho}$ and temperature T. That is

$$p = p(\bar{\rho}, T) \tag{2.62}$$

Specific form of the expression for $p(\bar{\rho}, T)$ depends upon the matter under consideration. In case of gases, ideal gas law $p = \bar{\rho}RT$ (R being gas constant) generally describes the dependence of p on $\bar{\rho}$ and T quite satisfactorily for most gases within limited range of $\bar{\rho}$ and T. For extended range of $\bar{\rho}$ and T or for heavy molecular weight gases (ratio of specific heat to gas constant greater than twenty), real gas models such as Van der Waals, Redlich-Kwang, Beattie-Bridgeman and Benedict-Webb-Rubin etc. may be employed. All these equations of state express p as a function of $\bar{\rho}$ and T (as in (2.62)). Thus from the point of view of the development of mathematical model of the deforming matter, (2.62) suffices as equation of state.

We remark that if p is maintained as a dependent variable in the development of the mathematical model, then the equation of state (2.62) becomes an additional equation as part of the mathematical model. This of course is essential in allowing interaction of a compressible medium with incompressible medium such as liquids (Newtonian or polymeric) in which p must be a dependent variable. If the physical process at hand only consists of compressible matter, then, there is no need to retain pressure p as a dependent variable and it can be substituted in terms of $\bar{\rho}$ and T using (2.62).

2.8 Specific Internal Energy $\bar{e}$

The energy equation requires material derivative of the specific internal energy $\bar{e}$. Thus, we must define $\bar{e}$ for compressible and incompressible matter and obtain explicit form of its material derivative.

2.8.1 Compressible matter

The specific internal energy i.e. internal energy per unit mass '$\bar{e}$' is a function of p, $\bar{\rho}$ and T for compressible matter.

$$\bar{e} = \bar{e}(p, \bar{\rho}, T) \tag{2.63}$$

But, $p = p(\bar{\rho}, T)$ from the equation of state (2.62). Substituting from (2.62) into (2.63) we obtain

$$\bar{e} = \bar{e}(\bar{\rho}, T) \tag{2.64}$$

From section 2.2, equation (2.13), we note that the energy equation requires $\bar{\rho}\frac{D\bar{e}}{Dt}$

$$\bar{\rho}\frac{D\bar{e}}{Dt} = \bar{\rho}\frac{\partial \bar{e}}{\partial t} + \bar{\rho}\frac{\partial \bar{e}}{\partial \bar{x}_i}v_i \tag{2.65}$$

and

$$\frac{\partial \bar{e}(\bar{\rho}, T)}{\partial \bar{x}_i} = \left(\frac{\partial \bar{e}}{\partial \bar{\rho}}\right)\frac{\partial \bar{\rho}}{\partial \bar{x}_i} + \left(\frac{\partial \bar{e}}{\partial T}\right)\frac{\partial T}{\partial \bar{x}_i} \tag{2.66}$$

$$\frac{\partial \bar{e}(\bar{\rho}, T)}{\partial t} = \left(\frac{\partial \bar{e}}{\partial \bar{\rho}}\right)\frac{\partial \bar{\rho}}{\partial t} + \left(\frac{\partial \bar{e}}{\partial T}\right)\frac{\partial T}{\partial t} \tag{2.67}$$

From continuity equation

$$\frac{\partial \bar{\rho}}{\partial t} = -\frac{\partial}{\partial \bar{x}_i}(\bar{\rho} v_i) \tag{2.68}$$

Substituting for (2.66)- (2.68) into (2.65), we obtain

$$\bar{\rho}\frac{D\bar{e}}{Dt} = \bar{\rho}\frac{\partial \bar{e}}{\partial T}\left(\frac{\partial T}{\partial t} + v_i \frac{\partial T}{\partial \bar{x}_i}\right) - \bar{\rho}^2 \frac{\partial \bar{e}}{\partial \bar{\rho}}\frac{\partial v_i}{\partial \bar{x}_i} \tag{2.69}$$

Explicit expression for $\frac{\partial \bar{e}}{\partial T}$ and $\frac{\partial \bar{e}}{\partial \bar{\rho}}$ can be obtained once we have an explicit expression for $\bar{e}(\bar{\rho}, T)$ for the compressible matter under consideration. As an example, we consider a gas with specific heat $C_v = C_v(T)$ and $p = p(\bar{\rho}, T)$, In this case we can write the following for $\bar{e}(\bar{\rho}, T)$.

$$\bar{e} = \int_{T_0}^{T} C_v dT - \int_{\bar{\rho}_0}^{\bar{\rho}} \frac{1}{\bar{\rho}^2}\left(\left(T\frac{\partial p}{\partial T}\right)_{\bar{\rho}} - p\right) d\bar{\rho} \tag{2.70}$$

and

$$C_v = \sum_{j=0}^{m} C_j T^j - T\int_{\bar{\rho}_0}^{\bar{\rho}} \frac{1}{\bar{\rho}^2}\left(\frac{\partial^2 p}{\partial T^2}\right)_{\bar{\rho}} d\bar{\rho} \tag{2.71}$$

C_j are known constants for the gas under consideration.

First, using $p = p(\bar{\rho}, T)$ in (2.71) we obtain an expression for $C_v(T)$. Then equation of state (2.62) and $C_v(T)$ can be used in $\bar{e}$ to obtain an explicit expression for $\bar{e} = \bar{e}(\bar{\rho}, T)$. Limit of integration $\bar{\rho}_0$ is not important due to the fact that (2.69) only requires derivatives of $\bar{e}(\bar{\rho}, T)$ with respect to $\bar{\rho}$ and T.

2.8.2 Incompressible matter

For incompressible matter, the specific internal energy $\bar{e}$ can be assumed to be of the form

$$\bar{e} = C_v T \tag{2.72}$$

in which C_v is constant hence, in (2.69), we have

$$\frac{\partial \bar{e}}{\partial \bar{\rho}} = 0 \qquad \text{and} \qquad \frac{\partial \bar{e}}{\partial T} = C_v \tag{2.73}$$

Thus, $\bar{\rho}\frac{D\bar{e}}{Dt}$ in the energy equation for such matter simplifies to

$$\bar{\rho}\frac{D\bar{e}}{Dt} = \bar{\rho}C_v \left(\frac{\partial T}{\partial t} + v_i \frac{\partial T}{\partial \bar{x}_i} \right) \tag{2.74}$$

2.9 Complete Mathematical Model

In this section we present descriptions of complete mathematical model for compressible as well as incompressible matter in Eulerian description including constitutive relations.

2.9.1 Conservation laws for compressible matter using $\bar{\rho}$, $\boldsymbol{v}$, p, $\bar{\boldsymbol{\tau}}$, T as dependent variables

The continuity equation remains the same as (2.11). In the momentum equations (2.12) deviatoric stress decomposition has already been used. In the energy equation (2.13), we substitute stress decomposition $[\bar{\sigma}] = -p(\bar{\rho}, T)[I] + [\bar{\tau}]$ in which $[\bar{\tau}]$ is deviatoric Cauchy stress (based on contra- or co- variant description). Additionally, we also sub-

stitute $\bar{\rho}\frac{D\bar{e}}{Dt}$ from (2.69) and the heat fluxes $\bar{q}_i$ from (2.61) into the energy equation.

$$\frac{\partial \bar{\rho}}{\partial t} + \frac{\partial}{\partial \bar{x}_i}(\bar{\rho} v_i) = 0 \tag{2.75}$$

$$\bar{\rho}\frac{\partial v_i}{\partial t} + \bar{\rho}\frac{\partial v_i}{\partial \bar{x}_j} v_j + \frac{\partial p}{\partial x_i} - \frac{\partial \bar{\tau}_{ij}}{\partial \bar{x}_j} - \bar{\rho} F_i^b = 0 \tag{2.76}$$

$$\bar{\rho}\frac{\partial \bar{e}}{\partial T}\left(\frac{\partial T}{\partial t} + v_i \frac{\partial T}{\partial \bar{x}_i}\right) - \frac{\partial}{\partial \bar{x}_i}\left(k_{ij}\frac{\partial T}{\partial \bar{x}_j}\right) - \left(p(\bar{\rho}, T) + \bar{\rho}^2 \frac{\partial \bar{e}}{\partial \bar{\rho}}\right)\frac{\partial v_i}{\partial \bar{x}_i} - \bar{\tau}_{ij}\frac{\partial v_i}{\partial \bar{x}_j} = 0 \tag{2.77}$$

$$p = p(\bar{\rho}, T) \tag{2.78}$$

These remain valid regardless of the constitution of the matter and hence hold for thermoelastic solids as well as thermoviscous fluids and polymeric fluids. Since $\bar{e} = \bar{e}(p, \bar{\rho}, T) = \bar{e}(\bar{\rho}, T)$, $\frac{\partial \bar{e}}{\partial T}$ and $\frac{\partial \bar{e}}{\partial \bar{\rho}}$ in the energy equation are strictly deterministic. $p(\bar{\rho}, T)$ in the energy equation is defined by the equation of state. $\frac{\partial p}{\partial \bar{x}_i}$ in the momentum equations can be defined using equation of state if we wish to eliminate pressure as a dependent variable.

$$\frac{\partial p}{\partial \bar{x}_i} = \left(\frac{\partial p}{\partial \bar{\rho}}\right)\frac{\partial \bar{\rho}}{\partial \bar{x}_i} + \left(\frac{\partial p}{\partial T}\right)\frac{\partial T}{\partial \bar{x}_i} \tag{2.79}$$

In (2.79), $\frac{\partial p}{\partial \bar{\rho}}$ and $\frac{\partial p}{\partial T}$ can be explicitly obtained using equation of state if pressure is to eliminated as a dependent variable.

The mathematical model defined by (2.75) - (2.78) requires definitions of $[\bar{\tau}]$, the Cauchy stress tensor using the constitutive equations to provide closure to the mathematical model.

2.9.2 Conservation laws for incompressible matter using $\boldsymbol{v}$, p, $\bar{\boldsymbol{\tau}}$, T as dependent variables

The continuity equation remains the same as (2.14). In the momentum equations (2.15) the deviatoric Cauchy stress decomposition has been used. In the energy equation (2.16), we substitute stress decomposition $[\bar{\sigma}] = -p[I] + [\bar{\tau}]$ in which $[\bar{\tau}]$ is deviatoric Cauchy stress (based on contra- or co- variant description). Additionally, we also substitute $\bar{\rho}\frac{D\bar{e}}{Dt}$ from (2.76) and the heat fluxes $\bar{q}_i$ from (2.61) into the energy equation. For incompressible matter $\bar{\rho} = \rho =$ constant.

$$\bar{\rho}\left(\frac{\partial v_i}{\partial \bar{x}_i}\right) = 0 \tag{2.80}$$

$$\bar{\rho}\frac{\partial v_i}{\partial t} + \bar{\rho}\frac{\partial v_i}{\partial \bar{x}_j}v_j + \frac{\partial p}{\partial \bar{x}_j} - \frac{\partial \bar{\tau}_{ij}}{\partial \bar{x}_j} - \bar{\rho}F_i^b = 0 \tag{2.81}$$

$$\bar{\rho}C_v\left(\frac{\partial T}{\partial t} + v_i\frac{\partial T}{\partial \bar{x}_i}\right) - \frac{\partial}{\partial \bar{x}_i}\left(k_{ij}\frac{\partial T}{\partial \bar{x}_j}\right) - \bar{\tau}_{ij}\frac{\partial v_i}{\partial \bar{x}_j} = 0 \tag{2.82}$$

These remain valid regardless of the constitution of the matter. In this case p is mechanical pressure which is not deterministic from the deformation field. In this case also we need constitutive equations to provide closure to the mathematical model defined by (2.80)- (2.82).

2.9.3 Constitutive equations

A summary of the constitutive equations presented earlier is given in the following.

Thermoviscous fluids

Compressible

$$[\bar{\tau}] = 2\eta(\bar{\rho}, T)\,[D] + \kappa(\bar{\rho}, T)\,\mathrm{tr}([D])[I] \tag{2.83}$$

Incompressible

$$[\bar{\tau}] = 2\eta(T)\,[D] \tag{2.84}$$

Thermoviscous polymeric fluids

We consider only incompressible case as the compressibility for such fluids is only significant at very high pressure.

Maxwell model (incompressible)

Using contra- and co- variant Cauchy stress tensors and their convected rates we have

$$[\bar{\tau}^{(0)}] + \lambda_1\,[\bar{\tau}^{(1)}] = 2\eta_0(T)\,[\gamma^{(1)}] \tag{2.85}$$

$$[\bar{\tau}_{(0)}] + \lambda_1\,[\bar{\tau}_{(1)}] = 2\eta_0(T)\,[\gamma_{(1)}] \tag{2.86}$$

Oldroyd-B model (incompressible)

$$[\bar{\tau}^{(0)}] + \lambda_1\,[\bar{\tau}^{(1)}] = 2\eta_0\,([\gamma^{(1)}] + \lambda_2\,[\gamma^{(2)}]) \tag{2.87}$$

$$[\bar{\tau}_{(0)}] + \lambda_1\,[\bar{\tau}_{(1)}] = 2\eta_0\,([\gamma_{(1)}] + \lambda_2\,[\gamma_{(2)}]) \tag{2.88}$$

Giesekus model (incompressible)

$$[\bar{\tau}^{(0)}] + \lambda_1\,[\bar{\tau}^{(1)}] - \alpha\frac{\lambda_1}{\eta_0}([\bar{\tau}^{(0)}] \cdot [\bar{\tau}^{(0)}]) = 2\eta_0\,[\gamma^{(1)}] \tag{2.89}$$

$$[\bar{\tau}_{(0)}] + \lambda_1\,[\bar{\tau}_{(1)}] - \alpha\frac{\lambda_1}{\eta_0}([\bar{\tau}_{(0)}] \cdot [\bar{\tau}_{(0)}]) = 2\eta_0\,[\gamma_{(1)}] \tag{2.90}$$

Solid matter (incompressible)

$$[\bar{\tau}^{(1)}] = 2\mu(T)\,[\gamma^{(1)}] \tag{2.91}$$

$$[\bar{\tau}_{(1)}] = 2\mu(T)\,[\gamma_{(1)}] \tag{2.92}$$

Remarks

(1) The mathematical model for compressible medium in dependent variables $\bar{\rho}$, $\boldsymbol{v}$, p, $[\bar{\tau}]$ and T (twelve dependent variables) has closure due to continuity, momentum equations, energy equation, equation of state for p and constitutive equations for $[\bar{\tau}]$ ($[\bar{\tau}^{(0)}]$ or $[\bar{\tau}_{(0)}]$)

(2) In case of incompressible matter the mathematical model in dependent variables $\boldsymbol{v}$, p, $[\bar{\tau}]$ and T (ten dependent variables) also has closure. In this case equation of state is absent.

(3) When $\bar{\tau}_{ij}$ in the constitutive equations are explicitly expressed in terms of $[D]$ and the transport properties of the matter as in case of gases, it is advisable to substitute them in the energy equation. This makes viscous dissipation positive in the energy equation regardless of the signs of the velocities gradients but $\bar{\tau}_{ij}$ still remain as dependent variables in the mathematical model and hence their appearance is maintained in the momentum equations (2.76) or (2.81). This is necessary for interactions of compressible media with incompressible media such as a gas with solid matter in which explicit expressions for $\bar{\tau}_{ij}$ in terms of convected time derivatives of the strain tensors and transport properties is not possible.

(4) If the process consists of a single compressible matter in which the constitutive

equations are such that $\bar{\tau}_{ij}$ can be expressed explicitly in terms of convected time derivatives of strain tensor and transport properties, then $\bar{\tau}_{ij}$ can be eliminated as dependent variables by substituting them in the momentum and energy equations. Additionally thermodynamic pressure p can also be eliminated from the mathematical model using the equation of state and

$$\frac{\partial p}{\partial \bar{x}_i} = \left(\frac{\partial p}{\partial \bar{\rho}}\right)\left(\frac{\partial \bar{\rho}}{\partial \bar{x}_i}\right) + \left(\frac{\partial p}{\partial T}\right)\left(\frac{\partial T}{\partial \bar{x}_i}\right) \tag{2.93}$$

in which $(\frac{\partial p}{\partial \bar{\rho}})$ and $(\frac{\partial p}{\partial T})$ are known explicitly.

The final form of the mathematical model contains only $\bar{\rho}$, $\boldsymbol{v}$ and T as dependent variables. Explicit form is rather straight forward to derive using (2.75) - (2.78) and (2.83).

(5) If the process consists of a single incompressible matter in which the constitutive equations are such that $\bar{\tau}_{ij}$ can be expressed explicitly in terms of convected time derivatives of strain tensor and transport properties as in Newtonian and generalized Newtonian fluids, then $\bar{\tau}_{ij}$ can also be eliminated as dependent variables by substituting them in the momentum and energy equations. The final form of the mathematical model contains only p, $\boldsymbol{v}$ and T as dependent variables. Explicit form is rather straight forward to derive using (2.80) - (2.82) and (2.84) - (2.92). This mathematical model is computationally more efficient but can not be used in multi-media interaction processes. We note that in this case the mechanical pressure p is not deterministic from the deformation field.

(6) In case of incompressible elastic solid matter, the rate constitutive equations are volume preserving, hence ensure conservation of mass. Therefore for such mat-

ter, the continuity equation should be removed from the mathematical model. Also, the pressure for such solid matter is mechanical pressure ($p = -\frac{\bar{\sigma}_{kk}}{3}$) which implies that $\bar{\tau}_{kk} = 0$ must hold. Thus, for incompressible elastic solid matter the continuity equation must be replaced with $\bar{\tau}_{kk} = 0$. The resulting model has closure.

(7) In this single mathematical model interactions of the various media of an interaction process are intrinsic in the mathematical model thereby eliminating the need for contraint equations at the mating boundaries between the different media.

2.10 Dimensionless Forms of the Mathematical Model

The governing differential equations in the mathematical model must be non-dimensionalized before using them in the methods of approximation for computing their numerical solutions. The non-dimensionalization process eliminates the magnitude differences between the various dependent and independent variables appearing in the mathematical model which leads to better conditioned algebraic system in the methods of approximation. In the mathematical models presented in section 2.9 all quantities have dimensions based on force (F), length (L) and time (t). In order to make these quantities dimensionless we must choose a set of reference quantities and divide the corresponding quantities with dimensions by the reference quantities. This process must be applied to all equations in the mathematical model. The end result is that all dependent and independent variables in the mathematical model now become dimensionless hence, the name 'dimensionless form of the mathematical model'. In addition, during this process of non-dimensionalizing the mathematical model we encounter dimensionless parameters that define the characteristics of the physical process described by the mathematical model.

We consider the complete mathematical model presented in section 2.9 and drop over bar (-) since all descriptions are understood to be Eulerian and introduce '$\hat{}$' over all quantities, meaning that all quantities now have their usual dimensions (in terms of F, L and t).

Next, we choose a consistent set of the reference quantities denoted by subscript '0'(zero). We divide the quantities with dimensions by the reference quantities to non-dimensionalize them (quantities without the hat). These are then introduced in each equation of the mathematical model. We choose the following reference quantities and dimensionless variables.

$$L=\hat{L}/L_0,\ x_i=\hat{x_i}/L_0\ ,\ F=\hat{F}/F_0\ ,\ v_i=\hat{v_i}/v_0\ ,\ \tau_{ij}=\hat{\tau}_{ij}/\tau_0, \sigma_{ij}=\hat{\sigma}_{ij}/\tau_0, p=\hat{p}/p_0\ ;$$

$$E=\hat{E}/E_0\ ,\ \rho=\hat{\rho}/\rho_0\ ,\ k_{ij}=\hat{k}_{ij}/k_0\ ,\ \mu=\hat{\mu}/\mu_0\ ,\ \eta=\hat{\eta}/\mu_0\ ,\ \eta_s=\hat{\eta_s}/\mu_0\ ,\ \eta_p=\hat{\eta_p}/\mu_0\ ;$$

$$\eta=(\hat{\eta_p}+\hat{\eta_s})/\mu_0\ ,\ \lambda=\hat{\lambda}/\lambda_0\ ,\ t=\hat{t}/t_0\ ,\ t_0=L_0/v_0\ ,\ C_v=\hat{C_v}/C_{v0}\ ,\ e=\hat{e}/e_0\ ,\ e_0=C_0T_0$$

We note that, τ_0, p_0 and E_0 all have the same dimensions ($\mathrm{Force}/(\mathrm{Length})^2$) and hence, care must be taken in their selection to ensure that $\tau_0 = p_0 = E_0$ always holds. For example, we can choose $\tau_0 = p_0 = E_0 = \rho_0 {v_0}^2$; characteristic kinetic energy. Then, if we choose $E_0 = \hat{E} = \rho_0 {v_0}^2$, we have, $v_0 = \sqrt{E_0/\rho_0}$ and $E = 1$ and τ_0, p_0 are now automatically defined. We can also choose $\tau_0 = p_0 = E_0 = \frac{\mu_0 v_0}{L_0}$; characterstic viscous stress, hence if we choose $E_0 = \hat{E} = \frac{\mu_0 v_0}{L_0}$, we have $v_0 = \frac{E_0 L_0}{\mu_0}$.

In the following we use this selection of reference quantities and dimensionless quantities to non-dimensionalize the mathematical models for compressible and incompress-

ible matter.

2.10.1 Conservation laws for compressible matter

Consider continuity, momentum and energy equations (2.75) - (2.77) with dimensions

$$\frac{\partial \hat{\rho}}{\partial \hat{t}} + \frac{\partial}{\partial \hat{x}_i}(\hat{\rho}\hat{v}_i) = 0 \tag{2.94}$$

$$\hat{\rho}\frac{\partial \hat{v}_i}{\partial \hat{t}} + \hat{\rho}\frac{\partial \hat{v}_i}{\partial \hat{x}_j}\hat{v}_j + \frac{\partial \hat{p}}{\partial \hat{x}_i} - \frac{\partial \hat{\tau}_{ij}}{\partial \hat{x}_j} - \hat{\rho}\hat{F}_i^b = 0 \tag{2.95}$$

$$\hat{\rho}\frac{\partial \hat{e}}{\partial \hat{T}}\left(\frac{\partial \hat{T}}{\partial \hat{t}} + \hat{v}_i\frac{\partial \hat{T}}{\partial \hat{x}_i}\right) - \frac{\partial}{\partial \hat{x}_i}\left(\hat{k}_{ij}\frac{\partial \hat{T}}{\partial \hat{x}_j}\right) - \left(\hat{p}(\hat{\rho}, \hat{T}) + \hat{\rho}^2\frac{\partial \hat{e}}{\partial \hat{\rho}}\right)\frac{\partial \hat{v}_i}{\partial \hat{x}_i} - \hat{\tau}_{ij}\frac{\partial \hat{v}_i}{\partial \hat{x}_j} = 0 \tag{2.96}$$

Using the dimensionless variables and reference quantities and noting that

$$\frac{\partial}{\partial \hat{T}} = \frac{1}{T_0}\frac{\partial}{\partial T}\ ;\quad \frac{\partial}{\partial \hat{x}_i} = \frac{1}{L_0}\frac{\partial}{\partial x_i}\ ;\quad \frac{\partial}{\partial \hat{\rho}} = \frac{1}{\rho_0}\frac{\partial}{\partial \rho}\ \text{ etc.}$$

We can obtain the following dimensionless forms of continuity, momentum and energy equations (2.94) - (2.96)

$$\frac{\partial \rho}{\partial t} + \frac{\partial}{\partial x_i}(\rho v_i) = 0 \tag{2.97}$$

$$\rho\frac{\partial v_i}{\partial t} + \rho\frac{\partial v_i}{\partial x_j}v_j + \left(\frac{p_0}{\rho_0 {v_0}^2}\right)\frac{\partial p}{\partial x_i} - \left(\frac{\tau_0}{\rho_0 {v_0}^2}\right)\frac{\partial \tau_{ij}}{\partial x_j} - \rho F_i^b = 0 \tag{2.98}$$

$$\left(\frac{1}{Ec}\right)\rho\frac{\partial e}{\partial T}\left(\frac{\partial T}{\partial t}+v_i\frac{\partial T}{\partial x_i}\right)-\left(\frac{1}{ReBr}\right)\frac{\partial}{\partial x_i}\left(k_{ij}\frac{\partial T}{\partial x_j}\right)$$
$$-\left(\frac{p_0}{\rho_0{v_0}^2}\right)\left(p(\rho,T)+\left(\frac{1}{Ec}\right)\rho^2\frac{\partial e}{\partial \rho}\right)\frac{\partial v_i}{\partial x_i}-\left(\frac{\tau_0}{\rho_0{v_0}^2}\right)\tau_{ij}\frac{\partial v_i}{\partial x_j}=0 \quad (2.99)$$

in which Re, Ec and Br are Reynolds number, Eckert number and Brinkman number and are defined as, $Re=\frac{\rho_0 v_0 L_0}{\mu_0}$, $Ec=\frac{{v_0}^2}{C_{v0}T_0}$ and $Br=\frac{\mu_0{v_0}^2}{k_0T_0}$ where $Br=PrEc$. The Prandtl number Pr is defined as $Pr=\frac{\mu_0 C_{v0}}{k_0}$.

We also note that the dimensionless body force F_i^b are defined as

$$F_i^b=\left(\frac{L_0}{{v_0}^2}\right)\hat{F}_i^b \quad (2.100)$$

Furthermore if we choose

$$p_0=\tau_0=E_0=\rho_0{v_0}^2 \quad (2.101)$$

Then $\frac{p_0}{\rho_0{v_0}^2}=1$, $\frac{\tau_0}{\rho_0{v_0}^2}=1$ in the energy equation (2.99). On the other hand, if we choose

$$p_0=\tau_0=E_0=\frac{\mu_0 v_0}{L_0} \quad (2.102)$$

Then, $\frac{p_0}{\rho_0{v_0}^2}=\frac{1}{Re}$ and $\frac{\tau_0}{\rho_0{v_0}^2}=\frac{1}{Re}$ in the energy equation (2.99). As a general guideline one choose larger of the two between (2.101) and (2.102) [54, 55].

2.10.2 Conservation laws for incompressible matter

Consider continuity, momentum and energy equations (2.80)- (2.82) with dimensions

$$\hat{\rho}\left(\frac{\partial \hat{v}_i}{\partial \hat{x}_i}\right) = 0 \tag{2.103}$$

$$\hat{\rho}\frac{\partial \hat{v}_i}{\partial \hat{t}} + \hat{\rho}\frac{\partial \hat{v}_i}{\partial \hat{x}_j}\hat{v}_j + \frac{\partial \hat{p}}{\partial \hat{x}_j} - \frac{\partial \hat{\tau}_{ij}}{\partial \hat{x}_j} - \hat{\rho}\hat{F}_i^b = 0 \tag{2.104}$$

$$\hat{\rho}\hat{C}_v\left(\frac{\partial \hat{T}}{\partial \hat{t}} + \hat{v}_i\frac{\partial \hat{T}}{\partial \hat{x}_i}\right) - \frac{\partial}{\partial \hat{x}_i}\left(\hat{k}_{ij}\frac{\partial \hat{T}}{\partial \hat{x}_j}\right) - \hat{\tau}_{ij}\frac{\partial \hat{v}_i}{\partial \hat{x}_j} = 0 \tag{2.105}$$

using

$$\frac{\partial}{\partial \hat{T}} = \frac{1}{T_0}\frac{\partial}{\partial T}\ ;\ \frac{\partial}{\partial \hat{x}_i} = \frac{1}{L_0}\frac{\partial}{\partial x_i}\ ;\ \frac{\partial}{\partial \hat{\rho}} = \frac{1}{\rho_0}\frac{\partial}{\partial \rho}\ \text{ etc.}$$

and the reference quantities and the dimensionless variables we obtain the following for (2.103) - (2.105).

$$\rho\left(\frac{\partial v_i}{\partial x_i}\right) = 0 \tag{2.106}$$

$$\rho\frac{\partial v_i}{\partial t} + \rho\frac{\partial v_i}{\partial x_j}v_j + \left(\frac{p_0}{\rho_0 {v_0}^2}\right)\frac{\partial p}{\partial x_i} - \left(\frac{\tau_0}{\rho_0 {v_0}^2}\right)\frac{\partial \tau_{ij}}{\partial x_j} - \rho F_i^b = 0 \tag{2.107}$$

$$\left(\frac{1}{Ec}\right)\rho C_v\left(\frac{\partial T}{\partial t} + v_i\frac{\partial T}{\partial x_i}\right) - \left(\frac{1}{ReBr}\right)\frac{\partial}{\partial x_i}\left(k_{ij}\frac{\partial T}{\partial x_j}\right) - \left(\frac{\tau_0}{\rho_0 {v_0}^2}\right)\tau_{ij}\frac{\partial v_i}{\partial x_j} = 0 \tag{2.108}$$

The dimensionless body force in (2.107) has the same definition as (2.100).

2.10.3 Constitutive equations

Viscous fluids

Compressible

$$\boldsymbol{\tau} = 2\left(\frac{\mu_0 v_0}{L_0 \tau_0}\right)\eta(T)\,\boldsymbol{D} + \left(\frac{\mu_0 v_0}{L_0 \tau_0}\right)\kappa(T)\,\mathrm{tr}\boldsymbol{D}[I] \tag{2.109}$$

Incompressible

$$\boldsymbol{\tau} = 2\left(\frac{\mu_0 v_0}{L_0 \tau_0}\right)\eta(T)\,\boldsymbol{D} \tag{2.110}$$

Viscoelastic polymeric fluids

Maxwell models (incompressible)

$$\boldsymbol{\tau}^{(0)} + De\boldsymbol{\tau}^{(1)} = \left(\frac{\mu_0 v_0}{L_0 \tau_0}\right)\eta(T)\boldsymbol{\gamma}^{(1)}; \quad \text{(contravariant)} \tag{2.111}$$

$$\boldsymbol{\tau}_{(0)} + De\boldsymbol{\tau}_{(1)} = \left(\frac{\mu_0 v_0}{L_0 \tau_0}\right)\eta(T)\boldsymbol{\gamma}_{(1)}; \quad \text{(covariant)}$$

in which $De = \frac{\lambda v_0}{L_0}$ is the Deborah number and μ_0 is dimensionless zero shear rate viscosity.

Oldroyd-B models (incompressible)

$$\boldsymbol{\tau}^{(0)} + De_1\boldsymbol{\tau}^{(1)} = \left(\frac{\mu_0 v_0}{L_0 \tau_0}\right)\eta(T)(\boldsymbol{\gamma}^{(1)} + De_2\boldsymbol{\gamma}^{(2)}); \quad \text{(contravariant)} \tag{2.112}$$

$$\boldsymbol{\tau}_{(0)} + De_1\boldsymbol{\tau}_{(1)} = \left(\frac{\mu_0 v_0}{L_0 \tau_0}\right)\eta(T)(\boldsymbol{\gamma}_{(1)} + De_2\boldsymbol{\gamma}_{(2)}); \quad \text{(covariant)}$$

in which $De_1 = \frac{\lambda_1 v_0}{L_0}$ and $De_2 = \frac{\lambda_2 v_0}{L_0}$. The Deborah number De_1 and De_2 are related

to relaxation time λ_1 and the retardation time λ_2.

Giesekus model (incompressible)

$$\boldsymbol{\tau}^{(0)} + De\boldsymbol{\tau}^{(1)} - \alpha\frac{De}{\eta}\left(\frac{\tau_0 L_0}{\mu_0 v_0}\right)\boldsymbol{\tau}^{(0)}\cdot\boldsymbol{\tau}^{(0)} = \left(\frac{\mu_0 v_0}{L_0\tau_0}\right)\eta(T)\boldsymbol{\gamma}^{(1)}; \quad \text{(contravariant)} \tag{2.113}$$

$$\boldsymbol{\tau}_{(0)} + De\boldsymbol{\tau}_{(1)} - \alpha\frac{De}{\eta}\left(\frac{\tau_0 L_0}{\mu_0 v_0}\right)\boldsymbol{\tau}_{(0)}\cdot\boldsymbol{\tau}_{(0)} = \left(\frac{\mu_0 v_0}{L_0\tau_0}\right)\eta(T)\boldsymbol{\gamma}_{(1)}; \quad \text{(covariant)}$$

α is dimensionless mobility factor.

Solid matter (incompressible)

$$\boldsymbol{\tau}^{(1)} = \overset{\nabla}{\frac{D\boldsymbol{\tau}}{Dt}} = \frac{D\boldsymbol{\tau}}{Dt} - \boldsymbol{L}\boldsymbol{\tau} - \boldsymbol{\tau}\boldsymbol{L}^T = \left(\frac{E_0}{\tau_0}\right)\mu\boldsymbol{\gamma}^{(1)}; \quad \text{Upper convected} \tag{2.114}$$

$$\boldsymbol{\tau}_{(1)} = \overset{\Delta}{\frac{D\boldsymbol{\tau}}{Dt}} = \frac{D\boldsymbol{\tau}}{Dt} + \boldsymbol{L}^T\boldsymbol{\tau} + \boldsymbol{\tau}\boldsymbol{L} = \left(\frac{E_0}{\tau_0}\right)\mu\boldsymbol{\gamma}_{(1)}; \quad \text{Lower convected} \tag{2.115}$$

$$\frac{{}^{J}D\boldsymbol{\tau}}{Dt} = \frac{D\boldsymbol{\tau}}{Dt} - \boldsymbol{W}\boldsymbol{\tau} + \boldsymbol{\tau}\boldsymbol{W} = \left(\frac{E_0}{\tau_0}\right)\mu\boldsymbol{\gamma}^{(1)} = \left(\frac{E_0}{\tau_0}\right)\mu\boldsymbol{\gamma}_{(1)}; \quad \text{Jaumann rate} \tag{2.116}$$

2.11 Summary

(1) The development of the mathematical model utilizes Eulerian descriptions for all media such as solids, liquids and gases.

(2) The choice of dependent variables is the same for all media (solids, liquids and gases) and is such that the same GDEs from the conservation laws remain valid for all media. Furthermore, the constitutive equations and the equations of state

for all media contain the same dependent variables as used in the conservation laws.

(3) Due to Eulerian description, all constitutive equations are rate constitutive equations [1–4].

(4) For compressible media, equations of state provides a relationship of the dependence of pressure on density and temperature. This is well established for gases. Ideal gas law and real gas models such as the Van der Waals equation of state, the Redlich-Kwang equation of state, the Beattie-Bridgeman equation of state and the Benedict-Webb-Rubin equation of state etc. can be used. For solids and liquids, compressibility is only important at very high pressures at which materials like metals may experience plasticity and other damage mechanisms. However, the framework used here allows one to have any desired equation of state for any media.

(5) For incompressible elastic solids, the constitutive rate equations contain the mechanism of isochronic deformation due to Poisson's ratio. Thus, for such materials the velocity field is not divergence free, hence, the continuity equation should not be used as part of the mathematical model. Furthermore, since the pressure for incompressible elastic solids is purely mechanical i.e. $p = -\frac{\bar{\sigma}_{ii}}{3}$, which implies $\bar{\tau}_{ii} = 0$ and hence this relationship should be used in place of continuity equation as part of the mathematical model.

(6) Fourier heat conduction law is generally accepted as constitutive relation for heat vector in terms of temperature gradients and the conductivity of the medium for solids, liquids as well as gases and hence, is considered here as well.

Chapter 3

hpk Finite Element Framework for Initial Value Problems

In this chapter we present details of the mathematical and computational framework for finite element processes for obtaining numerical solutions of the evolutions described by the IVPs in the interaction processes. First, we note that the IVPs described by the mathematical models are non-linear partial differential equations in dependent variables, space coordinates and time. Surana et. al. [7] have discussed details of mathematical and computational framework, and associated finite element processes for obtaining numerical solutions of such IVPs. We summarize the important features in the following. This is followed by the details of the finite element process and the solution procedure for the resulting non-linear algebraic systems.

Broadly speaking the computational methodologies for IVPs can be categorized as either space-time decoupled formulations or space-time coupled formulations. In space-time decoupled approaches, integral forms and discretizations in space and time are performed independent of each other i.e. non-concurrent. In contrast, the space-time

coupled approaches consider space-time integral forms in which the approximations exhibit simultaneous dependence on space coordinates and time. IVPs describe evolutions in which the dependent variables naturally exhibit simultaneous dependence on space coordinates as well as time. Space-time decoupled methods are contrary to physics, and raise serious issues of stability and accuracy, and hence are not considered in the present work. In space-time coupled methods, simultaneous dependence of the dependent variables on space and time is preserved. Thus, the space and time are naturally coupled in these methods hence, in these methods concurrent treatment in space and time is inherent. In space-time coupled methods we could either use space-time meshes or space-time strip or slab for an increment of time in conjunction with time marching procedures. If the IVP requires response for a large time then the space-time mesh may consist of a large number of elements in time, and as a result the size of the resulting set of assembled equations can become enormous for two and three dimensional problems. To circumvent this, a marching or time-stepping procedure can be utilized effectively for a space-time strip or slab. The solution is obtained for only one layer of elements in time (space-time strip or slab), at a time, in a sequential manner. The initial conditions for the current time step are supplied by the solution from the previous time step. Thus, in this procedure the IVPs are solved for each time step or time increment. For an increment of time we define a space-time strip or a space-time slab say ${}^{n}\bar{\Omega}_{xt}$ for n^{th} increment of time. Thus, we solve the IVP for a space-time slab or strip and then time march to obtain the desired evolution for subsequent values of time.

3.1 General Considerations

Let

$$A\boldsymbol{\varphi} - f = 0 \quad \text{in } \Omega_{xt} = \Omega_x \times \Omega_t = \Omega_x \times (0, \tau) \tag{3.1}$$

be an IVP (with some BCs and ICs) describing an evolution over a space-time domain Ω_{xt}. Let $\boldsymbol{\varphi}(\boldsymbol{x}, t)$ be analytic over Ω_{xt}. Let $\bar{\Omega}^T_{xt}$ be a space-time discretization of $\bar{\Omega}_{xt}$ such that (Figure 3.1)

$$\bar{\Omega}^T_{xt} = \bigcup_e \bar{\Omega}^e_{xt} \tag{3.2}$$

in which $\bar{\Omega}^e_{xt} = \Omega^e_{xt} \bigcup \Gamma^e$ is a space-time subdomain of $\bar{\Omega}^T_{xt}$. Ω^e_{xt} is interior of $\bar{\Omega}^e_{xt}$ and Γ^e is the closure of Ω^e_{xt}. Let $\boldsymbol{\varphi}_h(\boldsymbol{x}, t)$ and $\boldsymbol{\varphi}^e_h(\boldsymbol{x}, t)$ be approximations of $\boldsymbol{\varphi}(\boldsymbol{x}, t)$ over $\bar{\Omega}^T_{xt}$ and $\bar{\Omega}^e_{xt}$, and

$$\boldsymbol{\varphi}_h(\boldsymbol{x}, t) = \bigcup_e \boldsymbol{\varphi}^e_h(\boldsymbol{x}, t) \tag{3.3}$$

Then, the following must hold

(1) Since $\boldsymbol{\varphi} = \boldsymbol{\varphi}(\boldsymbol{x}, t)$ i.e., $\boldsymbol{\varphi}$ is simultaneously dependent on $\boldsymbol{x}, t$, the approximation $\boldsymbol{\varphi}_h(\boldsymbol{x}, t)$ must also exhibit the same. This requirement precludes space-time decoupled methods and necessitates the use of space-time coupled methods.

(2) $\boldsymbol{\varphi}_h$ must be admissible in the non-discretized form of GDEs (3.1) and furthermore

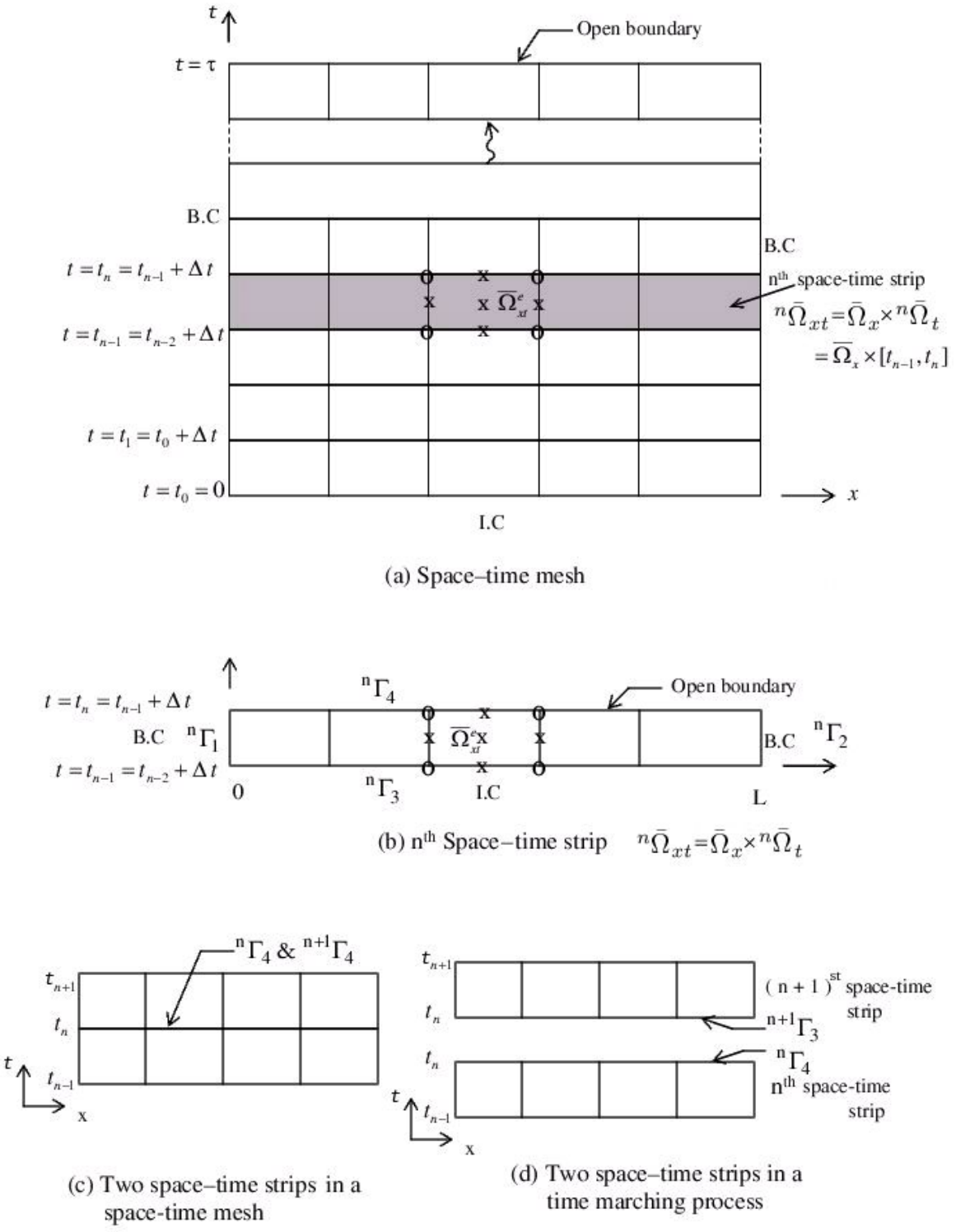

Figure 3.1: Space-time mesh and space-time strips

(a) Admissibility of $\boldsymbol{\varphi}_h(\boldsymbol{x},t)$ in (3.1) must be in the pointwise sense i.e., $\forall(\boldsymbol{x},t)\in\bar{\Omega}^T_{xt}$.

(b) If $E=A\boldsymbol{\varphi}_h-f$ is the residual or error in $\bar{\Omega}^T_{xt}$, then $E\rightarrow 0$ when $\boldsymbol{\varphi}_h\rightarrow\boldsymbol{\varphi}$ in the pointwise sense.

(c) When (b) holds, we also have $I=(E,E)_{\bar{\Omega}^T_{xt}}\rightarrow 0$ i.e., convergence of I to zero implies pointwise convergence of E to zero in $\bar{\Omega}^T_{xt}$ provided the integral in I is Riemann.

(3) If the space-time differential operator A in (3.1) is of order $2m_1$ in space and of order $2m_2$ in time (orders of highest derivatives in space and time), then (2) requires that $\boldsymbol{\varphi}_h(\boldsymbol{x},t)$ be at least of class C^{2m_1} and C^{2m_2} in space and time. If the theoretical solution $\boldsymbol{\varphi}(\boldsymbol{x},t)$ is of class C^{L_1}, C^{L_2} in space and time ($L_1\geq 2m_1$, $L_2\geq 2m_2$; $L_1,L_2\rightarrow\infty$ admissible), then the approximation $\boldsymbol{\varphi}_h(\boldsymbol{x},t)$ must be of class $C^{q_1},C^{q_2};2m_1\leq q_1\leq L_1,2m_2\leq q_2\leq L_2$ in space and time. Choice of q_1 and q_2 depends upon the continuity of the highest orders of the derivatives in space and time desired in $\bar{\Omega}^T_{xt}$ in the computational process. Thus, approximation $\boldsymbol{\varphi}_h(\boldsymbol{x},t)$ of $\boldsymbol{\varphi}(\boldsymbol{x},t)$ over $\bar{\Omega}^T_{xt}$ must posses higher order global differentiability in space and time. $q_1=2m_1$ and $q_2=2m_2$ correspond to the minimally conforming global differentiability in space and time. For this choice all space-time integrals over $\bar{\Omega}^T_{xt}$ are Riemann.

(4) Based on (3), the independent parameters $h,p,k;k=(k_1,k_2)=(\geq q_1+1,\geq q_2+1)$ must form the basis for the approximations in the space-time finite element processes.

(5) The mathematical framework must yield computational processes that remain unconditionally stable and non-degenerate.

(6) The mathematical and the computational framework must be applicable to all IVPs in the interaction processes with the same rigor regardless of their origin or field of application without the use of problem dependent ad-hoc treatments such as upwinding methods.

(7) The space-time differential operators appearing in the mathematical models of multi-physics processes (in Eulerian description) are always non-linear. Hence, the computational infrastructure must be able to treat non-linear PDEs in space and time in a rigorous and consistent manner.

3.2 Space-time Integral Forms and Space-time Methods of Approximation

In the methods of approximations that form the basis for space-time finite element processes for IVPs, one constructs a space-time integral form using GDEs describing the IVPs. One possible way to construct this is to use the fundamental lemma of the calculus of variations [39–41].

Lemma 1: *If* $\eta(\boldsymbol{x}, t)$ *is continuous in* ${}^n\bar{\Omega}_{xt} = {}^n\Omega_{xt} \bigcup {}^n\gamma$*, an* n^{th} *space-time strip or slab and if* $\int_{{}^n\Omega_{xt}} \eta(\boldsymbol{x}, t) h(\boldsymbol{x}, t) d\Omega_{xt} = 0 \; \forall \; h(\boldsymbol{x}, t) \in H^1\left({}^n\bar{\Omega}_{xt}\right)$ *such that* $h(\boldsymbol{x}, t) = 0$ *on* γ^* *then* $\eta(\boldsymbol{x}, t) = 0$ *every where in* ${}^n\Omega_{xt}$ ■

This lemma provides a means of constructing an integral form of the IVP defined by (3.1) in ${}^n\Omega_{xt}$. If we consider (3.1) with $\boldsymbol{\varphi} = \boldsymbol{\varphi}_0$ on γ^*, a portion of the boundary ${}^n\gamma$ of ${}^n\bar{\Omega}_{xt}$, then if we choose a function $v(\boldsymbol{x}, t)$ that is also continuous in ${}^n\Omega_{xt}$ such

that $v(\boldsymbol{x},t)=0$ on γ^*, then

$$\int_{{}^n\bar{\Omega}_{xt}}(A\boldsymbol{\varphi}(\boldsymbol{x},t)-f(\boldsymbol{x},t))v(\boldsymbol{x},t)d\Omega_{xt} \;=\; (A\boldsymbol{\varphi}(\boldsymbol{x},t)-f(\boldsymbol{x},t),v(\boldsymbol{x},t))_{{}^n\bar{\Omega}_{xt}}=0 \tag{3.4}$$

is valid based on lemma 1. Here $(\cdot,\cdot)$ denotes the scalar product of $A\boldsymbol{\varphi}-f$ and v over space-time domain ${}^n\bar{\Omega}_{xt}$. Thus, in (3.4) we have an integral form of the IVP over the space-time domain ${}^n\bar{\Omega}_{xt}$. If $v=\delta\boldsymbol{\varphi}$ (first variation of $\boldsymbol{\varphi}$), then v is admissible in (3.4). v is referred to as the test function. If $\boldsymbol{\varphi}(\boldsymbol{x},t)$ is analytic and f is smooth, then $(A\boldsymbol{\varphi}-f)$ and $v=\delta\boldsymbol{\varphi}$ are both continuous and hence the integrand in (3.4) is continuous also.

In classical space-time methods of approximation (no discretization of $\bar{\Omega}_{xt}$), $\boldsymbol{\varphi}(\boldsymbol{x},t)$ is approximated by $\boldsymbol{\varphi}_N(\boldsymbol{x},t)$ over $\bar{\Omega}_{xt}$. Surana et al. [7] have shown that space-time Galakin method, GM/WF, Petrov-Galakin method, weighted residual method are all STVIC and hence result in computational processes that have non-symmetric coefficient matrices with possibility of complex basis and lack of unconditional stability. On the other hand, space-time LSP for non-linear space-time differential operators can be designed to yield STVC integral forms. STVC computational process yield symmetric coefficient matrices with real basis and unconditionally stable computations during the entire evolution. STVC or STVIC of the integral form is determined by establishing a correspondence between the integral form (resulting from the desired method of approximation) and the calculus of variations (See reference [7] for details).

3.2.1 STVC or STVIC of space-time integral forms [7]

STVC space-time integral forms (definition): In finite element processes for IVPs, if one constructs a space-time integral form over ${}^n\bar{\Omega}^T_{xt}$ and then if one is able to show that

there exists a functional $I({}^n\boldsymbol{\varphi}_h(\boldsymbol{x},t))$ such that $\delta I({}^n\boldsymbol{\varphi}_h(\boldsymbol{x},t)) = 0$ yields the space-time integral form and $\delta^2 I({}^n\boldsymbol{\varphi}_h(\boldsymbol{x},t))$ yields a unique extremum principle then the space-time integral form conforms to the calculus of variations. Such integral forms are called STVC integral forms. ■

STVC space-time integral forms ensure unique solution ${}^n\boldsymbol{\varphi}_h(\boldsymbol{x},t)$ from the integral form. This stems from the fact that STVC integral forms yield unique extremum principle which ensures that the coefficient matrices in the algebraic systems remain unconditionally positive definite and hence the resulting computational processes remain unconditionally stable.

STVIC space-time integral forms (definition): In space-time finite element processes in which either existence of $I({}^n\boldsymbol{\varphi}_h(\boldsymbol{x},t))$ and/or existence of unique extremum principle is not possible, we are in violation with the principles of the calculus of variations. The space-time integral forms in such finite element processes are termed STVIC integral forms. ■

STVIC integral forms may not yield a unique extremum principle and hence may not ensure a unique numerical solution of the IVP. Such integral forms yield algebraic systems in which the coefficient matrices are nonsymmetric and are not ensured to be unconditionally positive definite and hence the resulting computational processes may not be unconditionally stable. In STVIC integral forms one must use Lax-Milgrim theorem, Inf-Sup condition etc., on problem by problem basis to establish ranges of computational and physical parameters for which the computational processes remain stable (as done currently in the finite element processes).

3.2.2 Classical space-time least square method based on residual functional [7–9]

Let

$$A\boldsymbol{\varphi} - f = 0 \quad \text{in } {}^{n}\Omega_{xt} \tag{3.5}$$

be an IVP defined over an n^{th} space-time strip ${}^{n}\Omega_{xt}$ in which $\boldsymbol{\varphi}$ is a list of dependent variables. We first consider classical space-time least square method based on residual functional. In this approach the space-time domain of definition of the IVP is not discretized. Let ${}^{n}\boldsymbol{\varphi}_N$ (and N-parameter approximation) be the approximation of $\boldsymbol{\varphi}$ over ${}^{n}\bar{\Omega}_{xt} = {}^{n}\Omega_{xt} \bigcup {}^{n}\Gamma$ where ${}^{n}\Gamma$ is the closure of ${}^{n}\Omega_{xt}$. Let

$$A({}^{n}\boldsymbol{\varphi}_N) - f_p = E \quad \text{in } {}^{n}\bar{\Omega}_{xt} \tag{3.6}$$

be the residual equations due to approximation ${}^{n}\boldsymbol{\varphi}_N$. Based on [7] a STVC integral form of (3.6) can be constructed using the residual functional leading to space-time least square finite element process (STLSFEP). Details are given in the following.

(i) *Existence of space-time residual functional* $I({}^{n}\boldsymbol{\varphi}_N)$ We define

$$I({}^{n}\boldsymbol{\varphi}_N) = (E, E)_{{}^{n}\Omega_{xt}} = \int_{{}^{n}\Omega_{xt}} E^T E \, d\Omega_{xt} \tag{3.7}$$

The approximation ${}^{n}\boldsymbol{\varphi}_N \in V$. $I({}^{n}\boldsymbol{\varphi}_N)$ defines a convex manifold regardless of the nature of E. $I : {}^{A}V^d \times {}^{A}V^d \rightarrow \mathbb{R}$, where ${}^{A}V^d$ is dual of V for operator A. f_p is the projection of f in ${}^{A}V^d$ and $A({}^{n}\boldsymbol{\varphi}_N) \in {}^{A}V^d$.

(ii) *Necessary conditions*

$$\delta I({}^n\boldsymbol{\varphi}_N) = 2(E, \delta E)_{{}^n\bar{\Omega}_{xt}} = 2\boldsymbol{g}({}^n\boldsymbol{\varphi}_N) = 0 \tag{3.8}$$

or

$$\boldsymbol{g}({}^n\boldsymbol{\varphi}_N) = 0$$

in which

$$\boldsymbol{g}({}^n\boldsymbol{\varphi}_N) = (A({}^n\boldsymbol{\varphi}_N) - f_p, Av + \delta A({}^n\boldsymbol{\varphi}_N)) \tag{3.9}$$

(iii) *Sufficient condition or extremum principle*: Based on reference [7], we define

$$\delta^2 I({}^n\boldsymbol{\varphi}_N) \cong (\delta E, \delta E)_{{}^n\bar{\Omega}_{xt}} > 0 \,\text{hence unique extremum principle} \tag{3.10}$$

When the space-time differential operator is nonlinear, $\boldsymbol{g}(\cdot)$ is a nonlinear function of ${}^n\boldsymbol{\varphi}_N$. Thus, we must find a ${}^n\boldsymbol{\varphi}_N$ that satisfies $\boldsymbol{g}(\cdot) = 0$ iteratively.

Let

$${}^n\boldsymbol{\varphi}_N = N_0(\boldsymbol{x}, t) + \sum_{i=1}^{N} N_i(\boldsymbol{x}, t) C_i \tag{3.11}$$

in which $N_i(\boldsymbol{x}, t); i = 1, \cdots, N$ are known basis functions and C_i are constants, yet to be determined. When we substitute (3.11) into (3.9), $\boldsymbol{g}(\cdot)$ becomes a nonlinear function of C_i, i.e.

$$\boldsymbol{g}({}^n\boldsymbol{\varphi}_N) = \boldsymbol{g}(C_i) = 0 \tag{3.12}$$

must hold. Additionally, with the approximation (3.11), the residual E and the residual functional I becomes nonlinear functions of $C_i; i = 1, 2, \cdots, N$.

$$\begin{aligned} E &= E(C_i); \forall \boldsymbol{x}, t \in {}^{n}\bar{\Omega}_{xt} \\ I &= (E, E)_{{}^{n}\bar{\Omega}_{xt}} = I(C_i) \end{aligned} \tag{3.13}$$

We choose Newton's linear method to find $C_i; i = 1, 2, \cdots, N$ that satisfy (3.12). Let $\{C\}_0$ be an assumed or initial guess of $\{C\}$, then

$$\boldsymbol{g}(\{C\}_0) \neq 0 \tag{3.14}$$

Let $\{\Delta C\}$ be a correction to $\{C\}_0$ such that

$$\boldsymbol{g}(\{C\}_0 + \{\Delta C\}) = 0 \tag{3.15}$$

Expanding $\boldsymbol{g}(\{C\}_0 + \{\Delta C\})$ in Taylor series about $\{C\}_0$ and retaining only up to linear term in $\{\Delta C\}$

$$\boldsymbol{g}(\{C\}_0 + \{\Delta C\}) \simeq \boldsymbol{g}(\{C\}_0) + \big[\frac{\partial \boldsymbol{g}}{\partial \{C\}}\big]_{\{C\}_0} \{\Delta C\} = 0 \tag{3.16}$$

$$\{\Delta C\} = -\big[\frac{\partial \boldsymbol{g}}{\partial \{C\}}\big]^{-1}_{\{C\}_0} \boldsymbol{g}(\{C\}_0) \tag{3.17}$$

Recall that $\boldsymbol{g} = (E, \delta E)_{{}^{n}\bar{\Omega}_{xt}}$ in which E and δE are functions of $\{C\}$, hence

$$\delta \boldsymbol{g} = (\delta E, \delta E)_{{}^{n}\bar{\Omega}_{xt}} + (E, \delta^2 E)_{{}^{n}\bar{\Omega}_{xt}} \tag{3.18}$$

Also

$$\delta^2 I = 2(\delta E, \delta E)_{n\bar{\Omega}_{xt}} + 2(E, \delta^2 E)_{n\bar{\Omega}_{xt}} \tag{3.19}$$

If we approximate $\delta^2 I$ by [7]

$$\delta^2 I \simeq 2(\delta E, \delta E)_{n\bar{\Omega}_{xt}} > 0; \quad \text{unique extremum principle} \tag{3.20}$$

Then

$$\delta \boldsymbol{g} = \frac{\partial \boldsymbol{g}}{\partial \{C\}} = (\delta E, \delta E)_{n\bar{\Omega}_{xt}} = \frac{1}{2}\delta^2 I \tag{3.21}$$

Thus

$$\{\Delta C\} = -\big[\frac{\partial \boldsymbol{g}}{\partial \{C\}}\big]^{-1}_{\{C\}_0} \boldsymbol{g}(\{C\}_0) = -\frac{1}{2}\big[\delta^2 I\big]^{-1}_{\{C\}_0} \boldsymbol{g}(\{C\}_0) \tag{3.22}$$

In which the coefficient matrix $\delta^2 I$ (defined by (3.21)) is symmetric and positive definite (due to (3.20)).

New updated solution $\{C\}$ is obtained using

$$\{C\} = \{C\}_0 + \alpha\{\Delta C\} \tag{3.23}$$

in which α is a scalar generally between $(0, 2)$ determined using $I(\{C\}) < I(\{C\}_0)$. This is called line search (see reference [7] for more details). With new $\{C\}$ we check if each component of $\boldsymbol{g}(\{C\})$ is close to zero or not using a threshold value Δ i.e. $\boldsymbol{g}_i \leq \Delta$. Generally $\Delta \leq 10^{-6}$ suffices. If this condition is satisfied, we have a solution

for $\{C\}$ that satisfies $\boldsymbol{g}(\{C\}) = 0$, If not, then we reset $\{C\}_0$ to $\{C\}$ and repeat the calculation for $\{\Delta C\}$ and the remaining steps.

3.2.3 Space-time least squares finite element process based on residual functional

Let $({}^n\bar{\Omega}_{xt})^T = \bigcup_e \bar{\Omega}^e_{xt}$ be discretization of ${}^n\bar{\Omega}_{xt}$ in which $\bar{\Omega}^e_{xt} = \Omega^e_{xt} \bigcup^e \Gamma$ is the domain of a space-time element e. $({}^n\bar{\Omega}_{xt})^T = \bar{\Omega}^T_x \times \bar{\Omega}^n_t = \bar{\Omega}^T_x \times [t_n, t_{n+1}]$ with $\Delta t = t_{n+1} - t_n$, an increment of time (see figure 3.2). Let ${}^n\boldsymbol{\varphi}_h(\boldsymbol{x}, t)$ be approximation of $\boldsymbol{\varphi}(\boldsymbol{x}, t)$ over $\bar{\Omega}^T_{xt}$ and $\boldsymbol{\varphi}^e_h(\boldsymbol{x}, t)$ be the local approximation of $\boldsymbol{\varphi}(\boldsymbol{x}, t)$ over $\bar{\Omega}^e_{xt}$ such that

$$ {}^n\boldsymbol{\varphi}_h(\boldsymbol{x}, t) = \bigcup_e \boldsymbol{\varphi}^e_h(\boldsymbol{x}, t) \tag{3.24} $$

Let V_h be the approximation space then

$$ {}^n\boldsymbol{\varphi}_h(\boldsymbol{x}, t) \ \in \ V_h(({}^n\bar{\Omega}_{xt})^T) \ ; \ \boldsymbol{\varphi}^e_h(\boldsymbol{x}, t) \ \in \ V_h(\bar{\Omega}^e_{xt}) \tag{3.25} $$

in which

$$ \boldsymbol{\varphi}^e_h(\boldsymbol{x}, t) = \sum_{i=1}^{N} N_i \delta^e_i = [N]\{\delta^e\} \ ; \quad N_i \in \ V_h(\bar{\Omega}^e_{xt}) \tag{3.26} $$

in which N_i are local approximation function and δ^e_i are nodal degree of freedom.

(i) *Residual functional $I({}^n\boldsymbol{\varphi}_h)$ over $V_h(({}^n\bar{\Omega}_{xt})^T)$* Let the residual function E^e over $\bar{\Omega}^e_{xt}$ be given by

$$ E^e = A\boldsymbol{\varphi}^e_h - f^e_p \quad \forall(\boldsymbol{x}, t) \in \bar{\Omega}^e_{xt} \tag{3.27} $$

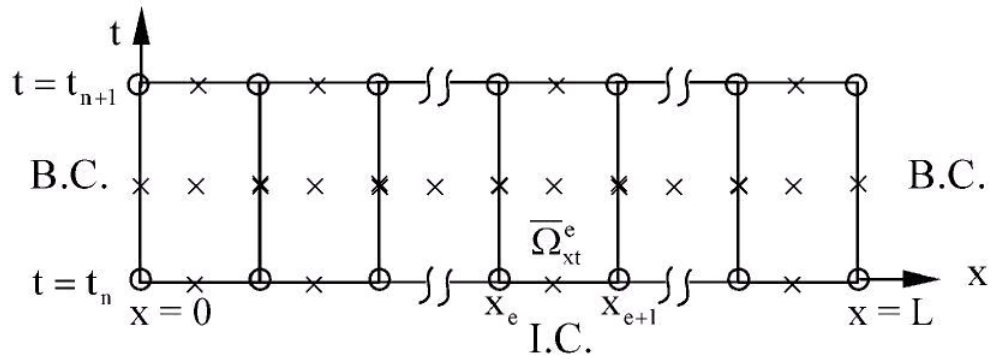

(a) Discretization $\left({}^{n}\overline{\Omega}_{xt}\right)^{T}$ for an n^{th} space-time strip

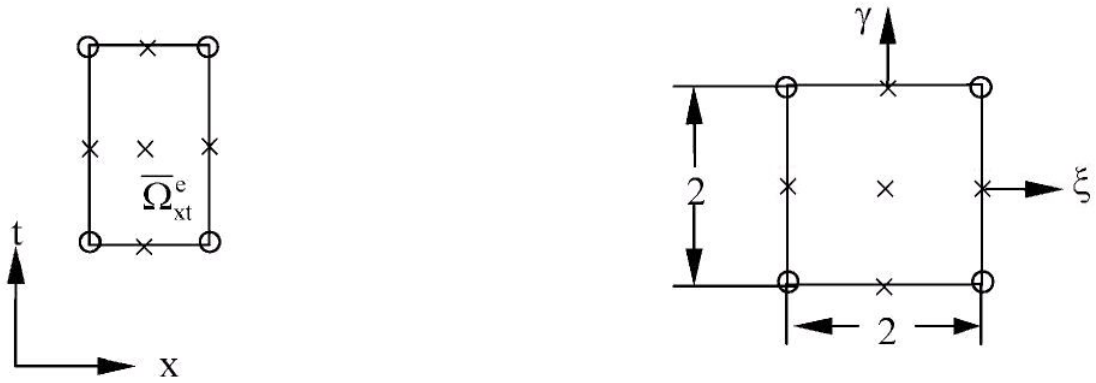

(b) A space-time element $\overline{\Omega}^{e}_{xt}$ (c) Map of $\overline{\Omega}^{e}_{xt}$ in natural coordinate space ξ,γ

Figure 3.2: Discretization for a space-time strip and element domains: (a) discretization $\left({}^{n}\bar{\Omega}_{xt}\right)^{T}$ for a space-time strip; (b) a space-time element $\bar{\Omega}^{e}_{xt}$; and (c) map of $\bar{\Omega}^{e}_{xt}$ in natural coordinate space ξ, γ.

then

$$I = \sum_{e} I^{e} = \sum_{e} (E^{e}, E^{e})_{\bar{\Omega}^{e}_{xt}} \tag{3.28}$$

in which $I : {}^{A}V_{h}^{d} \times {}^{A}V_{h}^{d} \rightarrow \mathbb{R}$ where ${}^{A}V_{h}^{d}$ is the dual of V_h for operator A. f_p^e is the projection of f in ${}^{A}V_{h}^{d}$ and $A\boldsymbol{\varphi}_{h}^{e} \in {}^{A}V_{h}^{d}$.

(ii) *Necessary condition*

$$\delta I({}^n\boldsymbol{\varphi}_h) = \sum_e \delta I^e(\boldsymbol{\varphi}_h^e) = 2\sum_e (E^e, \delta E^e)_{\bar{\Omega}_{xt}^e} = 2\sum_e \boldsymbol{g}^e(\boldsymbol{\varphi}_h^e) = 2\boldsymbol{g} = 0 \quad (3.29)$$

or

$$\boldsymbol{g} = 0 \quad (3.30)$$

When we substitute (3.26)) in E^e and I^e, these become functions of $\{\delta^e\}$ and hence I becomes a nonlinear function of $\{\delta\} = \bigcup_e \{\delta^e\}$, nodal degree of freedom for $\bar{\Omega}_{xt}^T$. Likewise $\boldsymbol{g}(\cdot)$ in (3.30)) becomes a nonlinear function of $\{\delta\}$.

Thus we have

$$\begin{aligned} E^e &= E^e(\{\delta^e\}), \quad I^e = I^e(\{\delta^e\}) \\ I &= I(\{\delta\}), \quad \boldsymbol{g} = \boldsymbol{g}(\{\delta\}) \end{aligned} \quad (3.31)$$

Since $g(\cdot)$ is a nonlinear function of $\{\delta\}$, we must find a $\{\delta\}$ that satisfies $g(\cdot) = 0$ iteratively. We choose Newton's linear method. Let $\{\delta\}_0$ be an assumed or initial guess of $\{\delta\}$, then

$$\boldsymbol{g}(\{\delta\}_0) \neq 0 \quad (3.32)$$

Let $\{\Delta\delta\}$ be a correction to $\{\delta\}$ such that

$$\boldsymbol{g}(\{\delta\}_0 + \{\Delta\delta\}) = 0 \quad (3.33)$$

Expanding $\boldsymbol{g}(\{\delta\}_0 + \{\Delta\delta\})$ in Taylor series about $\{\delta\}_0$ and retaining only up to

linear terms in $\{\Delta\delta\}$

$$\boldsymbol{g}(\{\delta\}_0 + \{\Delta\delta\}) \simeq \boldsymbol{g}(\{\delta\}_0) + \big[\frac{\partial \boldsymbol{g}}{\partial\{\delta\}}\big]_{\{\delta\}_0}\{\Delta\delta\} = 0 \tag{3.34}$$

$$\{\Delta\delta\} = -\big[\frac{\partial \boldsymbol{g}}{\partial\{\delta\}}\big]^{-1}_{\{\delta\}_0}\boldsymbol{g}(\{\delta\}_0) \tag{3.35}$$

Recall that $\boldsymbol{g} = \sum_e (E^e, \delta E^e)_{\bar{\Omega}^e_{xt}}$, hence

$$\delta\boldsymbol{g} = \sum_e (\delta E^e, \delta E^e)_{\bar{\Omega}^e_{xt}} + \sum_e (E^e, \delta^2 E^e)_{\bar{\Omega}_{xt}} \tag{3.36}$$

and

$$\delta^2 I = 2\sum_e (\delta E^e, \delta E^e)_{\bar{\Omega}^e_{xt}} + 2\sum_e (E^e, \delta^2 E^e)_{\bar{\Omega}^e_{xt}} \tag{3.37}$$

If we approximate $\delta^2 I$ by [7]

$$\delta^2 I \simeq 2\sum_e (\delta E^e, \delta E^e)_{\bar{\Omega}^e_{xt}} > 0; \quad \text{unique extremum principle} \tag{3.38}$$

Then

$$\delta\boldsymbol{g} = \frac{\partial \boldsymbol{g}}{\partial\{\delta\}} = \sum_e (\delta E^e, \delta E^e)_{\bar{\Omega}^e_{xt}} \tag{3.39}$$

Thus

$$\{\Delta\delta\} = -\big[\frac{\partial \boldsymbol{g}}{\partial\{\delta\}}\big]^{-1}_{\{\delta\}_0}\boldsymbol{g}(\{\delta\}_0) = -\frac{1}{2}\big[\delta^2 I\big]^{-1}_{\{\delta\}_0}\boldsymbol{g}(\{\delta\}_0) \tag{3.40}$$

In which the coefficient matrix in (3.40) given by $[\delta^2 I]_{\{\delta\}_0}$ is defined by (3.39))

i.e.

$$\{\Delta\delta\} = -\big[\sum_e (\delta E^e, \delta E^e)_{\bar{\Omega}^e_{xt}}\big]^{-1}_{\{\delta\}_0} \boldsymbol{g}(\{\delta\}_0) = -\frac{1}{2}\big[\sum_e [K^e]\big]^{-1}_{\{\delta\}_0} \boldsymbol{g}(\{\delta\}_0) \quad (3.41)$$

in which the element matrix $[K^e]$ is defined by

$$[K^e] = (\delta E^e, \delta E^e)_{\bar{\Omega}^e_{xt}} \quad (3.42)$$

New updated solution $\{\delta\}$ is obtained using

$$\{\delta\} = \{\delta\}_0 + \alpha\{\Delta\delta\} \quad (3.43)$$

in which α is a scalar generally between $(0, 2)$ determined using $I(\{\delta\}) < I(\{\delta\}_0)$. This is called line search (see reference [7] for more details). With new $\{\delta\}$ we check if each component of $\boldsymbol{g}(\{\delta\})$ is close to zero or not using a threshold value Δ i.e. $\boldsymbol{g}_i \leq \Delta$. Generally $\Delta \leq 10^{-6}$ suffices. If this condition is satisfied, we have a solution for $\{\delta\}$ that satisfies $\boldsymbol{g}(\{\delta\}) = 0$, If not, then we reset $\{\delta\}_0$ to $\{\delta\}$ and repeat the calculation for $\{\Delta\delta\}$ and the remaining steps.

Let $V_h(\bar{\Omega}^e_{xt})$ be the local approximation space. First, $V_h(\bar{\Omega}^e_{xt}) \subset H^{k,p}(\bar{\Omega}^e_{xt})$, the scalar product space of order k where $k = (k_1, k_2)$, $k_1 \geq 2p_1 - 1,\ k_2 \geq 2p_2 - 1$. k_1 and k_2 are the orders of the space $H^{k,p}$ space in space and time and p_1, p_2 are the corresponding p - levels (degrees of approximations). The minimally conforming choices of k_1 and k_2 must be based on the mathematical models with restriction of pointwise admissibility of ${}^n\boldsymbol{\varphi}_h(\boldsymbol{x}, t), \forall(\boldsymbol{x}, t) \in ({}^n\bar{\Omega}_{xt})^T$. This ensures that the integral in $I({}^n\boldsymbol{\varphi}_h)$ is Riemann. One could choose different k_1 and k_2 as well as p - levels p_1, p_2 for each dependent variable in $\boldsymbol{\varphi}$ based on the highest orders of their derivatives in space and time appearing in the mathematical model. Perhaps a more practical view point is to

choose the largest admissible k_1 and k_2 for all variables in $\boldsymbol{\varphi}$. The choice of k_1 and k_2 lower than minimally conforming are possible too, but we must keep in mind that for such choices the integrals in $I({}^n\boldsymbol{\varphi}_h)$ and the rest of the least squares process are not Riemann but will be in the Lebesgue sense. Thus if we choose local approximations function $[N^{(k_1-1,k_2-1),p}(\boldsymbol{x},t)] \in V_h(\bar{\Omega}^e_{xt}) \subset H^{(k_1,k_2),p}(\bar{\Omega}^e_{xt})$, then we can write

$$\boldsymbol{\varphi}^e_h(\boldsymbol{x},t) = [N^{(k_1-1,k_2-1),p}(\boldsymbol{x},t)]\boldsymbol{\varphi}^e \tag{3.44}$$

where $\boldsymbol{\varphi}^e$ are nodal degrees of freedom for the space-time element $\bar{\Omega}^e_{xt}$. Obviously $\boldsymbol{\varphi}^e_h(\boldsymbol{x},t) \in V_h(\bar{\Omega}^e_{xt})$

The hpk mathematical and computational finite element framework described here with STVC space-time integral forms ensures desired global differentially in space and time as well as unconditionally stable computations during the entire evolution regardless of the type of interaction process. This approach is used for obtaining numerical solutions of the model problems presented in chapters 4, 5, 6 and 7.

Chapter 4

The Rate Constitutive Equations and Their Validity for Progressive Increasing Deformation

4.1 Introducation

Since the constitutive theories in Eulerian description are rate constitutive theories that have been derived using contra- and co- variant bases [1–4], the performance of the mathematical models using these theories are of interest and concern for progressively increasing deformation. A systematic study is needed to determine the validity of rate theories in co- and contra- variant bases for progressively increasing deformation. This is essential to ensure that most appropriate constitutive theory is chosen in the interaction processes. Based on reference [1–4], it can be concluded that the rate constitutive theories based on contravariant basis are physical as they utilized true deformed volume in their development, whereas in case of development of the rate constitutive theories based on covariant basis, the true deformed volume is further disturbed (deformed

and/or rotated). A quantitative assessment is needed to establish guide line for the validity of rate constitutive equations in co- and contra- variant bases for progressively increasing deformation.

In the studies presented here we choose Giesekus constitutive model for dense polymeric liquids in co- and contra- variant bases derived using polymer stress [53], even though the choice of polymer stress in the rate constitutive equations has been demonstrated to be not in accordance with the derivation of this constitutive model based on axioms of continuum mechanics [3, 4]. In the present work we do not take an issue on this aspect. We consider fully developed flow between parallel plates as model problem to present numerical studies. We have intentionally chosen a model problem with simple physics so that behaviors of the solutions utilizing co- and contra- variant rate constitutive models can be clearly demonstrated.

Even for simplest possible flow such as fully developed flow between parallel plates, the BVP or the IVP described by the mathematical model resulting from the conservation laws and the Giesekus constitutive model does not permit theoretical solution. These are a system of non-linear PDEs in the dependent variables, spatial coordinates and time. Their solutions must be obtained numerically using methods of approximation. Based on reference [7, 9], the space-time coupled least square finite element process using space-time strip or slab with time marching in hpk-mathematical and computational framework [48–50] is an ideal method of approximation for obtaining the numerical solution of the BVPs and the IVPs associated with this mathematical model. In case of BVPs, the least square finite element method based on residual functional in hpk framework [48–50] is the best choice.

The mathematical model describing the physics of flow between parallel plates using Giesekus constitutive model is a system of non-linear PDEs in the dependent variables, a BVP. For such BVPs, the least square finite element processes yield variationally consistent integral forms [48–50] that ensure symmetric and positive definite coefficient matrices unconditionally. hpk mathematical and computational framework permits higher order global differentiability in the entire computational process and all integrals can be maintained in the Riemann sense. This permits accurate computations of the desired L_2-norms, $\sqrt{I} = \sqrt{\sum_i (E_i, E_i)}$ of the residuals, and E_i, the residuals resulting from the non-discretized governing differential equations. When $I \rightarrow 0$, we are assured that $E_i \rightarrow 0$ i.e. GDEs are satisfied accurately over the entire domain of definition of the BVP in the pointwise sense. In all numerical studies, low value of I ($O(10^{-8})$ or lower) is sought to ensure that GDEs are satisfied accurately. Details of the least square finite element method for BVPs in hpk framework can be found in reference [48–50].

4.2 Mathematical Model

Since the Giesekus constitutive model is derived using deviatoric Cauchy polymer stresses ($\boldsymbol{\tau}^p$), the most suitable choice of dependent variables is velocities, deviatoric Cauchy polymer stresses and pressure (p). We use hat ($\hat{}$) on all quantities to emphasize that all quantities have their appropriate dimensions in terms of force, length and time. Consider the schematic shown in Figure 4.1, where H is half of the distance between the parallel plates. We assume the fluid to be incompressible. In this case continuity equation is satisfied identically.

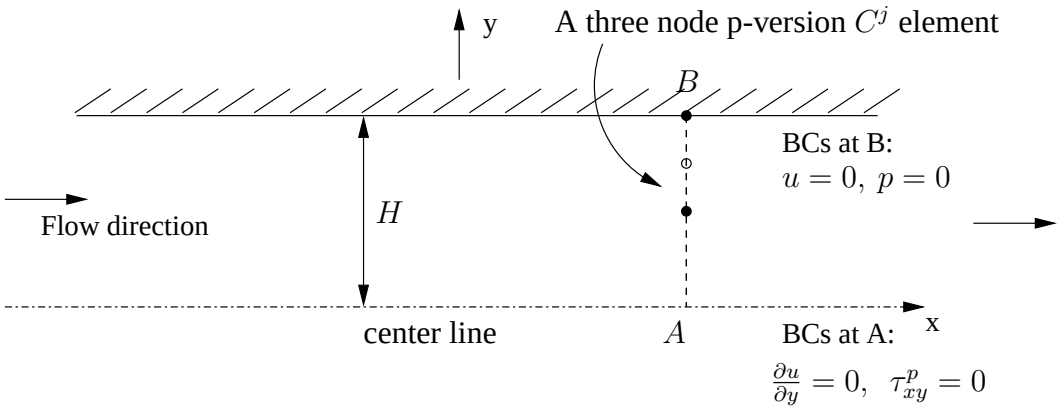

Figure 4.1: Schematic of 1-D fully developed flow between parallel plates (half domain)

Momentum equations:

In the absence of body forces, the momentum equations are given by (remain the same regardless of the choice of rate constitutive equations).

$$\frac{\partial \hat{p}}{\partial \hat{x}} - (\frac{\partial \hat{\tau}^p_{xy}}{\partial \hat{y}} + \hat{\eta}_s \frac{\partial^2 \hat{u}}{\partial \hat{y}^2}) = 0 \tag{4.1}$$

$$\frac{\partial \hat{p}}{\partial \hat{y}} - \frac{\partial \hat{\tau}^p_{yy}}{\partial \hat{y}} = 0 \tag{4.2}$$

We note that $\hat{\boldsymbol{\tau}}^p$ is upper convected or lower convected or Jaumann or Truesdell polymer Cauchy stress deviation tensor depending upon the choice of the rate constitutive theory.

Rate constitutive equations:

Explicit forms of the rate constitutive equations for upper convected, lower convected, Jaumann and Truesdell stress rates are given in the following.

Upper convected:

If $\hat{\boldsymbol{\tau}}^p$ is the contravariant Cauchy stress deviation tensor then, we have

$$\hat{\tau}^p_{xx} - 2\lambda_1 \hat{\tau}^p_{xy} \frac{\partial \hat{u}}{\partial \hat{y}} + \alpha \frac{\lambda_1}{\hat{\eta}_p} \left((\hat{\tau}^p_{xx})^2 + (\hat{\tau}^p_{xy})^2 \right) = 0 \tag{4.3}$$

$$\hat{\tau}^p_{yy} + \alpha \frac{\lambda_1}{\hat{\eta}_p} \left((\hat{\tau}^p_{xy})^2 + (\hat{\tau}^p_{yy})^2 \right) = 0 \tag{4.4}$$

$$\hat{\tau}^p_{xy} - \lambda_1 \hat{\tau}^p_{yy} \frac{\partial \hat{u}}{\partial \hat{y}} + \alpha \frac{\lambda_1}{\hat{\eta}_p} \hat{\tau}^p_{xy} \left(\hat{\tau}^p_{xx} + \hat{\tau}^p_{yy} \right) - \hat{\eta}_p \frac{\partial \hat{u}}{\partial \hat{y}} = 0 \tag{4.5}$$

Lower convected:

If $\hat{\boldsymbol{\tau}}^p$ is the covariant polymer deviatoric Cauchy stress tensor then, we have

$$\hat{\tau}^p_{xx} + \alpha \frac{\lambda_1}{\hat{\eta}_p} \left((\hat{\tau}^p_{xx})^2 + (\hat{\tau}^p_{xy})^2 \right) = 0 \tag{4.6}$$

$$\hat{\tau}^p_{yy} + 2\lambda_1 \hat{\tau}^p_{xy} \frac{\partial \hat{u}}{\partial \hat{y}} + \alpha \frac{\lambda_1}{\hat{\eta}_p} \left((\hat{\tau}^p_{xy})^2 + (\hat{\tau}^p_{yy})^2 \right) = 0 \tag{4.7}$$

$$\hat{\tau}^p_{xy} + \lambda_1 \hat{\tau}^p_{xx} \frac{\partial \hat{u}}{\partial \hat{y}} + \alpha \frac{\lambda_1}{\hat{\eta}_p} \hat{\tau}^p_{xy} \left(\hat{\tau}^p_{xx} + \hat{\tau}^p_{yy} \right) - \hat{\eta}_p \frac{\partial \hat{u}}{\partial \hat{y}} = 0 \tag{4.8}$$

Jaumann:

If $\hat{\boldsymbol{\tau}}^p$ is the Jaumann deviatoric Cauchy stress tensor then, we have

$$\hat{\tau}^p_{xx} - \lambda_1 \hat{\tau}^p_{xy} \frac{\partial \hat{u}}{\partial \hat{y}} + \alpha \frac{\lambda_1}{\hat{\eta}_p} \left((\hat{\tau}^p_{xx})^2 + (\hat{\tau}^p_{xy})^2 \right) = 0 \tag{4.9}$$

$$\hat{\tau}^p_{yy} + \lambda_1 \hat{\tau}^p_{xy} \frac{\partial \hat{u}}{\partial \hat{y}} + \alpha \frac{\lambda_1}{\hat{\eta}_p} \left((\hat{\tau}^p_{xy})^2 + (\hat{\tau}^p_{yy})^2 \right) = 0 \tag{4.10}$$

$$\hat{\tau}^p_{xy} + \frac{1}{2} \lambda_1 (\hat{\tau}^p_{xx} - \hat{\tau}^p_{yy}) \frac{\partial \hat{u}}{\partial \hat{y}} + \alpha \frac{\lambda_1}{\hat{\eta}_p} \hat{\tau}^p_{xy} \left(\hat{\tau}^p_{xx} + \hat{\tau}^p_{yy} \right) - \hat{\eta}_p \frac{\partial \hat{u}}{\partial \hat{y}} = 0 \tag{4.11}$$

Truesdell:

Since the polymeric liquid is assumed incompressible, the velocity field is divergence

free hence, for this the Truesdell rate constitutive equations are exactly same as those for upper convected case (i.e. (4.3) - (4.5)).

4.3 Dimensionless Form of the Mathematical Model

Let ρ_0, u_0, L_0, η_0, p_0 and τ_0 be the reference density, velocity, length, viscosity, pressure and stress respectively. Then we define the following dimensionless quantities.

$$\rho = \hat{\rho}/\rho_0 \, , u = \hat{u}/u_0 \, , x = \hat{x}/L_0 \, , y = \hat{y}/L_0 \, , p = \hat{p}/p_0$$
$$\tau^p = \hat{\tau^p}/\tau_0 \, , \eta = \hat{\eta}/\eta_0 \, , \eta_p = \hat{\eta}_p/\eta_0 \, , \eta_s = \hat{\eta}_s/\eta_0 \, , \hat{\eta} = \hat{\eta}_p + \hat{\eta}_s$$

We note that p_0 and τ_0 are not independent ($p_0 = \tau_0$ must hold). Generally we choose $\tau_0 = \max((\tau_0)_{cke}, (\tau_0)_{cvs})$ [54, 55]. In which $(\tau_0)_{cke}$ and $(\tau_0)_{cvs}$ are reference stresses based on characteristic kinetic energy and characteristic viscous stress and are given by $(\tau_0)_{cke} = \rho_0 u_0^2$ and $(\tau_0)_{cvs} = \eta_0 u_0 / L_0$. If we define $De = \lambda_1 u_0 / L_0$, Deborah number, then the dimensionless forms of the momentum and rate constitutive equations become

Momentum equations:

In the absence of body forces we have

$$\left(\frac{p_0}{\rho_0 u_0^2}\right)\frac{\partial p}{\partial x} - \left(\frac{\tau_0}{\rho_0 u_0^2}\right)\left(\frac{\partial \tau_{xy}^p}{\partial y} + \left(\frac{\eta_0 u_0}{L_0 \tau_0}\right)\eta_s \frac{\partial^2 u}{\partial y^2}\right) = 0 \tag{4.12}$$

$$\left(\frac{p_0}{\rho_0 u_0^2}\right)\frac{\partial p}{\partial y} - \left(\frac{\tau_0}{\rho_0 u_0^2}\right)\frac{\partial \tau_{yy}^p}{\partial y} = 0 \tag{4.13}$$

Rate constitutive equations:

Upper convected:

$$\tau_{xx}^p - 2De\ \tau_{xy}^p \frac{\partial u}{\partial y} + \alpha \frac{De}{\hat{\eta}_p} \left(\frac{L_0 \tau_0}{u_0 \eta_0} \right) \left((\tau_{xx}^p)^2 + (\tau_{xy}^p)^2 \right) = 0 \tag{4.14}$$

$$\tau_{yy}^p + \alpha \frac{De}{\eta_p} \left(\frac{L_0 \tau_0}{u_0 \eta_0} \right) \left((\tau_{xy}^p)^2 + (\tau_{yy}^p)^2 \right) = 0 \tag{4.15}$$

$$\tau_{xy}^p - De\ \tau_{yy}^p \frac{\partial u}{\partial y} + \alpha \frac{De}{\eta_p} \left(\frac{L_0 \tau_0}{u_0 \eta_0} \right) \tau_{xy}^p \left(\tau_{xx}^p + \tau_{yy}^p \right) - \left(\frac{u_0 \eta_0}{L_0 \tau_0} \right) \eta_p \frac{\partial u}{\partial y} = 0 \tag{4.16}$$

Lower convected:

$$\tau_{xx}^p + \alpha \frac{De}{\eta_p} \left(\frac{L_0 \tau_0}{u_0 \eta_0} \right) \left((\tau_{xx}^p)^2 + (\tau_{xy}^p)^2 \right) = 0 \tag{4.17}$$

$$\tau_{yy}^p + 2De\ \tau_{xy}^p \frac{\partial u}{\partial y} + \alpha \frac{De}{\eta_p} \left(\frac{L_0 \tau_0}{u_0 \eta_0} \right) \left((\tau_{xy}^p)^2 + (\tau_{yy}^p)^2 \right) = 0 \tag{4.18}$$

$$\tau_{xy}^p + De\ \tau_{xx}^p \frac{\partial u}{\partial y} + \alpha \frac{De}{\eta_p} \left(\frac{L_0 \tau_0}{u_0 \eta_0} \right) \tau_{xy}^p \left(\tau_{xx}^p + \tau_{yy}^p \right) - \left(\frac{u_0 \eta_0}{L_0 \tau_0} \right) \eta_p \frac{\partial u}{\partial y} = 0 \tag{4.19}$$

Jaumann:

$$\tau_{xx}^p - De\ \tau_{xy}^p \frac{\partial u}{\partial y} + \alpha \frac{De}{\eta_p} \left(\frac{L_0 \tau_0}{u_0 \eta_0} \right) \left((\tau_{xx}^p)^2 + (\tau_{xy}^p)^2 \right) = 0 \tag{4.20}$$

$$\tau_{yy}^p + De\ \tau_{xy}^p \frac{\partial u}{\partial y} + \alpha \frac{De}{\eta_p} \left(\frac{L_0 \tau_0}{u_0 \eta_0} \right) \left((\tau_{xy}^p)^2 + (\tau_{yy}^p)^2 \right) = 0 \tag{4.21}$$

$$\tau_{xy}^p + \frac{De}{2} \left(\tau_{xx}^p - \tau_{yy}^p \right) \frac{\partial u}{\partial y} + \alpha \frac{De}{\eta_p} \left(\frac{L_0 \tau_0}{u_0 \eta_0} \right) \tau_{xy}^p \left(\tau_{xx}^p + \tau_{yy}^p \right) - \left(\frac{u_0 \eta_0}{L_0 \tau_0} \right) \eta_p \frac{\partial u}{\partial y} = 0 \tag{4.22}$$

4.4 Numerical Studies

In this section we present numerical studies for fully developed flow of a Giesekus fluid between parallel plates using all three rate constitutive equations. We choose PIB/C14 [56] fluid with the following properties.

$\hat{\rho} = 800\ kg/m^3,\ \lambda = 0.06\ s,\ \hat{\eta}_s = 0.002\ Pa.s,\ \hat{\eta}_p = 1.424\ Pa.s,$
$\hat{\eta} = \hat{\eta}_s + \hat{\eta}_p = 1.426\ Pa.s,\ \alpha = 0.15.$

We also choose $\eta_0 = \hat{\eta} = 1.426\ Pa.s$, for which case we have $\eta_s = \hat{\eta}_s/\eta_0 = 0.0015$ and $\eta_p = \hat{\eta}_p/\eta_0 = 0.9985$ and the Reynolds number Re and Deborah number De are given by $Re = (\rho_0 L_0/\eta_0)u_0 = 1.781206u_0$ and $De = (\lambda_1/L_0)u_0 = 18.8976378u_0$ if we choose $L_0 = 0.003175 = \hat{H}$, half the distance between the parallel plates.

The flow is pressure driven and is fully developed hence, $\frac{\partial p}{\partial x}$ is known and must be specified for each study but $\frac{\partial p}{\partial y}$ is related to τ^p_{yy} through the y-momentum equation and is not known. We note that for the flow direction to be in the positive x direction, $\frac{\partial p}{\partial x}$ must be negative. Progressively increasing magnitude of $\frac{\partial p}{\partial x}$ result in progressively increasing flow rate and hence progressively increasing strain rates for which the behaviors of various rate constitutive equations can be investigated.

An analytical solution of this BVP is not obtainable, hence we must resort to methods of approximation for obtaining numerical solutions. We use least squares finite element process in hpk framework.

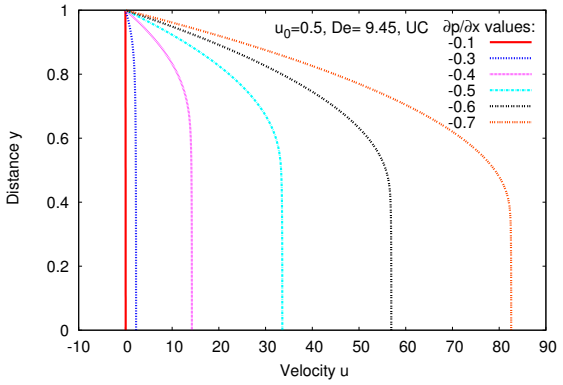

(a) Velocity u versus y

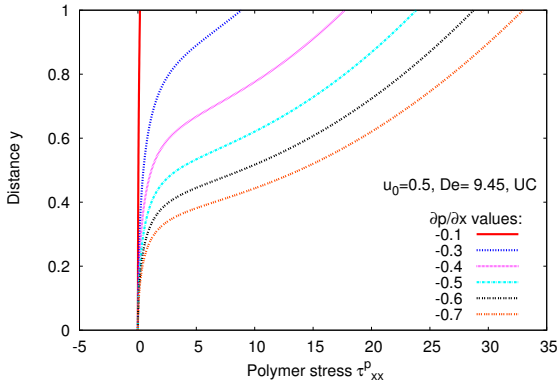

(b) Stress τ^p_{xx} versus y

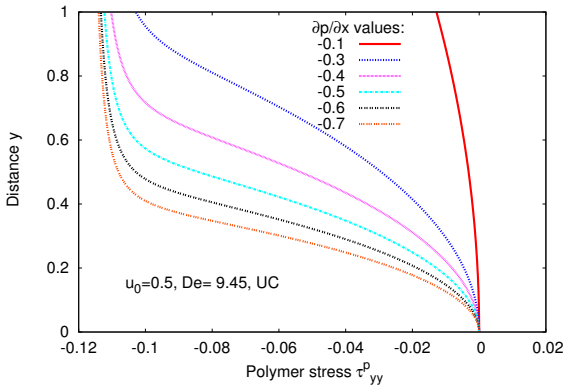

(c) Stress τ^p_{yy} versus y

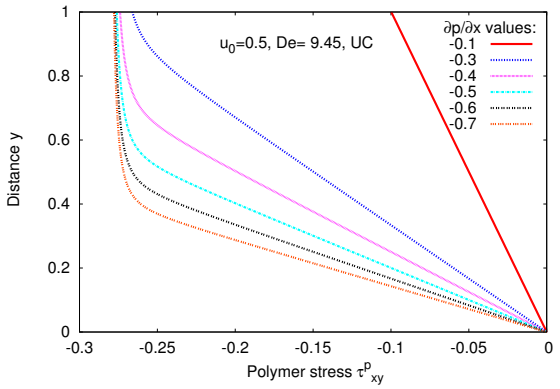

(d) Stress τ^p_{xy} versus y

Figure 4.2: Velocity u and stress $\boldsymbol{\tau}^p$ in Giesekus fluids for upper convected rate equations

Remarks

(i) For this simple flow the solutions are expected to be smooth. Thus a relatively coarse mesh with minimally conforming k (the order of the approximation space) with progressively incressing p-levels are expected to yield converged solutions that satisfy GDEs accurately. *If such solutions are in agreement with the flow physics then, these can be used as reference solutions.* In the numerical studies we first establish that the upper convected (UC) rate constitutive equations indeed yield converged solutions independent of hp and k and that these satisfy GDEs

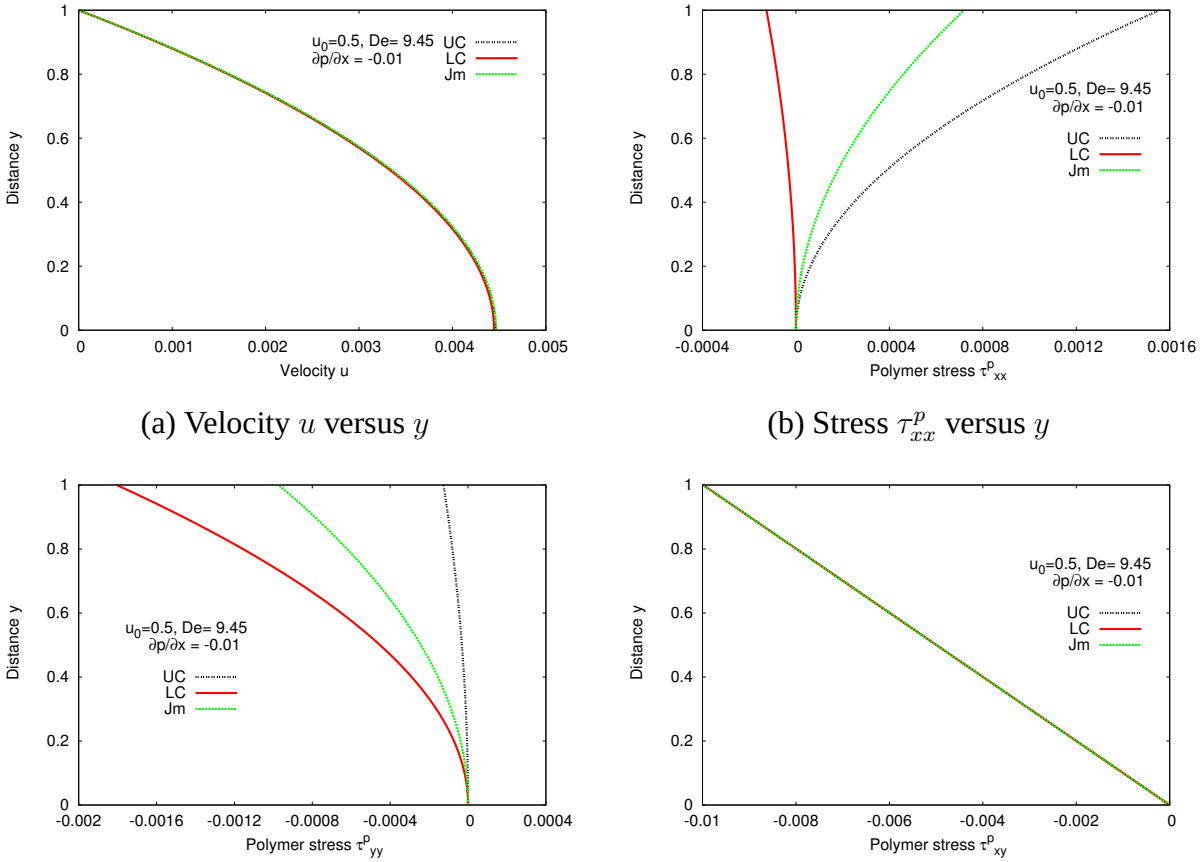

(a) Velocity u versus y

(b) Stress τ^p_{xx} versus y

(c) Stress τ^p_{yy} versus y

(d) Stress τ^p_{xy} versus y

Figure 4.3: Velocity u and stress $\boldsymbol{\tau}^p$ for upper, lower convected and Jaumann rate equations at $\frac{\partial p}{\partial x} = -0.01$

accurately in the pointwise sense over the entire domain of the BVP and are in agreement with the flow physics.

(ii) Converged solution obtained using lower convected (LC) and Jaumann (Jm) rate equations are then compared with those from the UC case to determine their validity: (a) for progressively increasing flow rate that correspond to the progressively increasing strain rates; (b) and for progressively increasing Deborah number (De) for a fixed $\frac{\partial p}{\partial x}$.

(iii) Surana et.al. [57] have shown that for this model problem a coarse uniform dis-

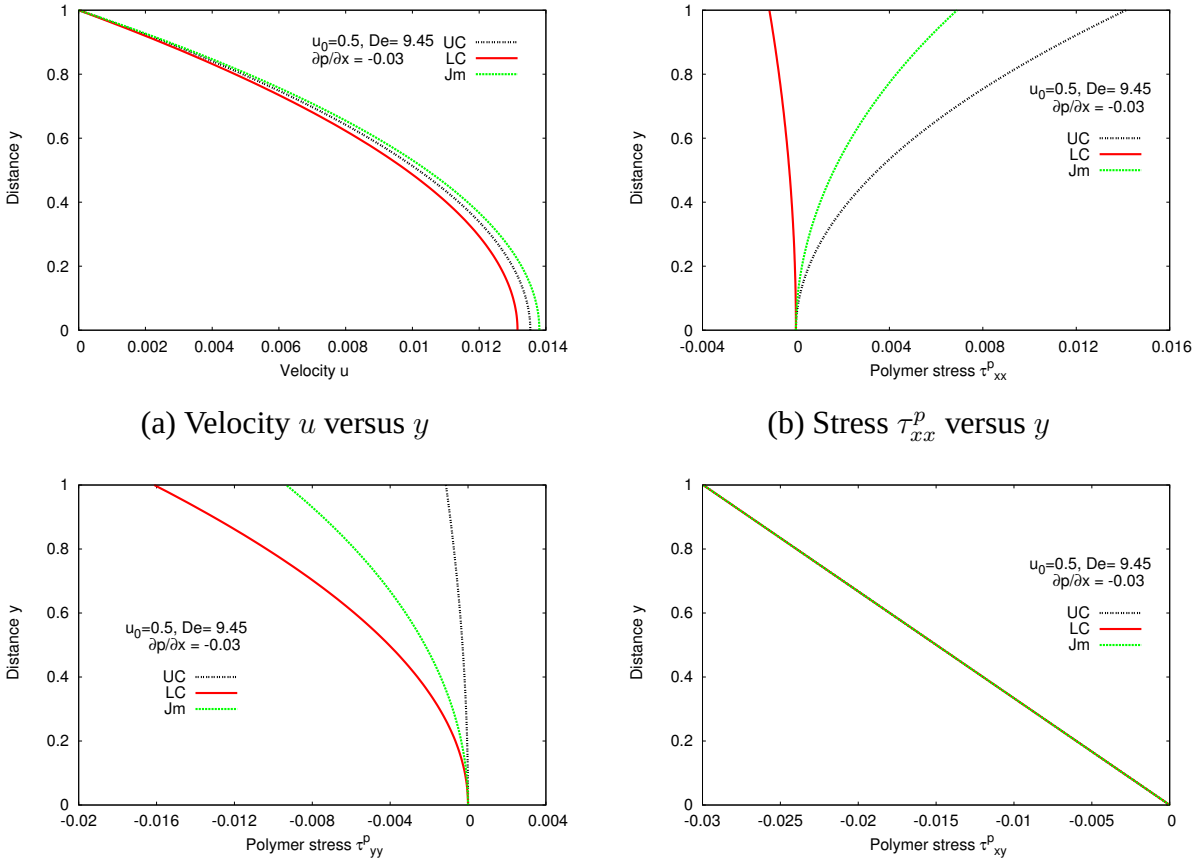

(a) Velocity u versus y

(b) Stress τ^p_{xx} versus y

(c) Stress τ^p_{yy} versus y

(d) Stress τ^p_{xy} versus y

Figure 4.4: Velocity u and stress $\boldsymbol{\tau}^p$ for upper, lower convected and Jaumann rate equations at $\frac{\partial p}{\partial x} = -0.03$

cretization of ten elements (half domain i.e. H) with p-levels $5 - 11$ for $k = 2$ (solution of class C^1 for u, p and $\boldsymbol{\tau}^p$) produces converged solutions that satisfy GDEs quite well. Numerical studies reported for a twenty element uniform discretization confirm that indeed the ten element discretization has the same convergence rate but substantially lower $I^e = \sum_e \sum_i (E^e_i, E^e_i)_{\bar{\Omega}^e}$; E^e_i being element residuals from the GDEs for a given DOFs due to the smoothness of the solution. Thus in all numerical studies we choose a ten element (p-version, 3-node elements) uniform discretization. We note that GDEs are a system of first order

PDEs in p and τ^p but the x-momentum equation contains second derivative of the velocity u. Thus minimally conforming k for p and $\boldsymbol{\tau}^p$ is two but $k = 3$ is needed for the velocity u if the integrals are to be in the Riemann sense. Surana et.al. [57] have shown that choice of $k = 2$ for velocity u suffices as well due to smoothness of the solution but for this choice the term corresponding to $\frac{\partial^2 u}{\partial y^2}$ in the integrals are in Lebesgue sense. However, upon convergence the desired smoothness in the numerical solution is achieved [57]. In summary, for all numerical solution we choose a ten element uniform discretization with $k = 2$ for u, p and $\boldsymbol{\tau}^p$. Based on reference [57] p-levels beyond 5 yield good accuracy of I. With p-levels of 11, I of the order of $O(10^{-8})$ or lower is achieved indicating that the GDEs are satisfied accurately by the computed solutions.

4.4.1 Numerical studies for 1D fully developed flow between parallel plates

In these studies we choose $u_0 = 0.5$ which yield $De = 9.45$ and $Re = 0.89$ we also choose a ten element uniform mesh for $\bar{\Omega} = H = 0 \leq y \leq 1$ using 3-node p-version elements with $k = 2$ i.e. local approximations of class $C^1(\bar{\Omega}^e)$ for u, p as well as $\boldsymbol{\tau}^p$. Based on reference [57] we choose $p = 11$ for all dependent variables. Thus the local approximations for all dependent variables is of the same order and same degree. Figure 4.1 shows a schematic of the flow domain as well as boundary condition. Due to symmetry only the half of the domain (in y - direction) needs to be modeled. We consider upper half. The origin of the coordinate system xy is located at the center of the flow domain. x is the direction of the flow (left to right).

(a) *Reference solution:*

First, we consider UC rate constitutive equations. We begin with $\frac{\partial p}{\partial x} = -0.1$ and increment it by -0.1 to obtain $\frac{\partial p}{\partial x} = -0.1, -0.2, \cdots$. For each $\frac{\partial p}{\partial x}$ we compute a numerical solution beginning with $\frac{\partial p}{\partial x} = -0.1$ and by using a continuation procedure in $\frac{\partial p}{\partial x}$. That is, when computing a solution for $\frac{\partial p}{\partial x} = -0.2$, the converged solution at $\frac{\partial p}{\partial x} = -0.1$ is used as initial solution or starting solution in Newton's linear method used for solving non-linear algebraic equations iteratively. This procedure is followed for each $\frac{\partial p}{\partial x}$ value. For each $\frac{\partial p}{\partial x}$ the least squares functional I of the order of $O(10^{-14})$ or lower is obtained indicating that the computed numerical solutions satisfy GDEs quite accurately. Newton's linear method converges in less than five iteration in all cases with good accuracy. The computed numerical results are shown in Figure 4.2(a)-(d). From the velocity profiles in Figure 4.2(a), we note the progressively increasing maximum velocity at the center ($y = 0$) for progressively increasing magnitude of $\frac{\partial p}{\partial x}$. As expected size of constant velocity core or plug at the center of the flow diminishes with increasing magnitude of $\frac{\partial p}{\partial x}$. Solutions for velocities are smooth, free of oscillations and conform to the flow physics. Plots of τ^p_{xx}, τ^p_{yy} and τ^p_{xy} verses distance y for different $\frac{\partial p}{\partial x}$ values are shown in Figure 4.2(b)-(d) are also smooth, oscillation free and conform to the flow physics (also see Surana et.al. [57]). Based on the values of I of $O(10^{-14})$, flow physics and the results shown in Figure 4.2: (i) We can treat these solutions as reference solutions for evaluating the accuracy and legitimacy of the numerical solutions obtained by using LC and Jm rate constitutive equations. (ii) If there is a need to obtain a new reference solution for a different $\frac{\partial p}{\partial x}$ (or De) then we can use UC rate constitutive equations to do so. Keeping in mind that the low values of the least squares functional I ($I \leq O(10^{-14})$) and agreement of the solutions with the flow physics are two essential elements

in judging whether a computed solution may serve as a reference solution. The numerical solution obtained using UC rate constitutive equations indeed satisfy these criteria.

(b) ***Comparisons of the solutions from UC, LC and Jm rate constitutive equations for a fixed*** De ***with increasing*** $\frac{\partial p}{\partial x}$***:***

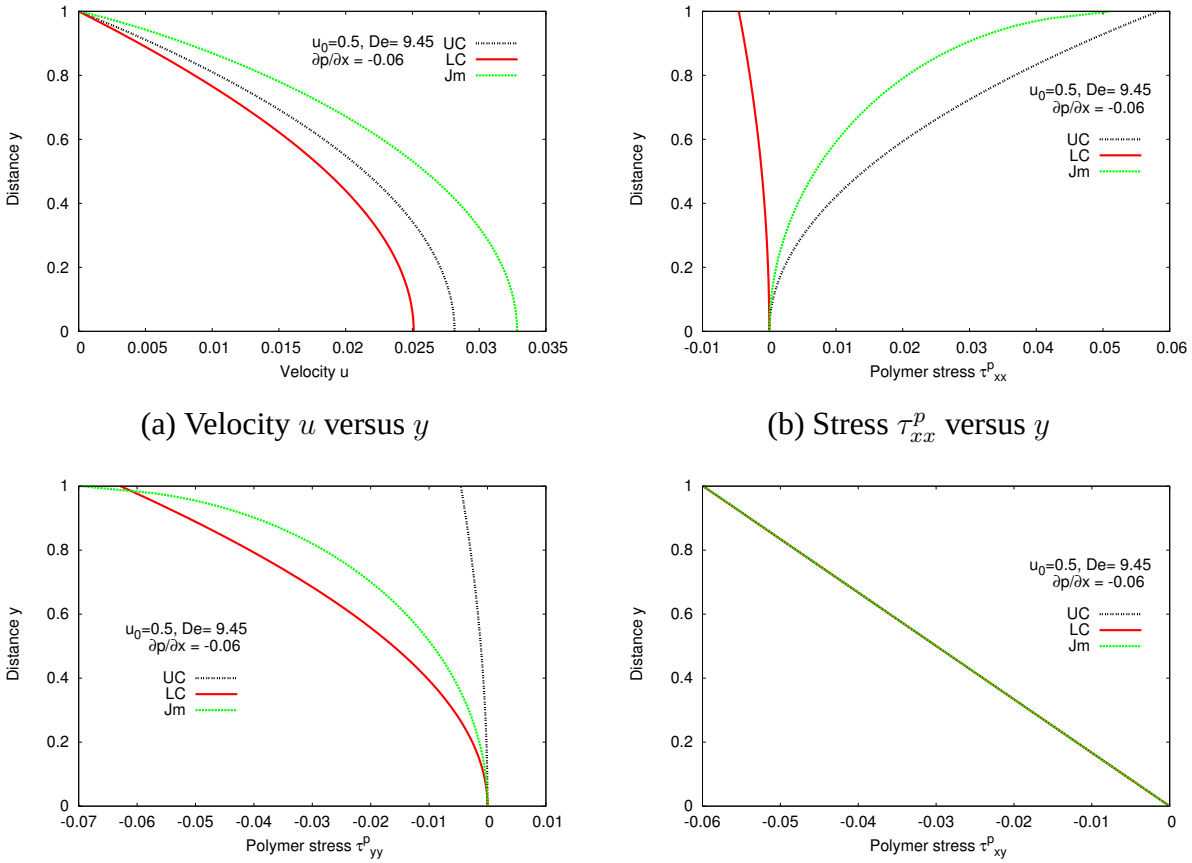

(a) Velocity u versus y

(b) Stress τ^p_{xx} versus y

(c) Stress τ^p_{yy} versus y

(d) Stress τ^p_{xy} versus y

Figure 4.5: Velocity u and stress $\boldsymbol{\tau}^p$ for upper, lower convected and Jaumann rate equations at $\frac{\partial p}{\partial x} = -0.06$

In this study we also choose $u_0 = 0.5$ yielding $De = 9.45$ and $Re = 0.89$. h, p and k remain the same as in the previous study i.e. $h^e = H/10$, $p = 11$ and $k = 2$.

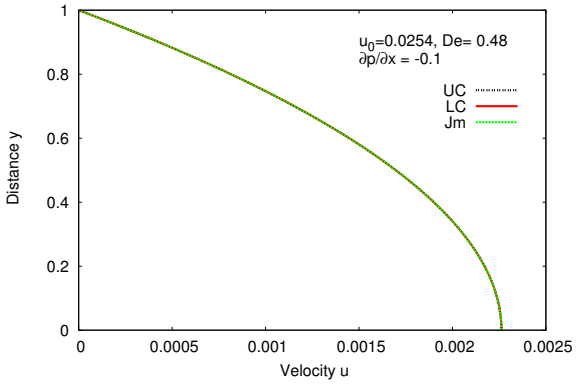

(a) Velocity u versus y

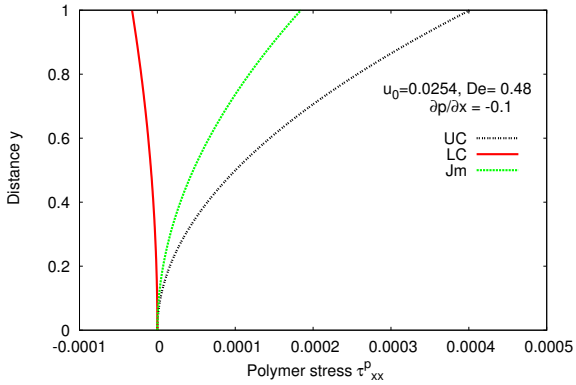

(b) Stress τ^p_{xx} versus y

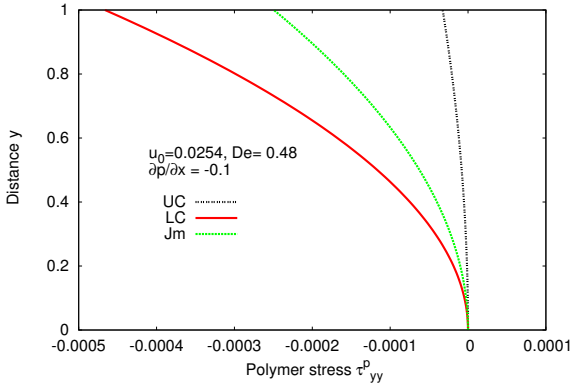

(c) Stress τ^p_{yy} versus y

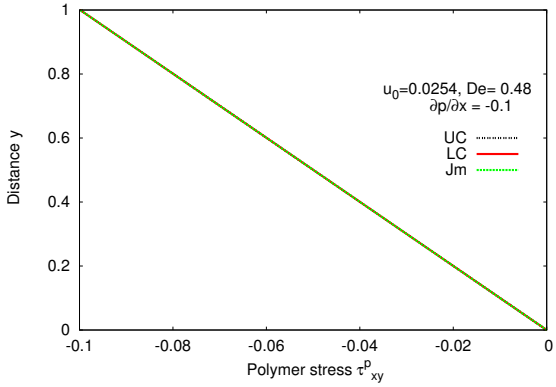

(d) Stress τ^p_{xy} versus y

Figure 4.6: Velocity u and stress $\boldsymbol{\tau}^p$ for upper, lower convected and Jaumann rate equations at $De = 0.48$

We choose $\frac{\partial p}{\partial x} = -0.01$. For this low value of $\frac{\partial p}{\partial x}$, we expect very low strain rates and hence UC, LC and Jm rate constitutive equations must show good agreement with each other. Next we consider $\frac{\partial p}{\partial x} = -0.03$, at this $\frac{\partial p}{\partial x}$, the strain rate(s) is much higher than at $\frac{\partial p}{\partial x} = -0.01$ and hence we shall observe some deviations of the results from LC and Jm when compared with UC. At $\frac{\partial p}{\partial x} = -0.06$, the strain rates are much higher and hence we shall observe the anomalous behaviors of LC and Jm rate constitutive equations and hence strong disagreement with UC. The computed numerical results for UC, LC and Jm rate constitutive equations for the three values of $\frac{\partial p}{\partial x}$ are shown in Figure 4.3 - Figure 4.5. In Figure 4.3(a)

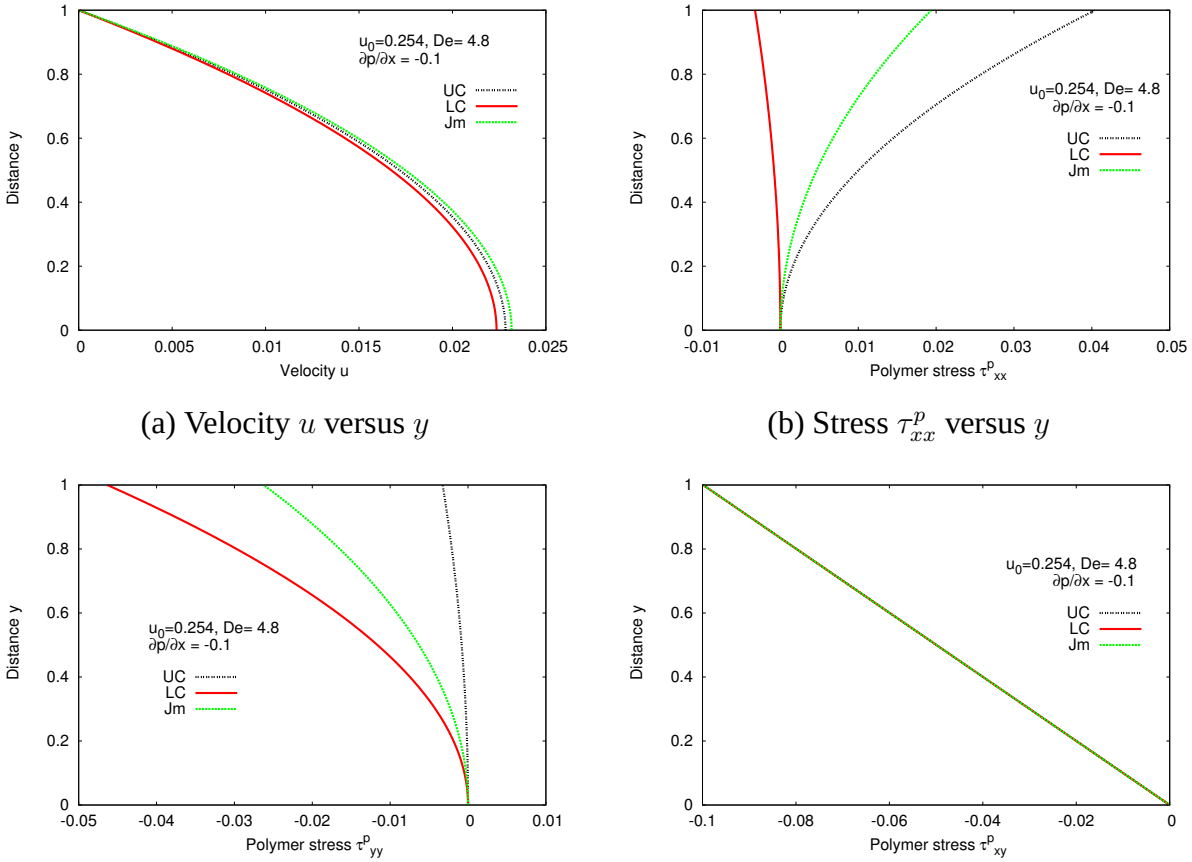

(a) Velocity u versus y

(b) Stress τ^p_{xx} versus y

(c) Stress τ^p_{yy} versus y

(d) Stress τ^p_{xy} versus y

Figure 4.7: Velocity u and stress $\boldsymbol{\tau}^p$ for upper, lower convected and Jaumann rate equations at $De = 4.8$

we note that the velocity profiles for UC, LC and Jm are all almost the same for $\frac{\partial p}{\partial x} = -0.01$. Hence for this case we expect the Jaumann stresses to be average of the UC and LC. This can be confirmed from Figure 4.3(b)-(d). We clearly see that the polymer stresses from LC and Jm rate equations are significantly different compared to UC even for such low $\frac{\partial p}{\partial x}$. At $\frac{\partial p}{\partial x} = -0.03$ (Figure 4.4(a)-(d)) the velocity obtained from LC and Jm begin to deviate compared to UC and hence the polymer stresses in Jm are no longer average of the polymer stress from UC and LC (except for τ^p_{xy}). This can be comfirmed from the graphs shown in Figure 4.4(b)-(d). At $\frac{\partial p}{\partial x} = -0.06$ the velocities from LC and Jm are sig-

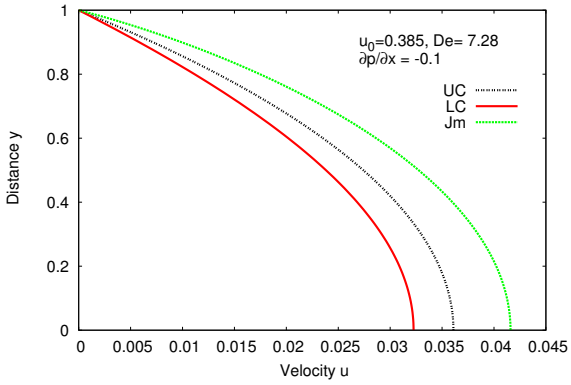

(a) Velocity u versus y

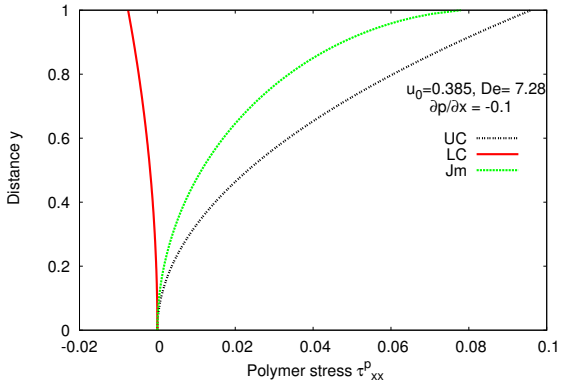

(b) Stress τ^p_{xx} versus y

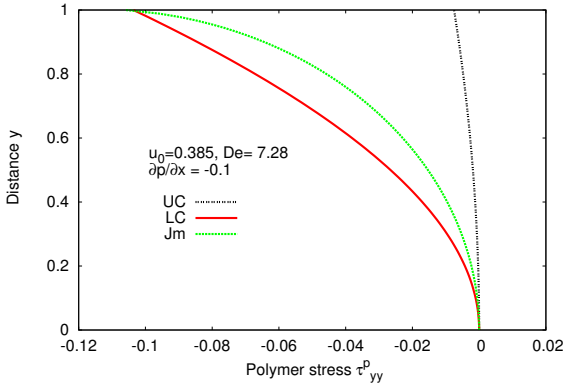

(c) Stress τ^p_{yy} versus y

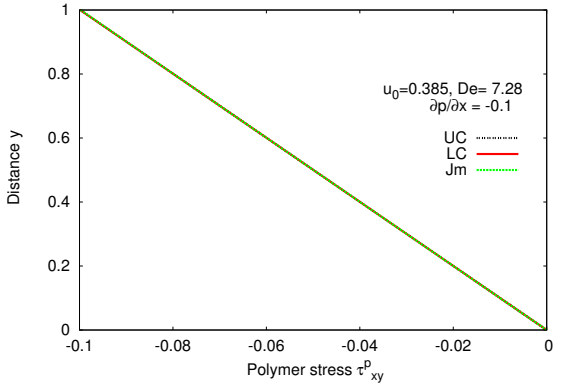

(d) Stress τ^p_{xy} versus y

Figure 4.8: Velocity u and stress $\boldsymbol{\tau}^p$ for upper, lower convected and Jaumann rate equations at $De = 7.28$

nificantly different compared UC (Figure 4.5(a)-(d)), keeping in mind that only UC results are physical as established earlier. The stresses τ^p_{xx} and τ^p_{yy} versus distance y in Figure 4.5(b)-(c) conform: (i) Anomalous behaviors of LC and Jm rate constitutive equations; (ii) τ^p_{xx} and τ^p_{yy} from Jm are no longer average of the corresponding polymer stresses from UC and LC due to the differences in the velocity fields. τ^p_{xy} continues to be linear (due to low value of $\frac{\partial p}{\partial x}$ and low De). For $\frac{\partial p}{\partial x}$ beyond -0.06, Jm rate constitutive equation model experiences problems in the convergence of the Newton's method but LC continues to yield solutions that progressively deviate more and more from those obtained by UC. This study

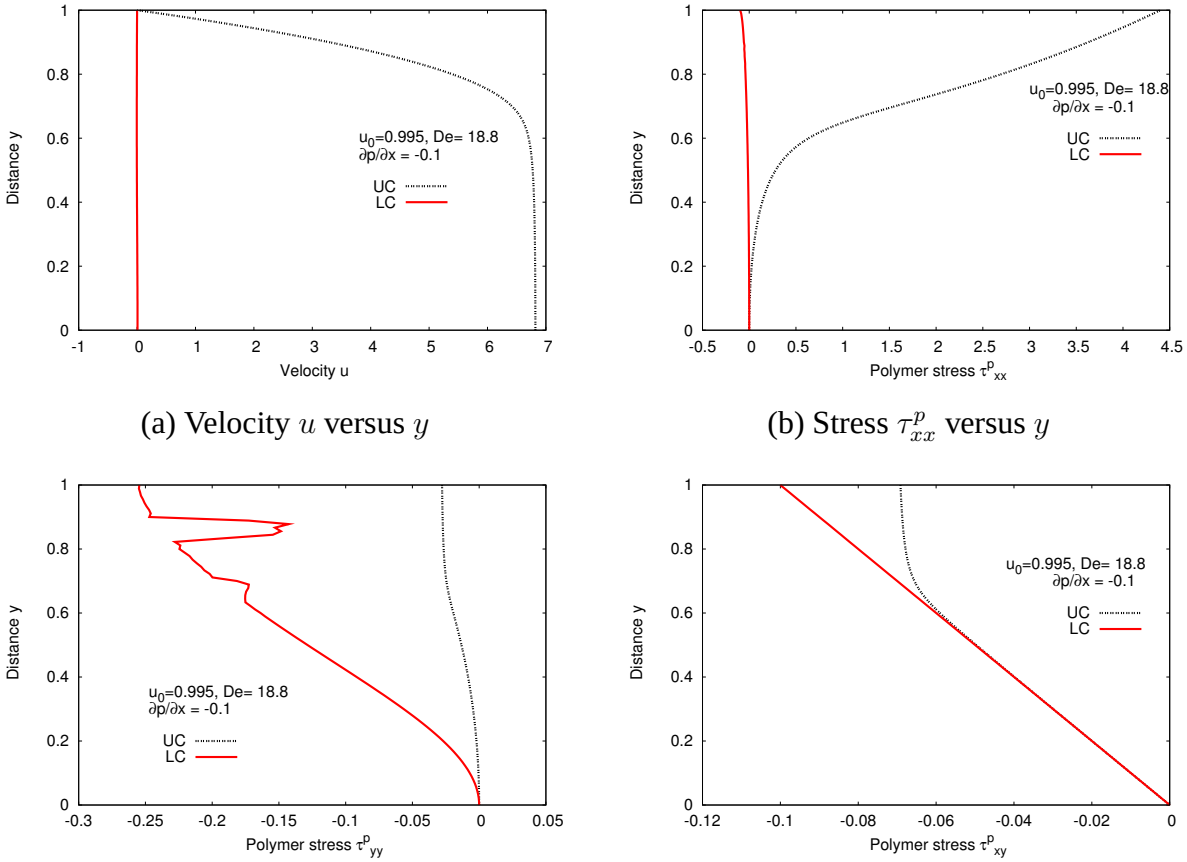

(a) Velocity u versus y

(b) Stress τ^p_{xx} versus y

(c) Stress τ^p_{yy} versus y

(d) Stress τ^p_{xy} versus y

Figure 4.9: Velocity u and stress $\boldsymbol{\tau}^p$ for upper, lower convected and Jaumann rate equations at $De = 18.8$

clearly demonstrates that infinitesimal strain assumption is essential for the validity of LC and Jm rate constitutive equations. The larger is the deviation from this assumption the more anomalous are the solutions of the BVPs incorporating the LC and Jm rate constitutive equations.

(c) *Comparisons of the solutions from UC, LC and Jm rate constitutive equations for a fixed $\frac{\partial p}{\partial x}$ with increasing De:*

In this study we choose a fixed value of $\frac{\partial p}{\partial x} = -0.1$ and vary Deborah number by

choosing $u_0 = 0.0254, 0.254$ and 0.385 that yield $De = 0.48, 4.8$ and 7.28 and Reynolds numbers of $0.045, 0.452$ and 0.686. We use uniform discretization of ten elements with $p = 11$ and local approximation of class C^1 for u, p and $\boldsymbol{\tau}^p$. In all numerical studies reported here the least square functional values of $O(10^{-14})$ or lower are achieved confirming that the computed solutions satisfy GDEs quite well. Just like in case of changing $\frac{\partial p}{\partial x}$ in previous numerical study, here also we use continuation in Deborah number whenever needed i.e. using converged solutions at lower Deborah numbers as initial starting solution for higher Deborah numbers in the Newton's linear method for solving system of non-linear algebraic equations resulting from the assembly of the element equations.

Figure 4.6(a)-(d) show graphs of $u, \tau^p_{xx}, \tau^p_{yy}$ and τ^p_{xy} verses y for $De = 0.48$. For this case, velocities u from UC, LC and Jm are in good agreement (due to very low strain rates) hence, polymer stresses from Jm are average of those from UC and LC as shown in Figure 4.6(b)-(d). However, even for such low strain rates the τ^p_{xx}, τ^p_{yy} from LC and Jm are significantly different compared to those from UC and hence are erroneous. Due to low strain rates for this De, τ^p_{xy} is almost linear for UC, LC and Jm rate constitutive equations (Figure 4.6(a)).

Figure 4.7(a)-(d) show plots of $u, \tau^p_{xx}, \tau^p_{yy}$ and τ^p_{xy} versus y for $De = 4.8$. From Figure 4.6(a) we note that for this Deborah number the velocity fields from LC and Jm begin to deviate slightly compared to the velocity field from UC rate constitutive equations and as a consequence τ^p_{xx} and τ^p_{yy} from Jm are no longer average of those from UC and LC (Figure 4.6(b)-(c)). τ^p_{xy} is linear for all three rate constitutive equations (Figure 4.6(d)).

Plots of $u, \tau_{xx}^p, \tau_{yy}^p$ and τ_{xy}^p verses y for $De = 7.28$ are shown in Figure 4.8(a)-(d). For the Deborah number the velocity profiles from LC and Jm deviate significantly from the velocity profile for UC case. From Figure 4.8(b)-(c) we clearly observe that τ_{xx}^p and τ_{yy}^p from Jm are no longer average of those from UC and LC and are clearly anomalous when compared with UC rate constitutive equation.

Figure 4.9(a)-(d) show plots of $u, \tau_{xx}^p, \tau_{yy}^p$ and τ_{xy}^p verses y for $u_0 = 0.995$ yielding $De = 18.8$ and $Re = 1.77$ (keeping $\frac{\partial p}{\partial x} = -0.1$). At this Deborah number Jm rate constitutive equations fail to yield results due to lack of convergence of the Newton's linear method. From Figure 4.9(a)-(d) we note that LC rate constitutive equations yield numerical solutions that are completely spurious. The solution from the UC rate constitutive equations is smooth, free of oscillations and is in agreement with the physics and the solutions reported in reference [57]. At this higher De, we note that τ_{xy}^p for UC rate constitutive equation is no longer linear (Figure 4.9(d)) whereas τ_{xy}^p for LC continues to be linear.

4.4.2 Numerical studies for 2D developing flow between parallel plates:

The numerical studies were also conducted for two dimensional developing flow between parallel plates for the same parameters as used for 1D fully developed flow presented here. These studies confirm that the fully developed flow results obtained from these (when converged) are in precise agreement with the solution presented here for UC, LC and Jm rate constitutive equations. The 2D developing flow studies presented by Surana et.al. [57] for UC rate constitutive equations also confirm this. The results of

these studies are not presented here for the sake of brevity.

4.5 Summary

Numerical studies are presented for fully developed flow of an incompressible Giesekus fluid between parallel plates using rate constitutive models based on UC, LC and Jm convected stress rates. Numerical solutions are obtained using least squares finite element methods in hpk framework. It is shown that the converged solutions (independent of h, p and k) obtained by using UC rate constitutive equations (when the least squares functional I is of the order of $O(10^{-14})$ or lower) can be used as reference solution. The numerical studies presented : (i) for a fixed Deborah number ($De = 9.45$) with progressively increasing magnitude of $\frac{\partial p}{\partial x}$; (ii) and those for a fixed $\frac{\partial p}{\partial x} = -0.1$ with progressively increasing Deborah number show that the converged solutions from the UC rate constitutive equations always remain physical regardless of the strain rates while those using LC and Jm stress rates become progressively more anomalous with progressively increasing strain rates.

We remark that a specific type of matter or a specific form of the rate equations is not the issue, the major issue is the choice of appropriate stress and strain measures and their convected time derivatives in the development of the rate constitutive theory. For example all rate constitutive equations regardless of the specific matter or their specific form that are based on, covariant and Jaumann measures are bound to be non-physical for finite deformation as these measures and their convected time derivatives are non-physical for finite deformation. Likewise the use of contravariant descriptions will incorporate the correct physics of the deforming matter and hence, is bound to yield more meaningful and physical response of the deforming matter.

Chapter 5

Computations of Evolutions for Isothermal Viscous and Viscoelastic Flows in open domains

5.1 Introduction

In multi-media interaction processes in which incompressible viscous or viscoelastic fluids may interact with other media (solid or fluid), the study of evolution of the deformation field in such media is obviously important. Numerical simulations of evolutions of incompressible fluids in open domains has been viewed difficult primary due to infinite speed of wave propagation because of incompressibility assumption in the derivations of the mathematical models [4, 6, 58]. In closed domain such as lid driven cavity the computation of evolution presents no special difficulty [54, 58, 59]. Since infinite wave speed is viewed as a problem, many remedies have been suggested and used to overcome this problem. In some works [60] it is suggested to introduce mild compressibility so that the speed of wave propagation is no longer infinite. This obvi-

ously requires a change in the mathematical model i.e. we are no longer considering the solution of the original IVP. With diminishing compressibility the solutions of the modified problem are expected to approach the solution of the original problem. Modified mathematical models considering mild compressibility require problem or application dependent treatments to ensure that within the limiting process the solution of the original problem is recoverable, and hence in our view can not be considered as a general methodology for such flows.

In some works [58, 59, 61] a known initial velocity field is specified for the first increment of time without explanation for the need of doing so. In our view there are two possibilities: (i) It could be that without doing so problems are encountered in the convergence of the iterative solution procedure for the system of non-linear algebraic equations resulting from the methods of approximation. (ii) or could it be that some how by doing so we elevate or circumvent the fundamental problem of infinite wave speed in such flows. From the published work no specific reasons are given for one or the other, nonetheless this approach is used commonly in flows with open domains. There are many more published works related to this issue than we have cited here. These consider finite difference, finite volume as well finite element approaches within the framework of space-time decoupled or space-time coupled methodologies with various stabilizing techniques.

In order to clearly understand the origin or the source of problem, we must examine the details of the mathematical model for incompressible viscous and viscoelastic liquids using continuum mechanics, its principles and axioms as foundation for deriving the mathematical models. We present details in the following. The fundamental developments of the mathematical model for any deforming matter must be based

on conservation laws: conservation of mass, balance of momenta, first law of thermodynamics (conservation of energy) and second law of thermodynamics (entropy or Clausius-Duhem inequality). A mathematical model based on these principles ensures thermodynamic equilibrium in the deforming matter. In case of isothermal, incompressible viscous and viscoelastic liquids, the conservation of mass yields continuity equation, balance of momenta yields momentum equations, the energy equation is not needed due to isothermal assumption. What remains is the second law of thermodynamics. First, we note that continuity equation is a statement of divergence free velocity field. The momentum equations require existence of the stress field regardless of the specific constitution of the matter. Thus continuity and momentum equations in velocities and stress tensor (total of nine) provide a mathematical model that does not have closure due to the fact that in their derivation constitution of the matter is not considered. Thus, we must consider constitutive equations that describe how the stress field is related to the kinematics of deformation and properties of the matter. We remark that first three conservation laws have already been used but the second law of thermodynamics has not been. Thus, the second law of thermodynamics must provide the basis for the development of the constitutive equations for the stress field for the deforming incompressible fluid. Of course, in this process we are free to use the other three conservation laws if so desired.

In case of fluids, Eulerian descriptions are preferred over Lagrangian description due to arbitrary large motion of material particles. The second law of thermodynamics leading to entropy or Clausius-Duhem inequality [4, 6, 62] can be expressed in either of the descriptions. It can be shown [4, 6, 62] that in case of fluids (compressible or incompressible), entropy inequality does not provide a mechanism for deriving constitutive equations for the stress field appearing in the momentum equations. To overcome this

difficulty we decompose the total stress tensor into equilibrium stress tensor and deviatoric stress tensor. In case of compressible fluids the entropy inequality can be used to determinate constitutive equation for the equilibrium stress. This results in equilibrium stress to be equal to thermodynamic pressure as a function of density and temperature in the current configuration. Thus if the density and the temperature in the current configuration are known then the thermodynamic pressure is strictly determinestic. This is commonly known as equation of state for compressible fluids such as gases. However, for incompressible fluids i.e. liquids, the entropy inequality only provides a mechanism for determining equilibrium stress if the incompressibility assumption is incorporated in the entropy inequality through Lagrange multiplier. This results in equilibrium stress to be equal to Lagrange multiplier, the mechanical pressure. For non-isothermal incompressible fluids the mechanical pressure becomes a function of temperature. In case of isothermal incompressible flows, the mechanical pressure is a function of spatial coordinates. Thus, it is clear that mechanical pressure introduced through Lagrange multiplier is obviously not deterministic from the kinematics of deformation. This is a significant distinction between thermodynamic pressure for compressible fluids and mechanical pressure for incompressible fluids which is important to note.

We still need to determine the constitutive equations for the deviatoric stress. It has been shown [4, 6, 62] that entropy inequality only requires that the viscous dissipation due to deviatoric stress be positive but provides no mechanism for determining constitutive equations for it. Based on references [1,3], the theory of generators and invariants can be used to determined the constitutive equation for viscous as well as viscoelastic liquids. These can be further simplified to obtain constitutive equations for Newtonian and Maxwell fluids [53]. Keeping in mind that the constitutive equations for Newtonian fluid as well as Maxwell fluid have assumption of small strain and small strain

rate. These constitutive equations in conjunction with continuity and momentum equation provide complete mathematical models for isothermal, incompressible viscous and viscoelastic liquids that are used in the present investigation.

5.2 Scope of Present Investigation

Based on the description of the developments of mathematical models presented in the introduction section, first we make some remarks. This is followed by a description of the scope of present investigation.

(i) In case of isothermal, incompressible fluids, the mechanical pressure is not deterministic from the kinematics of deformation due to the fact that it is the result of incorporating the incompressibility constraint through Lagrange multiplier in the entropy inequality.

(ii) Both pressure and deviatoric stress tensor must be retained as dependent variables in the mathematical models for Newtonian and Maxwell liquids.

(iii) In case of Newtonian fluids deviatoric stresses can be substituted in the momentum equations, thereby eliminating deviatoric stresses as dependent variables. In this case the mathematical model only contains pressure and velocities as dependent variables. However, in case of Maxwell constitutive model for viscoelastic liquids this is not possible as the rate constitutive equations are more complex PDEs in deviatoric stress tensor, velocity field and transport properties of the fluid.

(iv) It is obvious that infinite wave speed in viscous and viscoelastic incompressible fluids is due to incompressibility of the medium and is not influenced by the pressure field.

Thus, when using these mathematical models (for Newtonian or Maxwell model fluid) in the methods of approximation (say space-time finite element method) we must guarantee that specification of the boundary conditions ensure that the pressure is deterministic regardless of the kinematics of deformation. It is true that the pressure field and the velocity fields interact through the momentum equations and thus pressure field is continuously modified based on the velocity field during the iterative solution procedure for the system of non-linear algebraic equation and vice-verse, however, existence of a valid pressure field is essential for the development of a realistic velocity field. Since the momentum equations contain first order derivatives of the pressure in spatial coordinates, we require complete specification of the pressure field on at least one open boundary so that pressure field in the entire spatial domain becomes deterministic. The second important point to note is that we really have no control over the infinite wave speed, a consequence of incompressibility assumption in the mathematical model. Thus, it is perhaps fair to conclude that a good method of approximation must permit the simulations of evolutions in open domains with infinite wave speed as long as the pressure field is determinestic regardless of the kinematic of deformation.

In the present work we demonstrate that this in fact is the case if the method of approximation used for computing evolution has the following features:

(1) Space-time coupled method of approximation as opposed to space-time decoupled method [7, 9].

(2) Space-time finite element processes based space-time variationally consistent integral forms that ensure unconditionally stable computations during the entire evolution [7, 9].

(3) Higher order global differentiability feature in space and time i.e. hpk framework

in which the space-time local approximation over a space-time element are in higher order approximation spaces.

The space-time least squares finite element processes [7, 9] based on minimization of the space-time residual functional yielding space-time variationally consistent integral form with space-time local approximations in $H^{k,p}(\bar{\Omega}^e_{xt})$ spaces (higher order Hilbert spaces) is ideally suited for such applications. Details of the mathematical models are presented in section 5.3. The dimensionless form of the mathematical models and the details of the computational framework are given in sections 5.4 and 5.5. Numerical studies for time evolutions (that remain bounded) using flow between parallel plates and backward facing step as model problems for Newtonian as well as Maxwell constitutive equations are presented in section 5.6. Summary is given in section 5.7.

5.3 Mathematical Models

Since the main issues in this investigation are related to pressure field, choice of initial solution and infinite wave speed in incompressible isothermal flows, we consider the simplest possible constitutive models and hence choose Newtonian fluid and Maxwell model. Details of the mathematical model are given in the following. The continuity and momentum equations (in total stress tensor) remain valid for both fluids. Using Eulerian description with velocities $v_i, i = 1, 2, 3$ (or $\boldsymbol{v}$) in the fixed x-frame, spatial coordinates x_i (or $\boldsymbol{x}$), density $\bar{\rho}$ (fixed) and total Cauchy stress tensor $\bar{\sigma}_{ij}, i = 1, 2, 3$ (or $\bar{\boldsymbol{\sigma}}$), we have the following (in the absence of body forces, sources and sinks), in Einstein's notations [4, 6].

Continuity equation:

$$\bar{\rho}\left(\frac{\partial v_i}{\partial x_i}\right) = 0 \tag{5.1}$$

Momentum equations:

$$\bar{\rho}\frac{\partial v_i}{\partial t} + \bar{\rho}\frac{\partial v_i}{\partial x_j}v_j - \frac{\partial \bar{\sigma}_{ij}}{\partial x_j} = 0 \tag{5.2}$$

In $\bar{\sigma}_{ij}$ no distinction is made between co- and contra- variant bases [62] (valid for Newton's law of viscosity), hence we refer to $\bar{\sigma}_{ij}$ as Cauchy stress tensor. $\bar{\sigma}_{ij}$ is a symmetric tensor of rank two. (5.1) and (5.2) are a set of four partial differential equations in v_i and $\bar{\sigma}_{ij}$ (total of nine dependent variables), thus additional equations are needed to provide closure to the mathematical model described by (5.1) and (5.2). These are obtained by considering constitution of the matter i.e. constitutive equations.

Constitutive equations [4, 6]:

The second law of thermodynamics (Clausius-Duhem inequality) does not provide a mechanism for determining constitutive equations for $\bar{\sigma}_{ij}$. This problem can be overcome by decomposing the total stress tensor $\bar{\sigma}_{ij}$ into equilibrium stress ${}_e\bar{\sigma}_{ij}$ and deviatoric stress ${}_d\bar{\sigma}_{ij}$, both symmetric tensor of rank two.

$$\bar{\sigma}_{ij} = {}_e\bar{\sigma}_{ij} + {}_d\bar{\sigma}_{ij} = {}_e\bar{\sigma}_{ij} + \bar{\tau}_{ij} \tag{5.3}$$

The equilibrium stress ${}_e\bar{\sigma}_{ij}$ can be determined [4, 6] using entropy inequality by incor-

porating incompressibility constraint through Lagrange multiplier. This yields

$$ {}_e\bar{\sigma}_{ij} = -p\delta_{ij} \tag{5.4}$$

in which p is mechanical pressure (Lagrange multiplier) assumed positive when compressive. Additionally, the entropy inequality requires the viscous dissipation due to ${}_d\bar{\sigma}_{ij}$ to be positive but provides no mechanism for determining constitutive equations for it. The constitutive equations for ${}_d\bar{\sigma}_{ij}$ are determined using theory of generators and invariants [4, 6].

Incompressible Newtonian fluids:

Following reference [1, 6], we can establish the following (using theory of generators and invariants) for incompressible Newtonian fluids.

$$ \bar{\boldsymbol{\tau}}^{(0)} = 2\eta\boldsymbol{\gamma}^{(1)} = 2\eta\boldsymbol{D} \tag{5.5}$$

$$ \bar{\boldsymbol{\tau}}_{(0)} = 2\eta\boldsymbol{\gamma}_{(1)} = 2\eta\boldsymbol{D} \tag{5.6}$$

in which $\bar{\boldsymbol{\tau}}^{(0)}$ and $\bar{\boldsymbol{\tau}}_{(0)}$ are contravariant and covariant Cauchy stress deviatoric tensors. $\boldsymbol{\gamma}^{(1)}$ and $\boldsymbol{\gamma}_{(1)}$ are first convected time derivatives of the Almansi and Green's strain tensors in contravariant and covariant bases. We note that (5.5) and (5.6) are only valid for small strains and small strain rates for which the distinction between co- and contra- bases is not significant and hence (5.5) and (5.6) can be replaced by

$$ \bar{\boldsymbol{\tau}} = 2\eta\boldsymbol{D} \tag{5.7}$$

in which $\bar{\boldsymbol{\tau}}$ is Cauchy stress tensor in x-frame and $\boldsymbol{D}$ is the symmetric part of the velocity gradient tensor $\boldsymbol{L}$. η is viscosity of the medium. Thus for incompressible Newtonian fluids the constitutive equations become

$$\bar{\sigma}_{ij} = -p\delta_{ij} + 2\eta D_{ij} \tag{5.8}$$

or

$$[\bar{\sigma}] = -p[I] + 2\eta[D] \tag{5.9}$$

For isothermal incompressible Newtonian fluid flows the complete mathematical model consists of (5.1), (5.2) and (5.9) along with (5.3) and (5.4). A total of ten partial differential equations in ten dependent variables ($v_i, p, \bar{\tau}_{ij}$).

$$\bar{\rho}\left(\frac{\partial v_i}{\partial x_i}\right) = 0 \tag{5.10}$$

$$\bar{\rho}\frac{\partial v_i}{\partial t} + \bar{\rho}\frac{\partial v_i}{\partial x_j}v_j + \frac{\partial p}{\partial x_i} - \frac{\partial \bar{\tau}_{ij}}{\partial x_j} = 0 \tag{5.11}$$

$$\bar{\tau}_{ij} = \eta\left(\frac{\partial v_i}{\partial x_j} + \frac{\partial v_j}{\partial x_i}\right) \tag{5.12}$$

we note that (5.10)- (5.12) is a system of first order PDEs. In this particular case it is possible to substitute $\bar{\tau}_{ij}$ from (5.12) into (5.11) and obtain a mathematical model in dependent variables p and v_i. We do not do so in this work. The motivation being multimedia interaction applications [63] in which the constitutive equations for other interacting media may not be as simple as (5.12) and thereby not permitting elimination of $\bar{\tau}_{ij}$ as dependent variables as the case is for Maxwell constitutive model.

Maxwell constitutive model:

Following reference [3, 4], rate constitutive equations for $\bar{\tau}_{ij}$ for Maxwell fluid in contravariant basis can be derived using theory of generators and invariants.

$$\bar{\boldsymbol{\tau}}^{(0)} + \lambda \bar{\boldsymbol{\tau}}^{(1)} = 2\eta \boldsymbol{\gamma}^{(1)} \tag{5.13}$$

in which $\bar{\boldsymbol{\tau}}^{(1)}$ is the first convected time derivative of the contravariant Cauchy stress tensor $\bar{\boldsymbol{\tau}}^{(0)}$ in contravariant basis and $\boldsymbol{\gamma}^{(1)}$ is the first convected time derivative of the Almansi strain tensor in contravariant basis. Surana et.al. [62] have shown that covariant, Jaumann and all other measure that do not have contravariant basis lead to non-physical behavior when the strain and strain rates are finite while (5.13) remains valid. (5.13) is also referred to as upper convected rate constitutive equations. Thus, we have upper convected Maxwell model (UCMM). This model is generally good for dilute polymeric liquids in which the behavior is viscous dominated with small elastic effects. λ is relaxation time, a characteristic time constant of the polymeric liquid. If we drop the superscript $'(0)'$ in (5.13), we can write

$$\bar{\boldsymbol{\tau}} + \lambda \bar{\boldsymbol{\tau}}^{(1)} = 2\eta \boldsymbol{\gamma}^{(1)} \tag{5.14}$$

in which $\bar{\boldsymbol{\tau}}^{(1)}$ is given by

$$\bar{\boldsymbol{\tau}}^{(1)} = \frac{D[\bar{\tau}]}{Dt} - [L][\bar{\tau}] - [\bar{\tau}][L]^T \tag{5.15}$$

In (5.15) $\frac{D}{Dt}$ is the material derivative.

Thus, for isothermal, incompressible Maxwell fluid we have the following mathemati-

cal model (in the absence of body forces, sources and sinks).

$$\bar{\rho}\left(\frac{\partial v_i}{\partial x_i}\right) = 0 \tag{5.16}$$

$$\bar{\rho}\frac{\partial v_i}{\partial t} + \bar{\rho}\frac{\partial v_i}{\partial x_j}v_j + \frac{\partial p}{\partial x_i} - \frac{\partial \bar{\tau}_{ij}}{\partial x_j} = 0 \tag{5.17}$$

$$[\bar{\tau}] + \lambda\left(\frac{D[\bar{\tau}]}{Dt} - [L][\bar{\tau}] - [\bar{\tau}][L]^T\right) = 2\eta[D] \tag{5.18}$$

we note that in this case Cauchy stress deviations $\bar{\boldsymbol{\tau}}$ must be retained as dependent variables. This mathematical model also has closure.

5.4 Dimensionless Form of the Mathematical Models

First we recast the GDEs in both mathematical models using $\hat{}$ (hat) for all quantities indicating that all quantities have usual units based on force (F), length (L) and time (t).

Incompressible Newtonian fluids:

$$\hat{\rho}\left(\frac{\partial \hat{v}_i}{\partial \hat{x}_i}\right) = 0 \tag{5.19}$$

$$\hat{\rho}\frac{\partial \hat{v}_i}{\partial \hat{t}} + \hat{\rho}\frac{\partial \hat{v}_i}{\partial \hat{x}_j}\hat{v}_j + \frac{\partial \hat{p}}{\partial \hat{x}_i} - \frac{\partial \hat{\tau}_{ij}}{\partial \hat{x}_j} = 0 \tag{5.20}$$

$$\hat{\tau}_{ij} = \hat{\eta}\left(\frac{\partial \hat{v}_i}{\partial \hat{x}_j} + \frac{\partial \hat{v}_j}{\partial \hat{x}_i}\right) \tag{5.21}$$

Maxwell model:

The continuity and momentum equations remain the same as (5.19) and (5.20). The

constitutive equations are given by

$$[\hat{\tau}] + \hat{\lambda}(\frac{\hat{D}[\hat{\tau}]}{\hat{D}\hat{t}} - [\hat{L}][\hat{\tau}] - [\hat{\tau}][\hat{L}]^T) = 2\hat{\eta}[\hat{D}] \tag{5.22}$$

$$\hat{D}_{ij} = \frac{1}{2}\left(\frac{\partial \hat{v}_i}{\partial \hat{x}_j} + \frac{\partial \hat{v}_j}{\partial \hat{x}_i}\right) \tag{5.23}$$

We choose the following reference quantities and dimensionless variables.

$$\left.\begin{aligned} x_i = \hat{x}_i/L_0,\ v_i = \hat{v}_i/v_0,\ \tau_{ij} = \hat{\tau}_{ij}/\tau_0,\ p = \hat{p}/p_0,\ \eta = \hat{\eta}/\eta_0,\ t_0 = L_0/v_0,\ \rho = \hat{\rho}/\rho_0 \\ p_0 = \tau_0 = \begin{cases} \rho_0 {v_0}^2, & \text{characteristic kinetic energy} \\ \frac{\mu_0 v_0}{L_0}, & \text{characterstic viscous stress} \end{cases} \end{aligned}\right\} \tag{5.24}$$

We note that τ_0 and p_0 can not be chosen independently.

If the flow is inertia-dominated, i.e., if $\rho_0 {v_0}^2 > \frac{\mu_0 v_0}{L_0}$ then we choose $\tau_0 = \rho_0 {v_0}^2$. On the other hand, for viscous dominated flows we choose $\tau_0 = \frac{\mu_0 v_0}{L_0}$. In other words, we choose larger of $\rho_0 {v_0}^2$ and $\frac{\mu_0 v_0}{L_0}$ to be τ_0 [54]. Using (5.24), the mathematical models for Newtonian fluids can be non-dimensionalized to obtain

$$\rho \frac{\partial v_i}{\partial x_i} = 0 \tag{5.25}$$

$$\rho \frac{\partial v_i}{\partial t} + \rho \frac{\partial v_i}{\partial x_j} v_j + (\frac{p_0}{\rho_0 {v_0}^2})\frac{\partial p}{\partial x_i} - (\frac{\tau_0}{\rho_0 {v_0}^2})\frac{\partial \tau_{ij}}{\partial x_j} = 0 \tag{5.26}$$

$$\tau_{ij} = (\frac{\eta_0 v_0}{\tau_0 L_0})\eta \left(\frac{\partial v_i}{\partial x_j} + \frac{\partial v_j}{\partial x_i}\right) \tag{5.27}$$

For Maxwell fluid, (5.25) and (5.26) remain the same. The dimensionless form of the

constitutive equations become

$$[\tau] + De(\frac{D[\tau]}{Dt} - [L][\tau] - [\tau][L]^T) = 2(\frac{\eta_0 v_0}{\tau_0 L_0})\eta[D] \tag{5.28}$$

$$D_{ij} = \frac{1}{2}\left(\frac{\partial v_i}{\partial x_j} + \frac{\partial v_j}{\partial x_i}\right) \tag{5.29}$$

where De is Deborah number defined by $De = \frac{\hat{\lambda} v_0}{L_0}$, dimensionless time constant for the Maxwell fluid. We note that if we choose

$$\begin{aligned} &\tau_0 = \rho_0 {v_0}^2, \quad \text{then} \quad \frac{\tau_0}{\rho_0 {v_0}^2} = 1 \quad \text{and} \quad \frac{\mu_0 v_0}{\tau_0 L_0} = \frac{1}{Re} \\ &\tau_0 = \frac{\eta_0 v_0}{L_0}, \quad \text{then} \quad \frac{\mu_0 v_0}{\tau_0 L_0} = 1 \quad \text{and} \quad \frac{\tau_0}{\rho_0 {v_0}^2} = \frac{1}{Re} \end{aligned} \tag{5.30}$$

5.5 Method of Approximation for Obtaining Numerical Solutions of IVPs Resulting from the Mathematical Models

The mathematical models for both fluids are initial value problems in which the space-time differential operator is non-linear i.e. we have a system of non-linear PDEs in space and time. Based on many works by Surana et.al. [7, 48–50], we only consider space-time coupled finite element method of approximation in which the space-time integral forms are variationally consistent. Only space-time least squares processes based on minimization of the space-time residual functional yield space-time variationally consistent integral forms and hence are considered in the present work. For an increment of time, we consider a space-time strip or slab which is discretized in the spatial domain resulting in an assemblage of space-time finite element. Since in both mathematical models are a system of first order PDEs in the dependent variables p, v_i

and τ_{ij}, we consider space-time local approximations for a space-time element in the approximation space V_h such that

$$V_h \subset H^{k,p}(\bar{\Omega}^e_{xt}) \tag{5.31}$$

in which p is the degree of local approximation and $k = (k_1, k_2)$, k_1 and k_2 being orders of the approximation space in space and time. $\bar{\Omega}^e_{xt} = \Omega^e_{xt} \bigcup \Gamma^e$ is the space-time domain of a space-time element e, Γ^e being the closed boundary of Ω^e_{xt}.

Due to smoothness of the evolutions for the two model problems considered here we can choose $k_1 = k_2 = 1$ i.e. local approximation of class C^{00} in space and time. Keeping in mind that for this choice of the order of the space the space-time integrals over the discretization of the space-time strip or slab are in Lebesgue sense. However due to smoothness of the evolution we expect Lebesgue measure to approach Riemann measures upon convergence. The evolution is computed for the first space-time strip or slab using ICs and BCs and the solution is time marched only upon convergence to obtain the desired evolution. See reference [7] for details.

5.6 Numerical Studies

In this section we consider computations of evolutions for 2D transient developing flow between parallel plates and flow over a backward facing step for Newtonian as well as Maxwell fluids. In both model problems the emphasis is on computations of evolutions that remain bounded for all increments of time as opposed to their time accuracy. However, the discretizations and p-levels are chosen such that upon continued evolution accurate stationary states are achieved in both model problems. We reiterate that the

purpose of these studies is to demonstrate that computations of bounded evolutions are indeed possible in incompressible flows with open domains without any special treatments within the proposed infrastructure. In both model problems the least squares residual functional (I) values range from $o(10^{-3})$ to $o(10^{-5})$ corresponding first and the subsequent increments of time, confirming that evolutions for first few increments of time are not as accurate (and hence may not be time accurate) as compared to later time increments. Progressively reduced values of I for subsequent time increments confirm progressively increasing accuracy of the evolution that eventually (less than 10 increments of time) yields quite accurate stationary states. If one desires to seek the time accurate evolution for each increment of time, then it is a simple matter of hp refinement as the convergence of the computed solutions to the theoretical solutions is ensured by the computational framework used here due to space-time variationally consistent integral forms. We make further and more specific remarks regarding some of these aspects while discussing the numerical results for the two model problems.

5.6.1 Transient developing flow between parallel plates

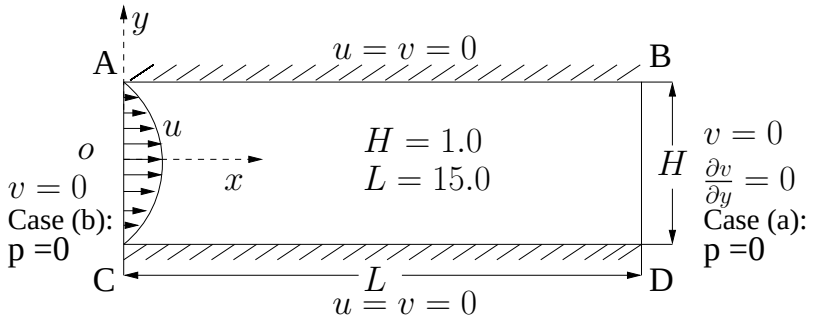

Figure 5.1: Developing flow between parallel plates: schematic and BCs

Figure 5.1 shows a schematic and the boundary conditions. In the first study for Newtonian fluid we choose $[L \times H] = [15 \times 1]$ and $[20 \times 1]$. The space-time domain of the space-time slab $[L \times H] \times [0, \Delta t] = [15 \times 1] \times [0, \Delta t]$ is discretized using

a (20×4) eighty 27-node p-version three dimensional space-time element uniform mesh with local approximations of class C^0 in space and time. The space-time domain $[20 \times 1] \times [0, \Delta t]$ is discretized using (24×4) mesh of 96 space-time 27 node $3D$ elements with local approximations of class C^0 in space and time. The axial domain $0 \leq x \leq 15$, $-0.5 \leq y \leq 0.5$ contain (20×4) uniform mesh (same as for $L = 15$) whereas the domain $15 \leq x \leq 20$, $-0.5 \leq y \leq 0.5$ contain (4×4) uniform mesh. The wall boundary conditions are standard no slip boundary conditions. i.e. $u = v = 0$.

At the inlet AC, the velocity profile defined by

$$u(t) = c_0 + c_1 t + c_2 t^2 + c_3 t^3 \quad ; \quad 0 \leq t \leq \Delta t \tag{5.32}$$

is applied such that

$$\begin{aligned} u(0) &= 0 \\ \frac{du}{dt}\Big|_{t=0} &= 0 \\ u(\Delta t) &= u_{\Delta t} = 3(0.5 - y)(0.5 + y) \\ \frac{du}{dt}\Big|_{t=\Delta t} &= 0 \end{aligned} \tag{5.33}$$

and for $t \geq \Delta t$, we consider $u = u_{\Delta t}$, where $u_{\Delta t}$ is the fully developed velocity for flow between parallel plates for the configuration shown in figure 5.1. Using conditions (5.33), the constants c_0, c_1, c_2 and c_3 in (5.32) can be evaluated and finally we have the following:

$$\begin{aligned} u(t) &= (\frac{3}{\Delta t^2} u_{\Delta t}) t^2 - (\frac{2}{\Delta t^3} u_{\Delta t}) t^3 \quad ; \quad 0 \leq t \leq \Delta t \\ u(t) &= u_{\Delta t} \quad ; \quad t \geq \Delta t \end{aligned} \tag{5.34}$$

(5.33) defines the inlet velocity at AC for all values of time. We note that (5.33) defines a continuously changing (increasing) flow rate at inlet AC for $0 \leq t \leq \Delta t$ that reaches a constant value only for $t = \Delta t$ and thereafter remains constant for all values of time greater than Δt. At time $t = 0$ (commencement of the evolution), the flow rate is zero.

Additionally we also impose $v = 0$ at the inlet AC. The initial velocity field at time $t = 0$ is assumed zero for all studies i.e. the fluid in the reference configuration is considered to be stationary. In all studies in this section we choose uniform p- level of 5 for all elements of the space-time slab. Solution is computed for the first space-time slab using Newton's linear method and then time marched to compute the evolution. We use $\Delta t = 0.2$ for all numerical studies. Newton's linear method with line search for solving non-linear algebraic equations is considered converged when the absolute value of each component of $\delta I = \{g\}$ is less than or equal to Δ, a threshold value for numerically computed zero. In the numerical studies $\Delta = 10^{-5}$ is chosen. For each space-time slab, Newton's linear method with line search converges in 3 to 4 iterations. The least squares or the residual functional (I) for each space-time slab during the time marching is of the order of $O(10^{-3})$ to $O(10^{-5})$ corresponding to the first and the subsequent space-time slabs, confirming the progressively increasing accuracy of the evolution with elapsing time. We make further remarks regarding these values of I and their adequacy in context with the accuracy of the evolution in the following sections.

5.6.1.1 Newtonian fluid

We consider the medium to be water with the following properties at NTP.
$\hat{\rho} = 998.2\ kg/m^3,\ \hat{\eta} = 1.002 \times 10^{-3} Pa\ s.$

The following reference quantities are used:

$\rho_0 = \hat{\rho} = 998.2\ kg/m^3,\ \eta_0 = \hat{\eta} = 1.002 \times 10^{-3} Pa\ s,\ L_0 = 0.01\ m\ ,\ v_0 = 2.008 \times 10^{-3}\ m/s.$

This results in:

$Re = 20,\ \rho_0 {v_0}^2 = 4.025 \times 10^{-3}\ Pa,\ \frac{\eta_0 v_0}{L_0} = 2.012 \times 10^{-4}\ Pa,\ t_0 = \frac{L_0}{v_0} = \frac{0.01}{2.008 \times 10^{-3}} s = 4.980\ s.$

Therefore we choose $p_0 = \tau_0 = \rho_0 {v_0}^2 = 4.025 \times 10^{-3}\ Pa.$

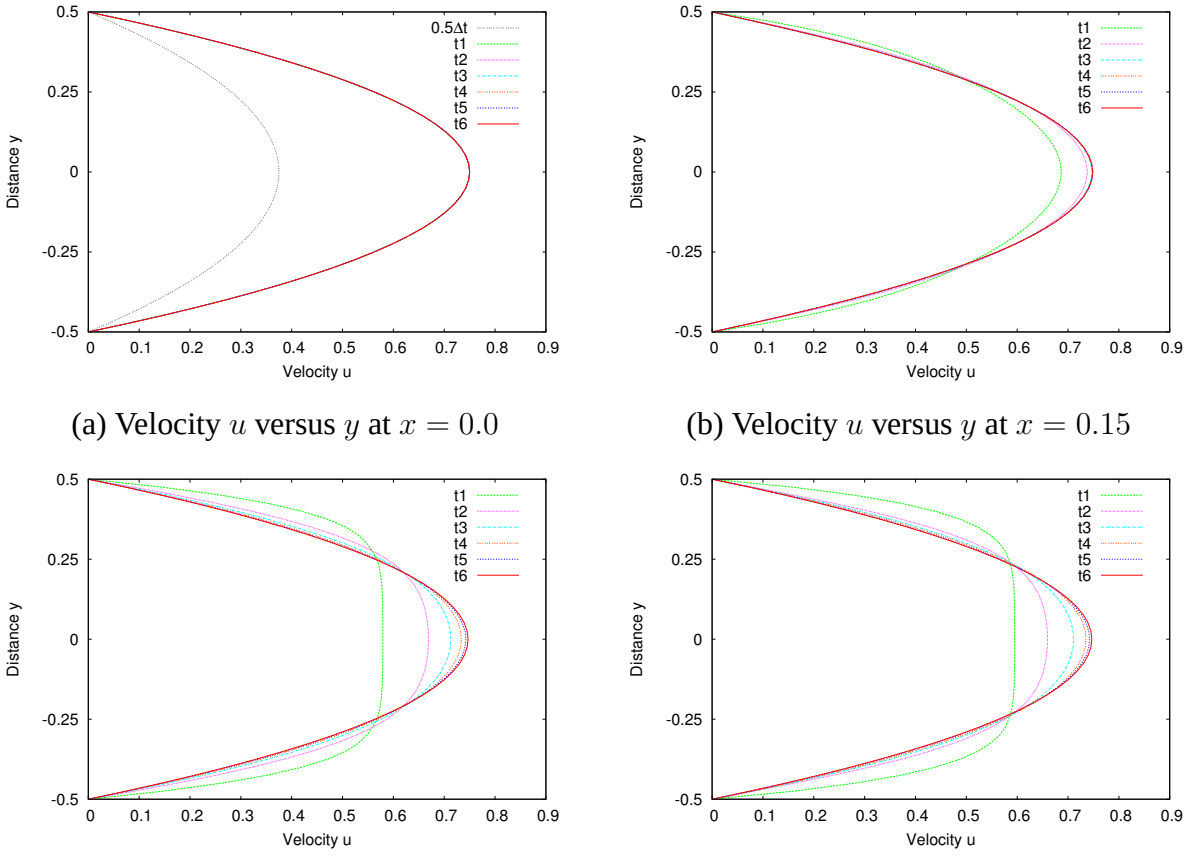

(a) Velocity u versus y at $x = 0.0$

(b) Velocity u versus y at $x = 0.15$

(c) Velocity u versus y at $x = 1.2$

(d) Velocity u versus y at $x = 15.0$

Figure 5.2: Flow between parallel plates, evolution of velocity u: Newtonian fluid, case (a): $p = 0$ at outflow boundary

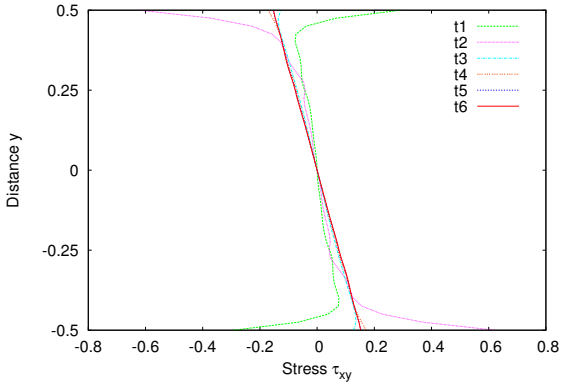

(a) Stress τ_{xy} versus distance y at $x = 0.0$

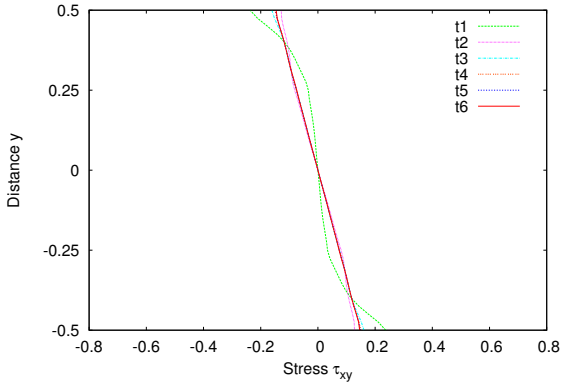

(b) Stress τ_{xy} versus distance y at $x = 0.15$

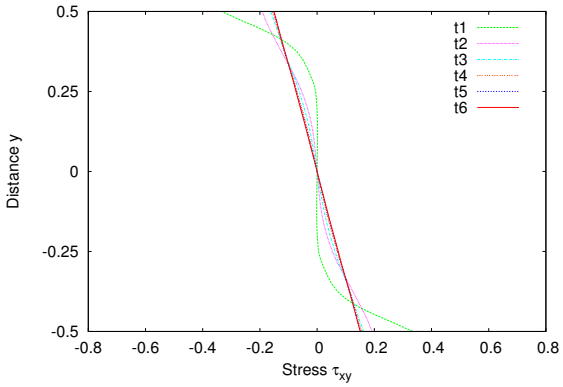

(c) Stress τ_{xy} versus distance y at $x = 1.2$

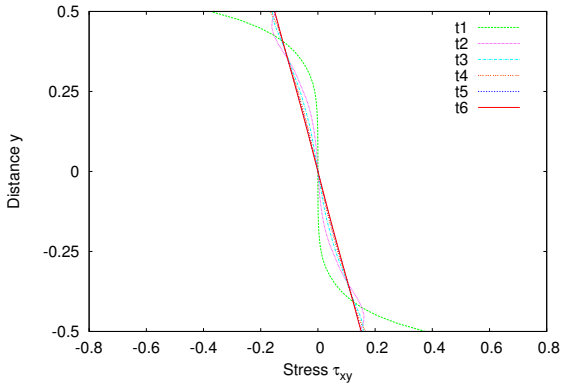

(d) Stress τ_{xy} versus distance y at $x = 15.0$

Figure 5.3: Flow between parallel plates, evolution of stress τ_{xy}: Newtonian fluid, case (a): $p = 0$ at outflow boundary

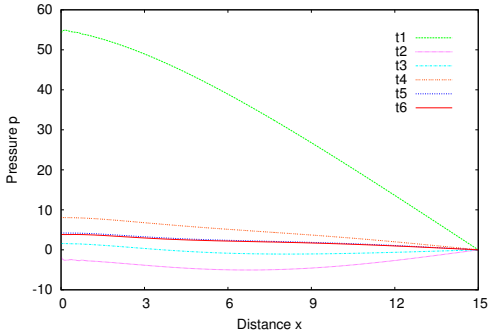

Pressure p versus distance x at $y = 0.0$

Figure 5.4: Flow between parallel plates, evolution of pressure p: Newtonian fluid, case (a): $p = 0$ at outflow boundary

Case (a): pressure $p = 0$ at the outflow boundary

In this study we choose $L = 15$. In addition to the boundary condition shown in figure 5.1, boundary conditions on pressure is needed at an open boundary BD or AC so that the pressure is deterministic regardless of the deformation field. In this study we impose $p = 0$ at the open outflow boundary BD. Evolution is computed for six increments of time using $\Delta = 0.2$. Figure 5.2 shows velocity profiles at $x = 0.0, 0.15, 1.2$ and 15.0 as a function of y for all six increments of time. Since the speed of wave propagation is infinity, at $t = \Delta t = 0.2$, the velocity field propagates in the entire spatial domain. Upon evolution the velocity field at each spatial location x approaches the fully developed velocity field. From fifth to sixth increment of time the velocity field virtually remains the same at all spatial location indicating the stationary state of the evolution i.e. fully developed velocity field at all spatial locations. Figure 5.3 shows evolution of shear stress τ_{xy} at the same axial location as used for velocity u. Between the fifth and the sixth time steps a linear shear stress distribution (as expected) is obtained at all spatial locations. Figure 5.4 shows evolution of pressure p at $y = 0.0$. At fifth and sixth time steps a linear pressure distribution along the length with $\frac{\partial p}{\partial x} = -0.253$, is obtained.

The choice of $L/H = 15$ is sufficiently large so that regardless of the specific description of the applied inlet velocity, the fully developed conditions are ensured at the outflow boundary. To demonstrate this point and to illustrate the time accuracy of the evolution we present next study in which L is increased to 20 with spatial discretization in the x direction containing 96 elements while discretization in y direction is kept same as in case of $L = 15$. Figure 5.5 shows evolutions of axial velocity u and shear stress τ_{xy} at $x = 1.2$ and $x = 15.0$ for first two increments of time and a comparison with the

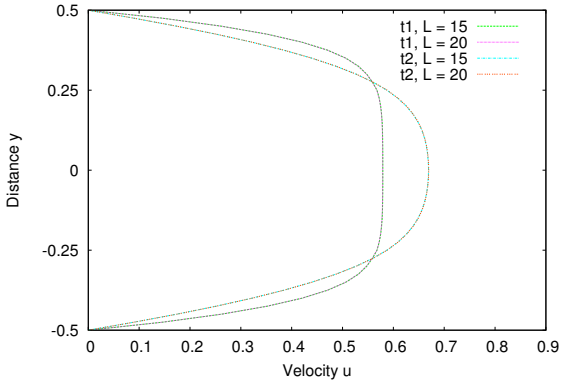

(a) Velocity u versus y at $x = 1.2$

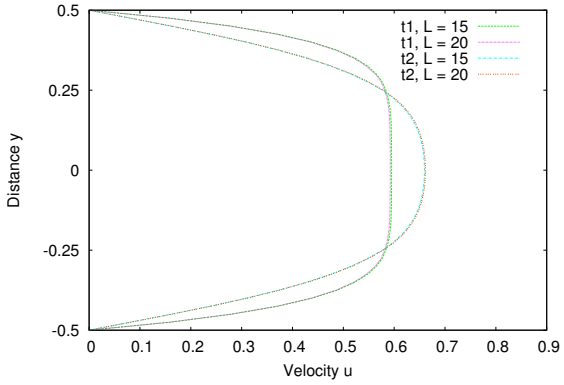

(b) Velocity u versus y at $x = 15.0$

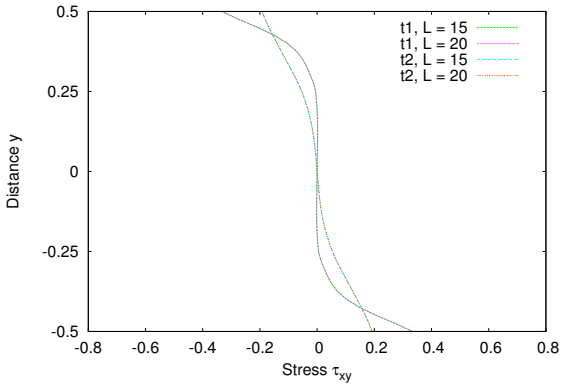

(c) Stress τ_{xy} versus distance y at $x = 1.2$

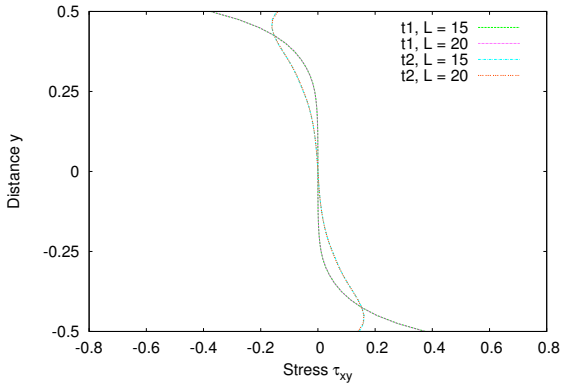

(d) Stress τ_{xy} versus distance y at $x = 15.0$

Figure 5.5: Flow between parallel plates, evolution of velocity u and stress τ_{xy}: Newtonian fluid, $L = 15$ and $L = 20$

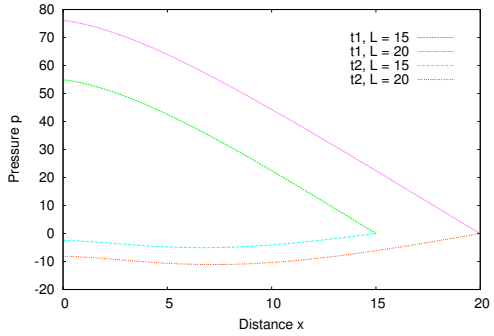

Pressure p versus distance x at $y = 0.0$

Figure 5.6: Flow between parallel plates, evolution of pressure p: Newtonian fluid, $L = 15$ and $L = 20$

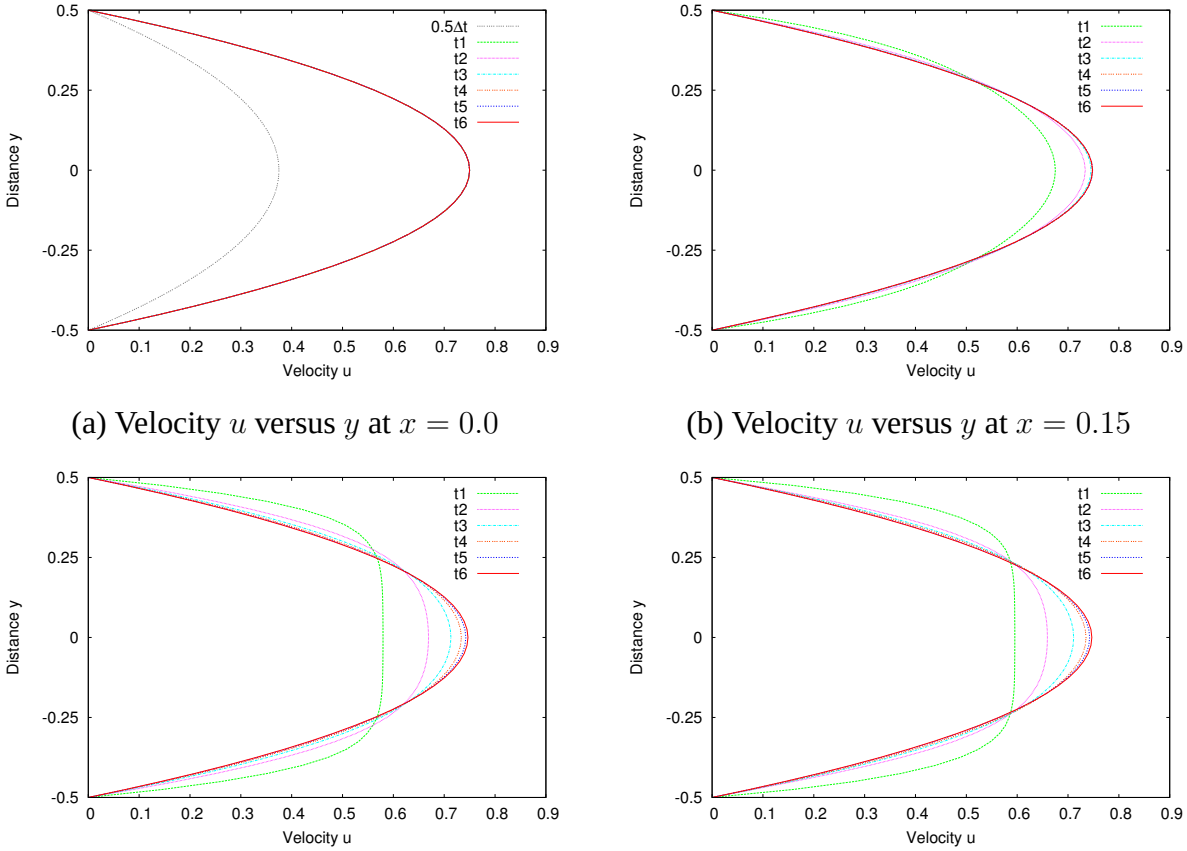

(a) Velocity u versus y at $x = 0.0$

(b) Velocity u versus y at $x = 0.15$

(c) Velocity u versus y at $x = 1.2$

(d) Velocity u versus y at $x = 15.0$

Figure 5.7: Flow between parallel plates, evolution of velocity u: Newtonian fluid, case (b): $p = 0$ at inlet boundary

results from the study with $L = 15$. The results for the two values of L match perfectly confirming that increasing L to 20 has no effect on the deformation field in the domain $0 \leq x \leq 15$. Figure 5.6 shows pressure distribution along length L at $y = 0$ for $L = 15$ and $L = 20$ for the first two increments of time. $\frac{\partial p}{\partial x}$ is identical for both choices of L for each of the two time increments.

Case (b): pressure $p = 0$ at the inlet boundary

In this study we choose $L = 15$ but specify the pressure boundary condition $p = 0$

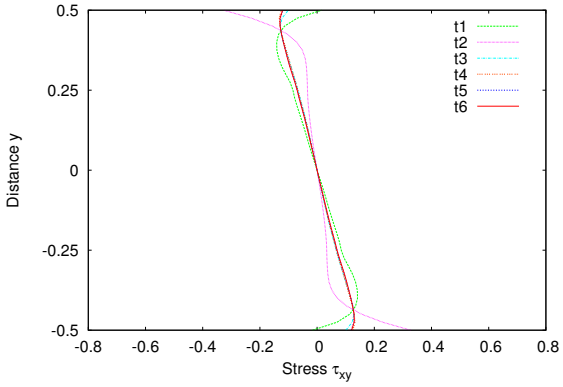

(a) Stress τ_{xy} versus distance y at $x = 0.0$

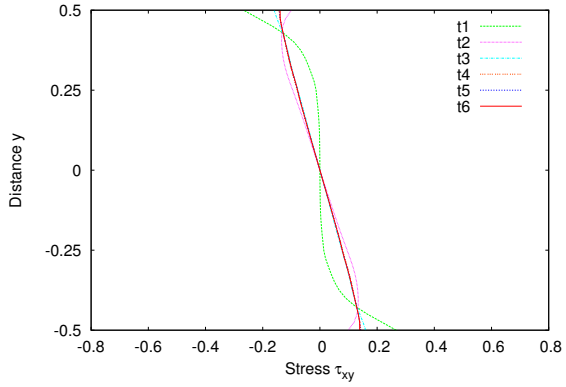

(b) Stress τ_{xy} versus distance y at $x = 0.15$

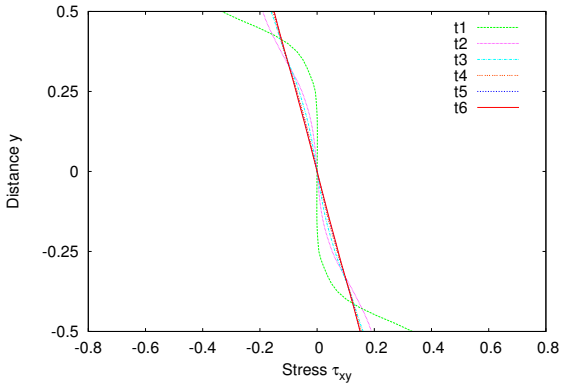

(c) Stress τ_{xy} versus distance y at $x = 1.2$

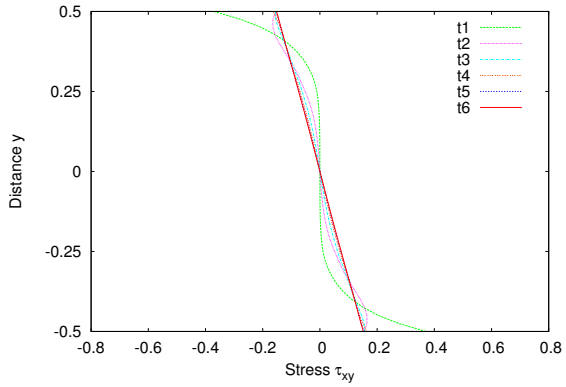

(d) Stress τ_{xy} versus distance y at $x = 15.0$

Figure 5.8: Flow between parallel plates, evolution of stress τ_{xy}: Newtonian fluid, case (b): $p = 0$ at inlet boundary

at the inlet instead of outflow boundary (as in case (a)). The purpose of this study is to demonstrate that since pressure is not deterministic from the deformation field, its specification at either of two open boundaries (i.e. inlet or outflow) is admissible without influencing the resulting deformation field. Figures 5.7 and 5.8 show axial velocity u and shear stress τ_{xy} as a function of y at $x = 0.0, 0.15, 1.2$ and 15.0 for first six increments of time. These are identical to those for case (a) in which the pressure boundary condition $p = 0$ is applied at the outflow boundary. Figure 5.9 shows evolution pressure p versus x at $y = 0.0$ for first six increments of time. We note that $\frac{\partial p}{\partial x} = -0.253$ (when stationary state of the evolution is reached), same as case (a).

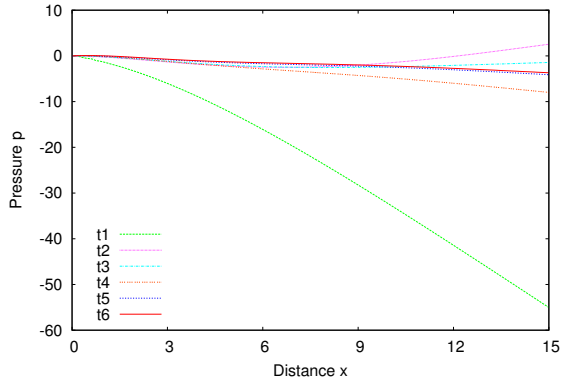

Pressure p versus distance x at $y = 0$

Figure 5.9: Flow between parallel plates, evolution of pressure p: Newtonian fluid, case (b): $p = 0$ at inlet boundary

5.6.1.2 Maxwell fluid

In this study we consider Maxwell fluid with the following properties [64]. All other details of the discretization, p-level, the orders of the approximation space and inlet velocity specification remain the same as in case of Newtonian fluid.

Maxwell fluid properties:

$\hat{\rho} = 868\ kg/m^3,\ \hat{\eta}_s = 2.7Pa\ s,\ \hat{\eta}_p = 0.3Pa\ s,\ \lambda = 0.1s$

The following reference quantities are used :

$\rho_0 = \hat{\rho} = 868\ kg/m^3,\ L_0 = 0.2\ m\ ,\ v_0 = 0.2\ m/s,\ \eta_0 = 3.0Pa\ s$

For this choice of reference quantities, we have

$\rho_0 {v_0}^2 = 34.72\ Pa,\ \frac{\eta_0 v_0}{L_0} = 3\ Pa,\ Re = 11.573,\ De = 0.1,\ t_0 = \frac{L_0}{v_0} = 1\ s.$

Therefore we choose $p_0 = \tau_0 = \rho_0 {v_0}^2 = 34.72\ Pa$.

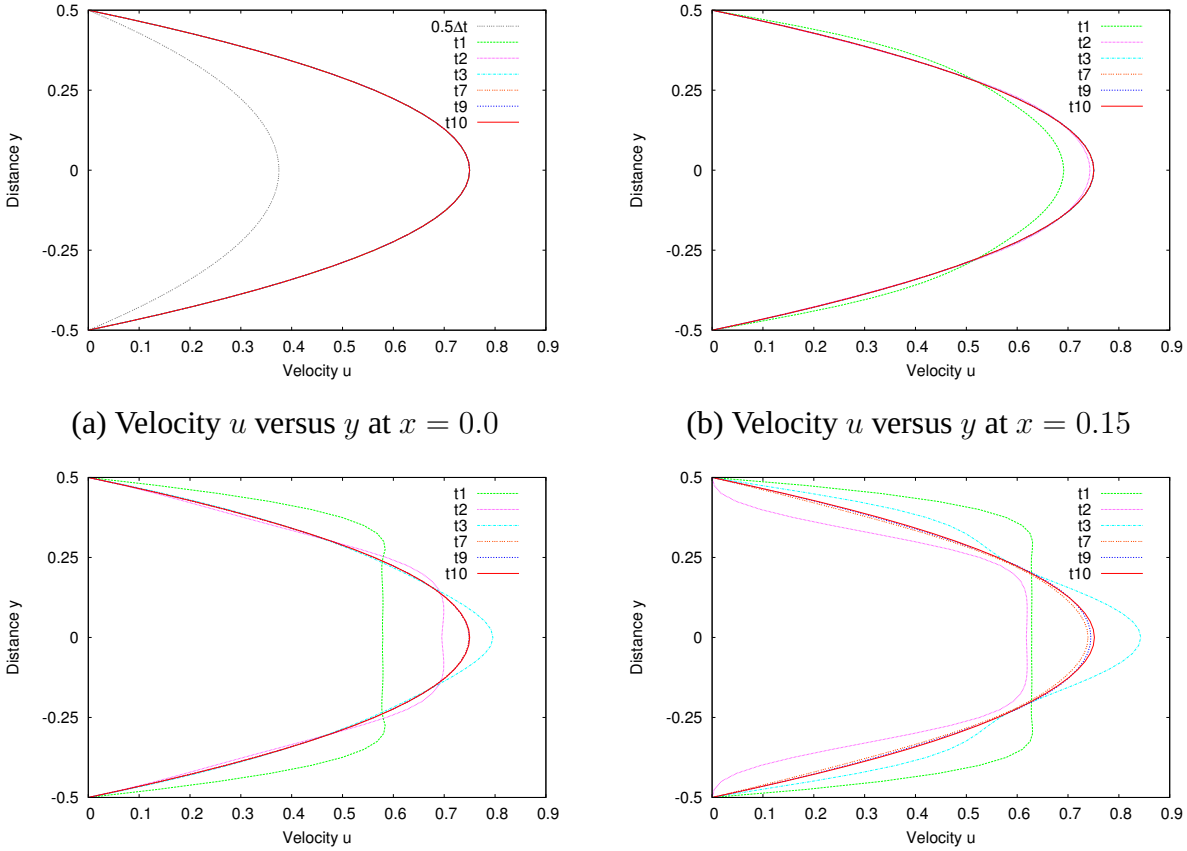

(a) Velocity u versus y at $x = 0.0$

(b) Velocity u versus y at $x = 0.15$

(c) Velocity u versus y at $x = 1.2$

(d) Velocity u versus y at $x = 15.0$

Figure 5.10: Flow between parallel plates, evolution of velocity u: Maxwell fluid: $p = 0$ at outflow boundary

We choose $L = 15$ and use the same discretization, p-levels of 5 and $\Delta t = 0.2$ as used in case of Newtonian fluid (section 5.6.1.1 case (a)). Values of I, $|g_i|_{\max}$, number of iterations for Newton's linear method with line search are all comparable to the Newtonian fluid study. In this study we consider pressure boundary condition $p = 0$ at the outflow boundary BD. Figures 5.10- 5.12 show evolution of axial velocity u, normal stress τ_{xx} and shear stress τ_{xy} at spatial locations $x = 0.0, 0.15, 1.2$ and 15.0 for time steps $1, 2, 3, 7, 9, 10$. At the end of the first time step the velocity field propages in the entire spatial domain (as expected due to incompressibility of the medium). As evolution proceeds the velocity field and the stress field at all spatial locations approach

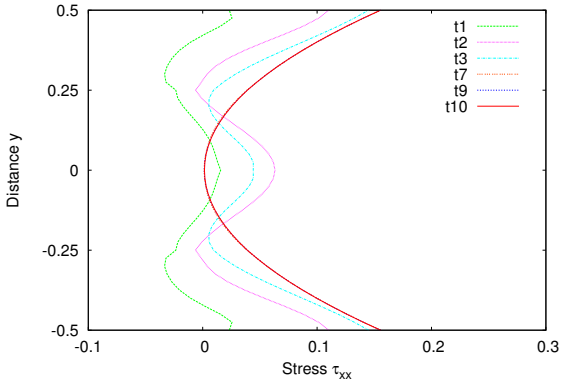

(a) Stress τ_{xx} versus distance y at $x = 0.0$

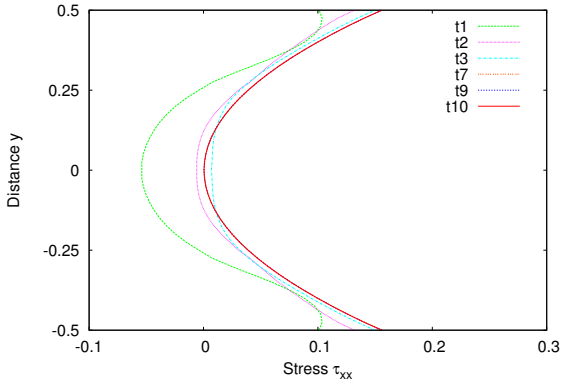

(b) Stress τ_{xx} versus distance y at $x = 0.15$

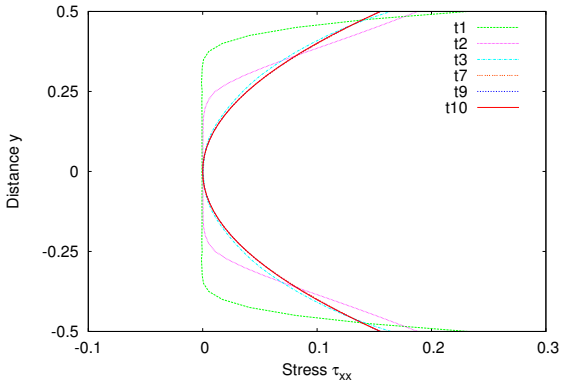

(c) Stress τ_{xx} versus distance y at $x = 1.2$

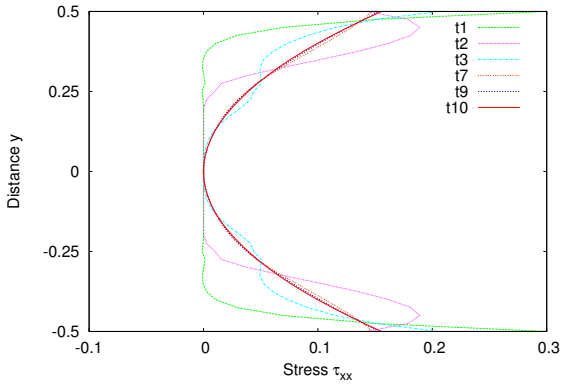

(d) Stress τ_{xx} versus distance y at $x = 15.0$

Figure 5.11: Flow between parallel plates, evolution of stress τ_{xx}: Maxwell fluid: $p = 0$ at outflow boundary

fully developed condition. Between time steps 9 and 10 the evolution at each spatial locations are virtually unchanged. Evolution of the pressure along the length at $y = 0$ is shown in figure 5.13. At time step 10 we have linear pressure distribution (as expected) with constant $\frac{\partial p}{\partial x} = -0.493$.

5.6.2 Transient developing flow over a 1:2 backward facing step

In this section we consider time dependent flows of Newtonian and Maxwell fluids over a 1:2 backward facing step. Schematic, dimensions and the boundary conditions are shown in figure 5.14. The choice of $L_2/H_2 = 15$ ensures that for the Reynolds

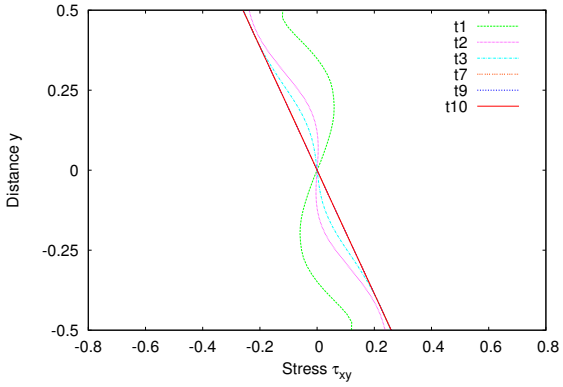

(a) Stress τ_{xy} versus distance y at $x = 0.0$

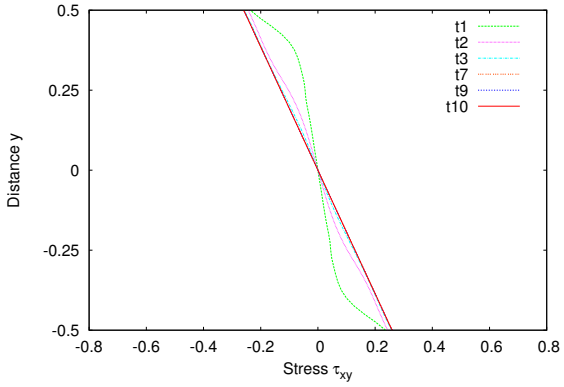

(b) Stress τ_{xy} versus distance y at $x = 0.15$

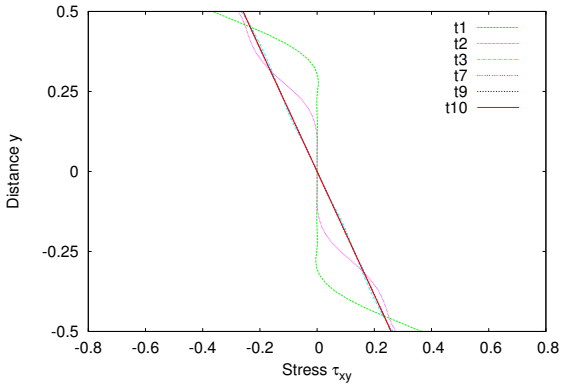

(c) Stress τ_{xy} versus distance y at $x = 1.2$

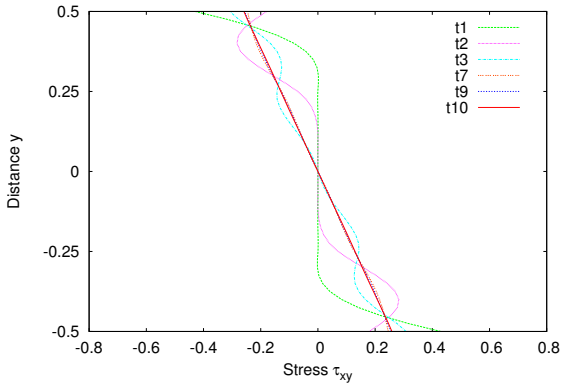

(d) Stress τ_{xy} versus distance y at $x = 15.0$

Figure 5.12: Flow between parallel plates, evolution of stress τ_{xy}: Maxwell fluid: $p = 0$ at outflow boundary

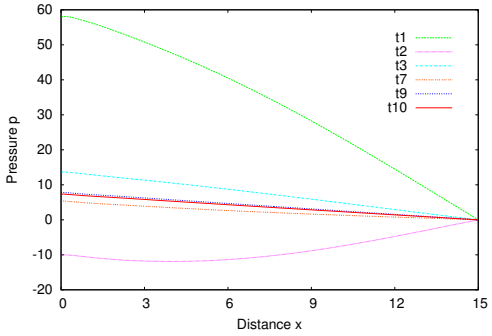

Pressure p versus distance x at $y = 0$

Figure 5.13: Flow between parallel plates, evolution of pressure p: Maxwell fluid: $p = 0$ at outflow boundary

number used in this study the flow would be fully developed at the outflow boundary BC. Hence $v = 0$ and $\frac{\partial v}{\partial y} = 0$ hold at outflow boundary BC. Additionally $p = 0$ (implying $\frac{\partial p}{\partial y} = 0$) is imposed at the outflow boundary (based on the studies for flow between parallel plate).

Following the developing flow between parallel plates, here also we define the inlet velocity at oA or (AF) using

$$\begin{aligned} u(t) &= (\frac{3}{\Delta t^2} u_{\Delta t}) t^2 - (\frac{2}{\Delta t^3} u_{\Delta t}) t^3 \quad ; \quad 0 \leq t \leq \Delta t \\ u(t) &= u_{\Delta t} \quad ; \quad t \geq \Delta t \end{aligned} \tag{5.35}$$

where $u_{\Delta t} = 24y(0.5 - y)$, $u_{\Delta t}$ being fully developed velocity for flow between parallel plates seperated by H_1. Additionally, we also specify $v = 0$ at the inlet oA or (AF). Clearly the velocity field (5.35) describes a continuously increasing flow rate for $0 \leq t \leq \Delta t$ at inlet that reaches a steady value at $t = \Delta t$ and thereafter remains constant.

The initial velocity field is set to $u = v = 0$ everywhere in the computational domain. Details of the graded spatial discretization are shown in Table 5.1. h_x and h_y in table 5.1 refer to element length in x and y spatial directions.

Table 5.1: Spatial discretization for flow over a 1:2 backward facing step

Edge FE (h_x)	3.0	1.6	0.398	0.002		
Edge AF (h_y)	0.25	0.25				
Edge DC (h_x)	0.001	0.004	0.04	0.2	0.755	15 of 0.933
Edge ED (h_y)	0.25	0.25				

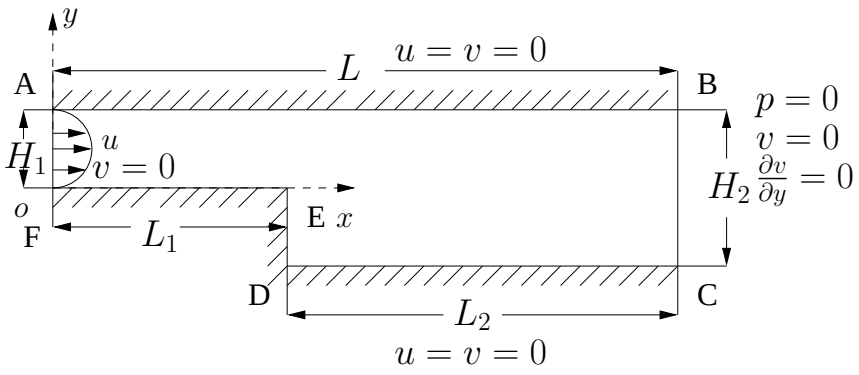

Figure 5.14: Developing flow over a 1:2 backward facing step

In all numerical studies we choose uniform p- level of 5 in spatial directions and time for all 27-node space-time elements of the space-time slab. Evolutions are computed using $\Delta t = 0.2$ with time marching. Details of I, $|g_i|_{\max}$, Δ and Newton's linear method with line search are parallel to those presented for flow between parallel plates and hence not repeated here.

5.6.2.1 Newtonian fluid

We use the same medium as in case of parallel plate with same properties, reference quantities and the dimensionless variables (see section 5.6.1.1). Evolution is computed for six time steps using space-time slab with time marching using constant $\Delta t = 0.2$ and uniform p-level of five. We discuss the results in the following.

Evolutions of the axial velocity field u and stress τ_{xy} at spatial locations $x = 0.0, 5.0,$ $5.205, 5.547, 6.0$ and 20.0 for six time steps are shown in figures 5.15 and 5.16. Figure 5.17 shows evolutions of pressure p along the length at spatial locations $y = 0.25$ and -0.25. Spatial locations in the x direction used in figures 5.15 and 5.16 are chosen to show the progression of the evolution of the velocity field from fully developed at inlet to the fully developed velocity field at the outflow boundary. In figure 5.15(b) at

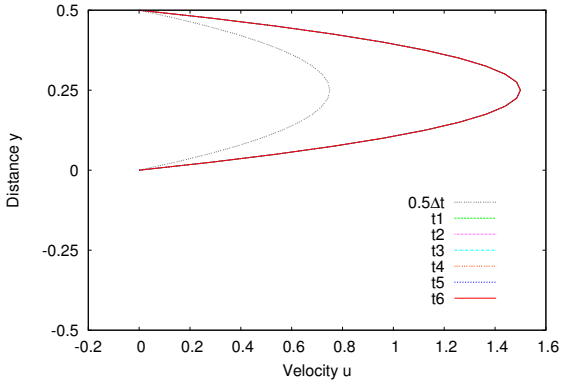

(a) Velocity u versus distance y at $x = 0.0$

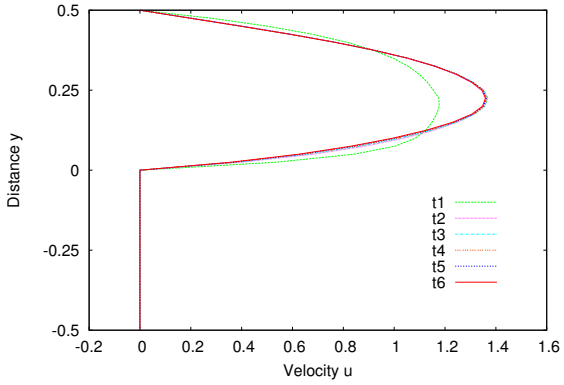

(b) Velocity u versus distance y at $x = 5.0$

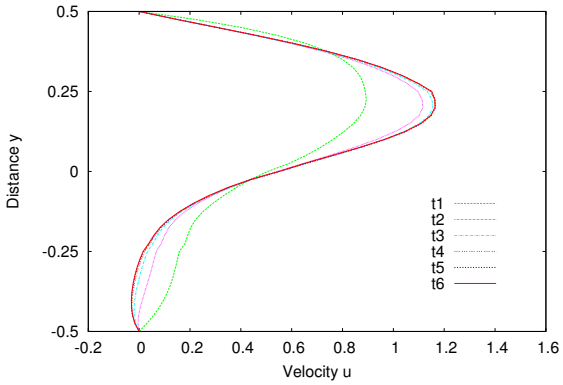

(c) Velocity u versus distance y at $x = 5.205$

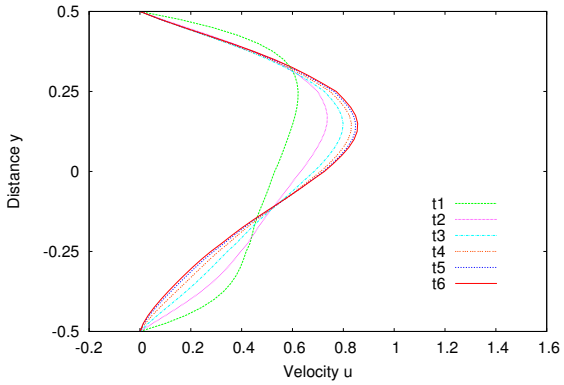

(d) Velocity u versus distance y at $x = 5.547$

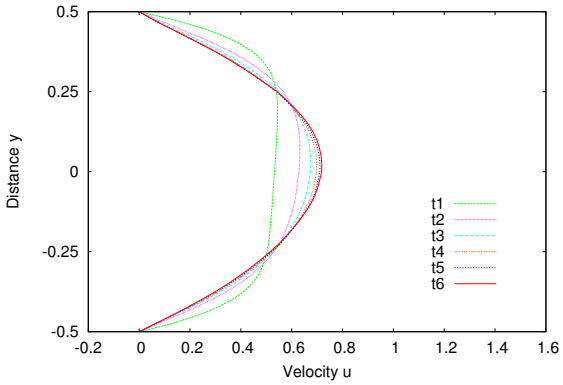

(e) Velocity u versus distance y at $x = 6.0$

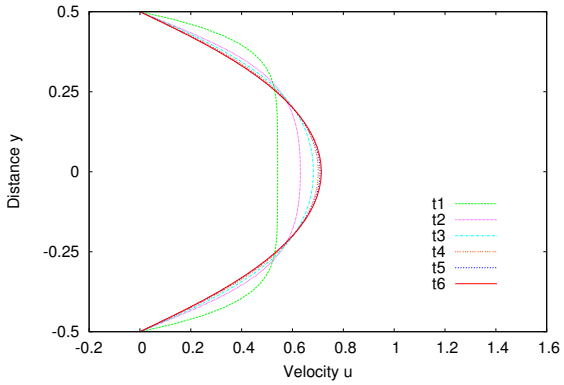

(f) Velocity u versus distance y at $x = 20.0$

Figure 5.15: Flow over backward facing step, evolution of velocity u: Newtonian fluid

$x = 5.0$, we observe similar fully developed velocity field at second time step and beyond as inlet velocity but with different peak value than that at the inlet. Figures 5.15(c)

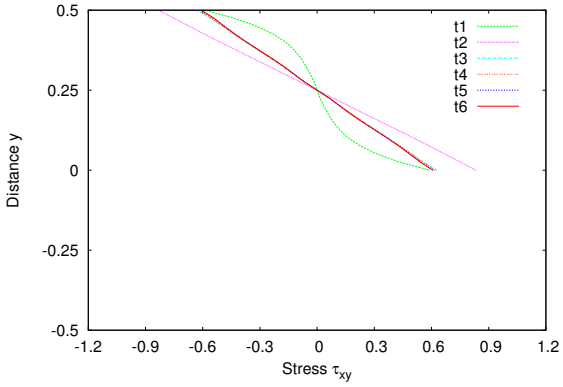

(a) Stress τ_{xy} versus distance y at $x = 0.0$

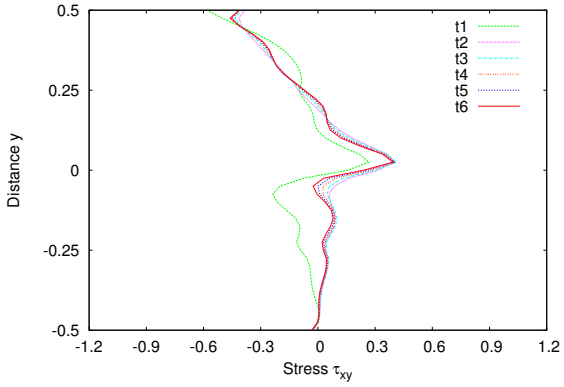

(b) Stress τ_{xy} versus distance y at $x = 5.0$

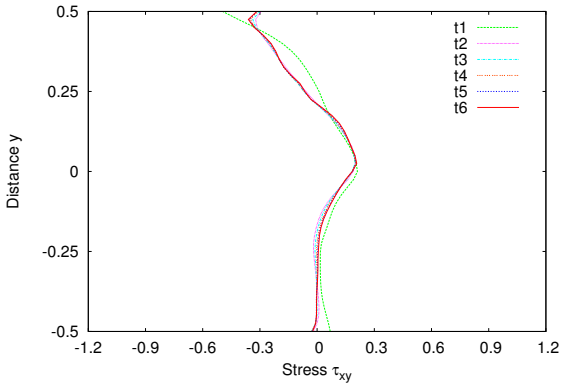

(c) Stress τ_{xy} versus distance y at $x = 5.205$

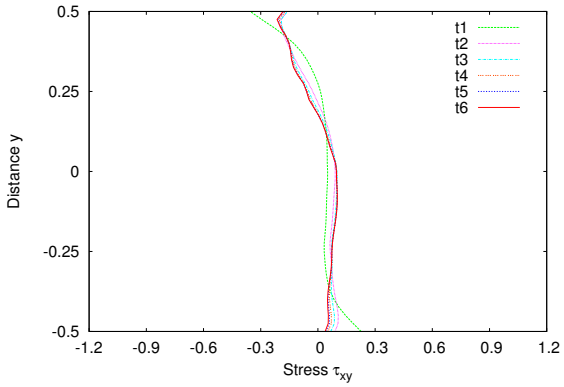

(d) Stress τ_{xy} versus distance y at $x = 5.547$

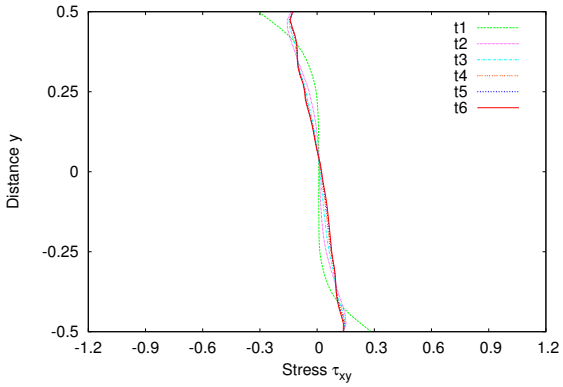

(e) Stress τ_{xy} versus distance y at $x = 6.0$

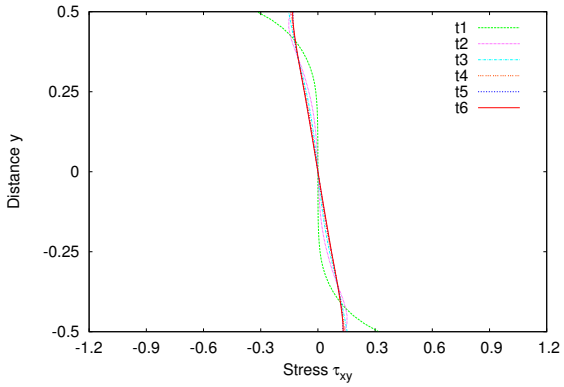

(f) Stress τ_{xy} versus distance y at $x = 20.0$

Figure 5.16: Flow over backward facing step, evolution of stress τ_{xy}: Newtonian fluid

and (d) show intermediate stages of the velocity fields from the two fully developed stages at inflow and outflow boundaries. At $x = 6.0$ (in figure 5.15(e)) the velocity

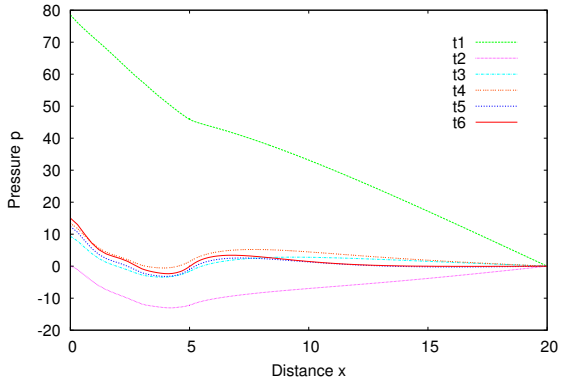

(a) Pressure p versus distance x at $y = 0.25$

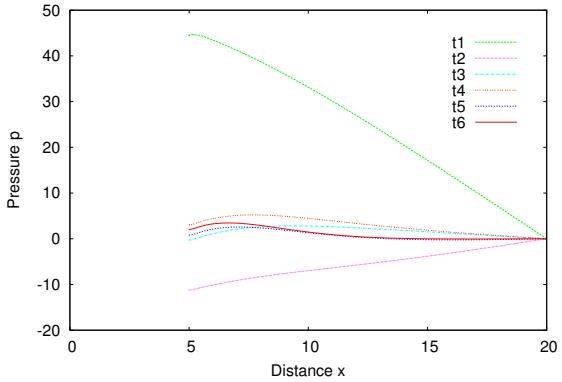

(b) Pressure p versus distance x at $y = -0.25$

Figure 5.17: Flow over backward facing step, evolution of pressure p: Newtonian fluid

field is almost same as at the outflow boundary. In figure 5.15(c), we observe negative velocity field at the stationary state in the portion of the y domain due to recirculation. Evolution of velocity at all x locations for time step five and six are almost identical confirming that the stationary state of the evolution has been reached at all spatial locations (x-locations). The residual functional I varies from $o(10^{-3})$ to $o(10^{-5})$ from the first time step to the sixth time step indicating that the evolution for the first time step is perhaps not good enough to claim time accuracy but the accuracy of the evolution improves with elapsing time. Evolution remains bounded and it is computed in a straight forward manner without using any other artificial means. The stationary state of the evolution is predicated quite accurately.

From figure 5.16(a), we observe fully developed linear τ_{xy} between fifth and sixth time steps at $x = 0$. We observe the same at $x = 6.0$ and $x = 20$ but with different slope due to $H_2 = 2H_1$. At other x locations time steps 5 and 6 confirm stationary state of τ_{xy} as well. Evolution of pressure shown in figure 5.17 also confirm stationary state of the evolution between fifth and sixth increments of time. Contours (carpet plots) of velocities u and v in the vicinity of the step presented in figures 5.18(a) and (b) show

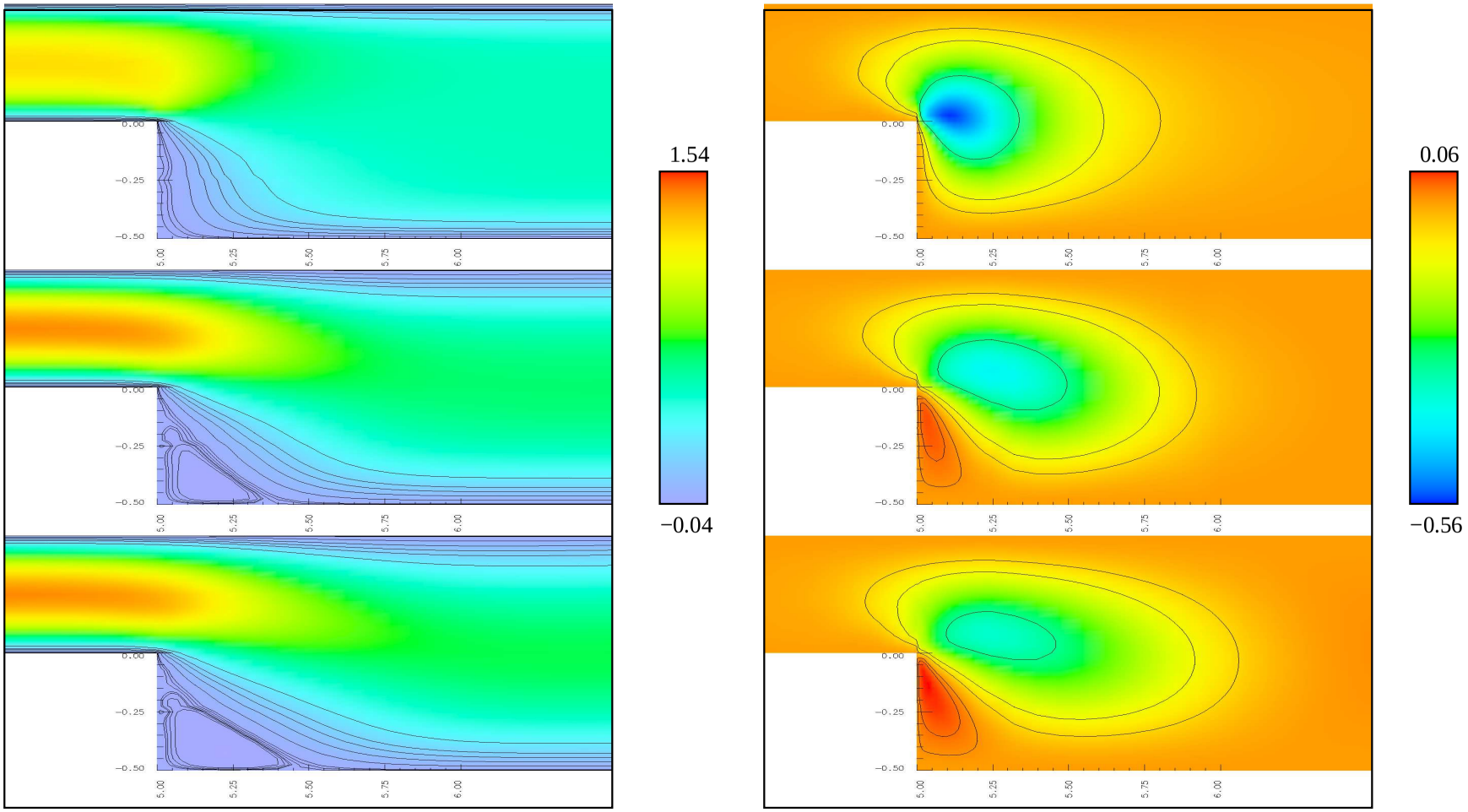

(a) Evolution of velocity u : Newtonian fluid

(b) Evolution of velocity v : Newtonian fluid

Figure 5.18: Flow over backward facing step, evolution of velocities u and v at the first, third and sixth time steps: Newtonian fluid

evolution of the recirculation zone and the evolution of the velocity field u and v at the corner for first, third and six time steps. In figures 5.18(a), we note that at the end of the first time there is no recirculation. The formation of the recirculation zone begins at the end of first time step. At the end of third time step we observe recirculation zone of substantial size. At sixth time step (stationary state) the length of the recirculation zone is 0.5 units (figures 5.18(a)).

5.6.2.2 Maxwell fluid

In this study also we use the same fluid, reference quantities, dimensionless variables and inlet velocity specification as used in case of flow of Maxwell fluid between parallel plates (section 5.6.1.2). Evolution is computed for ten time steps using space-time slab with time marching using constant $\Delta t = 0.2$ and uniform p-level of five. We present and discuss the results in the following. Figures 5.19- 5.21 show evolution of axial velocity u, axial stress τ_{xx} and shear stress τ_{xy} at axial location $x = 0.0, 5.0, 5.125, 5.205, 6.0$ and 20.0. Figure 5.22 shows evolution of pressure p along the length at spatial locations $y = 0.25$ and -0.25. The reason for choosing these spatial x-locations is exactly same as explained in case of Newtonian fluid. At $x = 5.0$ (figure 5.19(b)) velocity u at the tenth time step is converged to stationary state and is similar to inlet velocity but with a different peak value. Figures 5.19(b) and (c) show evolution of the intermediate velocity stages to stationary state at the tenth time step. At $x = 6.0$ the stationary state is almost same as the fully developed velocity field at the outflow boundary. In figures 5.19(c) and (d), we observe negative velocity field at the stationary state in the portion of the y-domains due to recirculation. The evolution of velocity u between ninth and tenth time step are almost identical confirming that a stationary state has been reached. Evolution of stress τ_{xx} shown in figure 5.20 clearly shows that τ_{xx} at ninth and tenth time step at each spatial (x-location) location are in

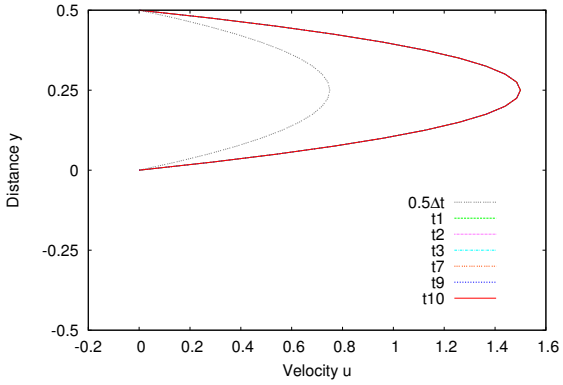

(a) Velocity u versus distance y at $x = 0.0$

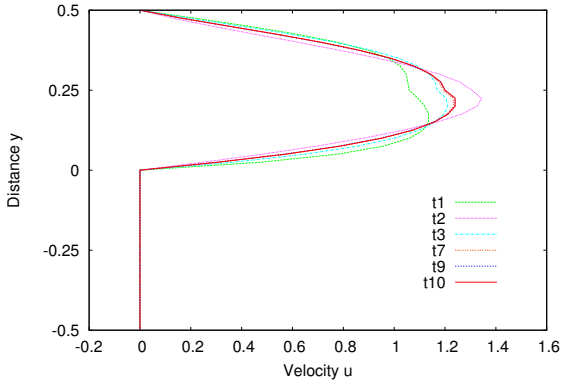

(b) Velocity u versus distance y at $x = 5.0$

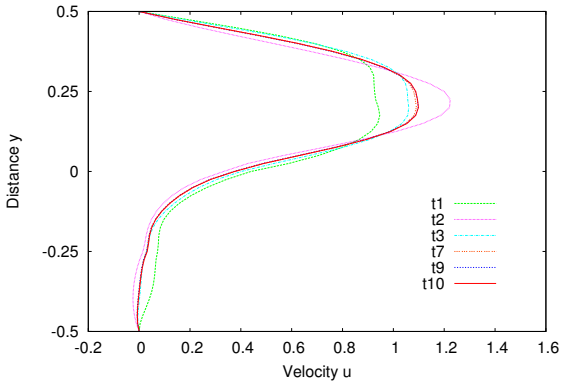

(c) Velocity u versus distance y at $x = 5.125$

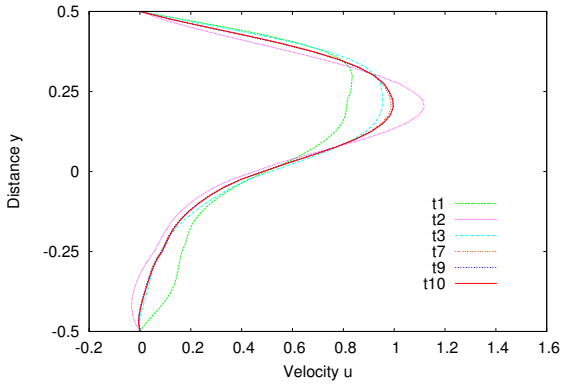

(d) Velocity u versus distance y at $x = 5.205$

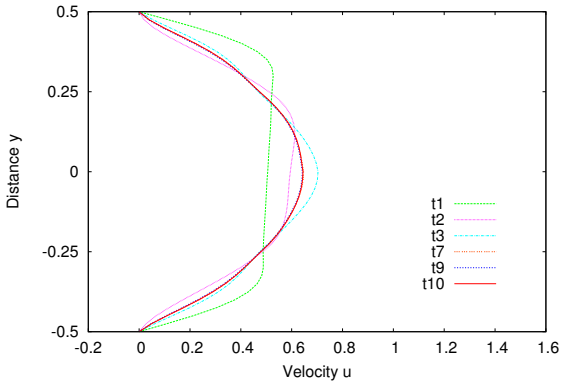

(e) Velocity u versus distance y at $x = 6.0$

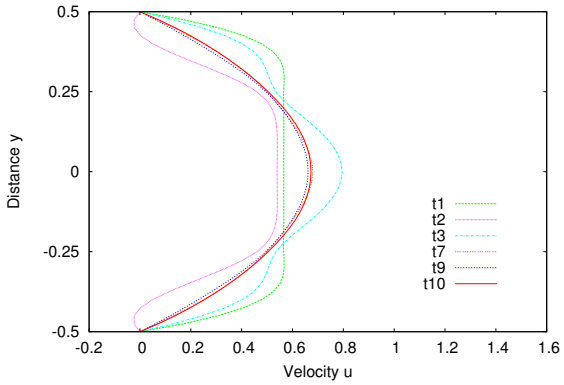

(f) Velocity u versus distance y at $x = 20.0$

Figure 5.19: Flow over backward facing step, evolution of velocity u: Maxwell fluid

very good agreement. Evolution of τ_{xy} in figure 5.21 clearly shows linear τ_{xy} profile at $x = 0.0, 6.0$ and 20.0 with correct slopes based on H_1 and H_2. Stationary state of τ_{xy}

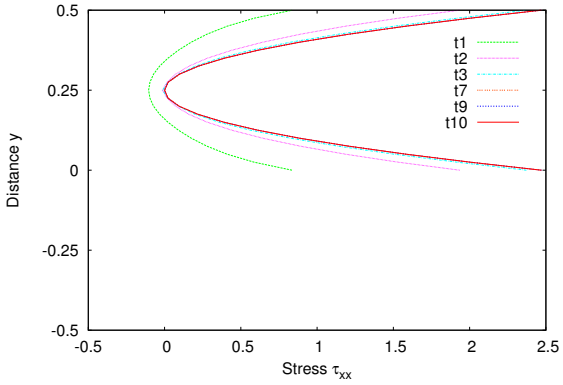

(a) Stress τ_{xx} versus distance y at $x = 0.0$

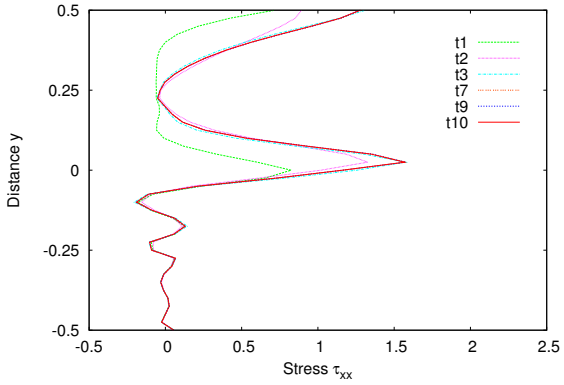

(b) Stress τ_{xx} versus distance y at $x = 5.0$

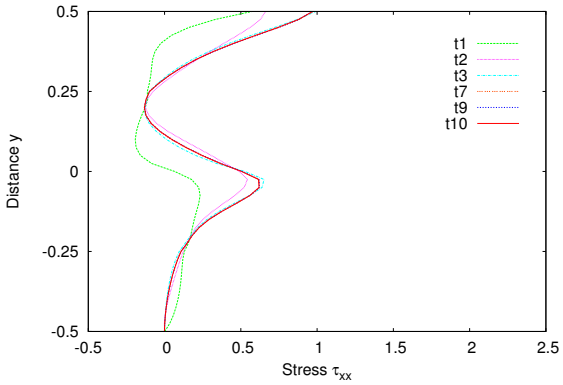

(c) Stress τ_{xx} versus distance y at $x = 5.125$

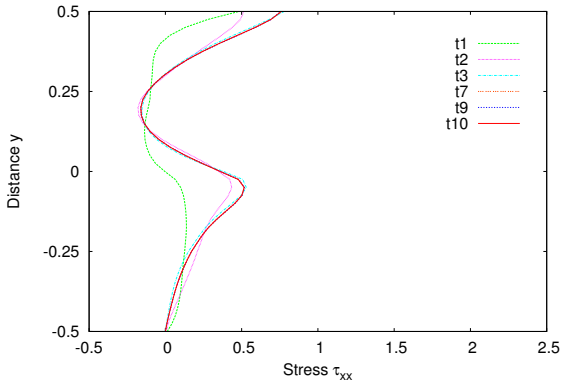

(d) Stress τ_{xx} versus distance y at $x = 5.205$

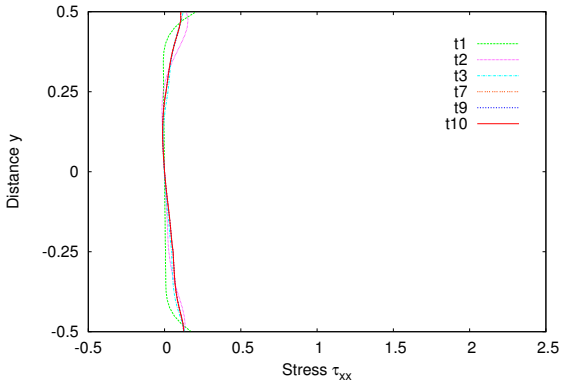

(e) Stress τ_{xx} versus distance y at $x = 6.0$

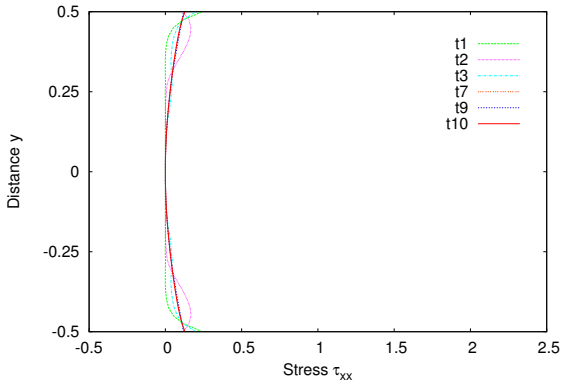

(f) Stress τ_{xx} versus distance y at $x = 20.0$

Figure 5.20: Flow over backward facing step, evolution of stress τ_{xx}: Maxwell fluid

at ninth and tenth time increments is clearly observed. Evolution of the pressure field shown in figure 5.22 also confirm stationary state at ninth and tenth time steps. Con-

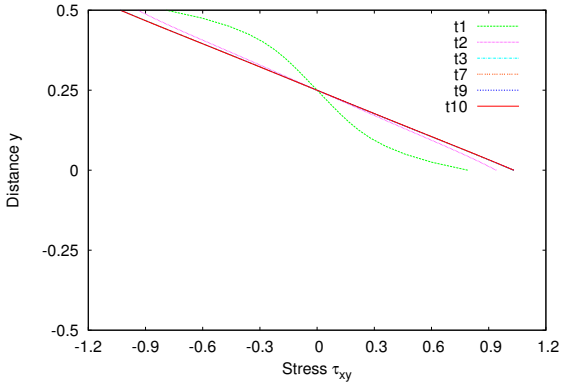

(a) Stress τ_{xy} versus distance y at $x = 0.0$

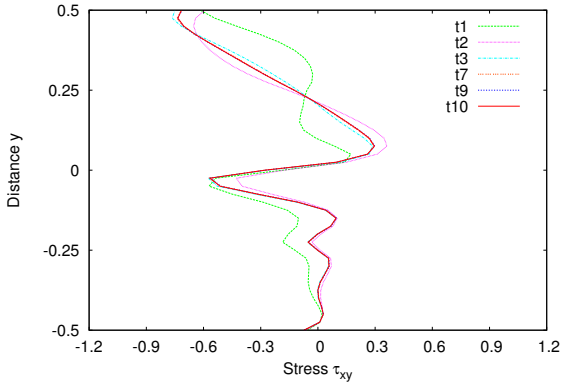

(b) Stress τ_{xy} versus distance y at $x = 5.0$

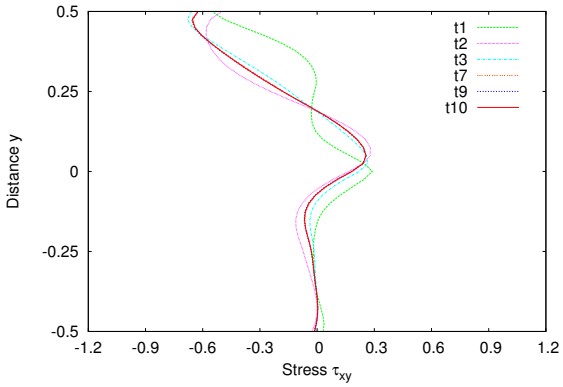

(c) Stress τ_{xy} versus distance y at $x = 5.125$

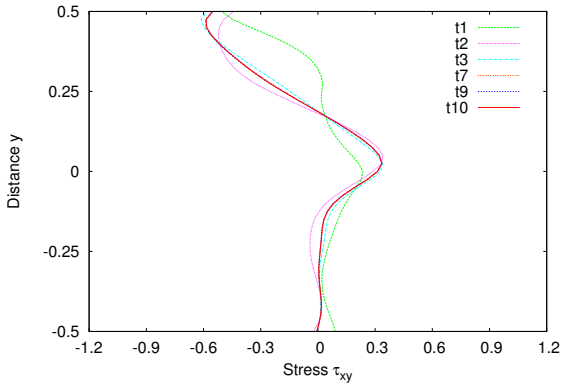

(d) Stress τ_{xy} versus distance y at $x = 5.205$

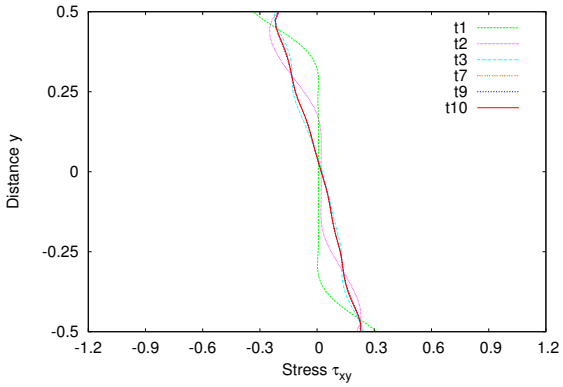

(e) Stress τ_{xy} versus distance y at $x = 6.0$

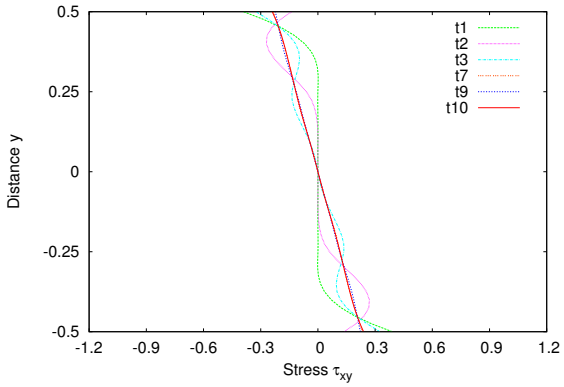

(f) Stress τ_{xy} versus distance y at $x = 20.0$

Figure 5.21: Flow over backward facing step, evolution of stress τ_{xy}: Maxwell fluid

tours (carpet plots) of velocities u and v in the vicinity of the step in figures 5.23(a) and (b) show evolution of the recirculation zone and the evolution of the velocity v around

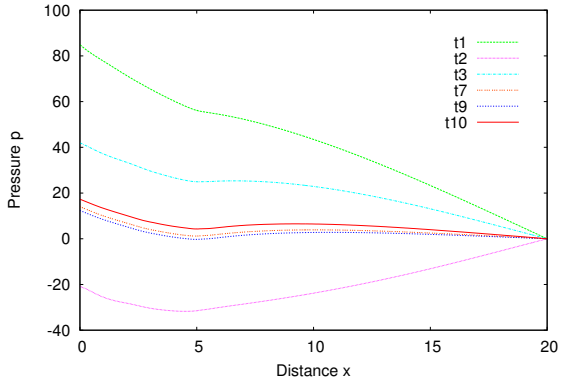

(a) Pressure p versus distance x at $y = 0.25$

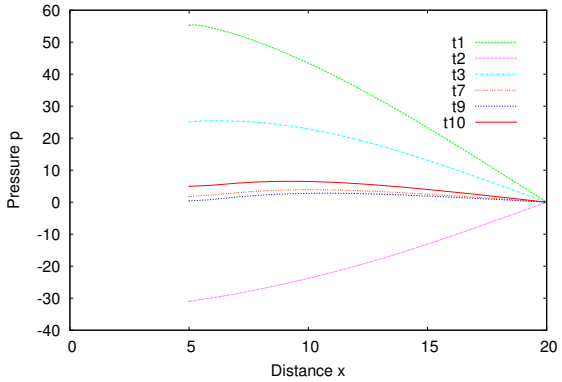

(b) Pressure p versus distance x at $y = -0.25$

Figure 5.22: Flow over backward facing step, evolution of pressure p: Maxwell fluid

the corner for first, fifth and tenth time steps. Just as in case of Newtonian fluid, here also we note the absence of recirculation at the end of first time step. But its substantial size is at the end of fifth time step. At tenth time step (stationary state) the length of recirculation zone is 0.3 units.

5.6.3 Remark on the numerical studies

The numerical studies presented in the section are designed to illustrate several significant points for time dependent flows of incompressible Newtonian and Maxwell fluids in open domains.

(1) The numerical studies presented for flow of Newtonian fluid between parallel plates clearly show that specification of pressure boundary conditions at inlet or outflow boundary is irrelevant as long as it specified at one of the open boundaries. This makes the pressure field deterministic regardless of the deformation field, an essential requirement based on the derivation of the constitutive equations using second law of thermodynamics. The two numerical studies in which the pressure p specified at outflow or inflow boundaries confirm that the

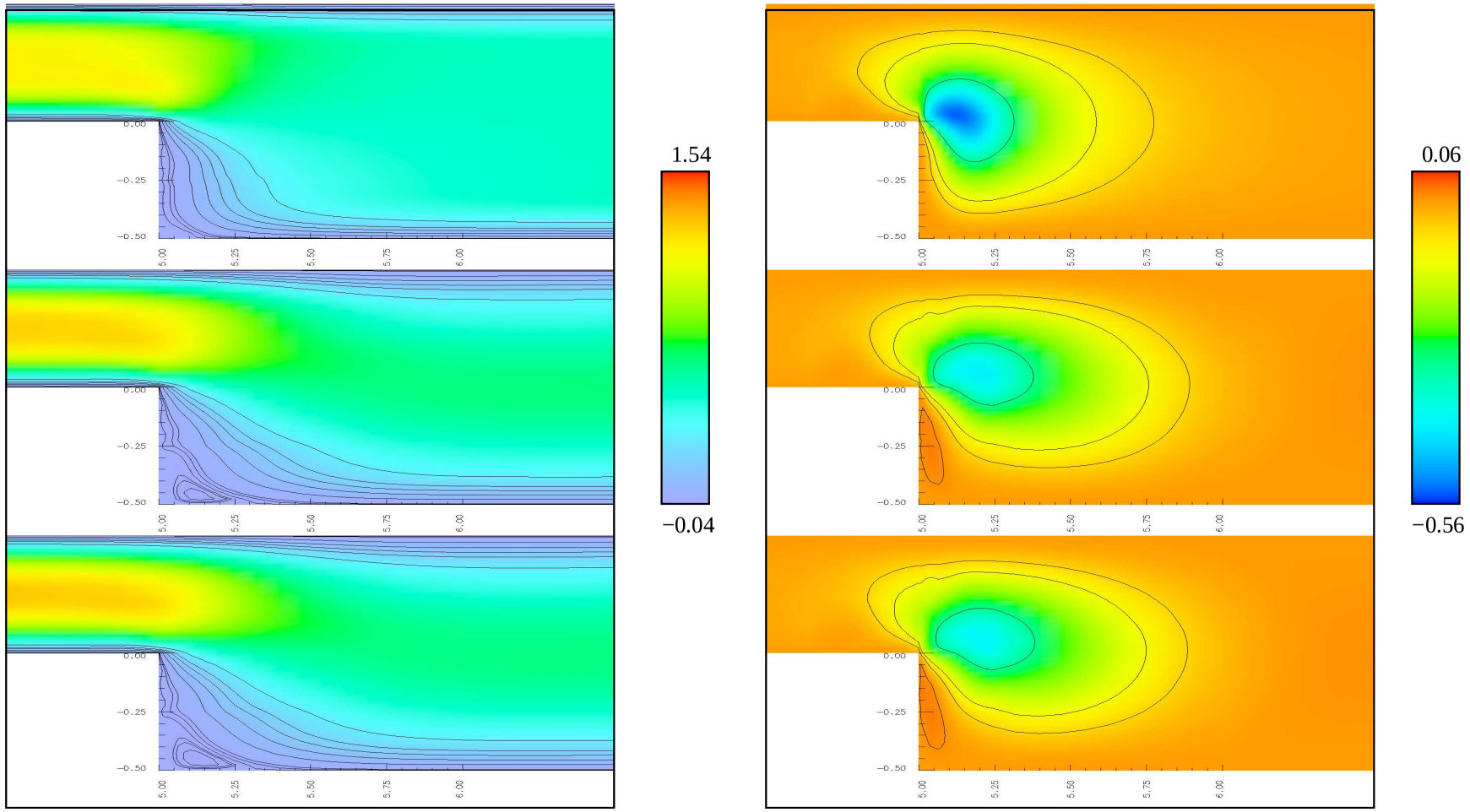

(a) Evolution of velocity u : Maxwell fluid

(b) Evolution of velocity v : Maxwell fluid

Figure 5.23: Flow over backward facing step, evolution of velocities u and v at the first, fifth and tenth time steps: Maxwell fluid

kinematic of the fluid flow is not influenced by either of the pressure boundary conditions.

(2) All numerical studies show that the speed of wave propagation is infinity in all cases due to which the applied velocity field at the inflow boundary propagates in the entire spatial domain for the first increment of time. This holds true regardless of the size of time increment. However, this posses no problems or difficulties in computing evolution that remains bounded for the first as well as subsequent increments of time.

(3) In all numerical studies, initially at the commencement of the evolution the fluid is assumed to be at rest i.e. initial solution or velocity field is assumed to be zero in the reference configuration. Newton's linear method with line search has good convergence with this zero initial solution ($3 - 5$ iterations). We remark that the numerical studies presented here are for very low Reynolds number. For such low Reynolds number as used here initial solution of zero is a good starting solution for Newton's linear method. However, this may not hold true for higher Reynolds number flows in which case converged solution at lower Reynolds number can be used as starting solution for Newton's linear method. We have used this procedure successfully.

(4) From the numerical studies presented (as well as other that were conducted but are not included here), it is conclusive that infinite wave speed and specification of initial velocity field have no relationship to each other. Infinite wave speed is a property of incompressibility of the medium while specification of initial solution is a requirement dictated by Newton's linear method (due to small radius of convergence) used for obtaining solution of non-linear algebraic systems.

(5) The section of $L/H = 15$ for parallel plates model problem ensures fully developed flow at the outflow regardless of the nature of the specified inlet velocity field. This is confirmed by increasing L/H to twenty and observing that the flow field for $0 \leq x \leq 15$ remain unaffected between $L/H = 15$ and 20 for all increments of time.

(6) Numerical studies for backward facing step for both Newtonian and Maxwell fluids show progressive evolution of the recirculation zone and the development of the fully developed flow condition past the recirculation zone in just ten increments of time.

(7) We present some discussion and remarks regarding the residual functional values and accuracy of evolution reported for both model problems. We note that continuously increasing flow rate for $0 \leq t \leq \Delta t$ at the inlet (for both model problems) that only reaches a steady value for $t = \Delta t$ and thereafter remains constant produces complex evolution for initial time steps. Thus, (for example) in case of flow between parallel plates, in our view it is not so straight forward to assertain the flow physics created by the varying inlet flow rate. From the velocity profiles for various values of time at different spatial locations one could compute the flow rate and perhaps make some arguments regarding the validity of the computed evolution. The oscillating pressure field during evolution is an indication of the complex flow physics created by varying flow rate at the inlet. The residual functional value of $o(10^{-3})$ for the first time step is an indication that perhaps the evolution for this time step may not be time accurate. However, the good accuracy of the stationary state when I is $o(10^{-5})$ and progressively reducing I values from $o(10^{-3})$ to $o(10^{-5})$ during the evolution leads us to believe that the reported evolutions for the first and subsequent time steps are not entirely

spurious.

(8) It is important to remark that the purpose of these studies is to demonstrate that in case of incompressible flows in open domains bounded evolutions leading to accurate stationary states can be computed in a straight forward manner using present framework without any ad-hoc treatments. The studies presented here clearly demonstrate this. Since the space-time integral forms are STVC, we are assured that if time accurate evolutions are desired, these can be obtained using hp refinements. We have not done so in the present work as this is not our objective.

5.7 Summary

Numerical computations of time accurate evolutions are presented for transient developing flows between parallel plates and 1:2 backward facing step for isothermal, incompressible Newtonian and Maxwell fluids. In all cases bounded evolutions are presented beginning from the commencement of the evolutions until they reach stationary states. The finite element computational framework used for computing evolutions is based on space-time variationally consistent integral forms with local approximation in hpk higher order spaces that ensure unconditionally stable computations during the entire evolution and provide mechanism for error control for each space-time slab. In all numerical studies integrated sum of squares of the residuals from the non-discretized GDEs are of the order of $O(10^{-3})$ to $O(10^{-5})$. The accuracy aspects of the solutions reported here have been discussed in remarks (7) and (8) in section 5.6.3 and hence are not reported.

(i) In all numerical studies we observe that even though initial velocity field in the

reference configuration at the commencement of the evolution is zero, the specified inlet velocity propages in the entire spatial domain during the first time step regardless of the size of the time step. This is obviously due to infinite wave speed in incompressible liquids.

(ii) From the first model problem (flow between parallel plates) with two open boundaries (inlet and outflow), complete specification of pressure is necessary at either of the two so that pressure field is deterministic in the entire domain regardless of the deformation field. Computations show that the deformation field remains unaffected due to pressure boundary condition either at inlet flow or outflow.

(iii) All computations of the evolution are performed without using initial non-zero velocity field. As pointed out in section 5.6, specification of initial velocity field may become necessary for higher Reynolds number due to Newton's linear method that has small radius of convergence. Continuation in Reynolds number is obviously a straight forward strategy to accomplish this. The infinite wave speed and initial solution issues are not related. Clearly infinite wave speed is the physics of incompressible liquids where as initial solution requirement is due to use of a specific method for solving non-linear algebraic equations (Newton's linear method in the present studies).

(iv) The infinite wave speed posses no problems in computing bounded evolutions from the commencement of the evolution till the stationary state is reached.

(v) In all studies stationary states of evolutions are reported that are in excellent agreement with fully developed conditions.

(vi) The work presented here clearly demonstrates that the mathematical and computational methodologies presented and used here permit computations of bounded

evolutions for incompressible flows with open domains from the commencement of the evolution leading to accurate stationary states in a straight forward but mathematically rigorous manner without the use of problem dependent special treatments.

Chapter 6

Multi-media Interaction Processes and Numerical Studies for One Dimensional Interaction IVPs

6.1 Introduction

In the chapter 2 complete development of the mathematical models for incompressible as well as compressible media have been presented. In the present approach, the interaction of different media in an interaction process is inherent in the mathematical model and hence no special treatment is needed at the interfaces between the media. We first consider typical examples of possible interactions of incompressible and compressible media in abstraction but with clarity to illustrate applications of the approach considered here. We consider three distinct categories of the interaction processes : (i) Interactions of compressible media (Fig.6.1(a)); (ii) Interactions of compressible media with incompressible media (Fig.6.1(b), (c)); (iii) Interactions of incompressible media (Fig.6.1(d)-(f)).

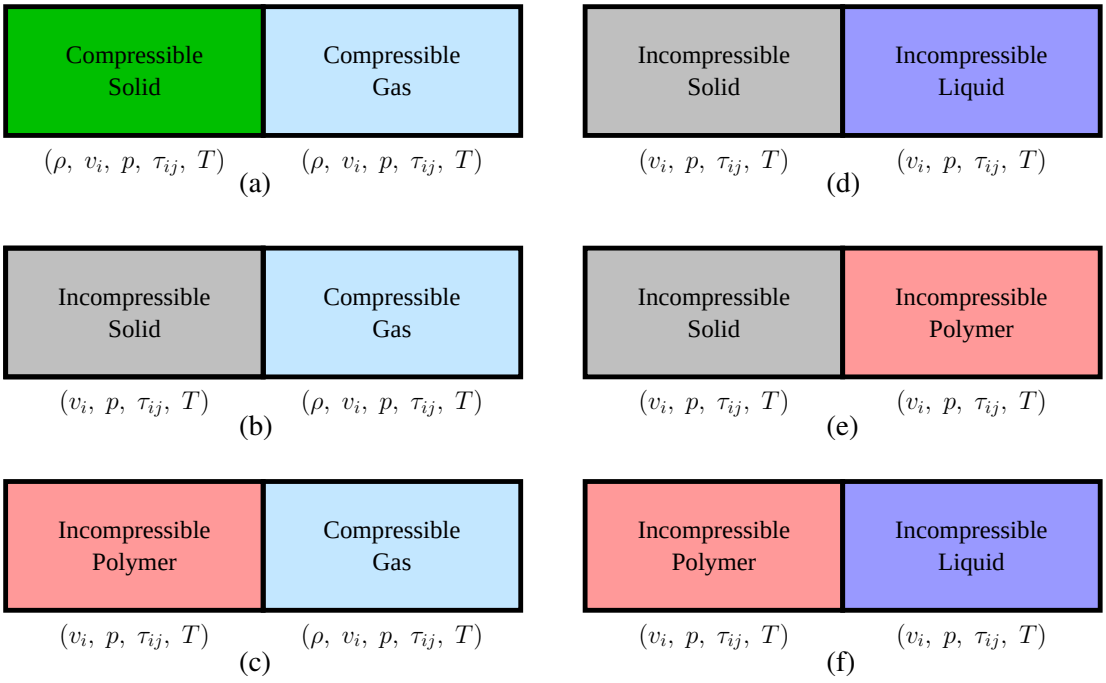

Figure 6.1: Multimedia interaction processes

This is followed by simple one dimensional model problems to demonstrate numerical simulations of multi-media interaction processes in which the interacting media are incompressible elastic solids and incompressible liquids such as Newtonian fluids, generalized Newtonian fluid, dilute polymeric liquids described by Maxwell and Oldroy-B models or dense polymers (polymer melts) with Giesekus constitutive equations. The development of the mathematical model and the computational finite element infrastructure for the initial value problems described by the mathematical models for the media considered in the numerical studies in this chapter have been presented in chapter two and three. In this chapter we borrow the dimensionless forms of the GDEs from chapter 2 and present explicit forms of the mathematical models for each medium that are utilized in the numerical studies. In specific, we consider the dimensionless forms of the mathematical models for purely 1D (axial) behavior of incompressible elastic solids and incompressible fluids. These models are useful in studying propagat-

ing disturbances such as velocity (or stress) waves, their transmission, reflection and subsequent propagations and interactions in the model problems containing bi-material interfaces. In all cases, the evolutions are computed using least squares space-time finite element formulation in hpk framework with a space-time strip and time marching.

6.2 Multi-media Interaction Processes

(i) **Interactions of compressible media:** When all media of a multimedia interaction process are compressible, the mathematical models for all media contain ρ, $\boldsymbol{v}$, p, $\boldsymbol{\tau}$ and T as dependent variables (Fig.6.1(a)). The GDEs resulting from the conservation laws are exactly same for all media but the constitutive equations and the equation of state may be media dependent, nonetheless, these are always defined in terms of the same dependent variables as those used in the GDEs resulting from the conservation laws. Thus, in this category of processes, the interaction is intrinsic in the mathematical model.

(ii) **Interactions of compressible media with incompressible media:** The dependent variables used in the mathematical models for compressible and incompressible media are same in both cases except density ρ (Fig.6.1(b), (c)). For incompressible media ρ = constant, whereas for compressible media $\rho = \rho(x_i, t)$. Thus, at the interface between compressible and incompressible media $\rho =$ constant must hold and must be equal to the density of the incompressible media. This is in agreement with the physics and is confirmed to work quite well in the computational processes. There are no other issues to consider in this category of interaction processes.

(iii) **Interactions of incompressible media:** When all media of an interaction pro-

cess are incompressible (Fig.6.1(d)-(f)), the mathematical models for all media contain $\boldsymbol{v}$, p, $\boldsymbol{\tau}$ and T as dependent variables. The GDEs resulting from the conservation laws are exactly the same for all media but the constitutive equations can be media dependent, but are always expressed in terms of the same dependent variables as used in deriving GDEs from the conservation laws. Thus for such interaction processes, the media interaction is obviously inherent in the mathematical model. For incompressible solid, the use of rate constitutive equations necessitates continuity equation not to be used but instead $\tau_{kk} = 0$ to be used as part of the mathematical model. In applications involving wave propagation, care must be taken for Newtonian and generalized fluids as the speed of the wave propagation in such media is infinity. This difficulty can be overcome by considering the media to be very mildly elastic (Maxwell or Oldroy-B constitutive equations). The other alternative of course is to consider the medium to be mildly compressible. Our experience in working with interaction processes shows the former to be a better alternative. We also remark that the successes of the numerical computations of the evolution for time processes for incompressible viscous liquids that do not have elasticity. Largely may depend upon how the problem is posed in terms of BCs and ICs.

6.3 One Dimensional Interaction Processes

6.3.1 Dimensionless forms of the mathematical models

Details of the derivations of mathematical models for compressible and incompressible matter were presented in chapter 2. In this chapter we describe the explicit forms of the dimensionless forms of the mathematical models for purely 1D behavior (axial)

of incompressible elastic solids and liquids in Eulerian description under isothermal conditions. The emphasis is placed on the explicit forms of the dimensionless forms of the GDEs in the mathematical models that are essential in the computations of the numerical solutions of the associated IVPs.

(a) Incompressible, homogeneous, isotropic hyper-elastic solids

Following the derivation presented in chapter 2, we can write the following dimensionless form of the equations in the mathematical model resulting from momentum, constitutive equations (upper convected rate constitutive equations) and the fact that pressure p is equal to the negative of the mean normal stress.

$$\rho\frac{\partial v_i}{\partial t}+\rho\frac{\partial v_i}{\partial x_j}v_j+(\frac{p_0}{\rho_0{v_0}^2})\frac{\partial p}{\partial x_i}-(\frac{\tau_0}{\rho_0{v_0}^2})\frac{\partial \tau_{ij}}{\partial x_j}-\rho F_i^b=0 \tag{6.1}$$

$$\frac{\partial \boldsymbol{\tau}}{\partial t}+\boldsymbol{v}\cdot(\nabla\boldsymbol{\tau})-\left[(\nabla\boldsymbol{v})^T\cdot\boldsymbol{\tau}+\boldsymbol{\tau}\cdot(\nabla\boldsymbol{v})\right]=(\frac{E_0}{\tau_0})\boldsymbol{\eta\gamma}^{(1)} \tag{6.2}$$

$$\tau_{kk}=0 \tag{6.3}$$

where $F_i^b=(\frac{L_0}{{v_0}^2})\hat{F}_i^b$. Equations (6.1)- (6.3) are a system of ten coupled partial differential equations in ten variables: v_i, p and τ_{ij} and hence, have closure. Expanded and explicit form of (6.1)- (6.3) for 3D and 2D cases can be easily obtained by expanding each term in them.

Explicit form for 1D axial behavior:

We present explicit form of (6.1)- (6.3) for purely 1-D axial behavior. In the following, we assume that $v_1=u$, $x_1=x$ and $\tau_{11}=\tau_{x_1x_1}=\tau_{xx}$. Except u, τ_{xx} and p, all other dependent variables are zero. For this particular case $p=-\frac{\sigma_{xx}}{3}$, $\sigma_{xx}=-p+\tau_{xx}$, hence $p=-0.5\tau_{xx}$. Thus we can eliminate pressure p from the momentum and rate

constitutive equations and we have the following for the momentum and constitutive equations.

$$\rho\frac{\partial u}{\partial t}+\rho u\frac{\partial u}{\partial x}-1.5(\frac{\tau_0}{\rho_0{v_0}^2})\frac{\partial \tau_{xx}}{\partial x}-\rho F_x^b=0 \tag{6.4}$$

$$\frac{\partial \tau_{xx}}{\partial t}+u\frac{\partial \tau_{xx}}{\partial x}-2.0\frac{\partial u}{\partial x}\tau_{xx}=(\frac{E_0}{\tau_0})E\frac{\partial u}{\partial x} \tag{6.5}$$

Equations (6.4) and (6.5) are two partial differential equations in axial velocity u and Cauchy stress deviation τ_{xx}. Elimination of pressure as a dependent variable was essential to allow the interaction of 1D solid with fluids in which $(\frac{\partial p}{\partial x})$ is a known quantity (a fixed value if the flow is pressure driven, otherwise zero) and hence pressure p can not be a dependent variable. For 1D linear elastic behavior, equations (6.4) and (6.5) constitutive the final mathematical model.

(b) Incompressible Newtonian and generalized Newtonian fluids

Based on the mathematical models presented in chapter 2, the dimensionless form of the continuity, momentum and constitutive equations can be written as

$$\rho\frac{\partial v_i}{\partial x_i}=0 \tag{6.6}$$

$$\rho\frac{\partial v_i}{\partial t}+\rho\frac{\partial v_i}{\partial x_j}v_j+(\frac{p_0}{\rho_0{v_0}^2})\frac{\partial p}{\partial x_i}-(\frac{\tau_0}{\rho_0{v_0}^2})\frac{\partial \tau_{ij}}{\partial x_j}-\rho F_i^b=0 \tag{6.7}$$

$$\tau_{ij}=(\frac{\mu_0 v_0}{\tau_0 L_0})\eta\left(\frac{\partial v_i}{\partial x_j}+\frac{\partial v_j}{\partial x_i}\right) \tag{6.8}$$

where $\eta=\mu$ for Newtonian fluids and $\eta=\eta(\dot{\gamma})$ for generalized Newtonian fluids. $\dot{\gamma}$ is the scalar strain rate. Viscosity $\eta(\dot{\gamma})$ can be defined using power law, Carreau model or Carreau-Yasuda Model. Details have been presented in chapter 2. For 2D and 3D cases, equations (6.6)- (6.8) can be expanded to yield the desired explicit forms.

Explicit form for 1D axial behavior:

For purely 1D axial behavior, the dependent variables are axial velocity u and stress τ_{xx}, but ($\frac{\partial p}{\partial x}$) is known. In this case we have momentum and constitutive equations.

$$\rho\frac{\partial u}{\partial t} + \rho u\frac{\partial u}{\partial x} + (\frac{p_0}{\rho_0 {v_0}^2})\frac{\partial p}{\partial x} - (\frac{\tau_0}{\rho_0 {v_0}^2})\frac{\partial \tau_{xx}}{\partial x} - \rho F_x^b = 0 \tag{6.9}$$

$$\tau_{xx} = (\frac{\mu_0 v_0}{\tau_0 L_0})2\eta\frac{\partial u}{\partial x} \tag{6.10}$$

we note that (6.9)- (6.10) provide interaction with the solids due to the choice of same dependent variables (u and τ_{xx}) and both being Eulerian description. If we choose, $p_0 = \tau_0 = \rho_0 {v_0}^2$, characteristic kinetic energy then, $\frac{\mu_0 v_0}{\tau_0 L_0} = \frac{\mu_0}{\rho_0 v_0 L_0} = \frac{1}{Re}$, $\frac{p_0}{\tau_0} = 1$ and $\frac{\tau_0}{\rho_0 {v_0}^2} = 1$, where Re is Reynolds number. On the other hand, if we choose $p_0 = \tau_0 = \frac{\mu_0 v_0}{L_0}$, characterstic viscous stress, then $\frac{\tau_0}{\rho_0 {v_0}^2} = \frac{1}{Re}$, $\frac{p_0}{\tau_0} = 1$ and $\frac{\mu_0 v_0}{\tau_0 L_0} = 1$. Generally, out of these two choices (characteristic kinetic energy or characterstic viscous stress), we choose the larger of the two while performing computations. Thus, obviously this choice is based on whether the flow is inertia dominated or shear dominated.

(c) Viscoelastic polymeric liquids

In this section we present dimensionless form of the mathematical model for viscoelastic polymeric incompressible liquids. We consider Maxwell, Oldroyd-B and Giesekus constitutive models.

Maxwell Model

Following chapter 2, we have the following for the dimensionless forms of the continu-

ity, momentum and constitutive equations.

$$\rho\frac{\partial v_i}{\partial x_i} = 0 \tag{6.11}$$

$$\rho\frac{\partial v_i}{\partial t} + \rho\frac{\partial v_i}{\partial x_j}v_j + (\frac{p_0}{\rho_0 {v_0}^2})\frac{\partial p}{\partial x_i} - (\frac{\tau_0}{\rho_0 {v_0}^2})\frac{\partial \tau_{ij}}{\partial x_j} - \rho F_i^b = 0 \tag{6.12}$$

$$\boldsymbol{\tau} + De\Big[\frac{\partial \boldsymbol{\tau}}{\partial t} + \boldsymbol{v}\cdot(\nabla\boldsymbol{\tau}) - \big((\nabla\boldsymbol{v})^T\cdot\boldsymbol{\tau} + \boldsymbol{\tau}\cdot(\nabla\boldsymbol{v})\big)\Big] = (\frac{\mu_0 v_0}{\tau_0 L_0})\eta\dot{\boldsymbol{\gamma}} \tag{6.13}$$

where $De = \frac{\lambda_1 v_0}{L_0}$ is Deborah number and η_0 is dimsionless zero shear rate viscosity and λ_1 is relaxation time. For 2D and 3D cases, equations (6.11)- (6.13) can be expanded to obtain explicit forms.

Explicit form for 1D axial behavior:

For purely 1D axial behavior, the explicit forms of the momentum and constitutive equations can be obtained using equations (6.11)- (6.13) in dependent variable u and τ_{xx}.

$$\rho\frac{\partial u}{\partial t} + \rho u\frac{\partial u}{\partial x} + (\frac{p_0}{\rho_0 {v_0}^2})\frac{\partial p}{\partial x} - (\frac{\tau_0}{\rho_0 {v_0}^2})\frac{\partial \tau_{xx}}{\partial x} - \rho F_x^b = 0 \tag{6.14}$$

$$\tau_{xx} + De(\frac{\partial \tau_{xx}}{\partial t} + u\frac{\partial \tau_{xx}}{\partial x} - 2.0\frac{\partial u}{\partial x}\tau_{xx}) = (\frac{\mu_0 v_0}{\tau_0 L_0})2\eta\frac{\partial u}{\partial x} \tag{6.15}$$

In this case also $(\frac{\partial p}{\partial x})$ is known depending whether the flow is pressure driven or not and hence pressure p is not a variable. This mathematical model also provides interaction with solids as well as Newtonian and generalized Newtonian fluids.

Oldroyd-B Model

The dimensionless form of the continuity, momentum and constitutive equations are in

chapter 2:

$$\rho\frac{\partial v_i}{\partial x_i} = 0 \tag{6.16}$$

$$\rho\frac{\partial v_i}{\partial t} + \rho\frac{\partial v_i}{\partial x_j}v_j + (\frac{p_0}{\rho_0 {v_0}^2})\frac{\partial p}{\partial x_i} - (\frac{\tau_0}{\rho_0 {v_0}^2})\frac{\partial \tau_{ij}}{\partial x_j} - \rho F_i^b = 0 \tag{6.17}$$

$$\begin{aligned}\boldsymbol{\tau} + De_1\big[\frac{\partial \boldsymbol{\tau}}{\partial t} + \boldsymbol{v}\cdot(\nabla\boldsymbol{\tau}) - \big((\nabla\boldsymbol{v})^T\cdot\boldsymbol{\tau} + \boldsymbol{\tau}\cdot(\nabla\boldsymbol{v})\big)\big] \\ = (\frac{\mu_0 v_0}{\tau_0 L_0})\eta\big[\dot{\boldsymbol{\gamma}} + De_2\big[\frac{\partial \dot{\boldsymbol{\gamma}}}{\partial t} + \boldsymbol{v}\cdot(\nabla\dot{\boldsymbol{\gamma}}) - \big((\nabla\boldsymbol{v})^T\cdot\dot{\boldsymbol{\gamma}} - \dot{\boldsymbol{\gamma}}\cdot(\nabla\boldsymbol{v})\big)\big]\big]\end{aligned} \tag{6.18}$$

where $De_1 = De = \frac{\lambda_1 v_0}{L_0}$ and $De_2 = \frac{\lambda_2 v_0}{L_0}$, λ_2 is retardation time and η_0 is dimensionless zero shear rate viscosity. Expanded form of equations (6.16)- (6.18) can be obtained for 2D and 3D cases.

Explicit form for 1D axial behavior:

In case of 1D axial behavior, equations (6.17) and (6.18) reduce to the following in terms of axial velocity u and Cauchy stress deviation τ_{xx}.

$$\rho\frac{\partial u}{\partial t} + \rho u\frac{\partial u}{\partial x} + (\frac{p_0}{\rho_0 {v_0}^2})\frac{\partial p}{\partial x} - (\frac{\tau_0}{\rho_0 {v_0}^2})\frac{\partial \tau_{xx}}{\partial x} - \rho F_x^b = 0 \tag{6.19}$$

$$\begin{aligned}\tau_{xx} + De_1(\frac{\partial \tau_{xx}}{\partial t} + u\frac{\partial \tau_{xx}}{\partial x} - 2.0\frac{\partial u}{\partial x}\tau_{xx}) = (\frac{\mu_0 v_0}{\tau_0 L_0})2\eta\frac{\partial u}{\partial x} \\ + 2De_2(\frac{\mu_0 v_0}{\tau_0 L_0})\eta(\frac{\partial^2 u}{\partial t \partial x} + u\frac{\partial^2 u}{\partial x^2} - 2.0(\frac{\partial u}{\partial x})^2)\end{aligned} \tag{6.20}$$

This mathematical model provides interaction of Oldroy-B fluids with solids, New-

tonian fluids, generalized Newtonian fluids and dilute polymeric liquids described by Maxwell constitutive model.

Giesekus Model

Using the mathematical models presented in chapter 2, we can obtain the dimensionless form of the continuity, momentum and constitutive equations.

$$\rho\frac{\partial v_i}{\partial x_i} = 0 \tag{6.21}$$

$$\rho\frac{\partial v_i}{\partial t} + \rho\frac{\partial v_i}{\partial x_j}v_j + (\frac{p_0}{\rho_0 {v_0}^2})\frac{\partial p}{\partial x_i} - (\frac{\tau_0}{\rho_0 {v_0}^2})\frac{\partial \tau_{ij}}{\partial x_j} - \rho F_i^b = 0 \tag{6.22}$$

$$\begin{aligned}\boldsymbol{\tau} - \eta_s(\frac{\mu_0 v_0}{\tau_0 L_0})\dot{\boldsymbol{\gamma}} + De\Big[\frac{\partial \boldsymbol{\tau}}{\partial t} + \boldsymbol{v}\cdot(\nabla\boldsymbol{\tau}) - \Big((\nabla\boldsymbol{v})^T\cdot\boldsymbol{\tau} + \boldsymbol{\tau}\cdot(\nabla\boldsymbol{v})\Big)\\ - (\frac{\mu_0 v_0}{\tau_0 L_0})\eta_s\Big(\frac{\partial\dot{\boldsymbol{\gamma}}}{\partial t} + \boldsymbol{v}\cdot(\nabla\dot{\boldsymbol{\gamma}}) - ((\nabla\boldsymbol{v})^T\cdot(\dot{\boldsymbol{\gamma}}) + (\dot{\boldsymbol{\gamma}})\cdot(\nabla\boldsymbol{v}))\Big)\Big]\\ - \alpha\frac{De}{\eta_p}\Big(\frac{\tau_0 L_0}{\mu_0 v_0}\Big)(\boldsymbol{\tau} - \eta_s(\frac{\mu_0 v_0}{\tau_0 L_0})\dot{\boldsymbol{\gamma}}\Big)\cdot\Big(\boldsymbol{\tau} - \eta_s(\frac{\mu_0 v_0}{\tau_0 L_0})\dot{\boldsymbol{\gamma}}\Big) = \eta_p(\frac{\mu_0 v_0}{\tau_0 L_0})\dot{\boldsymbol{\gamma}}\end{aligned} \tag{6.23}$$

Specific choice of τ_0 i.e. ${\rho_0 v_0}^2$ or $\frac{\mu_0 v_0}{L_0}$ will simplify the coefficient in (6.22) containing reference quantities i.e these will reduce to Re, $\frac{1}{Re}$ or simply 1. Explicit forms of the GDEs for 2D and 3D cases can be obtained using (6.21)- (6.23).

Explicit form for 1D axial behavior:

For purely 1D axial behavior, the mathematical model (6.21)- (6.23) reduces to the

following in terms of axial velocity u and Cauchy stress deviation τ_{xx}.

$$\rho\frac{\partial u}{\partial t}+\rho u\frac{\partial u}{\partial x}+(\frac{p_0}{\rho_0{v_0}^2})\frac{\partial p}{\partial x}-(\frac{\tau_0}{\rho_0{v_0}^2})\frac{\partial \tau_{xx}}{\partial x}-\rho F_x^b=0 \tag{6.24}$$

$$\begin{aligned}\tau_{xx}+De(\frac{\partial \tau_{xx}}{\partial t}+u\frac{\partial \tau_{xx}}{\partial x}-2.0\frac{\partial u}{\partial x}\tau_{xx})-2\eta_s De(\frac{\mu_0 v_0}{\tau_0 L_0})(\frac{\partial^2 u}{\partial t\partial x}+u\frac{\partial^2 u}{\partial x^2}-2.0(\frac{\partial u}{\partial x}^2))\\ -\alpha\frac{De}{\eta_p}(\frac{\tau_0 L_0}{\mu_0 v_0})(\tau_{xx}-2\eta_s(\frac{\mu_0 v_0}{\tau_0 L_0})\frac{\partial u}{\partial x})\cdot(\tau_{xx}-2\eta_s(\frac{\mu_0 v_0}{\tau_0 L_0})\frac{\partial u}{\partial x})=2\eta(\frac{\mu_0 v_0}{\tau_0 L_0})\frac{\partial u}{\partial x}\end{aligned} \tag{6.25}$$

Remarks:

(1) The dimensionless form of the mathematical models for incompressible elastic solids, Newtonian fluid, generalized Newtonian fluid, dilute polymeric liquids and polymer melts presented above contains inherent interaction capability between these media in a single process.

(2) Explicit form of the mathematical models for purely 1D axial behavior clearly demonstrates that the intrinsic interaction features of these models are due to the choice of a single framework for the development and secondly, due to the use of same dependent variables.

(3) The dimensionless form of the mathematical models is essential in finite element process due to varied magnitudes of the dependent variables to ensure that in the resulting computational process the coefficient matrices in the algebraic systems do not become ill-conditioned.

6.3.2 Mathematical and computational framework and finite element process

The mathematical models presented in chapter 2 yield a system of non-linear partial differential equations in the dependent variables, space coordinate and time and hence, are IVPs. The details of addressing numerical solution of such partial differential equations in time have been presented in reference [7]. Here, we present a short summary for the sake of completeness. We construct finite element processes for obtaining numerical solution of the IVPs described by these mathematical models using space-time integral forms that are STVC in h, p, k framework for a space-time strip (or slab) corresponding to an increment of time and then time match to obtain the evolution for the desired value of time. The h, p, k framework permits higher order global differentiability approximation in space and time due to k, the order of the approximation. This permits us to incorporate the desired physics as well as the higher order global differentiability features of the theoretical solution in the design of the computational process. The h, p, k framework also permits the use of GDEs with higher order derivative in the design of finite element processes. STVC integral forms ensure unconditionally stable computation during the entire evolution for all choice of h, p, k and the dimensionless parameters in the mathematical models. Surana et al. [7] have shown that only space-time least square process is STVC: (i) when in the second variation of the least square or residual functional, the second variations of the residuals are neglected and (ii) when the system of non-linear algebraic equations resulting from the first variation of the least square functional are solved iteratively using Newton's first order or linear method (Newton Raphson method). We utilize this approach in the work presented here.

6.3.3 Numerical studies

In this section we present a number of different numerical studies to demonstrate the applications and features of the mathematical models as well as significance of the finite element processes based on h, p, k framework and STVC integral forms. We consider two basic model problems. The first model problem consists of axial wave propagation in single medium. The second model problem consists of axial wave propagation in a medium containing two media with a bi-material interface. Using these two model problem, we demonstrate the highly significant feature of the proposed work in simulating interactions involving wave propagation, reflection, transmission, subsequent propagation as well as their interactions.

In all numerical studies for 1D model problem we use the following material properties.

Solid:

$\hat{E} = 2.0 \times 10^{11} Pa,\ \hat{\rho} = 7896\ kg/m^3$: steel (S_1)

$\hat{E} = 1.03 \times 10^{11} Pa,\ \hat{\rho} = 8830\ kg/m^3$: copper (S_2)

$\hat{E} = 4 \times 10^{2} Pa,\ \hat{\rho} = 2170\ kg/m^3$: softer solid (S_3)

Maxwell fluid: fluid M1 [64]

$\hat{\rho} = 868\ kg/m^3,\ \lambda_1 = 0.1\ s,\ \hat{\eta_s} = 2.7 Pa\ s,\ \hat{\eta_p} = 0.3 Pa\ s$

Oldroyd - B fluid: fluid M1 [64]

$\hat{\rho} = 868\ kg/m^3,\ \lambda_1 = 0.1\ s,\ \hat{\eta_s} = 2.7 Pa\ s,\ \hat{\eta_p} = 0.3 Pa\ s,\ \lambda_2 = 0.001\ s$

Giesekus fluid: PIB/C14 fluid [56]

$\hat{\rho} = 800\ kg/m^3,\ \lambda = 0.06\ s,\ \hat{\eta_s} = 0.002Pa\ s,\ \hat{\eta_p} = 1.424Pa\ s,\ \alpha = 0.15$

We present a number of numerical studies for these model problems to demonstrate wave propagation in single medium as well as wave propagation, reflection, transmission and subsequent propagation in a bi-material domain containing a single bi-material interface. A single medium consisting of elastic solid, Newtonian fluid as well polymeric liquid with constitutive equation based on Maxwell model, Oldroyd-B model and Giesekus as well as their various combination for bi-material case are used in the numerical studies.

Figure 6.2(a) and (b) show schematics of a single material model problem (domain M1) and the domain of a model problem consisting of two materials (M1 and M2). A uniform discretization consisting of a ten element space-time strip used for the single material model problem is shown in Figure 6.2(d). Figure 6.2(e) shows a graded discretization used for the model problem consisting of two materials. The right end, ($x = L$) in Figure 6.2(a), ($x = 2L$) in Figure 6.2(b), is subjected to a velocity pulse (Figure 6.2(c)) of duration $2\Delta t$ and peak value of 0.1. The time evolution is computed using the space-time strips (shown in Figure 6.2(d) and (e)) with time marching. In all studies we use $\Delta t = 0.01$, $p = 11$ (i.e. same p-level in space and time) and solution of class C^{11} in space and time. The numerical solutions are considered converged in the iterative solution procedure based on Newton's linear method with line search [7] when the absolute value of each component of δI (I, being residual functional) is less than or equal to 10^{-6}.

Model problem 1: 1D wave propagation in a single material domain

We consider the domain consisting of elastic solid (S1) as well as Maxwell fluid (M1),

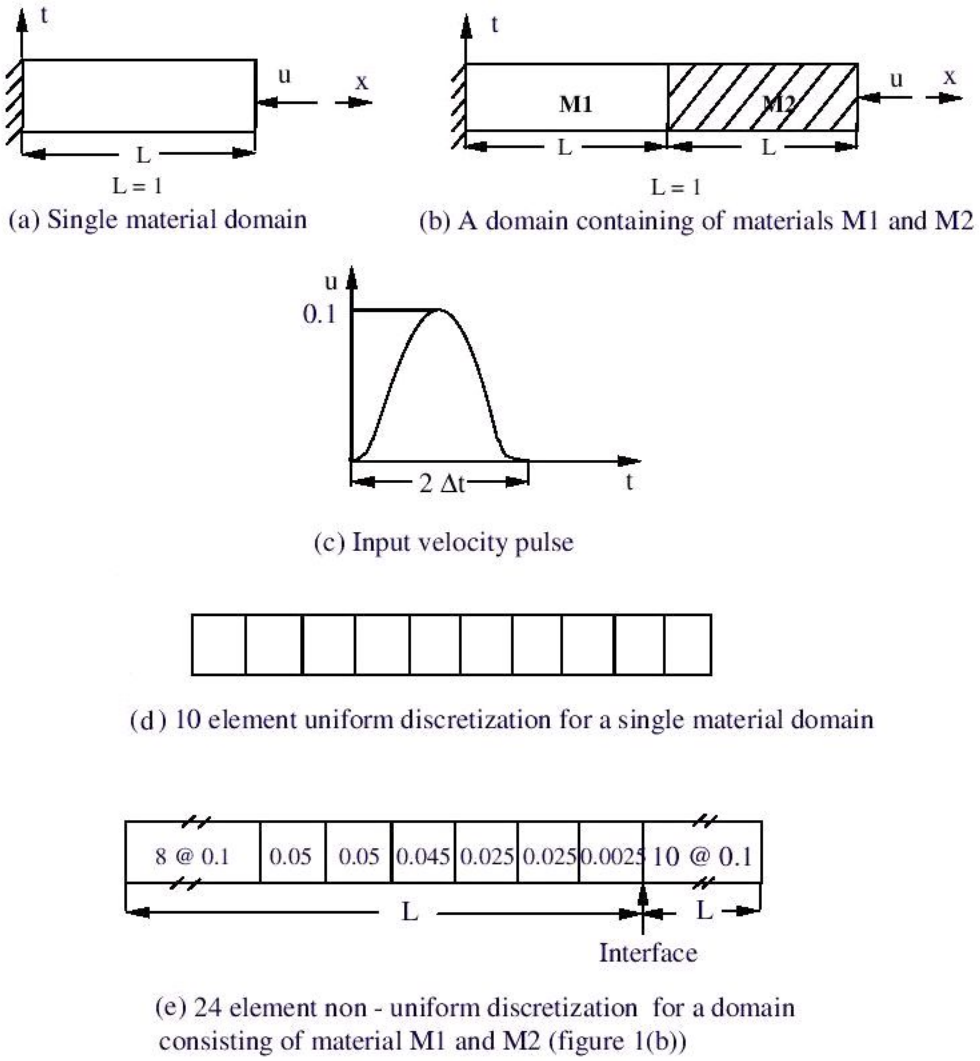

Figure 6.2: Schematics, disturbance and democratization

Oldroyd-B fluid and Giesekus fluid.

(a) Elastic solid

The GDEs are non-dimensionalized using:

$\rho_0 = 7896\ kg/m^3,\ L_0 = 0.02\ m\ ,\ v_0 = 500\ m/s,\ E_0 = 2.0 \times 10^{11}\ Pa,$

$\tau_0 = \rho_0 {v_0}^2 = 1.974 \times 10^9\ Pa.$

The evolution of velocity u and Cauchy stress deviation τ_{xx} are shown in Figure 6.3(a)

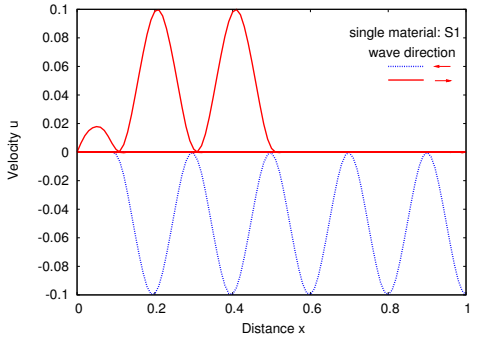

(a) Evolution of velocity u in solid (S1)

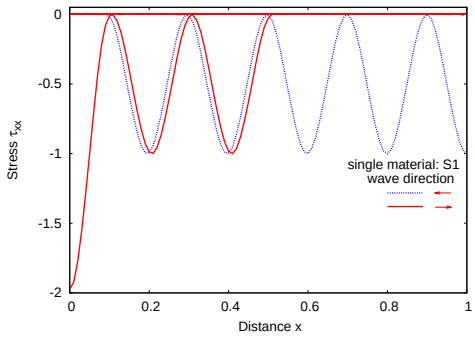

(b) Evolution of stress τ_{xx} in solid (S1)

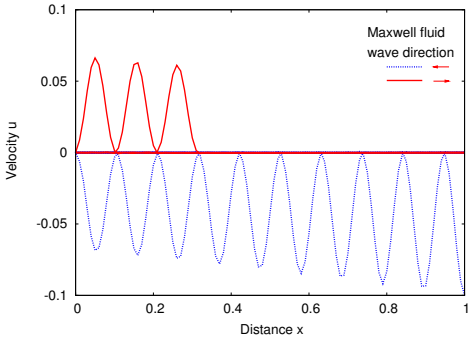

(c) Evolution of velocity u in Maxwell fluid

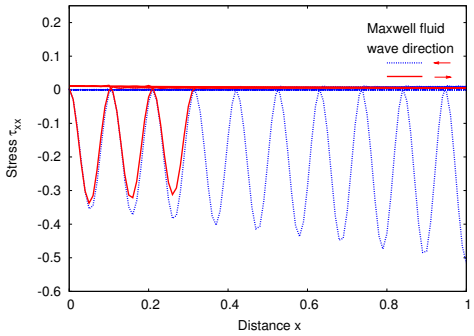

(d) Evolution of stress τ_{xx} in Maxwell fluid

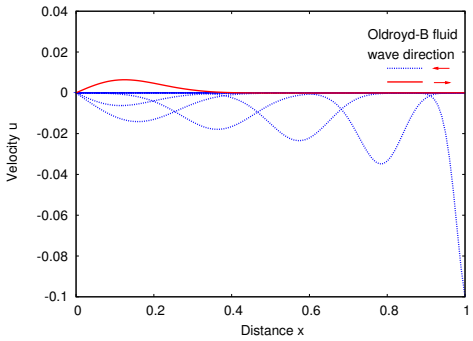

(e) Evolution of velocity u in Oldroyd - B fluid

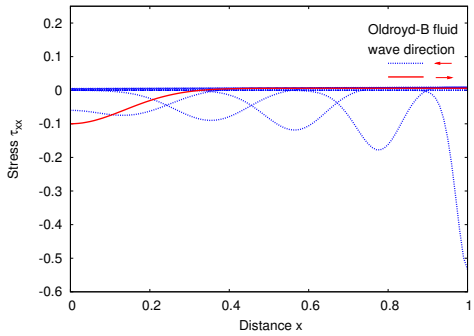

(f) Evolution of stress τ_{xx} in Oldroyd - B fluid

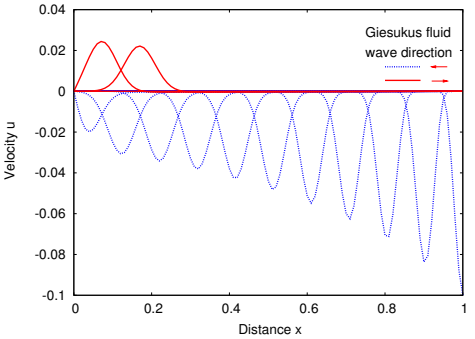

(g) Evolution of velocity u in Giesekus fluid

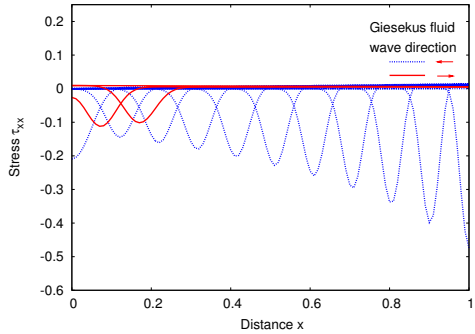

(h) Evolution of stress τ_{xx} in Giesekus fluid

Figure 6.3: Evolution of velocity u and stress τ_{xx} in solid (S1), Maxwell, Oldroyd - B and Giesekus fluids

and (b). Propagations of the velocity pulse and the associated stress pulse and their reflection from the impermeable boundary at $x = 0$ are oscillation free and are simulated accurately. For all space-time strips the residual functional I is of the order of (10^{-8}) or lower indicating that the computed solution satisfies the GDEs quite well.

(b) Maxwell fluid

In this case, the GDEs are non-dimensionalized using:

$\rho_0 = 868\ kg/m^3,\ L_0 = 0.02\ m\ ,\ v_0 = 0.05\ m/s,\ \mu_0 = 3.0Pa\ s\ ,$

$p_0 = \tau_0 = \rho_0 {v_0}^2 = 2.17\ Pa.$

The evolution of velocity u and stress τ_{xx} are shown in Figure 6.3(c) and (d). We observe: (i) wave propagation and reflection are smooth i.e oscillation free (ii) Due to viscosity of the medium, the incident as well as the reflected velocity and stress waves attenuate during the evolution (i.e. their magnitudes decreases and base elongates) as seen in Figure 6.3(c) and (d). (iii) Due to elasticity, the wave propagation speed in polymeric liquid is finite as clearly observed here. (iv) Since the visco-elastic fluids have relaxation phenomenon, we clearly note a finite stress field behind the travelling wave in Figure 6.3(d) that percussively decreases as evolution proceeds (due to relaxation of the fluid). A similar phenomenon is also observed behind the reflected stress wave (Figure 6.3(d)). Same accuracy of the result is achieved in the case of the elastic solid.

(c) Oldroyd - B fluid

We non-dimensionalize the GDEs in the mathematical model using:

$\rho_0 = 868\ kg/m^3,\ L_0 = 0.02\ m\ ,\ v_0 = 0.05\ m/s,\ \mu_0 = 3.0Pa\ s\ ,$

$p_0 = \tau_0 = \rho_0 {v_0}^2 = 2.17\ Pa.$

The evolution of axial velocity u and stress τ_{xx} are shown in Figures 6.3(e) and (f). As expected, much more rapid dispersion of the stress and velocity waves is observed here

compared to Maxwell model (Figure 6.3(c) and (d)). Progressive amplitude decay and based elongation of the incident travelling waves, as well as reflected waves are clearly observed in Figure 6.3(e) and (f), but no difficulty is encountered in the simulations. Accuracy of the entire evolution is similar to that achieved for solids (described in (a)). The non-zero stress field behind the wave is clearly observed in this case also.

(d) Giesekus fluid

The GDEs in the mathematical model are non-dimensionalized using:

$\rho_0 = 800\ kg/m^3,\ L_0 = 0.02\ m\ ,\ v_0 = 0.05\ m/s,\ \mu_0 = 1.426 Pa\ s\ ,$

$p_0 = \tau_0 = \rho_0 {v_0}^2 = 2.0\ Pa.$

Figure 6.3(g) and (h) show evolution of axial velocity u and stress τ_{xx}. Dispersion, i.e. base elongation and amplitude decay of incident travelling waves, as well as reflected waves are clearly seen in Figure 6.3(g) and (h). Evolutions are oscillation free and have the same accuracy as discussed in the case of solids (a).

(e) Newtonian fluids

In Newtonian fluids, due to incompressibility and lack of elasticity, the speed of wave propagation is infinite, hence, a study similar to that presented in section (a)-(d) can not be performed for Newtonian fluids. The alternative of course is to either incorporated artificial compressibility or artificial elasticity. Both approaches have been used successfully. For example, we could use Maxwell constitutive model but with very low elasticity (by controlling λ_1).

Model problem 2: 1D wave propagation in medium with bi-material interface

In these studies we consider a series of model problems similar to those in model problem 1, but the domain $2L$ consists of two materials M1 and M2 with a bi-material

interface at $x = L$ (Figure 6.2(b)). We choose different combinations of M1 and M2 to demonstrate the interaction feature intrinsic in the mathematical models.

(a) M1 - copper; M2 - steel :

In this case, we non-dimensionalized the GDEs by choosing following reference quantities:

$\rho_0 = 7896\ kg/m^3,\ L_0 = 0.02\ m,\ v_0 = 500\ m/s,\ E_0 = 2 \times 10^{11}\ Pa,$

$p_0 = \tau_0 = \rho_0 {v_0}^2 = 1.974 \times 10^9\ Pa.$

Figure 6.4(a) and (b) show evolutions of velocity u and stress τ_{xx}. The incident velocity wave propagates in steel (M2) without any attenuation. Upon reaching the interface at $x = L$, the process of transmission and reflection is clearly observed. The impendence of copper and steel determine the peaks of the transmitted and reflected waves and their moduii and densities determine the speed of propagation of the transmitted and the reflected waves. The tension caused in the steel by the reflected stress wave is seen in Figure 6.4(b). The velocity wave remains compressive due to the fact that the motion of the interface is into M1 (copper) medium upon the arrival of the incident wave at the interface. Accuracy of the entire evolution is excellent for each increment of time (I of the order of 10^{-8} or lower and $|\delta I|_{max} \leq 10^{-8}$).

(b) M1 - Maxwell fluid; M2 - steel(S1)

We use the following reference quantities to non-dimensionalize GDEs in the mathematical models.

$\rho_0 = 7896\ kg/m^3,\ L_0 = 0.02\ m,\ v_0 = 500\ m/s,\ E_0 = 2 \times 10^{11}\ Pa,$

$p_0 = \tau_0 = \rho_0 {v_0}^2 = 1.974 \times 10^9\ Pa.$

Figure 6.4(c) and (d) show evolutions of velocity u and stress τ_{xx}. Since the Maxwell fluid hardly offers much resistance to steel (due to impedance mismatch), the interface

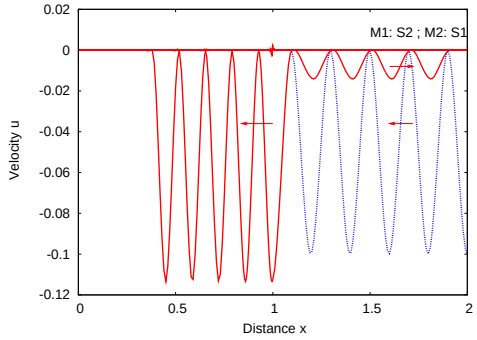

(a) Evolution of velocity u of M1 and M2

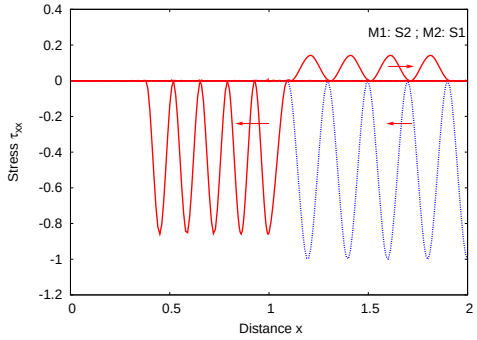

(b) Evolution of stress τ_{xx} of M1 and M2

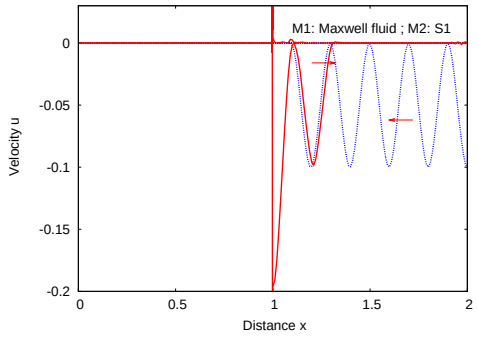

(c) Evolution of velocity u of M1 and M2

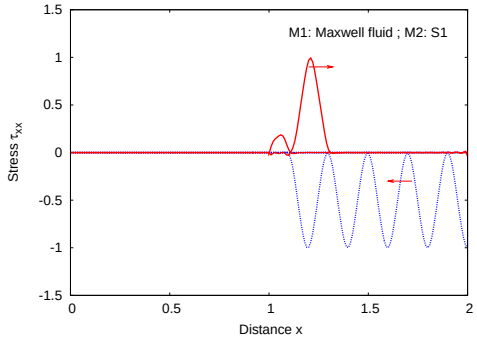

(d) Evolution of stress τ_{xx} of M1 and M2

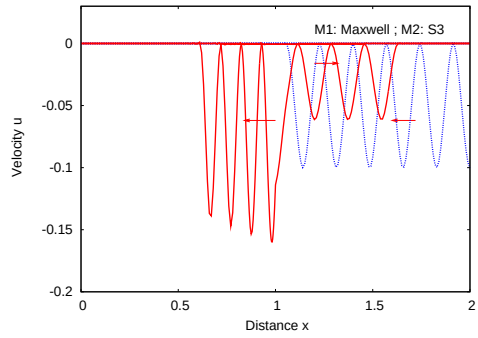

(e) Evolution of velocity u of M1 and M2

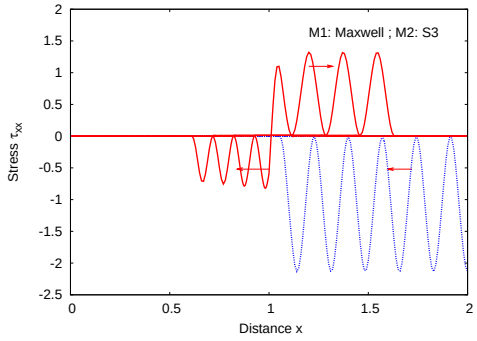

(f) Evolution of stress τ_{xx} of M1 and M2

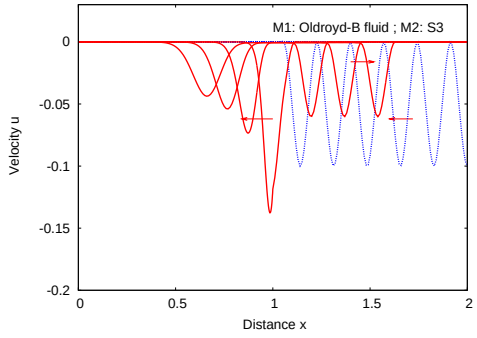

(g) Evolution of velocity u of M1 and M2

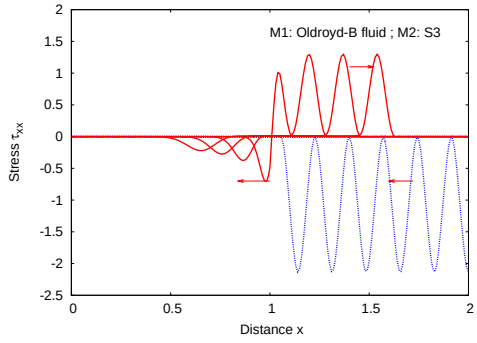

(h) Evolution of stress τ_{xx} of M1 and M2

Figure 6.4: Evolution of velocity u and stress τ_{xx} in bi-material model problems

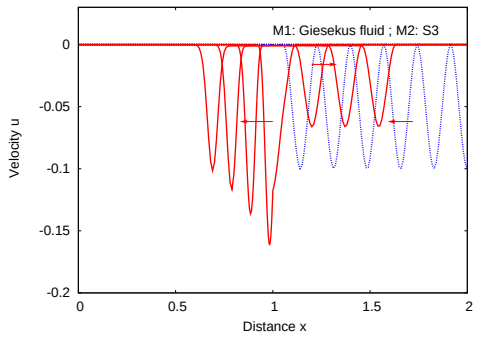

(a) Evolution of velocity u of M1 and M2

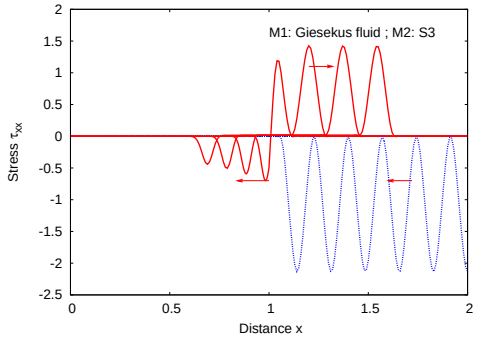

(b) Evolution of stress τ_{xx} of M1 and M2

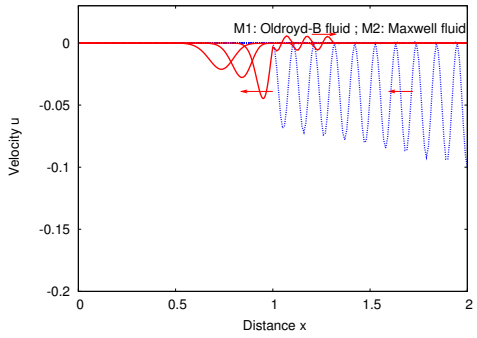

(c) Evolution of velocity u of M1 and M2

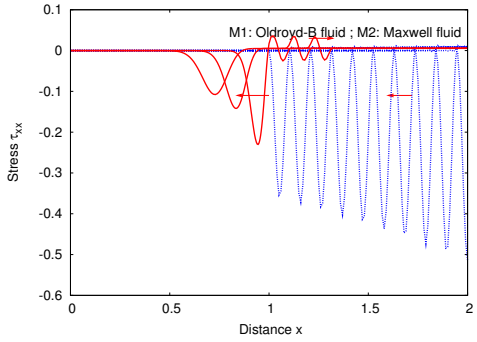

(d) Evolution of stress τ_{xx} of M1 and M2

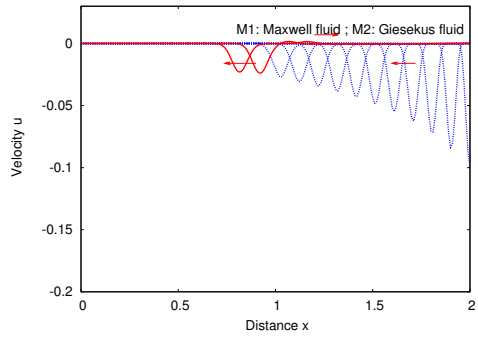

(e) Evolution of velocity u of M1 and M2

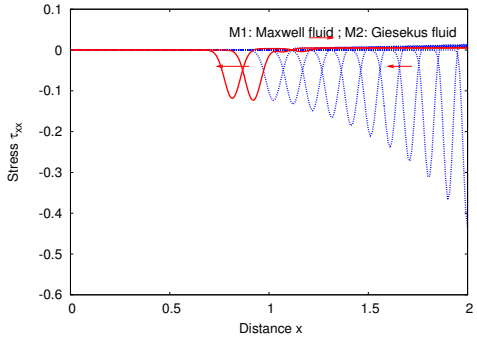

(f) Evolution of stress τ_{xx} of M1 and M2

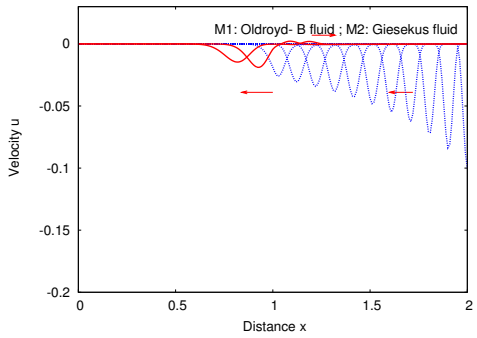

(g) Evolution of velocity u of M1 and M2

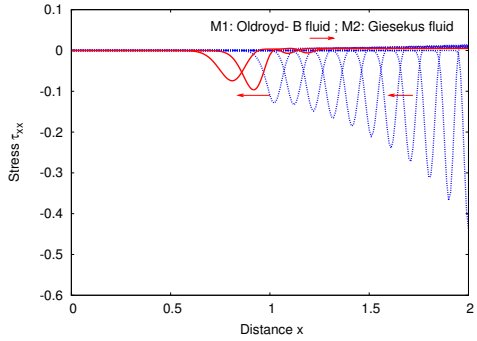

(h) Evolution of stress τ_{xx} of M1 and M2

Figure 6.5: Evolution of velocity u and stress τ_{xx} in bi-material model problems

between M1 and M2 behaves like a free boundary for steel and as a consequence, nothing much happens in M1 medium. But in steel, we find a tensile stress wave of the same magnitude as incident compressive stress wave (Figure 6.4(d)) while the reflected velocity wave remains compressive (Figure 6.4(c)). Evolutions are oscillation free and smooth with value of I and $|\delta I|_{max} \leq 10^{-8}$ indicating good accuracy of the evolution. Similar behaviors are also observed when M1 is Oldroyd-B or Giesekus fluid and M2 is steel (S1).

(c) M1 - Maxwell fluid; M2 - softer solid (S3)

The GDEs are non-dimensionalized using:

$\rho_0 = 868\ kg/m^3,\ L_0 = 0.02\ m\ ,\ v_0 = 0.05\ m/s,\ \mu_0 = 3.0Pa\ s\ ,\ E_0 = 400\ Pa,$

$p_0 = \tau_0 = \rho_0 {v_0}^2 = 2.17\ Pa.$

Figure 6.4(e) and (f) show evolution of velocity u and stress τ_{xx}. Since in this case, we do not have drastic impedance mismatch, wave reflection and transmission are observed clearly. The reflected tensile stress wave in the solid (S3) clearly demonstrates the interface between M1 and M2 is moving to the left due to the fact that M1 is softer than M2. Other numerical studies are summarized in the following:

(d) M1 - Oldroyd-B fluid; M2 - softer solid (S3) : Figure 6.4(g) and (h)

(e) M1 - Giesekus fluid; M2 - softer solid (S3) : Figure 6.5(a) and (b)

(f) M1 - Oldroyd-B fluid; M2 - Maxwell fluid : Figure 6.5(c) and (d)

(g) M1 - Maxwell fluid; M2 - Giesekus fluid : Figure 6.5(e) and (f)

(h) M1 - Oldroyd-B fluid; M2 - Giesekus fluid : Figure 6.5(g) and (h)

Remarks

(1) The numerical studies demonstrate the ability of a single mathematical model to accurately describe the interaction between different media at the bi-material interface.

(2) STVC space-time integral forms yield unconditionally stable computations.

(3) In all cases for each space time strip $I \leq 10^{-8}$ and $|\delta I|_{max} \leq 10^{-8}$ indicate good accuracy of the computed solutions as well as convergence of the Newton Raphson method.

(4) The physics of velocity and stress wave propagation, transmission and reflection at the bi-material interface are simulated accurately.

(5) In all studies, evolution remains oscillation free and smooth for all increments of time.

(6) Influence of medium viscosity in dispersing the waves is clearly simulated and observed in all cases presented.

Convergence studies

Figure 6.6(a), (b), (c) and (d) show plots of $\sqrt{I} = L_2$-norm of the residual = $(\sum_i \sum_e (E_i{}^e, E_i{}^e))^{\frac{1}{2}}$ (where $E_i{}^e$ are the element residuals) versus degrees of freedom for a single material domain consisting of 10 and 20 element uniform discretization in a space-time strip for progressively increasing p-levels beginning with $p = 3$ and increasing in increments of two. For most part, the 10 element uniform discretization yields the lowest $\sqrt{I}$ for a given dofs with comparable or better convergence rate compared to the 20 element uniform discretization, confirming the smoothness of the theoretical solution.

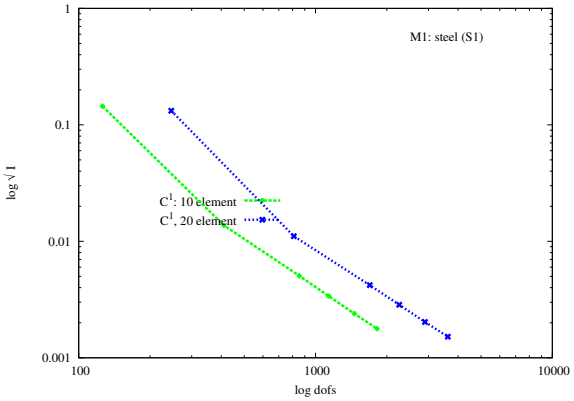

(a) I versus dofs : steel (S1)

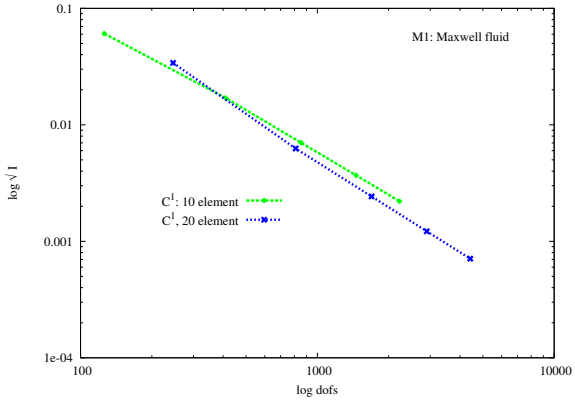

(b) I versus dofs : Maxwell fluid

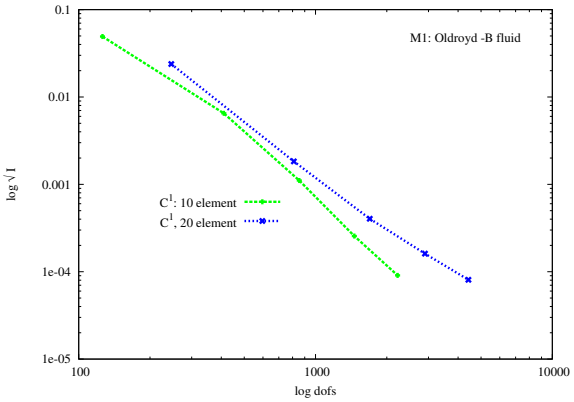

(c) I versus dofs : Oldroyd-B fluid

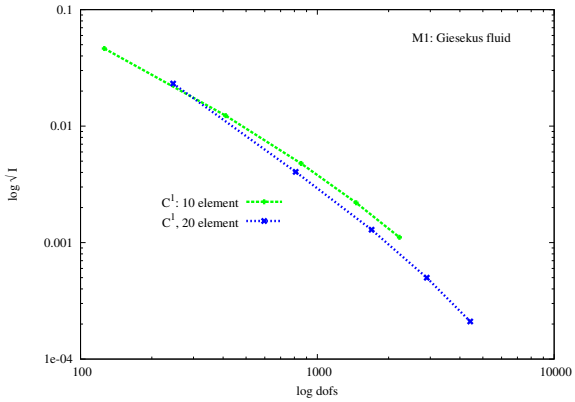

(d) I versus dofs : Giesekus fluid

Figure 6.6: Least square function I versus degree of freedom for the first space-time strip

6.4 Summary

(1) The mathematical models for incompressible matter developed in chapter 2 using Eulerian description are used to present explicit forms of the GDEs for 1D axial behavior of linear elastic solids, Newtonian fluids, generalized Newtonian fluids and polymeric liquids using Maxwell, Oldroyd-B and Giesekus constitutive models.

(2) h, p, k mathematical and computational finite element framework using STVC. Space-time integral forms is proposed and used for obtaining numerical solu-

tions of the IVPs described by these non-linear partial differential equations in the mathematical models. h, p, k framework permits higher order global differentiability approximation in space and time necessitated by the physics and higher order global differentiability features of the theoretical solutions. STVC integral forms ensure unconditionally stable computations during the entire evolution, thereby eliminating the need for upwinding methods.

(3) A significant aspect of the work presented here is that interactions of solids and liquids are inherent in the mathematical models, thus, completely eliminating the constraint equations at the interfaces between the media. The choice of Eulerian description and identical dependent variables for each media ensure the interaction between the media to be intrinsic in the mathematical model.

(4) A number of 1D numerical studies are presented for wave propagation and reflection in solids, and polymeric liquids to demonstrate that the mathematical models in h, p, k framework with STVC integral forms yield very accurate evolution and that the Newton's method with line search has good convergence characteristics.

(5) The 1D numerical studies containing a bi-material interface show that wave propagation, transmission, reflection and subsequent propagation are simulated accurately.

   (a) For viscoelastic medium, progressive wave dispersion i.e. base elongation and amplitude decay, is clearly observed due to viscosity of the medium.

   (b) In case of viscoelastic medium the stress relaxation phenomenon behind the travelling stress wave is observed as well.

   (c) The numerical studies clearly establish the ability of the mathematical models in simulating interactions between any two desired incompressible me-

dia.

(6) The strength of this work lies in the fact that mathematical models utilize a single description using same dependent variables for all media and that STVC integral forms ensure unconditionally stable computations during the entire evolution. The methodology presented here is natural, straight forward, avoids upwinding methods and has built in measures of accuracy of the computed evolution (element residuals for each space-time element of each space-time strip).

Chapter 7

Numerical Studies for Two Dimensional Model Problems

In this chapter we consider two dimensional model problems to demonstrate numerical simulations of multi-media interaction in which the interacting media are incompressible elastic solids and incompressible liquids such as Newtonian fluids and Maxwell model fluids. The development of the mathematical model and the computational finite element infrastructure for the initial value problems described by the mathematical models for the media considered in the numerical studies in this chapter have been presented in chapter two and three. In this chapter we borrow the dimensionless forms of the GDEs from chapter 2 and present explicit forms of the mathematical models for each medium that are utilized in the numerical studies. In all cases, the evolutions are computed using least squares space-time finite element processes in hpk framework using a space-time strip or slab with time marching.

7.1 Explicit Forms of the Dimensionless Mathematical Models

Details of the derivations of mathematical models for compressible and incompressible matter were presented in chapter 2. In this chapter we describe the explicit forms of the dimensionless forms of the mathematical models for 2D behavior of incompressible elastic solids and liquids in Eulerian description under isothermal conditions. The emphasis is placed on the explicit forms of the dimensionless forms of the GDEs in the mathematical models that are essential in the computations of the numerical solutions of the associated IVPs.

7.1.1 2D incompressible hyper-elastic solids

Following the mathematical model presented in chapter 2, we present explicit form of 2-D dependent variables (u, v, p, τ_{xx}, τ_{yy} and τ_{xy}) the momentum and constitutive equations are

$$\rho(\frac{\partial u}{\partial t}+u\frac{\partial u}{\partial x}+v\frac{\partial u}{\partial y})+(\frac{p_0}{\rho_0 {v_0}^2})\frac{\partial p}{\partial x}-(\frac{\tau_0}{\rho_0 {v_0}^2})\frac{\partial \tau_{xx}}{\partial x}-(\frac{\tau_0}{\rho_0 {v_0}^2})\frac{\partial \tau_{xy}}{\partial y}-\rho F_x^b=0 \quad (7.1)$$

$$\rho(\frac{\partial v}{\partial t}+u\frac{\partial v}{\partial x}+v\frac{\partial v}{\partial y})+(\frac{p_0}{\rho_0 {v_0}^2})\frac{\partial p}{\partial y}-(\frac{\tau_0}{\rho_0 {v_0}^2})\frac{\partial \tau_{xy}}{\partial x}-(\frac{\tau_0}{\rho_0 {v_0}^2})\frac{\partial \tau_{yy}}{\partial y}-\rho F_y^b=0 \quad (7.2)$$

$$\begin{aligned}\frac{\partial \tau_{xx}}{\partial t}+u\frac{\partial \tau_{xx}}{\partial x}+v\frac{\partial \tau_{xx}}{\partial y}-(2\tau_{xx}\frac{\partial u}{\partial x}+2\tau_{xy}\frac{\partial u}{\partial y})\\ =(\frac{E_0}{\tau_0})E(D_{11}\frac{\partial u}{\partial x}+D_{12}\frac{\partial v}{\partial y}+D_{13}(\frac{\partial u}{\partial y}+\frac{\partial v}{\partial x}))\end{aligned} \quad (7.3)$$

$$\begin{aligned}\frac{\partial \tau_{yy}}{\partial t}+u\frac{\partial \tau_{yy}}{\partial x}+v\frac{\partial \tau_{yy}}{\partial y}-(2\tau_{yy}\frac{\partial v}{\partial y}+2\tau_{xy}\frac{\partial v}{\partial x})\\ =(\frac{E_0}{\tau_0})E(D_{21}\frac{\partial u}{\partial x}+D_{22}\frac{\partial v}{\partial y}+D_{23}(\frac{\partial u}{\partial y}+\frac{\partial v}{\partial x}))\end{aligned} \quad (7.4)$$

$$\frac{\partial \tau_{xy}}{\partial t} + u\frac{\partial \tau_{xy}}{\partial x} + v\frac{\partial \tau_{xy}}{\partial y} - (\tau_{xx}\frac{\partial v}{\partial x} + \tau_{yy}\frac{\partial u}{\partial y} + \tau_{xy}(\frac{\partial u}{\partial x} + \frac{\partial v}{\partial y})) \\ = (\frac{E_0}{\tau_0})E(D_{31}\frac{\partial u}{\partial x} + D_{32}\frac{\partial v}{\partial y} + D_{33}(\frac{\partial u}{\partial y} + \frac{\partial v}{\partial x})) \tag{7.5}$$

Where the (3×3) matrix $[D]$ contains the coefficients from the fourth order material tensor $\boldsymbol{\eta}$. For the material under consideration, assuming 2D plane strain case, we can write the following for the components of $[D]$ matrix

$$d_{11} = E(1-\nu)/(1+\nu)(1-2\nu)$$
$$D_{11} = D_{22} = d_{11}, \quad D_{12} = D_{21} = d_{11}\nu/(1-\nu)$$
$$D_{33} = d_{11}(1-2\nu)/(1-\nu), \quad D_{13} = D_{31} = D_{23} = D_{32} = 0$$

Where E is the modulus of elasticity and ν is the Poisson's ratio of the solid matter.

$$p + \tau_{xx} + \tau_{yy} = 0 \tag{7.6}$$

Equations (7.1)- (7.6) are six partial differential equations in six variables. These are valid in the contra-variant basis related to the convected coordinate system.

7.1.2 2D incompressible Newtonian and generalized Newtonian fluids

The continuity, momentum and constitutive equations for this case are

$$\rho(\frac{\partial u}{\partial x} + \frac{\partial v}{\partial y}) = 0 \tag{7.7}$$

$$\rho(\frac{\partial u}{\partial t} + u\frac{\partial u}{\partial x} + v\frac{\partial u}{\partial y}) + (\frac{p_0}{\rho_0 {v_0}^2})\frac{\partial p}{\partial x} - (\frac{\tau_0}{\rho_0 {v_0}^2})\frac{\partial \tau_{xx}}{\partial x} - (\frac{\tau_0}{\rho_0 {v_0}^2})\frac{\partial \tau_{xy}}{\partial y} - \rho F_x^b = 0 \tag{7.8}$$

$$\rho(\frac{\partial v}{\partial t}+u\frac{\partial v}{\partial x}+v\frac{\partial v}{\partial y})+(\frac{p_0}{\rho_0{v_0}^2})\frac{\partial p}{\partial y}-(\frac{\tau_0}{\rho_0{v_0}^2})\frac{\partial \tau_{xy}}{\partial x}-(\frac{\tau_0}{\rho_0{v_0}^2})\frac{\partial \tau_{yy}}{\partial y}-\rho F_y^b=0 \quad (7.9)$$

$$\tau_{xx}=(\frac{\mu_0 v_0}{\tau_0 L_0})2\eta\frac{\partial u}{\partial x} \quad ; \quad \tau_{yy}=(\frac{\mu_0 v_0}{\tau_0 L_0})2\eta\frac{\partial v}{\partial y} \quad ; \quad \tau_{xy}=(\frac{\mu_0 v_0}{\tau_0 L_0})\eta(\frac{\partial v}{\partial x}+\frac{\partial u}{\partial y}) \quad (7.10)$$

we note that (7.7)- (7.10) provide interaction with the solids due to the choice of same dependent variables (u, v, p, τ_{xx}, τ_{yy} and τ_{xy}) and all being Eulerian description. If we choose, $p_0=\tau_0=\rho_0{v_0}^2$, characteristic kinetic energy then, $\frac{\mu_0 v_0}{\tau_0 L_0}=\frac{\mu_0}{\rho_0 v_0 L_0}=\frac{1}{Re}$, $\frac{p_0}{\tau_0}=1$ and $\frac{\tau_0}{\rho_0{v_0}^2}=1$, where Re is Reynolds number. On the other hand, if we choose $p_0=\tau_0=\frac{\mu_0 v_0}{L_0}$, characterstic viscous stress, then $\frac{\tau_0}{\rho_0{v_0}^2}=\frac{1}{Re}$, $\frac{p_0}{\tau_0}=1$ and $\frac{\mu_0 v_0}{\tau_0 L_0}=1$. Generally, out of these two choices (characteristic kinetic energy or characterstic viscous stress), we choose the larger of the two while performing computations. Thus, obviously this choice is based on whether the flow is inertia dominated or shear dominated. In case of generalized Newtonian fluids $\eta=\eta(I_2)$ where I_2 is the second invariant of the tensor $[D]$ (based on characteristic equations for $[D]$)

7.1.3 2D viscoelastic polymeric liquids

Maxwell model

Based on the mathematical models presented in chapter 2 for 2D behavior, we have the following for the dimensionless continuity, momentum and constitutive equations.

$$\rho(\frac{\partial u}{\partial x}+\frac{\partial v}{\partial y})=0 \quad (7.11)$$

$$\rho(\frac{\partial u}{\partial t}+u\frac{\partial u}{\partial x}+v\frac{\partial u}{\partial y})+(\frac{p_0}{\rho_0{v_0}^2})\frac{\partial p}{\partial x}-(\frac{\tau_0}{\rho_0{v_0}^2})\frac{\partial \tau_{xx}}{\partial x}-(\frac{\tau_0}{\rho_0{v_0}^2})\frac{\partial \tau_{xy}}{\partial y}-\rho F_x^b=0 \quad (7.12)$$

$$\rho(\frac{\partial v}{\partial t}+u\frac{\partial v}{\partial x}+v\frac{\partial v}{\partial y})+(\frac{p_0}{\rho_0 {v_0}^2})\frac{\partial p}{\partial y}-(\frac{\tau_0}{\rho_0 {v_0}^2})\frac{\partial \tau_{xy}}{\partial x}-(\frac{\tau_0}{\rho_0 {v_0}^2})\frac{\partial \tau_{yy}}{\partial y}-\rho F_y^b=0 \quad (7.13)$$

$$\tau_{xx}+De(\frac{\partial \tau_{xx}}{\partial t}+u\frac{\partial \tau_{xx}}{\partial x}+v\frac{\partial \tau_{xy}}{\partial y}-2.0(\tau_{xx}\frac{\partial u}{\partial x}+\tau_{xy}\frac{\partial u}{\partial y}))=(\frac{\mu_0 v_0}{\tau_0 L_0})2\eta\frac{\partial u}{\partial x} \quad (7.14)$$

$$\tau_{yy}+De(\frac{\partial \tau_{yy}}{\partial t}+u\frac{\partial \tau_{yy}}{\partial x}+v\frac{\partial \tau_{yy}}{\partial y}-2.0(\tau_{xy}\frac{\partial v}{\partial x}+\tau_{yy}\frac{\partial v}{\partial y}))=(\frac{\mu_0 v_0}{\tau_0 L_0})2\eta\frac{\partial v}{\partial y} \quad (7.15)$$

$$\tau_{xy}+De(\frac{\partial \tau_{xy}}{\partial t}+u\frac{\partial \tau_{xy}}{\partial x}+v\frac{\partial \tau_{xy}}{\partial y}-(\tau_{xx}\frac{\partial v}{\partial x}+\tau_{yy}\frac{\partial u}{\partial y}+\tau_{xy}(\frac{\partial u}{\partial x}+\frac{\partial v}{\partial y}))=(\frac{\mu_0 v_0}{\tau_0 L_0})\eta(\frac{\partial v}{\partial x}+\frac{\partial u}{\partial y}) \quad (7.16)$$

7.2 Numerical Studies : Lid Driven Cavity and Flow Between Parallel Plates

In this section we present a number of different numerical studies to demonstrate the applications and features of the mathematical models as well as significance of the finite element processes based on h, p, k framework and STVC integral forms. We consider two basic model problems. The first model problem consists of a lid driven square cavity with Newtonian fluid. The second model problem we consider transient developing flow of Maxwell fluid between parallel plates. Using these two model problems, we demonstrate the highly significant feature of the proposed work in simulating interactions.

7.2.1 Lid driven cavity

In this model problem we consider a lid driven square cavity with Newtonian fluid. The problem is characterized by a square cavity in which the driving force for the flow is the shear created by a sliding lid. In the first case, we consider rigid cavity, and in the

second case, the cavity has elastic bottom consisting of steel as well as a softer material. The schematics, dimensions and the discretizations for both cases are shown in Figure 7.1. We choose $L = 1$ and a velocity distribution that is continuous, differentiable and varies from $u = 0$ at point A and B to $u = 1$ at a distance $h_d = 0.025$ away from the corners. The elastic bottom consists of ($L \times L/4$) (figure 7.1(b)).

We consider details of the boundary conditions in the following:

Rigid square cavity [54]:

$u = v = 0$ on the walls AD, BC and CD; specified velocity u on the wall AB (see figure 7.1(a))

Cavity with the elastic bottom [65]:

$u = v = 0$ on the walls AD, BC and EF; $\tau_{xy} = 0$ on the walls DE and CF(see figure 7.1(b))

At time $t = 0$ (reference configuration) the cavity is at rest and free of stress field and pressure field. The velocity distribution shown in figure 7.1(a) is applied over an increment of time with $h_d = 0.025$.

We consider the following material properties of the fluid and elastic bottom.

Newtonian fluid (M_1) [66] : $\hat{\rho} = 1075\ kg/m^3,\ \hat{\eta} = 0.5375 Pa\ s$

Steel (M_2): $\hat{E} = 2.0 \times 10^{11}\ Pa,\ \hat{\rho} = 7896\ kg/m^3, \nu = 0.0$

Softer solid (M_2): $\hat{E} = 2.58 \times 10^{6}\ Pa,\ \hat{\rho} = 1075\ kg/m^3, \nu = 0.0$

We consider the following reference quantities in both studies (rigid cavity and cavity with elastic bottom):

$\rho_0 = 1075\ kg/m^3,\ L_0 = 0.02\ m\ ,\ v_0 = 10\ m/s,\ E_0 = 1.075 \times 10^5\ Pa,$
$\tau_0 = \rho_0 {v_0}^2 = 1.075 \times 10^5\ Pa,\ \eta_0 = 0.5375 Pa\ s$

These result in Reynolds number of 400.

For an increment of time the space-time slab for the square rigid cavity is discretized using 12×20 graded mesh (figure 7.1(c)) of 27-node p-version three dimensional hexahedron space-time elements. The space-time slab for the cavity with elastic bottom is discretized using 12×28 graded mesh (figure 7.1(d)) of 27-node p-version three dimensional hexahedron space-time elements. We choose local approximation space of class C^0 in space and time for all dependent variables ($u, v, \tau_{xx}, \tau_{xy}, \tau_{yy}, p$) with uniform p-level of five. Evolutions are computed using uniform $\Delta t = 0.1$. For these choice of h, p and k the least squares functional for all space-time slabs during the computations of the evolutions is of the order of $O(10^{-5})$ or lower. Newton's linear method with line search is considered converged when $|\delta I|_{max} \leq 10^{-5}$. Newton's linear method converges in 4 to 14 iterations for all space-time slabs. The contour plots of the velocities, stresses and pressure for various stages of the solution corresponding to the various time steps are presented and discussed in the following.

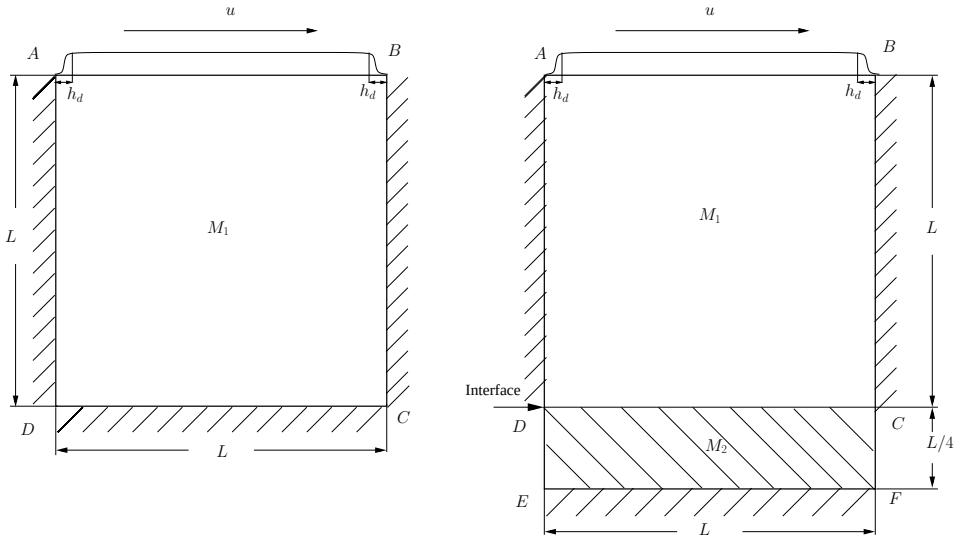

(a) Rigid lid driven cavity

(b) Lid driven cavity with elastic bottom

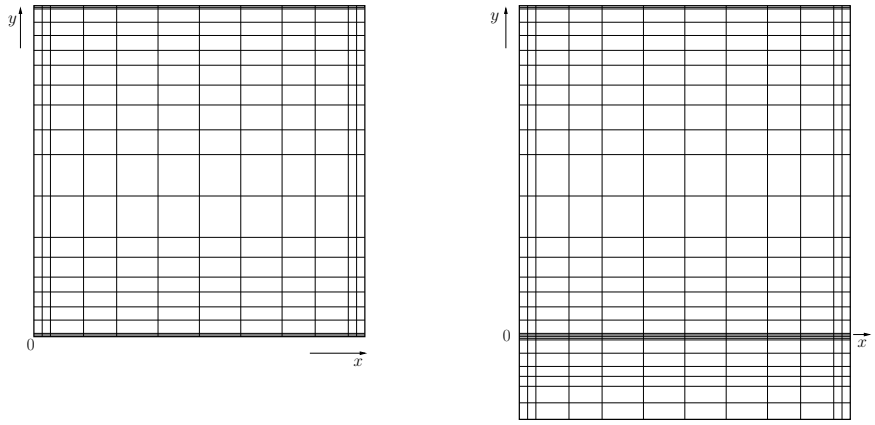

(c) 240 element non−discretization for rigid lid driven cavity

(d) 336 element non−discretization for lid driven cavity with elastic bottom

Figure 7.1: Lid driven cavity : schematics and discretizations

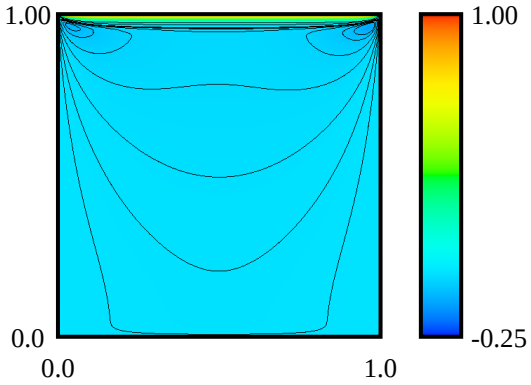

(a) velocity u for the first time step

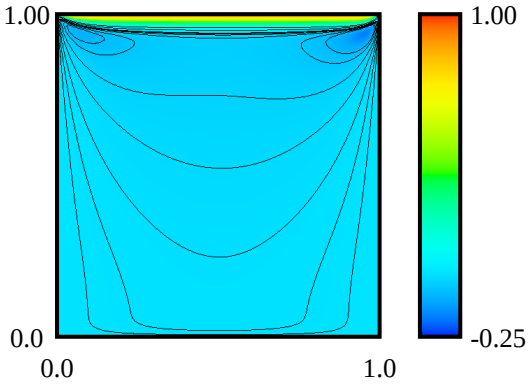

(d) velocity u for the second time step

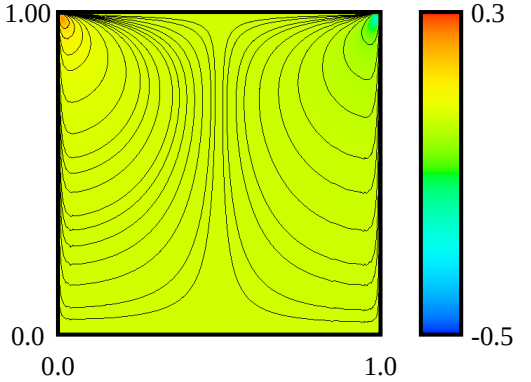

(b) velocity v for the first time step

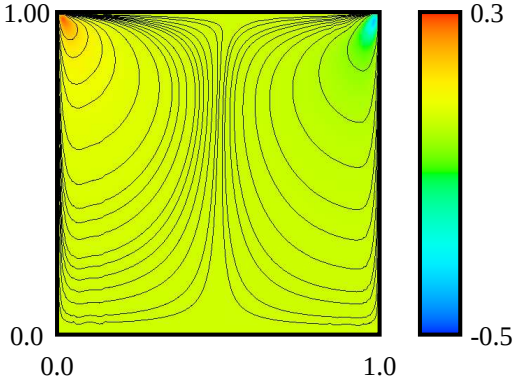

(e) velocity v for the second time step

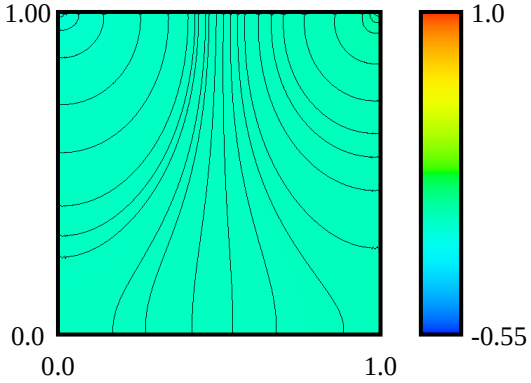

(c) pressure p for the first time step

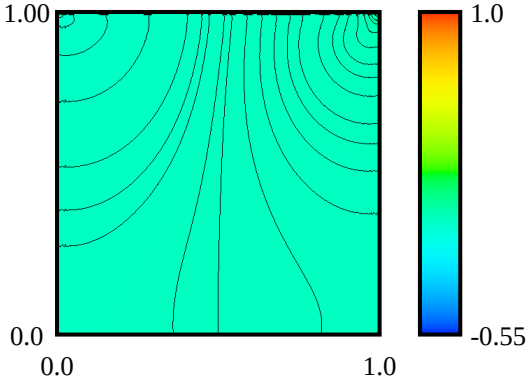

(f) pressure p for the second time step

Figure 7.2: Rigid cavity: first and second time steps

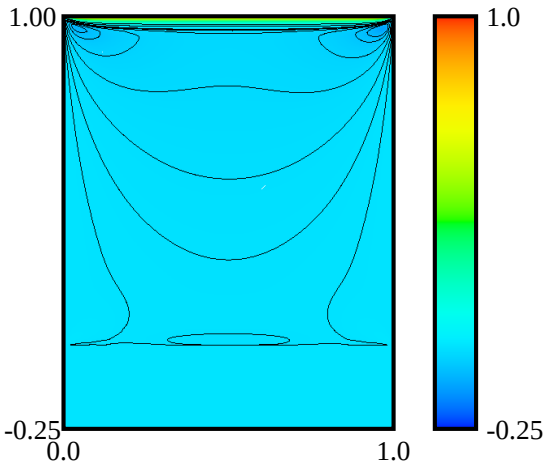

(a) velocity u for the first time step

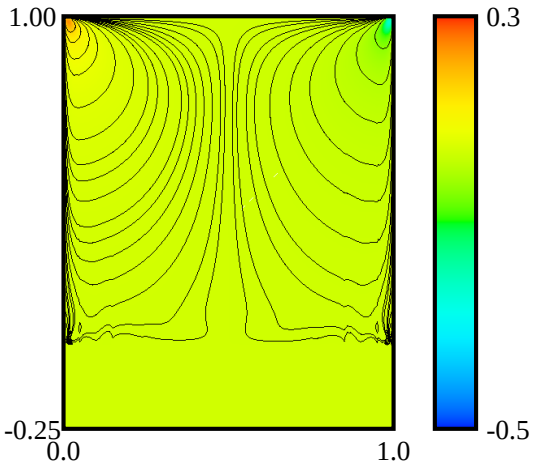

(b) velocity v for the first time step

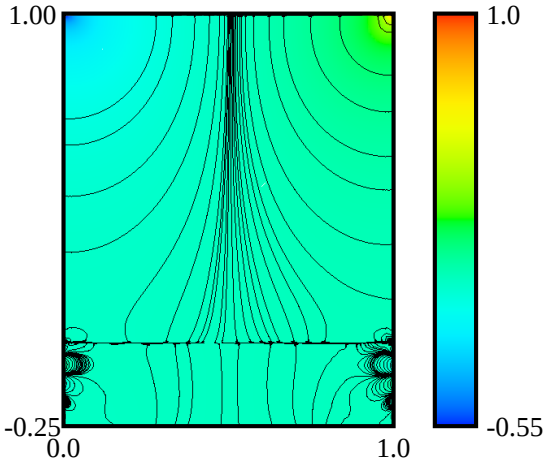

(c) pressure p for the first time step

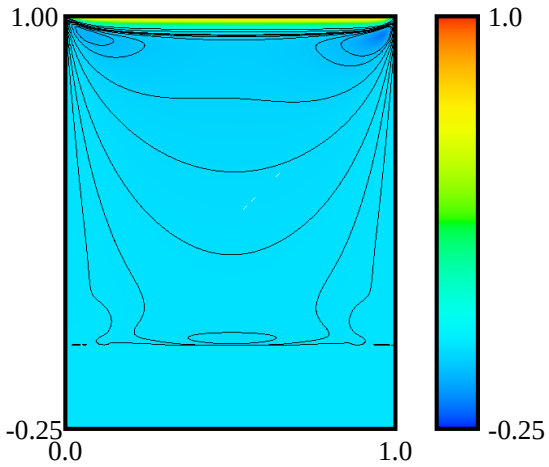

(d) velocity u for the second time step

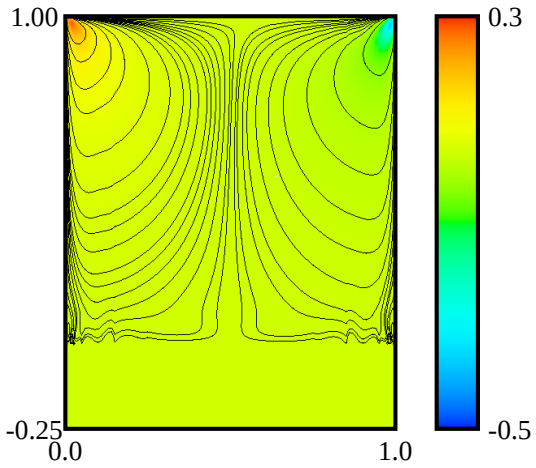

(e) velocity v for the second time step

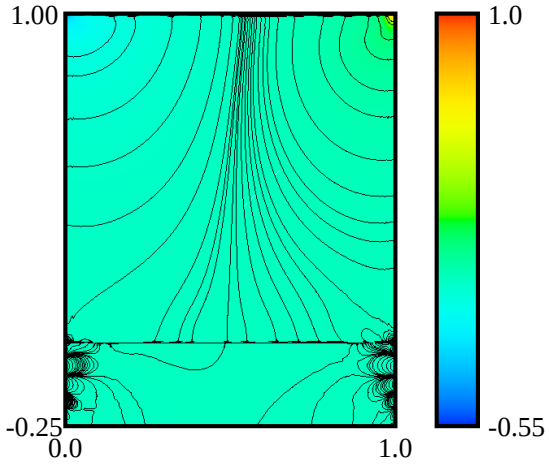

(f) pressure p for the second time step

Figure 7.3: Cavity with steel bottom: first and second time steps

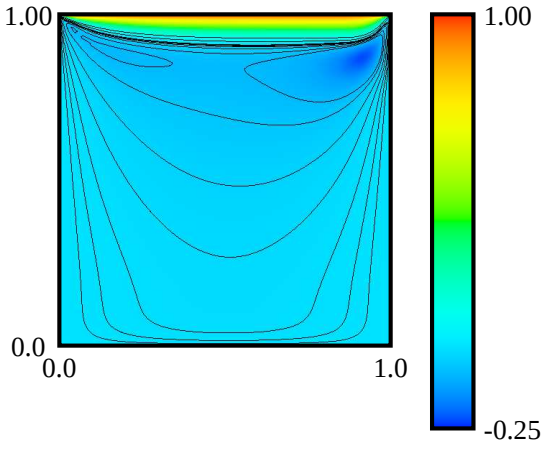

(a) velocity u for rigid cavity

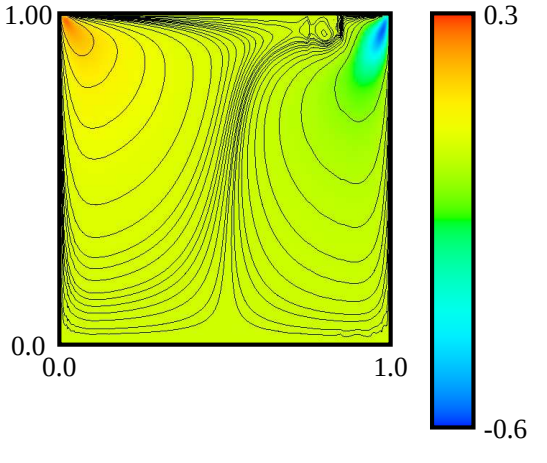

(b) velocity v for the rigid cavity

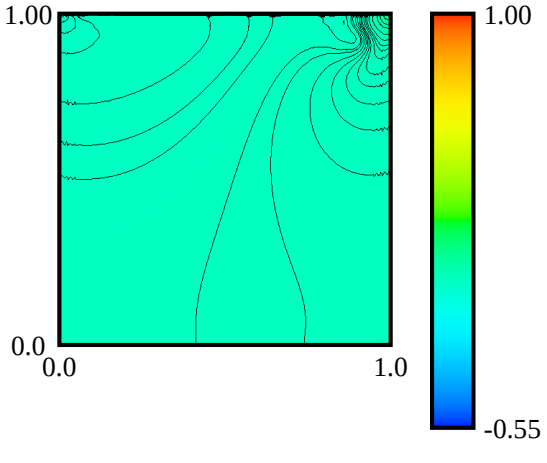

(c) pressure p for the rigid cavity

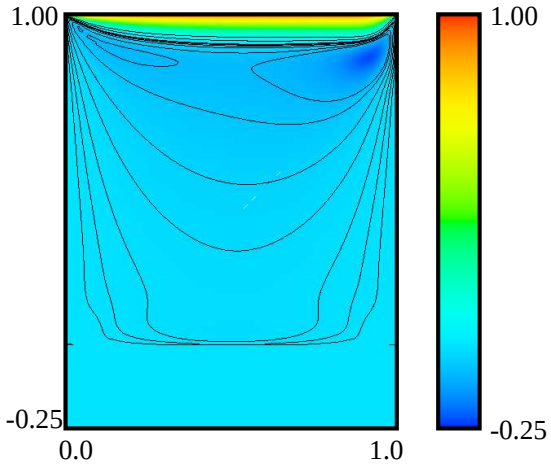

(d) velocity u for the steel bottom cavity

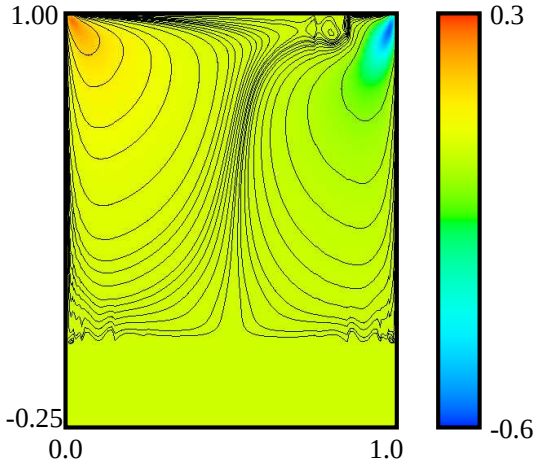

(e) velocity v for the steel bottom cavity

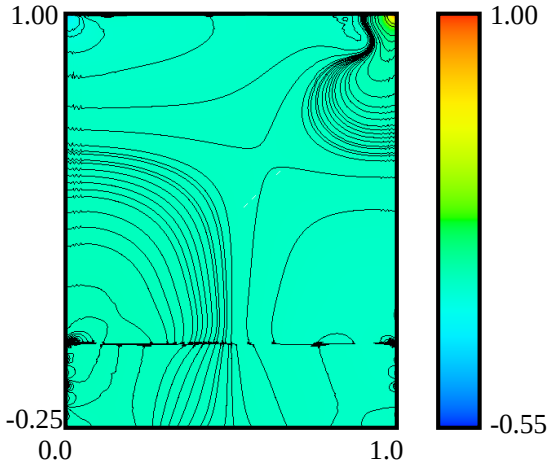

(f) pressure p for the steel bottom cavity

Figure 7.4: Cavity and steel bottom : sixth time step

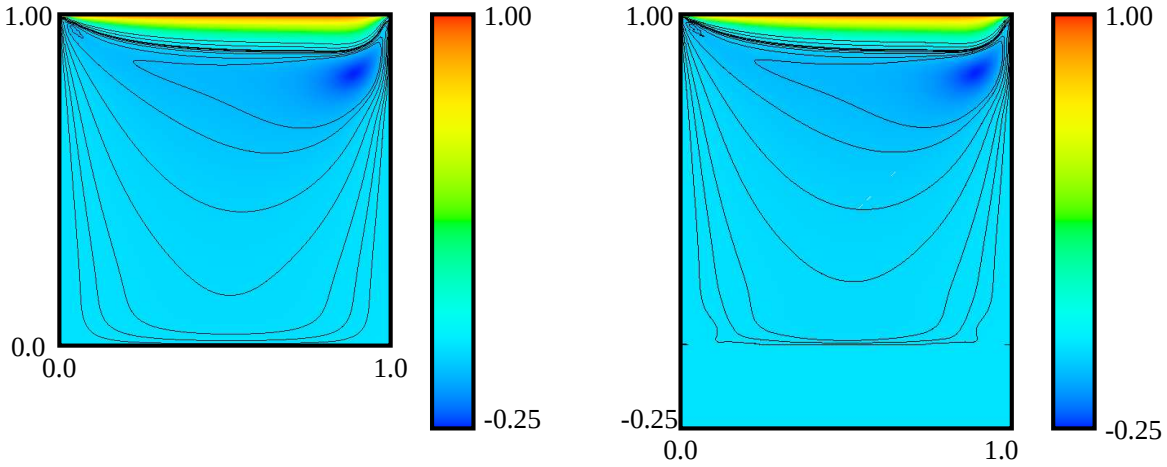

(a) velocity u for rigid cavity

(d) velocity u for the steel bottom cavity

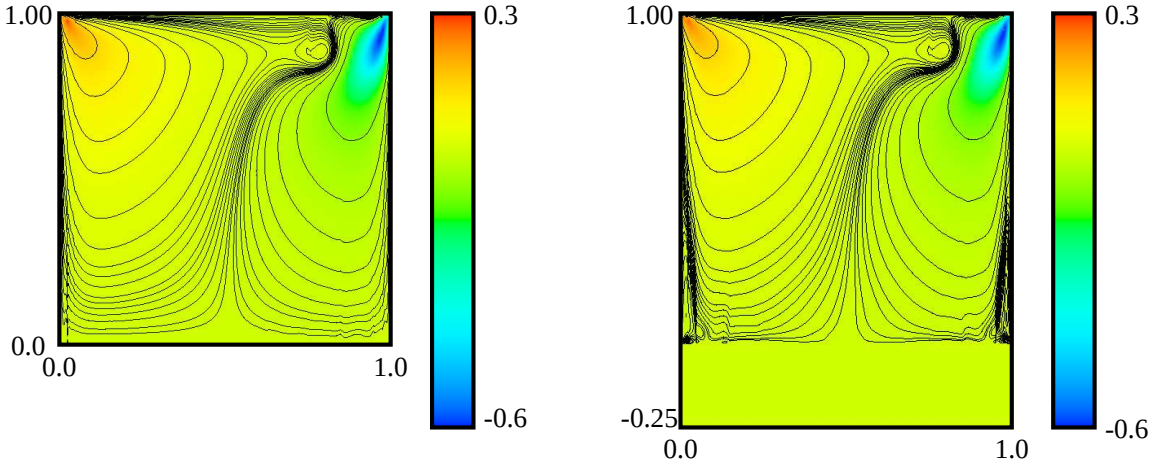

(b) velocity v for the rigid cavity

(e) velocity v for the steel bottom cavity

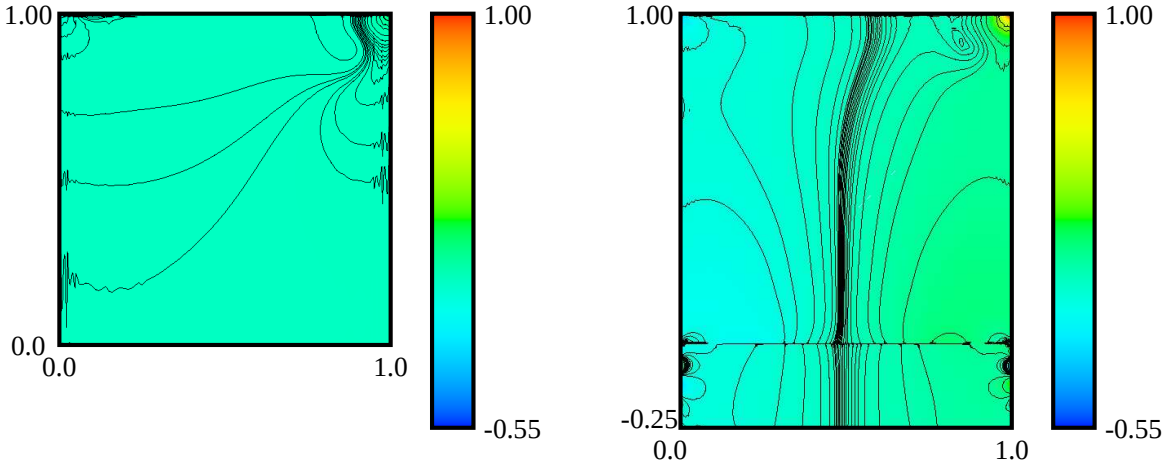

(c) pressure p for the rigid cavity

(f) pressure p for the steel bottom cavity

Figure 7.5: Cavity and steel bottom : ninth time step

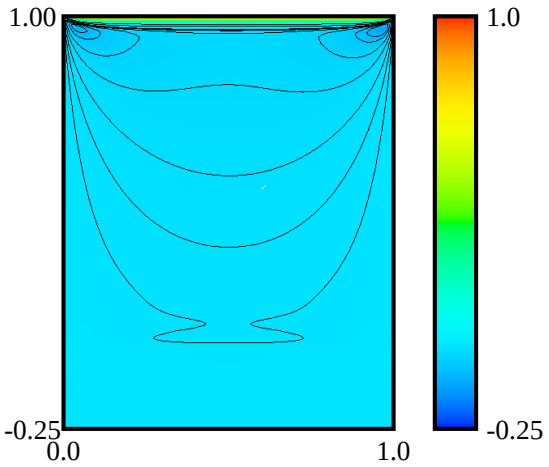

(a) velocity u for the first time step

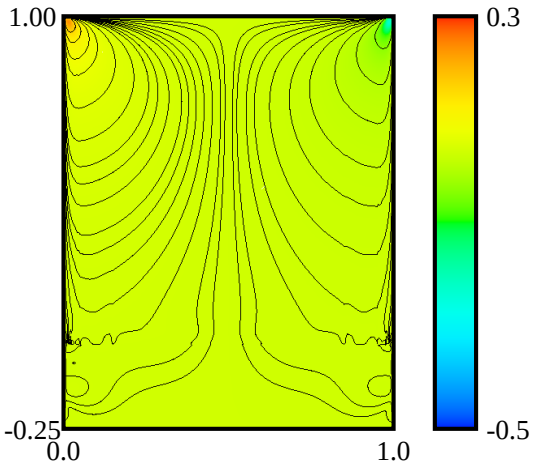

(b) velocity v for the first time step

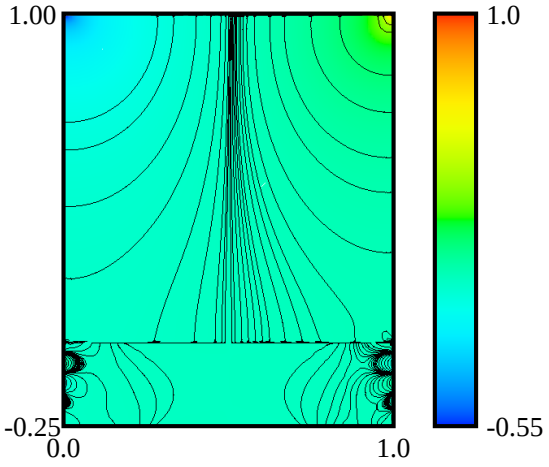

(c) pressure p for the first time step

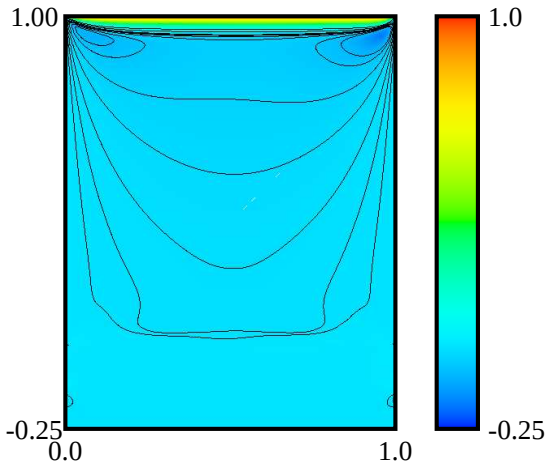

(d) velocity u for the second time step

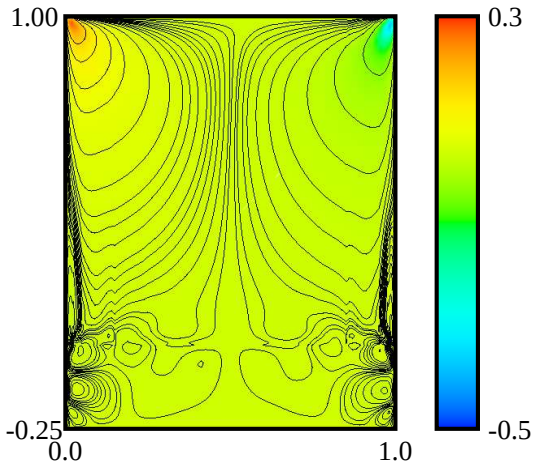

(e) velocity v for the second time step

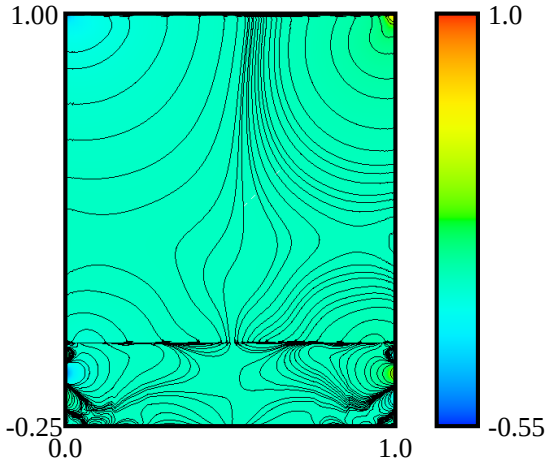

(f) pressure p for the second time step

Figure 7.6: Cavity with soft bottom: first and second time steps

Figure 7.2(a)-(c) and (d)-(f) show contours of velocities u and v and pressure p for the first and second increments of time for the square rigid cavity. Plots of u and v and p for the cavity with steel bottom for first and second time steps are shown in figures 7.3(a)-(f). As expected the steel bottom almost behaviors like an impermeable boundary. Velocities fields in figures 7.2 and 7.3 for corresponding time steps show extremely good agreement. Pressure field has similar behavior in both cases, however we note significant pressure values in the elastic bottom (as expected). Figure 7.4(a)-(c) show contour plots of u, v and p for rigid square cavity at the end of sixth time step. The contour plots of u, v and p for the cavity with steel bottom are shown in figure 7.4(d)-(f). We observe almost no activity in the steel bottom in figure 7.4(d) and (e) i.e. almost zero velocity field and a good match between the two in the square domain. As expected the pressure field is quite different between the two (figure 7.4(c) and (f)). Similar results with similar features are observed in figures 7.5(a)-(f) at the end of ninth time step. When the cavity bottom is a relatively softer elastic material compared to steel, we observe significant velocity field in the elastic bottom of the cavity. Figure 7.6(a)-(f) show contour of u, v and p for softer elastic bottom cavity for the first two increments of time.

Even though for this model problem we don't have a theoretical solution, however the values of the residual functional I of the order of $O(10^{-5})$ or lower during the entire evolution ensure extremely good accuracy of the computed results. A significant point to note is that interaction of Newtonian fluid and elastic solid in two dimensions is described by a single mathematical model and is simulated accurately in the proposed computational frame without requiring special treatment at the fluid-solid boundary in their respective mathematical models.

7.2.2 Transient developing flow of Maxwell fluid between parallel plates

In this study we consider transient developing flow of Maxwell fluid between parallel plates. A portion of the domain ($L_1 = 6$) has rigid boundary conditions at the plates. The remaining portion ($L_2 = 2$) has elastic boundaries. The schematics of domain, boundary condition and dimensions are shown in figure 7.7.

Following the developing flow between parallel plates, here also we define the inlet velocity at CF using

$$\begin{aligned} u(t) &= (\frac{3}{\Delta t^2} u_{\Delta t}) t^2 - (\frac{2}{\Delta t^3} u_{\Delta t}) t^3 \quad ; \quad 0 \leq t \leq \Delta t \\ u(t) &= u_{\Delta t} \quad ; \quad t \geq \Delta t \end{aligned} \tag{7.17}$$

where $u_{\Delta t} = u = 7.5(0.2 - y)(0.2 + y)$, $u_{\Delta t}$ being fully developed velocity. Additionally, we also specify $v = 0$ at the inlet CF. Clearly the velocity field (7.17) describes a continuously increasing flow rate for $0 \leq t \leq \Delta t$ at inlet that reaches a steady value at $t = \Delta t$ and thereafter remains constant.

Details of the discretization in the spatial domain are given in Table 7.1. A space-time slab for an increment of time Δt is discretized using 27 node p-version 3D hexahedron space-time elements.

We consider following properties of the Maxwell fluid and the elastic solid.

Maxwell fluid [64]: $\hat{\rho} = 868\ kg/m^3,\ \lambda_1 = 0.1\ s,\ \hat{\eta_s} = 2.7Pa\ s,\ \hat{\eta_p} = 0.3Pa\ s$

Elastic solid (Bone): $\hat{E} = 9.0 \times 10^9\ Pa,\ \hat{\rho} = 1900\ kg/m^3$

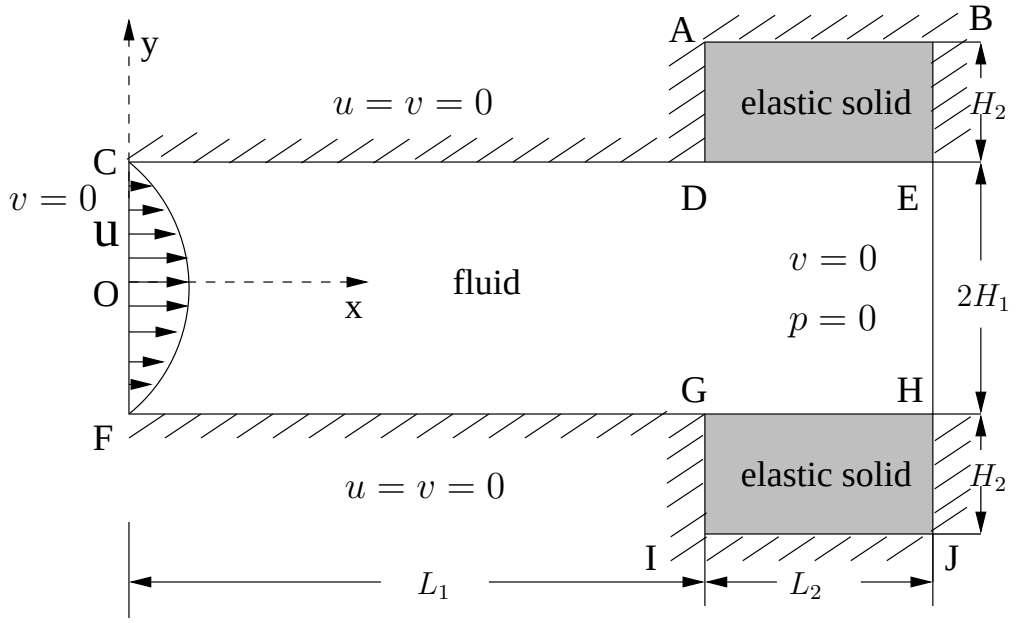

Figure 7.7: Schematics for flow between parallel plates

Value of reference quantities used are:

$\rho_0 = 868\ kg/m^3,\ L_0 = 0.2\ m\ ,\ v_0 = 0.2\ m/s,\ E_0 = 34.72\ Pa,\ \tau_0 = \rho_0 {v_0}^2 = 34.72\ Pa,\ \eta_0 = 3.0 Pa\ s$

These yield Reynolds number of 11.573 and Deborah number of 0.1.

Local approximation of class C^0 in space and time with p-level of 5 are considered with uniform Δt of 0.2. Due to local approximation of class C^0 all space-time integral over the space-time discretization are in Lebesgue sense. For the choice of h, p and k considered here, the least squares functional is of the order of $O(10^{-5})$ or lower for each space-time slab confirming that GDEs are satisfied accurately during the entire evolution. Newton's linear method with line search converges in 2 to 9 iterations for each space-time slab with $|\delta I|_{max} \leq 10^{-5}$.

Table 7.1: Spatial discretization for flow between parallel plates

Edge AB (h_x)	14 of 0.143					
Edge CD (h_x)	10 of 0.6					
Edge BE (h_y)	0.025	0.025	0.05			
Edge EH (h_y)	0.025	0.075	0.1	0.1	0.075	0.025
Edge HJ (h_y)	0.025	0.025	0.05			

We note that for the choices of dimensions $L_1/2H_1 = 15$ i.e. L_1 is sufficiently large for $2H_1 = 0.4$ for the flow to be fully developed in the later stage of $0 \leq x \leq L_1$. Evolution is completed for six time increments. Figure 7.8 shows evolutions of velocity u, axial stress τ_{xx} and shear stress τ_{xy} as a function of y at $x = 0.0$ and 3.0. We observe that in six increments of time the evolution reaches stationary state at both axial locations. u, τ_{xx} and τ_{xy} verse y at $x = 6.2$ and 7.2 (domain with elastic boundaries) for six time increments are shown in figure 7.9. First we note that due to infinite speed of wave propagation (due to open domain) the applied disturbance at inflow boundary propagates through the entire spatial domain in the first increment of time. Secondly at these spatial locations evolutions of u, τ_{xx} and τ_{xy} are complex and we do not have stationary state in six increments of time. This of course is due to complex wave phenomenon in the solid medium and its interaction with the Maxwell fluid. Evolution of velocity v and normal stress τ_{yy} verse y at $x = 6.2$ and 7.2 are shown in figures 7.10(a)-(d). Evolution of pressure p verse x at $y = 0$ is shown in figure 7.10(e) and (f). As in figure 7.9, here also evolutions are complex and don't reach stationary state in six increments of time. Pressure evolution becomes increasing more complex with time. Since the pressure in elastic solid is mean normal stress, the complexity of the pressure is clearly due to complex wave phenomena in the solid and its interaction with the Maxwell fluid.

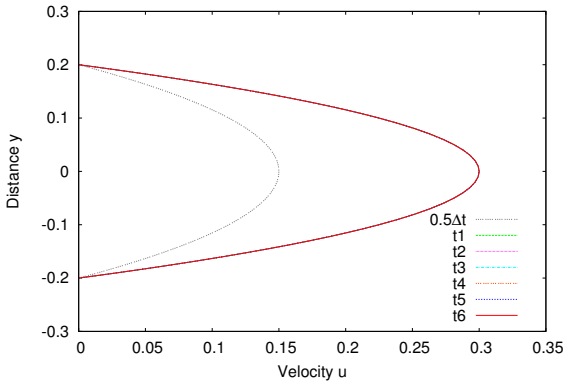

(a) Velocity u versus distance y at $x = 0.0$

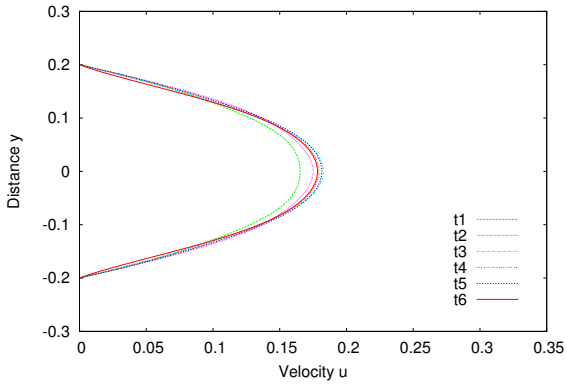

(b) Velocity u versus distance y at $x = 3.0$

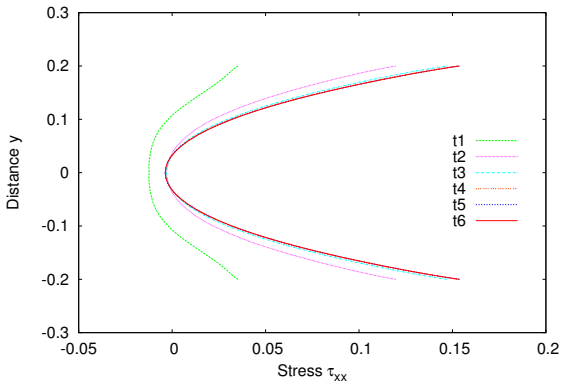

(c) Stress τ_{xx} versus distance y at $x = 0$

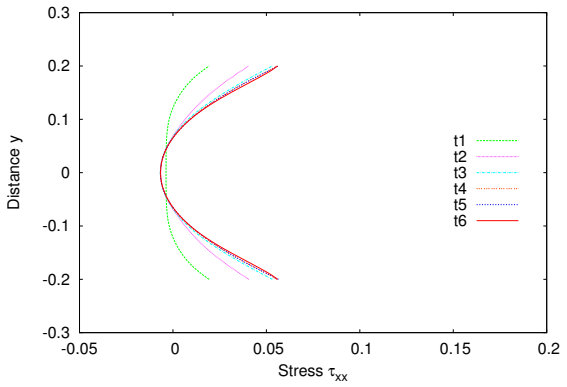

(d) Stress τ_{xx} versus distance y at $x = 3.0$

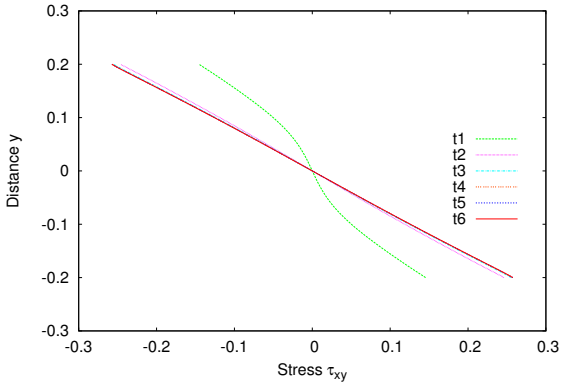

(e) Stress τ_{xy} versus distance y at $x = 0$

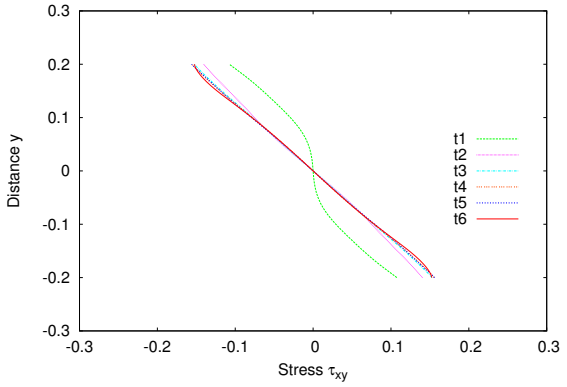

(f) Stress τ_{xy} versus distance y at $x = 3.0$

Figure 7.8: Evolutions of velocity u, stress τ_{xx} and stress τ_{xy} for pure fluid part

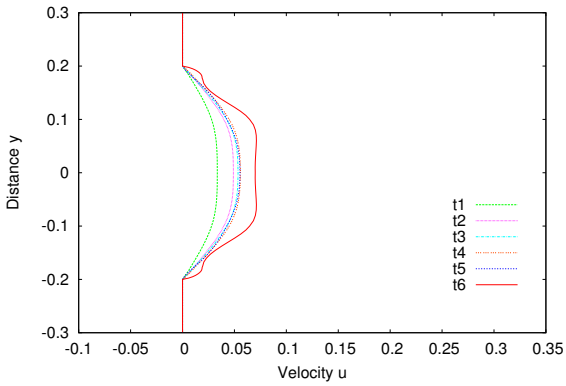

(a) Velocity u versus distance y at $x = 6.2$

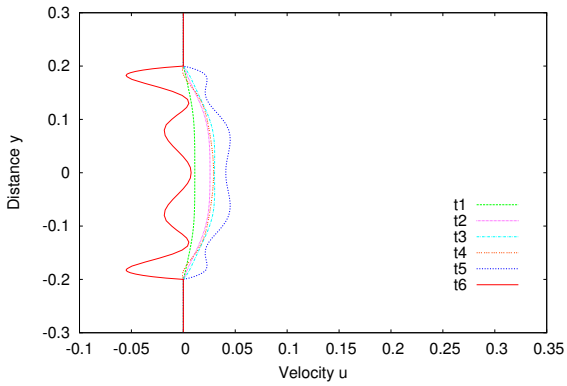

(b) Velocity u versus distance y at $x = 7.2$

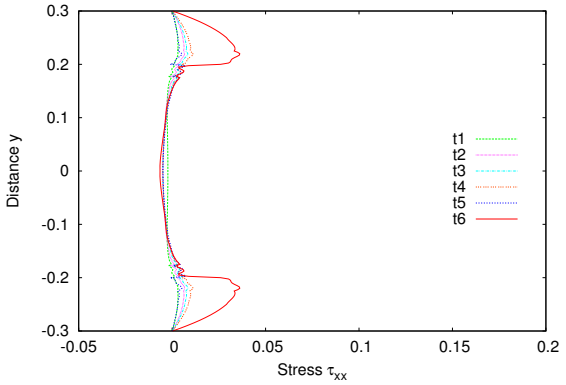

(c) Stress τ_{xx} versus distance y at $x = 6.2$

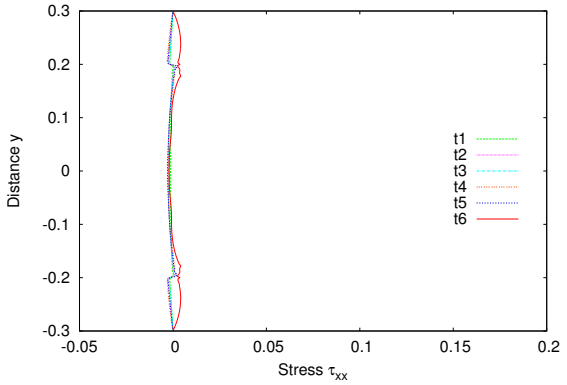

(d) Stress τ_{xx} versus distance y at $x = 7.2$

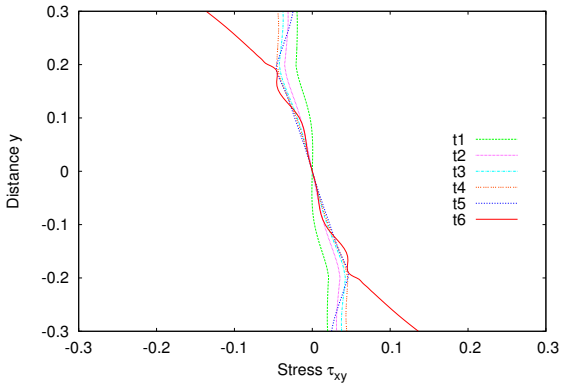

(e) Stress τ_{xy} versus distance y at $x = 6.2$

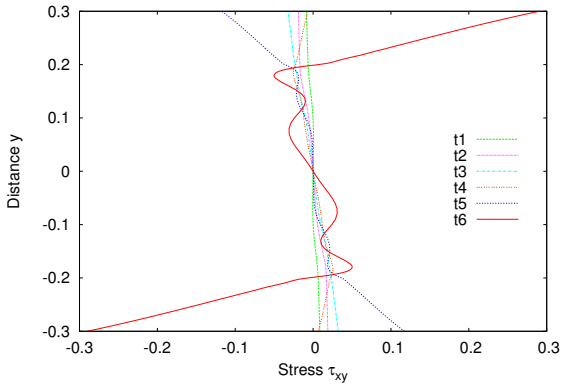

(f) Stress τ_{xy} versus distance y at $x = 7.2$

Figure 7.9: Evolutions of velocity u, stress τ_{xx} and stress τ_{xy} for interaction part

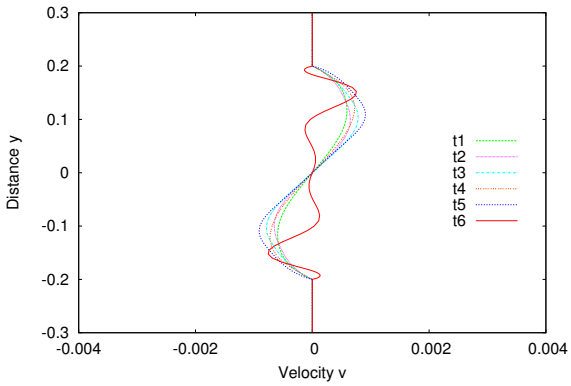

(a) Velocity v versus distance y at $x = 6.2$

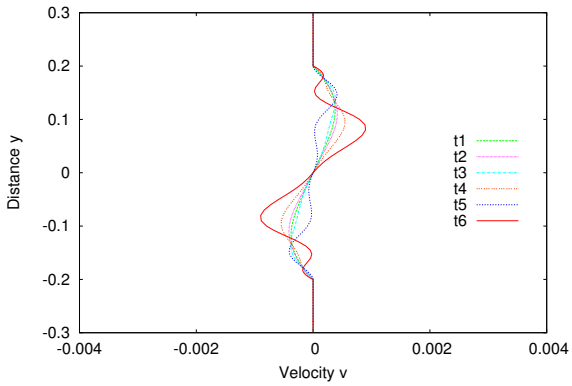

(b) Velocity v versus distance y at $x = 7.2$

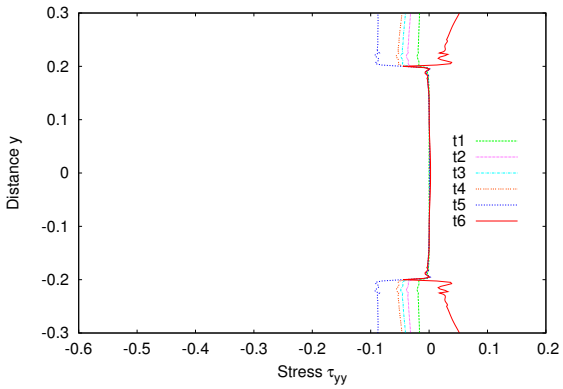

(c) Stress τ_{yy} versus distance y at $x = 6.2$

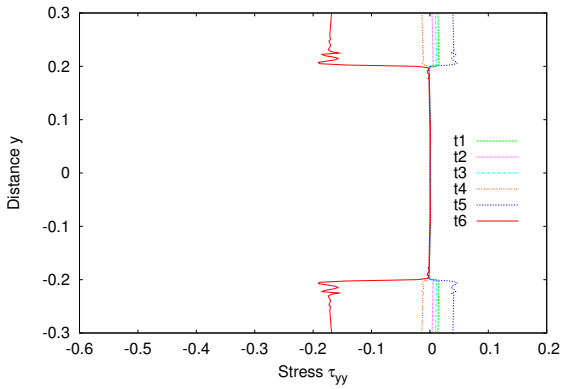

(d) Stress τ_{yy} versus distance y at $x = 7.2$

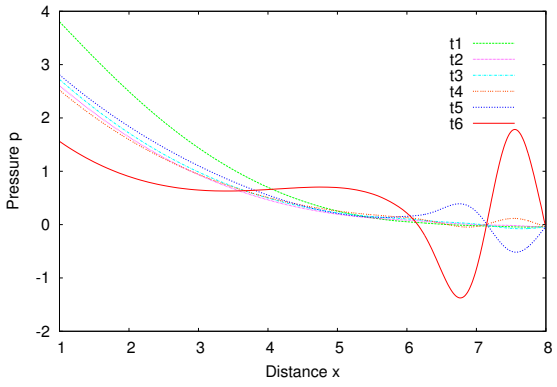

(e) Pressure p versus distance x at $y = 0$

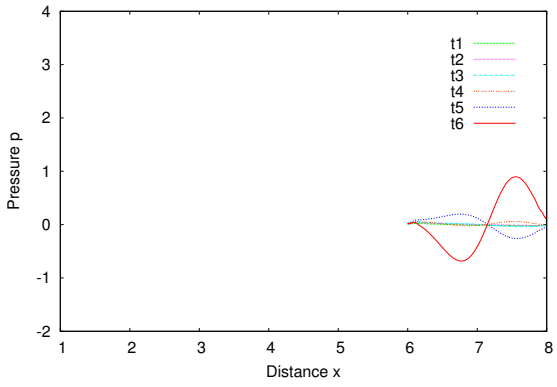

(f) Pressure p versus distance x at $y = 0.3$

Figure 7.10: Evolutions of velocity v, stress τ_{yy} and pressure p for interaction part

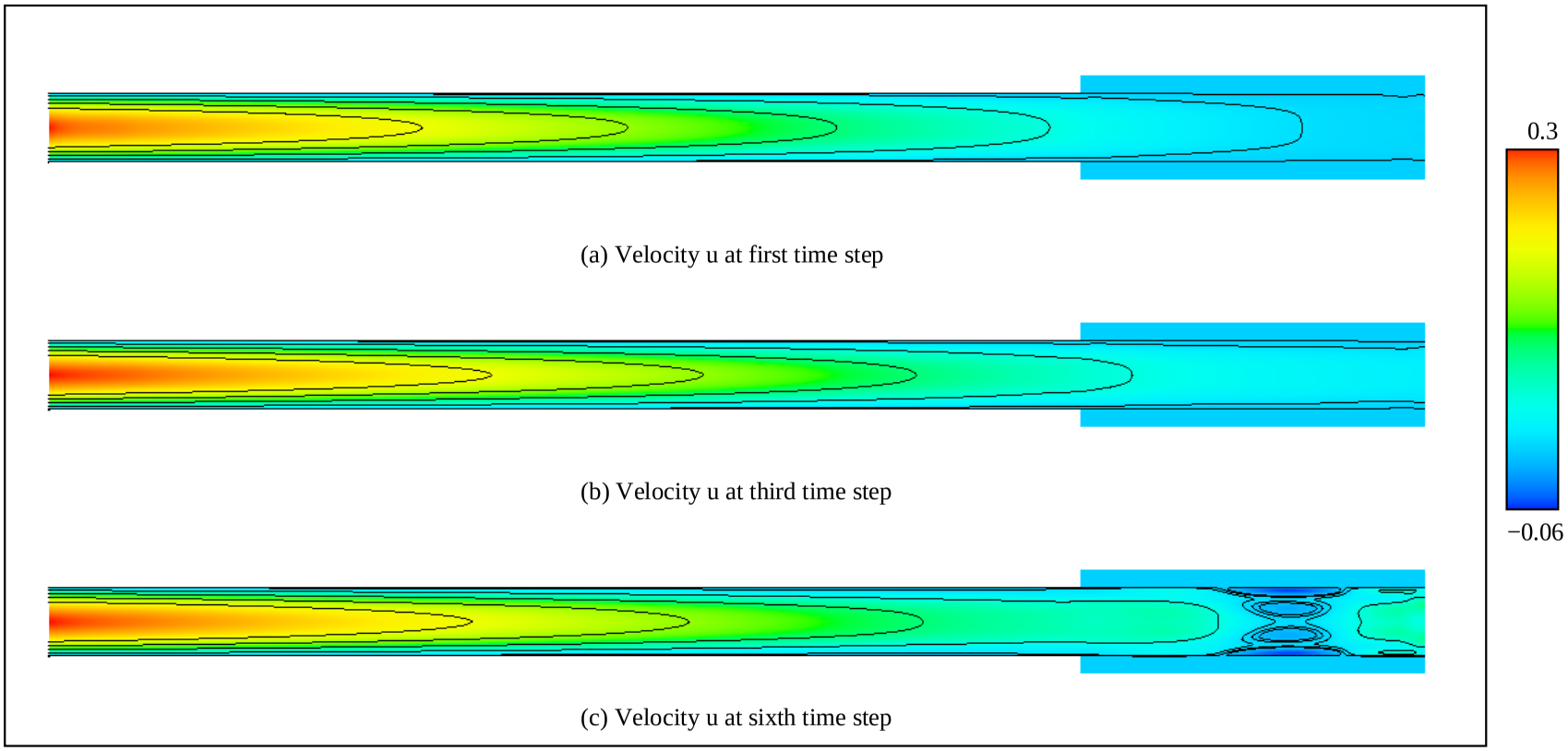

(a) Velocity u at first time step

(b) Velocity u at third time step

(c) Velocity u at sixth time step

Figure 7.11: Flow between parallel palate : velocity u at first, third and sixth time steps

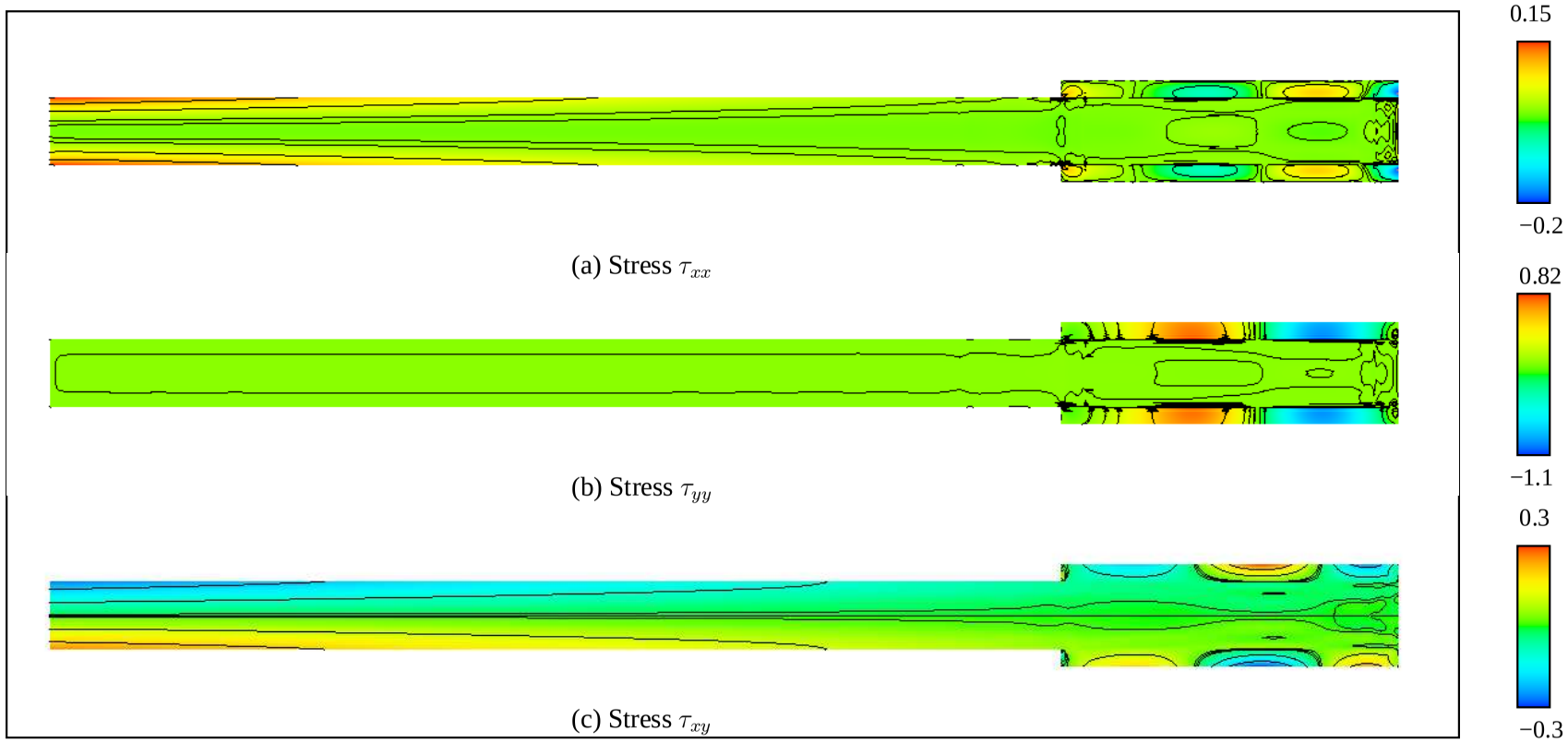

(a) Stress τ_{xx}

(b) Stress τ_{yy}

(c) Stress τ_{xy}

Figure 7.12: Flow between parallel palate : stresses τ_{xx}, τ_{yy} and τ_{xy} at sixth time step

Evolution of velocity u in the entire spatial domain for first, third and sixth time steps are shown in figure 7.11. Evolutions of stresses τ_{xx}, τ_{yy} and τ_{xy} in the entire spatial domain at the end of sixth time step are shown in figure 7.12. While the velocity field u in the solid portion is relatively small compared to the field portion, this is not the case for stress. In all cases symmetry (or antisymmetry) of results is clearly observed.

We remark that residual functional values of the order of $O(10^{-5})$ or lower ensures accurate evolution for all time increments. The complexity of interaction between Maxwell fluid and the elastic solid are simulated accurately without any special treatments at the interface boundary and without the use of stabilizing methods.

Remarks

(1) The numerical studies demonstrate the ability of a single mathematical model to accurately describe the interaction between two different media at the bi-material interface.

(2) STVC space-time integral forms yield unconditionally stable computations.

(3) In all cases for each space time strip $I \leq 10^{-5}$ and $|\delta I|_{max} \leq 10^{-5}$ indicate good accuracy of the computed solutions as well as convergence of the Newton Raphson method.

(4) We clearly observe that the results for the ninth time increments for both, rigid square cavity and the cavity with elastic bottom (steel) are in good agreement, indicating that the elastic steel bottom of the cavity compared to the Newtonian fluid used in the cavity, behaviors almost as an impermeable boundary.

(5) When the elastic bottom is a much softer material than steel, we can see the measurable differences in the velocity and pressure fields.

(6) In case of flow between parallel plates, infinite wave speed posses no problem in the computation of the evolution. Complex interaction of the waves in the solid with Maxwell fluid produces complex evolution for all dependent variables but no difficulties are encountered in the computation of the evolution.

7.3 Summary

(1) Dimensionless form of the mathematical models for incompressible hyper-elastic solids, Newtonian and generalized Newtonian fluid and polymeric liquids utilizing Maxwell model for constitutive equations are presented.

(2) A significant aspect of the work presented here is that interactions of solids and liquids are inherent in the mathematical models, thus, completely eliminating the need for constraint equations at the interfaces between the media. The choice of Eulerian description and identical dependent variables for each media ensure the interaction between the media to be intrinsic in the mathematical model.

(3) The numerical studies for the lid driven cavity and the flow between parallel plates with elastic boundary demonstate the interaction features of the elastic bottom of the cavity and the Newtonian fluid and the influence of elastic walls in case of parallel plates model problem.

(4) The methodology presented here is natural, straight forward, avoids upwinding methods and has built in measures of accuracy of the computed evolution (element residuals for each space-time element of each space-time strip or slab).

Chapter 8

Summary and Conclusions

In this thesis, numerical solutions of the interactions of solids, liquids both Newtonian and polymeric and gases in a single process have been addressed by constructing a single mathematical model for all media in Eulerian description and by utilizing hpk mathematical and computational space-time finite element framework in which the space-time integral forms are ensured to be space-time variationally consistent. A summary of the work and some conclusion are presented in the following.

(1) A single mathematical model based on conservation laws ensure that the interaction of various media of a single process are intrinsic in the mathematical model. The constitutive equations are obviously media specific but care is taken in choosing the dependent variables in the mathematical model to ensure that the constitutive equations for all media can also utilize the same dependent variables as those used in conservation laws. In case of compressible media density $\bar{\rho}$, velocities $\boldsymbol{v}$, thermodynamic pressure $p(\bar{\rho}, T)$ and deviatoric Cauchy stress tensor $\bar{\boldsymbol{\tau}}$ (in contra- and co- variant basis) are dependent variables of choice. For incompressible medium velocities $\boldsymbol{v}$, mechanical pressure $p(T)$ and deviatoric Cauchy stress tensor $\bar{\boldsymbol{\tau}}$ are dependent variables. For compressible medium, the thermodynamic

pressure is retained as a dependent variable to allow interaction of such media with incompressible media in which mechanical pressure $p(T)$ must remain a dependent variable in the mathematical model. The equation of state for compressible medium becomes an additional equation in the mathematical model.

(2) The mathematical model in (1), results in a system of non-linear partial differential equations in the dependent variables, spatial coordinates and time describing evolutions and hence are initial value problems. Numerical solution of the IVPs resulting from the mathematical model are obtained using space-time coupled finite element method in hpk framework with space-time variationally consistent integral form that ensure unconditionally stable computations during the entire evolution. As shown by Surana et. al. [7–9], the space-time least squares process based on space-time residual incorporating Newton's linear method for solving non-linear algebraic equations is the only method of approximation that yields STVC integral form and hence is used in the present work. For an increment of time the space-time strip or slab is discretized in spatial domain resulting in a space-time discretization containing space-time elements. A numerical solution is computed for an increment of time and then time march to obtain the desired evolution. In the approach the solution can be time marched only upon convergence for the current increment of time and hence ensuring desired accuracy of evolution for the entire space-time domain.

(3) Combining (1) and (2) provides a most general yet complete mathematical modelling and computational infrastructure for all interaction processes regardless of the application.

(4) Two significant and important investigations presented in this work that directly influence computations of evolutions for interaction processes are

(a) Investigation of the validity of rate constitutive equations in contra- and co-variant bases (and others such as Jaumann rate equations) for progressively increasing deformation using Giesekus constitutive model (holds for other constitutive models as well). The studies confirm that the rate constitutive theories in contravariant basis continue to produce physical deformation behaviors compared the rate constitutive theories in covariant basis and others with progressively increasing strains and strain rates. Thus, only contravariant rate constitutive theories are worthy of consideration when the deformation deviates from infinitesimal assumption.

(b) Investigation related to infinite wave speed, pressure field and the initial velocity field specification in incompressible flows in open domains reveal that the issues of infinite wave speed (inherent in the mathematical model due to incompressibility assumption) and the initial velocity field specification are completely unrelated. Initial velocity field may be necessary in iterative methods for solving non-linear algebraic equation resulting from the space-time methods of approximation but it has no influence on the wave speed or the pressure field. Secondly, the pressure field in case of incompressible liquids is mechanical and hence is not deterministic from the deformation field. Thus, when simulating flows in open domains, adequate specification of BCs on pressure such that it is deterministic regardless of the deformation field is essential. Numerical studies presented in the present work confirm this. Thirdly, since infinite wave speed is intrinsic in the mathematical model, it can not be altered without changing the mathematical model. Studies presented in this work show that in a single time step (regardless of its magnitude) the applied disturbance propagates in the whole domain as it should, but no problems are encountered in the computations

of the bounded evolutions that eventually lead to accurate stationary states. Numerical studies presented for developing transient flow between parallel plates and backward facing step with Newtonian and Maxwell fluids clearly demonstrate these aspects.

(5) A number of one dimensional wave propagation numerical studies have been presented using bi-material interfaces to demonstrate : (a) that a single mathematical model indeed contains all interaction features (b) Wave propagation, reflections and transmissions at the bi-material interface and subsequent interactions of the waves are simulated accurately without any difficulty or special treatments. Two dimensional numerical studies reaffirm these features of the proposed mathematical models and computational infrastructure.

(6) Since the interactions of the different media in a process are intrinsic in the mathematical model, the constraint equation at the interfaces between the media (used presently) are completely eliminated. Constraint equations are mathematical statements of the perceived physics at the interface and hence are highly prone to errors and often lead to corruption at the interface and in their vicinity.

(7) The present work is limited to small motion of the interfaces, boundaries and free surfaces due to the fact that in Eulerian descriptions motion of the material particles can not be monitored easily. However, within this assumption the approach presented in this work for constructing a single mathematical model for all media of an interaction process and for obtaining the numerical solution of the associated IVPs using hpk framework with space-time integral forms that are space-time variationally consistent is rather straight forward, application independent and ensures unconditionally stable computations during the entire evolution. When the minimally conforming approximation spaces are chosen based

on the highest order of the derivatives of the dependent variables in the mathematical model, the integrals in the entire computational process are Riemann and hence the space-time residual functionals for the space-time elements are true measures of the errors in the computed solution without the knowledge of theoretical solution. This features provide an inherent and built in mechanism for reducing errors in the computed solution through h-p adaptivity for each space-time strip or slab and, hence possibility of obtaining time accurate evolutions.

Bibliography

[1] K.S. Surana, D. Nunez, J.N. Reddy, and A. Romkes. Rate Constitutive Theory for Ordered Thermofluids. *Manuscript in preparation*, 2011.

[2] K.S. Surana, D. Nunez, J.N. Reddy, and A. Romkes. Rate Constitutive Theory for Ordered Thermoviscoelastic Solids. *Manuscript in preparation*, 2011.

[3] K.S. Surana, D. Nunez, J.N. Reddy, and A. Romkes. Rate Constitutive Theory for Ordered Thermoviscoelastic Fluids. *Manuscript in preparation*, 2011.

[4] K.S. Surana. *ME 840 Continuum Mechanics I and ME 841 Continuum Mechanics II class notes*. Mechanical Engineering Department, the University of Kansas, 2011 (Manuscript of the text book "Continuum Mechanics" in preparation, 2011).

[5] A. C. Eringen. *Nonlinear Theory of Continuous Media*. McGraw-Hill book company, Inc., 1962.

[6] A. C. Eringen. *Mechanics of Continua*. John Wiley& Sons, 1967.

[7] K.S. Surana, J.N. Reddy, and S. Allu. The k-Version of Finite Element Method for IVPs: Mathematical and Computational Framework. *International Journal for Computational Methods in Engineering Science and Mechanics*, 8(3):123–136, 2007.

[8] K.S. Surana, S. Allu, P.W. Tenpas, and J.N. Reddy. k-Version of Finite Element Method in Gas Dynamics: Higher Order Global Differentiability Numerical Solutions. *International Journal Numerical Methods in Engineering*, 69:1109–1157, 2006.

[9] K.S. Surana, S. Allu, J.N. Reddy, and P.W. Tenpas. Least Squares Finite Element Processes in h, p, k Mathematical and Computational Framework for a Nonlinear Conservation Law. *International Journal of Numerical Methods in Fluids*, 57:1545–1568, 2008.

[10] X. Wang and K.J. Bathe. Displacement/Pressure Based Mixed Finite Element Formulations for Acoustic Fluid–structure Interaction Problems. *International Journal for Numerical Methods in Engineering*, 40(11):2001–2017, 1997.

[11] K.C. Park, C.A. Felippa, and R. Ohayon. Partitioned Formulation of Internal Fluid-structure Interaction Problems by Localized Lagrange Multipliers. *Computer Methods in Applied Mechanics and Engineering*, 190(1):2989–3007, 2001.

[12] C. Michler, S.J. Hulshoff, E.H. van Brummelen, and R. de Borst. A Monolithic Approach to Fluid-structure Interaction. *Computers & Fluids*, 33:839–848, 2004.

[13] J.J. Heys, T.A. Manteuffel, S.F. McCormick, and J.W. Ruge. First-order System Least Squares (FOSLS) for Coupled Fluid-elastic Problems. *Journal of Computational Physics*, 195(2):560–575, 2004.

[14] D.J. Benson. A Multi-material Eulerian Formulation for the Efficient Solution of Impact and Penetration Problems. *Computational Mechanics*, 15(6):558–571, 1995.

[15] R.P. Fedkiw, T. Aslam, B. Merriman, and S. Osher. A Non-oscillatory Eulerian Approach to Interfaces in Multimaterial Flows(the Ghost Fluid Method). *Journal of Computational Physics*, 152(2):457–492, 1999.

[16] D.J. Benson. An Implicit Multi-material Eulerian Formulation. *International Journal for Numerical Methods in Engineering*, 48:475–499, 2000.

[17] D.J. Benson and L. Stainier. An Eulerian Shell Formulation for Fluid-structure Interaction. *Computer Methods in Applied Mechanics and Engineering*, 187(3):571–590, 2000.

[18] H.S. Udaykumar, L.B. Tran, D.M. Belk, and K.J. Vanden. An Eulerian Method for Computation of Multimaterial Impact with ENO Shock-capturing and Sharp Interfaces. *Journal of Computational Physics*, 186(1):136–177, 2003.

[19] L.B. Tran and H.S Udaykumar. A Particle-level Set- Based Sharp Interface Cartesian Grid Method for Impact, Penetration and Void Collapse. *Journal of Computational Physics*, 193:469–510, 2004.

[20] G.H. Cottet, E Maitre, and T. Milcent. An Eulerian Method for Fluid-structure Coupling with Biophysical Applications. *European Conference on Computational Fluid Dynamics*, pages 1–16, 2006.

[21] T. Dunne. An Eulerian Approach to Fluid-structure Interaction and Goal-oriented Mesh Adaptation. *International Journal for Numerical Methods in Fluids*, 51:1017–1039, 2006.

[22] T. Belytschko, W.K. Liu, and B. Moran. *Nonlinear Finite Elements for Continua and Structures*. John Wiley& Sons, 2000.

[23] M. Sussman, P. Smereka, and S. Osher. A Level Set Approach for Computing Solutions to Incompressible Two-phase Flow. *Journal of Computational Physics*, 114(1):146–159, 1994.

[24] M. Arienti, P. Hung, E. Morano, and J.E. Shepherd. A Level Set Approach to Eulerian–Lagrangian Coupling. *Journal of Computational Physics*, 185(1):213–251, 2003.

[25] R. Caiden, R.P. Fedkiw, and C. Anderson. A Numerical Method for Two-phase Flow Consisting of Separate Compressible and Incompressible Regions. *Journal of Computational Physics*, 166(1):1–27, 2001.

[26] B. Koren, M.R. Lewis, E.H. van Brummelen, and B. van Leer. Riemann-problem and Level-set Approaches for Homentropic Two-fluid Flow Computations. *Journal of Computational Physics*, 181(2):654–674, 2002.

[27] S. Groß, V. Reichelt, and A. Reusken. A Finite Element Based Level Set Method for Two-phase Incompressible Flows. *Computing and Visualization in Science*, 9(4):239–257, 2006.

[28] J. Chessa and T. Belytschko. An Enriched Finite Element Method and Level Sets for Axisymmetric Two-phase Flow with Surface Tension. *Int. J. Numer. Meth. Engng*, 58:2041–2064, 2003.

[29] A.A. Amsden. YAQUI: An Arbitrary Lagrangian-Eulerian Computer Program for Fluid Flow at All Speeds. Technical report, LA–5100, Los Alamos Scientific Lab., N. Mex.(USA), 1973.

[30] C.W. Hirt, A.A. Amsden, and J.L. Cook. An Arbitrary Lagrangian-Eulerian Computing Method for All Flow Speeds. *Journal of Computational Physics*, 14(3):227–253, 1974.

[31] T.J.R. Hughes, W.K. Liu, and T.K. Zimmermann. Lagrangian-Eulerian Finite Element Formulation for Incompressible Viscous Flows. *Computer Methods in Applied Mechanics and Engineering*, 29(3):329–349, 1981.

[32] C.Y. Lepage and W.G. Habashi. Fluid-structure Interactions Using the ALE Formulation. *AIAA, Aerospace Sciences Meeting and Exhibit, 37th, Reno, NV*, 1999.

[33] E. Lefrancois, G. Dhatt, and D. Vandromme. Fluid-structural Interaction with Application to Rocket Engines. *International Journal for Numerical Methods in Fluids*, 30(7):865–895, 1999.

[34] P.A. Mendes and F.A. Branco. Analysis of Fluid–structure Interaction by an Arbitrary Lagrangian–Eulerian Finite Element Formulation. *International Journal for Numerical Methods in Fluids*, 30(7):897–919, 1999.

[35] M. Souli, A. Ouahsine, and L. Lewin. ALE Formulation for Fluid-structure Interaction Problems. *Comput. Methods Appl. Mech. Engrg*, 190:659–675, 2000.

[36] Q. Zhang and H. Toshiaki. Analysis of Fluid-structure Interaction Problems with Structural Buckling and Large Domain Changes by ALE Finite Element Method. *Comput. Methods Appl. Mech. Engrg*, 190:6341–6357, 2001.

[37] P. Le Tallec and J. Mouro. Fluid Structure Interaction with Large Structural Displacements. *Comput. Methods Appl. Mech. Engrg*, 190:3039–3067, 2001.

[38] A. R. Pishevar. An ALE Method for Compressible Multifluid Flow: Application to Underwater Explosion. *CFD 2003, Vancouver, May 28-30, Cananda*, 2003.

[39] I.M. Gelfand and S.V. Fomin. *Calculus of Variations*. Dover Publications Inc. New York, 2000.

[40] S.G. Mikhlin. *Variational Methods in Mathematical Physics*. Pergamon Press New York, 1964.

[41] C. Johnson. *Numerical Solution of Partial Differential Equations by Finite Element Method*. Cambridge University press, 1987.

[42] K.S. Surana, R.K. Mahanti, and J.N. Reddy. Galerkin/least Squares Finite Element Processes for BVPs in h, p, k Mathematical Framework. *International Journal of Computational Engineering Sciences and Mechanics*, 8:439–462, 2007.

[43] H.S. Udaykumar and W. Shyy. A Grid-supported Marker Particle Scheme for Interface Tracking. *Numerical Heat Transfer. Part B, Fundamentals*, 27(2):127–153, 1995.

[44] H.S. Udaykumar, R. Mittal, and W. Shyy. Computation of Solid-Liquid Phase Fronts in the Sharp Interface Limit on Fixed Grids. *Journal of Computational Physics*, 153(2):535–574, 1999.

[45] T. Ye, R. Mittal, H.S. Udaykumar, and W. Shyy. An Accurate Cartesian Grid Method for Viscous Incompressible Flows with Complex Immersed Boundaries. *Journal of Computational Physics*, 156(2):209–240, 1999.

[46] H.S. Udaykumar, R. Mittal, P. Rampunggoon, and A. Khanna. A Sharp Interface Cartesian Grid Method for Simulating Flows with Complex Moving Boundaries. *Journal of Computational Physics*, 174(1):345–380, 2001.

[47] H.S. Udaykumar, R. Mittal, and P. Rampunggoon. Interface Tracking Finite Volume Method for Complex Solid-fluid Interactions on Fixed Meshes. *Communications in Numerical Methods in Engineering*, 18:89–97, 2002.

[48] K.S. Surana, A.R. Ahmadi, and J.N. Reddy. The k-Version of Finite Element Method for Self-adjoint Operators in BVPs. *International Journal of Computational Engineering Science*, 3(2):155–218, 2002.

[49] K.S. Surana, A.R. Ahmadi, and J.N. Reddy. The k-Version of Finite Element Method for Non-self-adjoint Operators in BVPs. *International Journal of Computational Engineering Sciences*, 4(4):737–812, 2003.

[50] K.S. Surana, A.R. Ahmadi, and J.N. Reddy. k-Version of Finite Element Method for Non-linear Operators in BVPs. *International Journal of Computational Engineering*, 5(1):133–207, 2004.

[51] C. A. Truesdell and R. A. Toupin. *The Classical Field Theories of Mechanics*. Handbuch der physik vol 3/1, 1963.

[52] C. A. Truesdell and W. Noll. *The Non-linear Field Theories of Mechanics*. Handbuch der physik vol 3/3, 1965.

[53] R.B. Bird, R.C. Armstrong, and O. Hassager. *Dynamics of Polymeric Liquids, Vol. 1, Fluid Mechanics*. John Wiley& Sons, 1987.

[54] B.C. Bell and K.S. Surana. A Space-time Coupled p-Version Least-squares Finite Element Formulation for Unsteady Fluid Dynamic Problem. *International Journal Numerical Methods in Engineering*, 37:3545–3569, 1994.

[55] B. Bell and K.S. Surana. p-Version Space-time Coupled Least Squares Finite Element Formulation for Two-dimensional Unsteady Incompressible, Newtonian Fluid Flow. *ASME Winter Annual Meeting*, 1993.

[56] L.M. Quinzani, R.C. Armstrong, and R.A. Brown. Use of Coupled Birefringence and LDV Studies of Flow through a Planar Contraction to Test Constitutive Equations for Concentrated Polymer Solutions. *Journal of Rheology*, 39(6):1201–1227, 1995.

[57] K.S. Surana, K. M. Deshpande, A. Romkes, and J.N. Reddy. Computations of Numerical Solutions in Polymer Flows using Giesekus Constitutive Model in hpk Framework and Variationally Consistent Integral Forms. *International Journal for Computational Methods in Engineering Science and Mechanics*, 10:317–344, 2009.

[58] J.P. Pontaza and J.N. Reddy. Space-time Coupled Spectral/hp Least-squares Finite Element Formulation for the Incompressible Navier-Stokes Equations. *Journal of Computational Physics*, 197(2):418–459, 2004.

[59] J.P. Pontaza and J.N. Reddy. Spectral/hp Least-squares Finite Element Formulation for the Navier-Stokes Equations. *Journal of Computational Physics*, 190(2):523–549, 2003.

[60] A. Povitsky. Numerical Study of Wave Propagation in a Nonuniform Compressible Flow. *Physics of Fluid*, 14(8):2657–2672, 2002.

[61] P.M. Gresho, D.K. Gartling, J.R. Torczynski, K.A. Cliffe, K.H. Winters, T.J. Garrat, A. Spence, and J.W. Goodrich. Is the Steady Viscous Incompressible Two-dimensional Flow Over a Backward-facing Step at Re=800 Stable? *International Journal of Numerical Methods in Fluids*, 17:501–541, 1993.

[62] K.S. Surana, Y.T. Ma, A. Romkes, and J.N. Reddy. The Rate Constitutive Equations and Their Validity for Progressively Increasing Deformation. *Mechanics of Advanced Materials and Structures*, Vol.17:509–533, 2010.

[63] K.S. Surana, Y.T. Ma, A. Romkes, and J.N. Reddy. Development of Mathematical Models and Mathematical, Computational Framework for Multi-physics Interaction Processes. *Mechanics of Advanced Material and Structures*, Vol.17:488–508, 2010.

[64] C. Bodart and M.J. Crochet. The Time Dependent Flow of a Viscoelastic Fluid Around a Sphere. *Journal of Non-Newtonian Fluid Mechanics*, 54:303–329, 1994.

[65] T. Dunne and R. Rannacher. Adaptive Finite Element Approximation of Fluid Structure Interation Based on an Eulerian Variational Formulation. *Fluid-structure Interaction : Modelling, Simulation, Optimization*, 53:110–145, 2006.

[66] M. Schafer, M. Heck, and S. Yigit. An Implicit Partitioned Method for the Numerical Simulation of Fluid-structure Interaction. *Fluid-structure Interaction : Modelling, Simulation, Optimization*, 53:171–194, 2006.